Representation of Water Table Dynamics In a Land Surface Scheme: Observations, Models, and Analyses

by

Pat Jen –Feng Yeh

B.E. in Civil Engineering, National Taiwan University (1992)
M.S. in Environmental Engineering, National Chiao-Tung University (1994)

Submitted to the Department of Civil and Environmental Engineering
in partial fulfillment of the requirement for the degree of

Doctor of Philosophy in the Field of Hydrology

at the

MASSACHUSETTS INSTITUTE OF TECHNOLOGY

February 2003
[June 2003]

Author.....
Department of Civil and Environmental Engineering
September 24, 2002

Certified by.....
Elfatih A. B. Eltahir
Associate Professor of Civil and Environmental Engineering
Thesis Supervisor

Accept by.....
Oral Buyukozturk
Chairman, Department of Committee on Graduate Studies

Representation of Water Table Dynamics In a Land Surface Scheme: Observations, Models, and Analyses

by

Pat Jen–Feng Yeh

Submitted to the Department of Civil and Environmental Engineering on September 24, 2002, in partial fulfillment of the requirement for the degree of Doctor of Philosophy in the Field of Hydrology

Abstract

A recent regional-scale water balance analysis has indicated that the groundwater storage and groundwater runoff are significant terms in the monthly and annual water balance for areas with a shallow water table. However, most of the current land surface parameterization schemes lack any representation of regional groundwater aquifers. Such a simplified representation of subsurface hydrological processes would result in significant errors in the predicted land-surface states and fluxes especially for the shallow water table areas in humid regions. This study attempts to address this deficiency. To incorporate the water table dynamics into a land surface scheme LSX, a lumped aquifer model is developed to represent the regional unconfined aquifer as a nonlinear reservoir, in which the aquifer simultaneously receives the recharge from the overlying soils, and discharges runoff into streams. The dependence of groundwater runoff on the water table depth (WTD), i.e., groundwater rating-curve, is parameterized empirically based on the observations in Illinois. The unconfined aquifer model is linked to the soil model in a land surface scheme LSX through the groundwater recharge flux (i.e., soil drainage flux). The total thickness of the unsaturated zone varies in response to the water table fluctuations, thereby interactively couples the aquifer model with the soil model.

The second issue to be addressed in this thesis is the representation of the sub-grid variability of water table depths (WTD) in the coupled model LSXGW. A statistical-dynamical (SD) approach is used to account for the effects of the unresolved sub-grid variability of WTD in the grid-scale groundwater runoff. The probability distribution function (PDF) of WTD is specified as a two-parameter Gamma distribution based on observations. The scale of this PDF is dynamic according to the varying grid-mean WTD at each time step. The shape parameter of the PDF describing the WTD is kept constant. The grid-scale groundwater rating-curve (i.e., aquifer storage-discharge relationship) is derived statistically by integrating a point groundwater runoff model with respect to the PDF of WTD. Next, a mosaic approach is utilized to account for the effects of sub-grid variability of WTD in the grid-scale groundwater recharge. According to the time-varying PDF, a grid-cell is categorized into different sub-grids based on WTD. The fraction describing each sub-grid can be determined from the WTD PDF; hence it varies with time. The grid-scale hydrologic fluxes are computed by averaging all the sub-grid fluxes weighted by their fractions. This new methodology combines the strengths of the SD approach and the mosaic

approach. The developed model has been successfully tested in Illinois for an 11-year period (1984-1994). The results indicate that the simulated hydrologic variables (soil saturation and WTD) and fluxes (evaporation, runoff, and groundwater recharge) agree well with the observations in Illinois. Nevertheless, it is recognized that the excellent performance of LSXGW in the Illinois simulation is significantly attributed to the reliable estimation of the macro-scale groundwater rating-curve. Due to the paucity of the large-scale observations on WTD, the development of a practical parameter estimation procedure is indispensable before the global implementation of the LSXGW in climate models. A procedure using the observed daily streamflow records to calibrate the model parameters is proposed and its applicability is demonstrated in several watersheds in Illinois.

Thesis Supervisor: Eltahir A. B. Eltahir

Title: Associate Professor of Civil and Environmental Engineering

Acknowledgements

First, I would like to express my gratitude and appreciation for the countless ways my advisor Elfatih Eltahir has supported me over the past six years. I am so grateful for his academic support and infinite patience on me. Without his instructions, this work will never be fulfilled. I am grateful to the other three members in my committee: Professor Peter Stone, Professor Charles Harvey, and Dr. Randy Koster. Professor Stone has been exceptionally kind to me in a very supportive and encouraging way. Professor Harvey has provided me many instructions that have benefited my research significantly. I am especially thankful to Dr. Koster, who has spent tremendous time and energy on instructing my research. Thank him for always being there whenever I need his advice.

I want to thank Professor Dennis McLaughlin and Professor Chiang Mei for their support during my first years at MIT when I struggled to survive in a totally unfamiliar environment.

Special thanks go to Guiling Wang and Jingfeng Wang. I am indebted to their encouragement and instruction in both my academic and private life. Many members in the Eltahir research group, Julie Kiang, Michelle Irizarry, Kirsten Findell, Anke Hildebrandt, Yeonjoo Kim, have been the source of countless help, joy and comfort over the past six years.

I would like to thank Sheila Frankel and Cynthia Stewart for taking care of me from the first day I arrived MIT. Also Vicky, Liz, Jim all treat me so well to make me feel like at home. Steve Margulis, who came to the Parsons Lab at the same time with me, is especially supportive and one of my best friends. Many thanks are also due my classmates in Parsons Lab for helping me in many ways: Xin Fu, Yang-hsin Shih, Zhenhua Huang, Enrique Vivoni, Frederic Chagnon, Susan Dunne, Sam Arey, Jean Fitzmaurice, Meng-Yi Chen, Virat Chatdarong, Venessa Teles, Rachel Adams, Giacomo Falorni, Ramahi Sarma-Rupartarm, Yuhua Zhou, Yoshimitsu Tajima, and many others.

Finally and most importantly, I dedicate this PhD work to my parent with love, respect, and appreciation. They are the two persons who love me most and as well whom I love most in the world.

Contents

List of Figures

List of Tables

Chapter 1 Introduction

1.1 The Representation of Water Table Dynamics in Land Surface Schemes

Atmospheric General Circulation Models (GCMs) are widely used for predicting the impacts of natural and anthropogenic perturbations on the Earth's climate. With the increased recognition of the importance of feedback between land surface processes and climate (*Charney et al.* 1977; *Shukla and Mintz,* 1982; *Delworth and Manabe*, 1988), and the interest in evaluation of hydrological and agricultural impacts under the changed climate conditions (*Manabe et al.*, 1981; *Rind et al.*, 1990; *Wetherald and Manabe*, 1995), the development of realistic parameterizations of land surface processes compatible with the scale of a climate model grid cell (~ 50-500 km) has been an area of active research over the last decade (*Dickinson et al.*, 1993; *Sellers et al.*, 1986, *Abramopoulis et al.*, 1988; *Verseghy,* 1991; *Wood et al.,* 1992). Moreover, the impact of land surface process representation on GCM simulations of climate sensitivity to the increasing greenhouse gases has become the focus of much public concern (*Houghton et al.*, 1995).

Land surface parameterization schemes (LSPs) are now an important component of Numerical Weather Prediction models and General Circulation Models. They calculate the water and heat fluxes from land surface to atmosphere and update the surface and subsurface variables affecting these fluxes. The earliest LSP used in climate models was the simple "bucket" model (*Manabe*, 1969). In this model, evaporation was calculated as the product of the potential evaporation and a factor depending on soil moisture, and runoff was assumed to occur whenever the surface water storage exceeds the specified bucket size. Schemes of this type generally assumed a geographically constant value of the bucket size and neglected the impact of vegetation control on the land surface fluxes of water, heat and momentum. Later in the 80's-90's, a new generation of LSPs was proposed (*Sellers et al.,* 1986; *Dickinson et al.*, 1993) to improve the limitations of the "bucket" model. Most of these LSPs were based on the knowledge gained from laboratory experiments or field work at the small scale. These schemes were often

referred to as big-leaf models since they assumed horizontal homogeneity of the land surface characteristics within a grid cell. LSPs usually include considerable vertical resolution and physical realism in the transfer of energy, mass, and momentum. However, the soil hydrology treatment is rather simple and spatial variability is ignored altogether in most LSPs. The common practice is to use a single soil column with 2-10 sub-layers to simulate the surface heat and water fluxes. The use of such simplified "big leaf - single soil column" models is justified in terms of computational efficiency, a lack of information about the detailed distribution of vegetation types, and the lack of appropriate approaches to accommodate spatial heterogeneity at the land surface.

The Biosphere Atmosphere Transfer Scheme (BATS) [*Dickinson et al.*, 1993] and the Simple Biosphere Schemes (SiB) [*Sellers et al.,* 1986] are the most commonly used "big leaf-single soil column" models in global and regional climate studies. Typically, these models solve the energy and water balance equations for only the "single soil column" and for the "big leaf". To characterize the various soil and vegetation properties as well as the hydrological and biogeochemical processes at the Earth's surface, these models require a large number of empirical constants that in practice are difficult to estimate. Moreover, there are still unresolved issues as to whether the use of point or small-scale parameters is valid at the atmospheric model grid scale. Because these point parameters might vary over an atmospheric model grid cell, it is not clear how these small-scale, local parameters could be aggregated to provide the grid-scale "representative" values that could account for the non-linearity of the underlying land-surface processes [*Wood et al.* 1992].

Offline tests such as the PILPS (i.e., the Project for Intercomparison of Land Surface Parameterization Schemes, see http://www.cic.mq.edu.au/pilps-rice/ and the overview by *Henderson-Sellers et al.,* 1995) and the GSWP (The Global Soil Wetness Project, see http://grads.iges.org/gswp/ and the overview by *Dirmeyer et al.,* 1999) have demonstrated that small differences in the model physics among various schemes can lead to a wide spread in the simulation results. Although many model parameterizations responsible for the simulation biases were diagnosed and corrected by the individual modeling group participating the PILPS and

GSWP, it is still unclear how to resolve the differences among schemes, and most importantly, how this spread would be affected by coupling the LSPs to their host climate models.

The current LSPs designed for use in climate models in general do not include the representation of shallow water table. According to the analysis by *Zektser and Loaiciga* [1993], the global averages of baseflow/precipitation ratio and baseflow/streamflow ratio are about 10% and 30%, respectively. Why should the water table dynamics be included in the land surface parameterization schemes (LSPs) used in climate models? Most importantly, since all the LSPs are developed based on the concept of water balance, it is unrealistic to expect that these schemes would reproduce the correct water balance without considering the entire set of significant processes involved in the hydrological cycle. At least for the humid climates, water table usually lies near ground surface and for these areas groundwater runoff (baseflow) is often the dominant streamflow generation mechanism. Under such conditions, the regional climate directly interacts with groundwater through the water fluxes near the water table, namely groundwater recharge and capillary rise (*Levine and Sulvucci*, 1999). Unlike the relatively steady and uniform soil moisture distribution under the deep water table condition, the presence of a shallow water table would significantly alter the vertical soil moisture profile at least in the lower part of the vadose zone. Given that most of the land surface hydrological processes (e.g., infiltration, evapotranspiration, drainage, streamflow, etc.) are highly dependent on soil moisture, the role of shallow water table must be incorporated in any LSPs. Comparing to the deep water table conditions, the presence of a shallow water table results in a decrease of the infiltration and an increase of the evapotranspiration principally due to the downward increase of moisture content. Moreover, field evidence points to the close correlation between plant species and water table depth (*Nichols*, 1993, 1994). The proximity of the capillary fringe to the land surface allows plant root to enter the saturated zone, while the root penetration is constrained by the anaerobic condition of saturated zone (*Miller and Eagleson*, 1982).

Despite its importance, it is not clear why the water table depth, a basic hydrologic variable, has not been a standard component in the LSPs. One possible explanation is that the current generation of LSPs views the soil column as the fundamental hydrologic unit. The large grid scale and thin soil layers (usually 1-5 m) typically considered in LSPs render the groundwater

dynamics a seemingly insignificant hydrologic process in LSPs. It is also possible due to ignorance or simplicity rather than reasonable scale arguments (*Chen et al.*, 1996). From the atmospheric point of view, it might be argued that because water table dynamics only impact evaporation on a small fraction of a GCM grid element so that its significance can be neglected. At least for the regions with a shallow water table, however, such an inaccurate representation of subsurface hydrological processes might result in significant errors in the predicted runoff, and hence affect the accuracy of the predicted evaporation in climate models.

Due to the absence of the groundwater representation, the specification of the lower boundary condition of the soil moisture in the current generation of LSPs is somewhat unrealisitc. The common practice in most LSPs is to apply a gravity drainage condition (i.e., drainage flux equals to the unsaturated conductivity) at the bottom of the lowest layer, or a linear function of gravity drainage condition with an empirical coefficient accounting for other factors than hydraulic conductivity that affect soil drainage such like the topographic slope and amplitude, or the location of bed rocks (see the summary in Table 3 of *Boone and Wetzel,* 1996, p.166). The application of gravity drainage condition implicitly assumes that the vertical soil moisture profile is nearly constant at the bottom of a soil column, thus the upward diffusion flux at the bottom is negligible. However, this assumption is valid only when water table is deep relative to the thickness of the soil column (typically 2-5m in LSPs) so that the unsaturated-saturated zone interactions are insignificant. If water table is shallow, the sharp moisture gradient right above water table would significantly enhance the upward diffusion flux. The outcome is a wetter soil moisture condition in the root-zone resulting in a decreased infiltration and an increased evapotranspiration.

Moreover, for those schemes specifying the lower boundary condition of soil moisture as a linear function of gravity drainage condition, the coefficients (or functions) multiplying the unsaturated hydraulic conductivity (see Table 3 of *Boone and Wetzel,* 1996) have rather ambiguous physical reality. For example, in the SiB model (*Sellers et al.*, 1986) this coefficient is defined as the sine of the slope angle. Apprently, it makes little sense to specify a single slope angle to represent the drainage condition for a model grid with the size as large as Illinois. Moreover, in the BATS model (*Dickinson et al.,* 1993), the drainage at the bottom of the soil

column was assumed empirically as a constant (4×10^{-4} mm/s) independent of soil type multiplied by a nonlinear function of soil saturation, because of "it is difficult to relate the drainage at the bottom of the subsoil layer (at 5-10m) to soil properties at the surface,..." (*Dickinson et al.,* 1993, p.37).

In fact, there exists several land surface models developed with the concept of water table representation. The earliest one is the TOPLATS model (TOPMODEL-basd Land Atmosphere Transfer Scheme) proposed by *Famiglietti and Wood* [1994a, b, c]. In their model, the knowledge on the spatial distribution of the topographic-soil index [*Beven*, 1986] was employed to model the spatial pattern of water table depths, thus coupling the grid elements within a study domain through the groundwater flow (baseflow). The key assumption behind this model is that the groundwater flow between grid elements is controlled by the spatial variability in topographic and soil properties so that the topographic-soil index was used to parameterize this variation. Moreover, in TOPLATS the rate of capillary rise was modeled according to the empirical formula for the steady groundwater flow proposed by *Gardner* [1958], and the baseflow parameterization was based on the analytical expression of *Sivapalan et al.,* [1987]. Following this line are the LSPs developed by *Stieglitz et al.,* [1997], *Koster et al.,* [2000] which are both based on TOPMODEL framework. In these LSPs, the water table position is modeled by invoking the hydrostatic approximation. More detailed discussions on these LSPs with the groundwater concept and the comparisons with our proposed model will be given in Chapter 7.

1.2 The Representation of Land Surface Sub-grid Heterogeneity

The second major issue to be addressed in this thesis is the spatial heterogeneity of land surface properties, also called sub-grid heterogeneity since their length scales are usually smaller than a typical climate model grid scale. A natural land surface usually exhibits considerable heterogeneity in vegetation cover, topography, soil characteristics (e.g., soil texture, hydraulic properties, organic content), and the depth to water table. These land surface characteristics may vary over a wide spectrum of spatial scales. Moreover, climate forcing (e.g., precipitation, radiation, temperature, etc.) may also vary over the unresolved spatial scales of typical atmospheric models. Due to the nonlinear nature of land surface processes, these heterogeneities can significantly affect the exchanges of momentum, water, and energy between the soil, the leaves, and the lower atmosphere. Therefore, a physically sound parameterization used in the climate models should be developed based on the physics known at smaller scales, while incorporating important spatial variability in the land surface properties.

The traditional approach used in BATS and SiB to account for the mixture of surface covers assumes that a single surface cover dominates the entire grid cell. This dominant vegetation type is usually derived by subjective analysis from the available maps or satellite images of land covers. When more than one vegetation coexist within a grid cell, a simple parameter aggregation procedure (usually by averaging arithmetically) is employed with respect to the vegetation characteristics to derive a representative, homogeneous mixture of surface types. Note that the traditional approach does not represent different vegetation types simultaneously within a grid cell. Rather, the characteristics of different vegetation types are lumped together into a single effective value. Traditional approach is conceptually less satisfying, but computationally more efficient than the mosaic approach described later. In the following, the current available approaches in the representation of spatial sub-grid heterogeneity are reviewed, and their major strengths and limitations are summarized.

Statistical-Dynamical (SD) Approach

The statistical-dynamical (SD) approach consists of using probability density functions (PDF) for describing the various parameters in the soil-vegetation-atmosphere system (see *Entekhabi and Eagleson*, 1989; and *Avissar*, 1992). It assumes that land surface characteristics (i.e., vegetation, soil, topography, etc.) or climate forcing (precipitation, temperature, humidity, etc.) vary according to the distributions that can be approximated by continuous analytical PDFs rather than a single representative value. The grid-scale surface fluxes can be calculated using numerical or analytical integration over appropriate PDFs.

Entekhabi and Eagleson [1989] prescribed PDFs to represent the sub-grid variability of soil moisture and precipitation. Based on that, the analytical expressions for the runoff, bare soil evaporation, and transpiration were derived. These hydrologic fluxes are calculated not from the grid-scale soil moisture, but from the PDFs of soil moisture and precipitation. However, their determination of the PDFs was based on heuristic arguments rather than the site-specific information. The variability in topography (i.e., elevation) has no been addressed explicitly in this study. *Famiglietti and Wood* [1990] proposed the use of the TOPMODEL framework to parameterize the spatial variability of soil moisture and the land surface fluxes within a catchment. They used a simple model linking soil moisture to the site-specific soil-topography index developed by *Beven and Kirkby* [1979]. Only the statistics of the soil-topography index are required as the model input. However, their model has not been implemented in a land surface scheme. *Pitman et al.* [1990] used a LSP driven by the GCM-generated climate forcing to investigate the impact of the sub-grid variability of precipitation on the surface water balance. Similar to *Entekhabi and Eagleson* [1989], an idealized PDF of precipitation was specified in their work. *Wood et al.* [1992] present a generalization of the simple bucket model by assigning a statistical distribution of bucket sizes within a grid cell. The Variable Infiltration Capacity (VIC) concept they proposed is defined as the total volumetric capacity of a soil column to hold water. Since the VIC concept is closely related to the saturation excess mechanism, their model is specifically suitable in dealing with the heterogeneity associated with the generation of saturated excess (Dunne-type) runoff, while the treatments in infiltration excess runoff and groundwater runoff (baseflow) are overly simplified.

Avissar [1992] proposed a parameterization based on the SD approach to represent the land surface heterogeneity in numerical atmospheric models. A 25% difference was predicted between the sensible and latent heat fluxes computed with this SD approach and that computed by a "big-leaf " model. *Bonan et al.* [1993] used a LSP to examine the influence of sub-grid variability in leaf area index, stomata resistance, and soil moisture on the surface energy balance, but prescribed periodically a spatially uniform precipitation. *Leung and Gahn* [1995] proposed a sub-grid parameterization of orographic precipitation for the regions with complex topography, by assuming that land surface processes, precipitation, and clouds are all related to the surface elevation. The sub-grid variations of surface elevation are aggregated to a limited number of elevation classes, each assigned with vegetation and surface parameters to compute the area-weighted average fluxes. This study has been extended (*Leung and Gahn*, 1998) to include a sub-grid vegetation scheme based on the statistical relationship between surface elevation and vegetation. *Stieglitz et al.* [1997] investigated specifically the importance of topography on the partitioning of surface water and energy fluxes by developing a sub-grid parameterization of topography. This scheme uses an analytical form of TOPMODEL equations and the statistics of the topography distribution, and then couples with a one-dimensional soil column model to account for the topographic effect.

Mosaic Approach

The mosaic approach assumes that the different vegetation types within a model grid cell separately exchange momentum, energy, and water mass with the atmosphere. The various vegetation types do not interact with each other but interact vertically with the atmosphere directly above them. This method groups all the vegetation of similar types within a grid cell into a "tile" or "patch". The land surface model calculates separate energy balances for each tile using mean grid cell atmospheric forcing and computes the area-weighted grid-average fluxes of heat, moisture, and momentum.

Avissar and Pielke [1989] was the first study to suggest this modeling approach within a meso-scale atmospheric model, while *Koster and Suarez* [1992] was the first study to develop the method and implement it in a GCM. Moreover, *Seth et al.* [1994] presented an approach that explicitly incorporates multiple sub-grid heterogeneities of land surface characteristics. *Giorgi* [1998a, 1998b] proposed a methodology to combine the mosaic and statistical-dynamical approach. A grid cell is divided into fractional areas covered by various surface types. Within each surface type, soil moisture content and surface temperature are assumed to follow continuous analytical PDFs. However, only linear and symmetric PDFs are chosen by the author since their simplicity allows ready analytical integration. Most recently, *Koster et al.*, [2000] developed a catchment-based approach for modeling the land surface processes in GCMs by partitioning continental areas into a mosaic of hydrologic catchments through analysis of surface elevation data. The sub-grid variability of soil moisture was related to topographic characteristics and to bulk soil moisture variables.

Discussion

By using the SD approach, complex soil-vegetation-atmosphere representations may not need to be parameterized explicitly. However, depending on how many variables are represented as probability distributions and how many integration intervals are used, this approach can be computationally expensive. Moreover, to apply the SD approach one has to determine a priori the desired probability density functions of certain land surface variables. However, in practice this task is limited by the difficulty of identifying these distributions. Also, the derived functions may be dependent on the specific PDFs assumed for the relevant land surface characteristics.

Another difficulty in the use of the SD approach is associated with description of the overlying atmospheric forcing (*Seth et al.*, 1994; *Sivapalan and Woods*, 1995). Since GCM only provides the grid-scale average precipitation, the exact location of precipitation is unknown. Although the use of a wetting fraction in current LSPs can nominally account for the sub-grid variability of precipitation (*Warrilow et al.*, 1986; *Shuttleworth*, 1988); however, the wetting fraction concept is unable to carry any information on the spatial pattern of precipitation from

time step to time step. Because only the grid-mean values of soil moisture or canopy storage are updated for each time step, the detailed information within each sub-gird region from the previous time step is lost. As a result, the persistence and amplification of the hydroclimatic anomalies within sub-grids cannot be reflected in the SD approach.

The problem discussed above can be avoided by using the mosaic approach. Since unique energy and water budgets are maintained for each sub-grid tile in the mosaic approach, there is no loss of memory from one step to the next and the evolution of prognostics in each sub-grid can be traced with consistency. However, given that the typical scale of hydrologic processes is at the order of less than 100 meters, significantly more detailed than that can be achieved by grid subdivision, the problem of parameter aggregation still exists, but just simply transferred to another scale (*Johnson et al.,* 1992). Moreover, recall that in this approach various sub-grids do not interact with each other, which means the horizontal cross-grid water transport is actually neglected. This transport may become more important as the grid subdivision become finer and finer such that a sub-grid might not be a closed hydrologic unit. Finally, the mosaic approach not only shares the same computational constraint as the SD approach, but it requires a larger amount of data than the SD approach does. Therefore, depending on the degree of grid subdivision the mosaic approach sometimes might be computationally too expensive for the use in operational climate models.

1.3 Research Objectives

A recent analysis of the regional hydroclimatology in Illinois (*Yeh et al.*, 1998) has shown that groundwater storage and groundwater runoff are significant terms in the monthly and annual water balance for areas with a shallow water table (see section 2.3). In Illinois, the state-average seasonal cycle of water table depth ranges between 2 to 4 meters below the surface. The monthly changes in saturated (groundwater) storage and unsaturated (soil moisture) storage are equally significant in shaping the seasonal hydrologic cycles. The monthly regional water balance in Illinois could not be closed without the consideration of the changes in groundwater storage. Moreover, the annual change in groundwater storage does not always integrate to zero especially during the drought and flood years. Therefore, the incorporation of a groundwater representation is indispensable for applying LSPs to the shallow water table regions such as Illinois.

This research aims to improve the ability of a land surface scheme to model the land surface hydrology at the large scale compatible to the grid size of General Circulation Models or weather forecast models. The ultimate goal is to improve the quality of climate model simulations by developing a state-of-the-art land surface scheme that can better simulate water and energy balance near the land surface. This goal has important implications regarding the evaluation of the impact on regional water resources due to climate change. It has been recognized (*Rind et al.*, 1990; *Wetherald and Manabe*, 1995) that the credibility of the climate model predictions is rather limited because of the inaccuracies in the parameterizations of land surface processes. Specifically, most of the current land surface schemes lack any representation of regional groundwater aquifers. Soil moisture is the sole state variable that exerts influences on the land-surface hydrological fluxes. Such a simplified representation of subsurface hydrology would result in significant errors in the predicted land-surface states and fluxes especially for the shallow water table areas. This study attempts to address this deficiency. In addition, the second central issue to be addressed in this thesis is the representation of the land-surface heterogeneity. Due to the nonlinear nature of surface and subsurface hydrological processes as well as the large scale of climate model applications, the spatial variability of atmospheric forcing (primarily precipitation) and land-surface properties would exert significant impacts on the large-scale water, heat and

momentum fluxes. Therefore, the sub-grid heterogeneity issue should be dealt with for any land surface schemes to be applied at the large scale. Above all, only by formulating the individual land surface physical components to be as realistic as possible can we expect to make progress in the prediction of the impact caused by climate change. This reasoning hence calls for the most realistic representations to be incorporated into the modeling process, which is the main objective to be achieved in this thesis.

One of the crucial requirements for the development of macro-scale land surface models is the availability of the spatially distributed data on various land surface properties necessary for the model input. Model validation also requires long-term observations on relevant hydrologic states and fluxes. Although several large-scale field campaigns held in the past decade (e.g., FIFE, HAPEX-MOBILHY, HAPEX–Sahel, BOREAS) have aimed at the development and the testing of parameterizations in LSPs, the spatial scales of these field campaigns are still relatively small in comparison with the scale typical of a climate model grid-cell. In addition, the simulation periods during these field campaigns as well as during various phases of the PILPS (*Henderson-Sellers et al.,* 1995) are within one year (except the more recent PILPS phase 2c experiment at the Arkansas-Red River Basin, phase 2d experiment at Vaidai in Russia, and phase 2e in Torne-Kalix Basin in Sweden). For the experiments with a simulation period less than 1-year, the LSPs are run until the equilibrium conditions are reached. This leads to two significant problems. First, the LSPs' ability to simulate inter-annual variability cannot be evaluated from the 1-year simulation. Second, the equilibrium-year assumption does not usually hold in reality, especially when groundwater is an important component of land surface water balance. In Illinois, there are long-term (more than 10 years) hydrometeorological data including precipitation measurements from more than 150 gauges, air temperature and humidity observations from NCDC (National climate Data Center) climate stations, bi-weekly soil moisture measurements using neutron probe from 19 sites, monthly shallow groundwater observations from 16 monitoring wells, and a dense streamflow observational network maintained by USGS. These comprehensive hydrometeorological data in Illinois collectively provide a unique opportunity to test LSPs on a multi-year basis at a scale (i.e., $\cong 10^5 km^2$) close to the size of a climate model grid.

This thesis is organized into 7 chapters. The next chapter presents the regional-scale water balance study in Illinois. Using a 12-year comprehensive hydrometeorological dataset, the unmeasured evaporation flux can be estimated from both the surface/subsurface and the atmospheric water balance computations whereby the regional-scale water balance in Illinois is closed. Chapter 3 discusses the statistical analysis of the relationships between the water balance components in Illinois with the objective of identifying the important role that shallow aquifers play in the regional-scale hydroclimatology in Illinois. In Chapter 4, the deficiencies caused by neglecting the groundwater representation in a LSP is demonstrated by applying a traditional land surface scheme (LSX) to the Illinois where the average water table depth is rather shallow. A lumped groundwater model that describes processes over large areas is then developed and interactively coupled to the LSX. The coupled land surface scheme (LSXGW) is tested in Illinois against the observational data from 1983-1994. The significant issue of sub-grid variability is addressed in Chapter 5. A new methodology combining the strength of the statistical-dynamical approach and the mosaic approach is proposed to incorporate the effects of the sub-grid variability of water table depth in the LSXGW. The LSXGW is again tested in Illinois to show the advantages of the scheme proposed to account for sub-grid variability. In Chapter 6, the problem of global applicability of the LSXGW is considered. A parameter calibration approach based on the comparison of the LSXGW simulations and the observed streamflow is proposed as a practical solution to estimate the groundwater parameters in LSXGW. The application of this approach to several watersheds in Illinois is summarized. This is followed by the summary of the conclusions and the future research directions in Chapter 7.

Chapter 2 The Regional-scale Water Balance in Illinois

2.1 Water Balance Computations

Hydrology is the science of the water cycle within the global domain including the land surface, the atmosphere, and the ocean. This cycle encompasses a wide spectrum of hydrological processes including precipitation, evaporation, runoff, snowfall, water vapor transport, and so on. These processes take place at a hierarchy of spatial scales: point scale, hillslope scale, watershed scale, regional scale, and continental scale. However, most of the past hydrologic research dealt with the phenomena occurring in the land surface branch of hydrology at the spatial scales comparable to or smaller than the size of a typical watershed (<10,000 km^2).

In recent years there has been increasing interest in the role of the water cycle in the climate system at large spatial scales. This interest has been motivated by the need to assess the impact on the water cycle due to the evident change in the chemical composition of the Earth atmosphere, and the observed change in the natural global land cover. To deal with these two environmental issues, it requires a solid understanding of hydrological phenomena occurring at large spatial scales and includes the land, the atmosphere, and the ocean.

In this chapter, we will study the regional-scale hydrological cycle in Illinois, including both the land and atmospheric branches of hydrology. The hydrological cycle of North America (including Illinois) has been the subject of several past large-scale water balance studies: *Benton et al.* [1950], *Benton and Estoque* [1954], *Rasmusson* [1967, 1968, 1971], among others. These studies used the atmospheric water balance computations to estimate the evaporation and runoff fluxes at the continental scale. On the other hand, several small-scale studies were performed on the hydroclimatology of small watersheds in Illinois, mostly by scientists from the Illinois State Water Survey (ISWS) [e.g., *Schicht and Walton*, 1961; *Walton*, 1964]. In this chapter, we study the regional-scale hydroclimatology in Illinois by using a dataset on most of the hydrological variables, i.e., precipitation, streamflow, soil water content, snow depth, groundwater level, and

atmospheric flux of water vapor. The water balance approach is employed to estimate those components in the hydrological cycle (e.g., evaporation, groundwater recharge, surface runoff, etc.) whose direct observations are usually not available. The unique availability of a comprehensive dataset covering the large area of Illinois facilitates such a large-scale water balance study. In the following, we start by introducing the theories of two water balance approaches that will be used in this study: the surface/subsurface water balance (SWB) and the atmospheric water balance (AWB).

Surface/Subsurface Water Balance (SWB)

The large-scale water balance equation for the unsaturated soils can be written as follows:

$$\overline{nD}\frac{\partial \bar{s}}{\partial t} = \overline{P} - \overline{E} - \overline{R_S} - \overline{P_G} \tag{2.1}$$

where $\overline{nD}$ [mm] is the available storage depth of the soil: the product of soil porosity and root zone depth. (Throughout this chapter the overbar denotes the regional scale spatially average value.). $\bar{s}$ [%] is the soil relative saturation (i.e. soil moisture content divided by soil porosity), $\overline{P}$ [mm/mo.] is the precipitation, $\overline{E}$ [mm/mo.] is the evaporation, $\overline{R_S}$ [mm/mo.] is the surface runoff and $\overline{P_G}$ [mm/mo.] is the downward percolation flux into the groundwater aquifer (i.e. groundwater recharge). Illinois has a rather uniform terrain with the local relief in most counties less than 200 feet [*Leighton et al.* 1948], hence the interflow is not a significant mechanism of runoff generation.

The water balance equation for the unconfined aquifer can be described as

$$\overline{S_y}\frac{\partial \overline{H}}{\partial t} = \overline{P_G} - \overline{R_G} \tag{2.2}$$

where $\overline{S_y}$ [%] is the specific yield, $\overline{H}$ [mm] is the groundwater level and $\overline{R_G}$ [mm/mo.] is the groundwater discharge. $\overline{S_y}$ is the fraction of water volume that can be drained by gravity in an unconfined aquifer [*Domenico* and *Schwartz*, 1990].

The regional-scale evaporation can be estimated from the soil moisture water balance equation if all the other terms in (2.1) are known. However, the measurements of groundwater recharge ($\overline{P_G}$) and surface runoff ($\overline{R_S}$) are rarely available especially at the large scale. Although hydrograph separation can be employed to separate streamflow into surface runoff component and groundwater runoff component, its application is an unresolved issue still under extensive debate in hydrology [*Gutpa and Furey*, 2001].

However, this difficulty can be avoided by adding (2.1) and (2.2) together

$$\overline{nD}\frac{\partial \bar{s}}{\partial t}+\overline{S_y}\frac{\partial \overline{H}}{\partial t}=\overline{P}-\overline{E}-\overline{R} \tag{2.3}$$

where $\overline{R}=\overline{R_S}+\overline{R_G}$ [mm/mo.] is the total (measured) runoff. This equation describes the surface/subsurface water balance in a drainage basin or a physiographic unit where there is no water movement between the adjacent units. From (2.3), regional evaporation $\overline{E}$ can be estimated which facilitates the surface/subsurface water balance computations by avoiding the necessity of hydrograph separation and the estimation of groundwater recharge.

For regions where the snow accumulation and ablation are important hydrological quantities, the combination of unsaturated and saturated water balances in (2.1) and (2.2) into (2.3) are not sufficient to accurately describe water balance. The snow accumulation and ablation can be incorporated into water balance computations by adding another equation representing the surface water storage as follows:

$$\frac{\partial \overline{W_S}}{\partial t} = \overline{P} - \overline{I} - \overline{V_S} - \overline{V_M} \tag{2.4}$$

where $\overline{W_S}$ [mm] is the accumulated depth of snowpack (liquid equivalent), $\overline{I}$ [mm/mo.] is infiltration rate, $\overline{V_S}$ [mm/mo.] is the sublimation rate, and $\overline{V_M}$ [mm/mo.] is snow melting rate. Under such a condition, (2.1) should be modified into the following:

$$\overline{nD}\frac{\partial \overline{s}}{\partial t} = \overline{I} + \overline{V_M} - \overline{E} - \overline{R_S} - \overline{P_G} \tag{2.5}$$

Therefore, the equations for the water balance of the surface and the subsurface can be combined (by adding equations 2.2, 2.4, and 2.5) and rearranging to result in

$$\overline{E} + \overline{V_S} = \overline{P} - (\overline{R} + \overline{nD}\frac{\partial \overline{s}}{\partial t} + \overline{S_y}\frac{\partial \overline{H}}{\partial t} + \frac{\partial \overline{W_S}}{\partial t}) \tag{2.6}$$

where the left hand side denotes the combination of the rates of evaporation and snow sublimation.

Atmospheric Water Balance (AWB)

The atmospheric water balance equation can be written as [*Peixoto and Oort*, 1992]:

$$\frac{\partial \overline{W_a}}{\partial t} = \overline{E} - \overline{P} + \overline{C} \tag{2.7}$$

where $\overline{W_a}$ is the mean precipitable water (or water vapor storage) within the atmospheric column, $\overline{C}(=-\nabla \cdot \overline{Q})$ is the mean convergence of lateral atmospheric vapor flux. $\overline{Q}$ is the vertically integrated mean total water vapor flux. $\overline{W_a}$ and $\overline{Q}$ can be calculated by integrating the

profiles of specific humidity q, zonal and meridional wind components, u and v, from the pressure at the ground surface p_s to that above which water vapor content becomes negligible p_u (i.e., $p_u = 300mb$ in this study) as follows: [*Rasmusson*, 1967, 1968; *Peixoto and Oort*, 1992]

$$\overline{W_a} = \frac{1}{g}\int_{p_u}^{p_s}\overline{q}dp \qquad \overline{Q_\lambda} = \frac{1}{g}\int_{p_u}^{p_s}\overline{qu}dp \qquad \overline{Q_\phi} = \frac{1}{g}\int_{p_u}^{p_s}\overline{qv}dp \tag{2.8}$$

where g is the acceleration of gravity, λ and ϕ represent the longitude and latitude, respectively. The most convenient way of calculating the mean atmospheric vapor flux convergence $\overline{C}$ is through the application of the Gauss Theorem:

$$\nabla \cdot \overline{Q} = \frac{1}{A}\oint_S \overline{Q} \cdot nds \tag{2.9}$$

where A is the corresponding area over which the convergence is being calculated. Hence $\overline{C}$ can be calculated by taking the line integral of the water vapor flux around the area under study.

By using the aerological data to calculate the convergence $\overline{C}$ and change in atmospheric water vapor storage with respect to time $\partial\overline{W_a}/\partial t$, (2.7) can be solved for the unknown regional evaporation:

$$\overline{E} = \overline{P} - \overline{C} + \frac{\partial \overline{W_a}}{\partial t} \tag{2.10}$$

The mean precipitable water, and mean zonal and meridional water vapor fluxes are calculated at each grid points by integrating vertically with respect to pressure using the trapezoidal method. Once these vertically integrated fluxes are determined, the convergence can be calculated for a given area by (2.9). The approach used here was essentially identical to that used by *Rasmusson* [1968, 1971].

By averaging (2.3) and (2.10) over long time series, all the derivative terms can be assumed negligible. Thus, by equating the two estimates of long-term evaporation, we derive

$$\overline{R} = \overline{C} = -\nabla \cdot \overline{Q} \tag{2.11}$$

which is an expression of the fact that, for any climate equilibrium, the long term convergence of atmospheric moisture towards any hydrologic unit has to be balanced by the long term net discharge of water out of the same hydrologic unit. Therefore, (2.11) can be conceived as a criterion for evaluating the agreement between the atmospheric and hydrological datasets.

In the next section, a comprehensive hydrological dataset of Illinois from 1983-1994 that will be used in this study will be described. By using this dataset, the unmeasured regional-scale evaporation in Illinois is estimated in Section 2.3 by applying the two water balance approaches introduced in the above, thus completes the quantitative descriptions of the regional hydrological cycle in Illinois. The 12-year (1983-1994) average climatology of the regional-scale hydrological cycle in Illinois is summarized in Section 2.4.

2.2 Data Summary

The Illinois dataset used in this study consists of the following hydroclimatic variables: atmospheric specific humidity, wind velocity, precipitation, streamflow, snow depth, soil moisture content, and water table depth to the ground surface. The locations of all various measurement stations are shown in Figure 2.1. A brief summary of the data used in this study is given in Table 2.1.

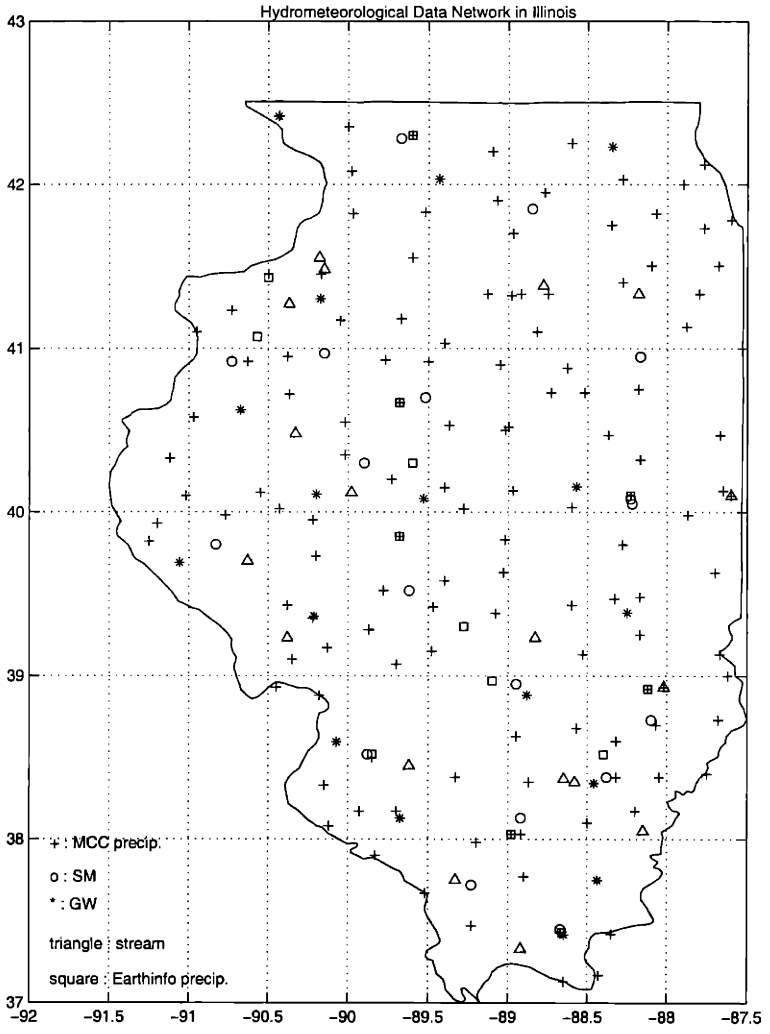

Figure 2.1 The locations of the measurement stations of the hydrometeorological variables in Illinois. The area of the study region is about 240,000 km^2.

Data	Number of Stations	Resolution	Sources
Precipitation	129	Daily	MCC
	52	Hourly	EarthInfo. Inc.
Wind/Humidity	9 grids (global $2.5^{\circ} \times 2.5^{\circ}$	6 hours	NCEP/NCAR
Snow	129	daily	MCC
Soil Moisture	16	1-4 times/month	ISWS
Groundwater depth	15	monthly	ISWS
Streamflow	3	daily	USGS

MCC, Midwest Climate Center; ISWS, Illinois State Water Survey; NCEP, National Center for Environmental Prediction; and NCAR, National Center for Atmospheric Research.

Table 2.1. A Summary of the Data Sets in Illinois Used in the Chapters 2 and 3

The data on specific humidity and wind speed is a subset of the National Center for Environmental Prediction/National Center for Atmospheric Research (NCEP/NCAR) global reanalysis data [*Kalnay et al.* 1996]. This dataset has daily and six-hourly temporal resolutions, and a $2.5^{\circ} \times 2.5^{\circ}$ horizontal resolution. It includes the mean specific humidity at eight pressure levels, and wind velocity at seventeen pressure levels in the atmosphere. In this study, we use data of six-hourly resolution at the following eight pressure levels: 1000, 925, 850, 700, 600, 500, 400, 300 mb. Above 300 mb, the atmospheric water vapor content is negligible. The NCEP/NCAR global reanalysis data have been used by *Higgins et al.* [1996] and *Gutowski et al.* [1997] to evaluate the moisture budget in the Central United States.

The data on precipitation has been supplied by two sources: Midwest Climate Center (MCC) [*Kunkel et al.,* 1990] and EarthInfo. Inc. The MCC dataset consists of daily precipitation at 129 NWS cooperative observe weather stations within Illinois. The EarthInfo dataset consists of hourly precipitation at 52 stations within the same areas. Area-average precipitation observations from 181 stations were used in this water balance study.

The snow data were also provided by MCC. The 129 rainfall stations of MCC reported daily records of snowfall as well. The snow data included both records of the snowfall and snow depth.

The daily streamflow records collected by the U.S. Geological Survey (USGS) were used in this water balance study. Daily discharge measurements at 3 hydrological stations were used in this study: Illinois River at Valley city, which drains about 69,237 km^2; Rock River near Joslin, which drains about 24,721 km^2; and Kaskaskia River near Venedy Station, which drains about 11,373 km^2. These 3 streamflow-gauging stations were selected as downstream as possible with the largest drainage areas along the 3 major rivers in Illinois. The station at Valley City represents the outflow from the total Illinois River Basin, consisting of the Upper and Lower Illinois River basins which encompass 28032 km^2 and 45978 km^2 of central and western Illinois, respectively. Rock and Kaskaskia River basins represent northern and southern Illinois, respectively. Their integrated monthly discharges were weighted by drainage areas to give an estimate of average streamflow in Illinois. The total drainage area of these 3 rivers exceeds two thirds of the total area of Illinois.

The data on soil moisture was collected by the Illinois State Water Survey (ISWS). Since 1981, ISWS has been collecting measurements on the soil moisture content at 8 grass-covered sites around Illinois using the neutron probe technology. Seven additional sites were added in 1982, two more in 1986, and by 1992 the total increased to 19. Sixteen of these 19 sites cover the period 1983 to 1994, and hence will be used in this study. Biweekly (March through October) and monthly (November through February) measurements of soil wetness were taken at 11 different soil layers with a resolution of about 20 centimeters down to 2 meters below the surface. The data on soil porosity, field capacity, and permanent wilting point were also provided in this dataset which enables us to estimate the water-holding capacity of soil layers. The details about this extensive soil moisture dataset has been published elsewhere [*Hollinger and Isard*, 1994]. *Findell and Eltahir* [1997] used this dataset to investigate the soil moisture-rainfall feedback mechanism in Illinois.

The dataset on the depth to water table was provided by the Groundwater Division of ISWS, which consists of monthly measurements of shallow groundwater level at 18 wells scattered throughout the state of Illinois from the 1960s till now. These 18 wells are located far away from pumping centers and streams. All of these 18 wells are under unconfined conditions where the average water table levels range between 1 to 10 meters below the surface. 15 wells with

complete records from 1983 to 1994 were used in this study to represent the regional groundwater system in Illinois. This dataset has been used to investigate the 1980-81 drought in Southern Illinois by *Changnon et al.* [1982] and the statistical relationships between precipitation and groundwater level in Illinois by *Changnon et al.* [1988].

The 12-year (1983-1994) time series describing the spatial averages of monthly atmospheric moisture convergence, precipitation, soil moisture content, groundwater level, and river flow in Illinois are presented in Figure 2.2. These data will be used in this chapter to study various aspects of the regional hydrological cycle in Illinois.

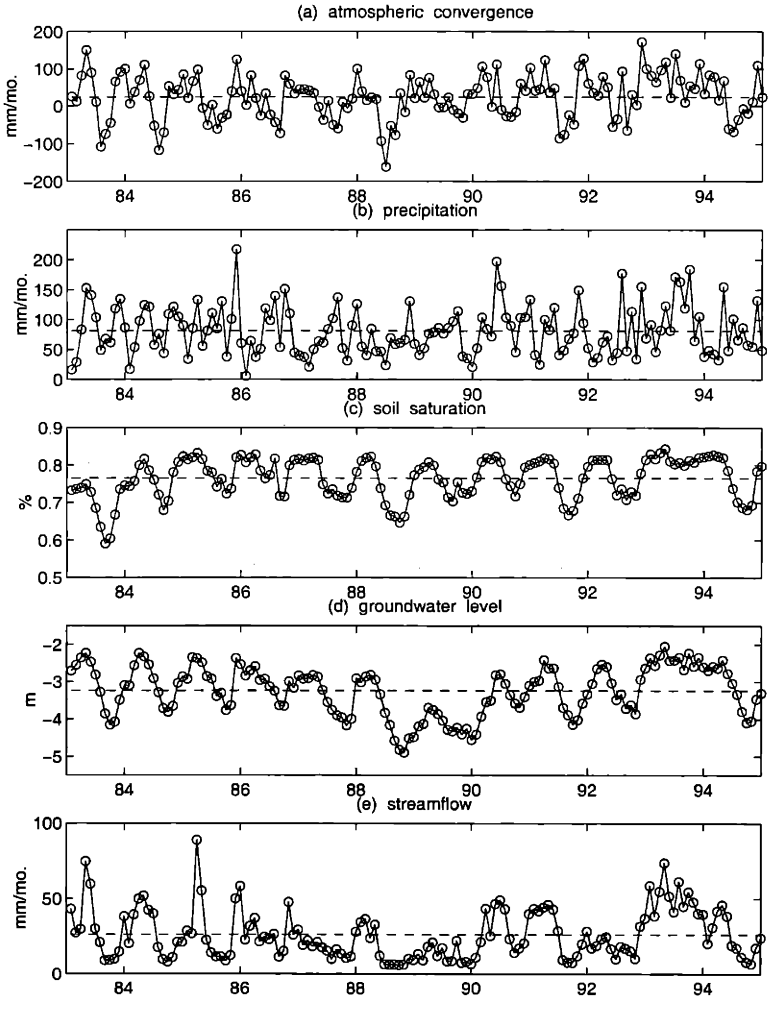

Figure 2.2 12-year (1983-1994) time series of (a) atmospheric water vapor convergence (b) precipitation (c) soil relative saturation (d) groundwater level (e) streamflow in Illinois. The dashed lines shown in the figure denote the long-term average from 1983 to 1994.

2.3 Estimation of the Regional-scale Evaporation

The atmospheric water balance (AWB) has been applied by several previous studies to estimate evaporation for large areas [*Benton et al.* 1950; *Rasmusson*, 1967, 1968, 1971]. However, the surface/subsurface water balance (SWB) has not been applied at a large scale about the size of Illinois ($\approx 2.5\times10^5\ km^2$). In this section, we utilize the extensive hydrological dataset in Illinois to estimate the regional-scale evaporation in Illinois at the monthly timescale from 1983-1994 using the SWB (equation 2.3) and the AWB (equation 2.10) computations. Thus, we will be able to compare the two estimates of regional evaporation in Illinois.

2.3.1 Introduction

Evaporation refers to the part of precipitation converted into water vapor and subsequently transported into the atmosphere [*Shuttleworth,* 1979; *Brutsaert,* 1982]. Evaporation together with precipitation govern the amount of runoff available to the planning and management of water resources, hence accurate knowledge of evaporation is required in the design of water resources systems such as storage reservoirs, agricultural irrigation schemes, municipal and industrial water supply systems, etc. In addition, evaporation links the land and atmospheric branches of the hydrological cycle by dictating exchanges of heat and moisture between the atmosphere and the land surface, thus exerting a strong influence on the patterns of atmospheric water vapor transport that are essential in shaping our climate. Evidence from General Circulation Model (GCM) experiments has suggested that the Earth's climate is sensitive to variations in regional evaporation [*Shukla and Mintz*, 1982; *Delworth and Manabe*, 1988], hence it is important for climate change studies to model evaporation accurately. However, since evaporation is difficult to estimate at a regional scale, GCM studies have used parameterizations of evaporation that are difficult to validate due to the lack of data at a compatible scale.

Traditionally, point measurements of evaporation can be performed with lysimeters [*Pruitt and Angus*, 1960] or evaporation pans [*Gangopadhyaya et al.*, 1966]. While such ground-based measurements of evaporation could be expensive and laborious, they become especially

impractical when regional scale coverage is of interest. Estimation of regional scale evaporation still relies on modeling techniques. Perhaps the most conceptually simple tool for modeling regional evaporation is through classical water balance computation. *Thronwaite* [1948] and *Penman* [1950] pioneered studies of land surface water balance for small catchments. *Baumgartner and Reichel* [1975] studied the world water balance and developed global maps for the distributions of precipitation, evaporation and runoff. These and other water balance computations have been discussed by *Street-Perrott et al.* [1983] and *Van der Beken and Herrmann* [1985]. Although numerous previous studies have attempted to estimate land-surface water balances [e.g. *McGowan and Williams*, 1980; *Ernstberger and Sokolleck*, 1983; *Alley,* 1984; *Kattelmann and Elder*, 1991; *Vandewiele et al.*, 1992, *Lesack*, 1993; *Xu and Halldin,* 1996; *Roberts and Harding*, 1996; *Malek et al.*, 1997; among others], most of these studies have focused on watersheds with the scale from $10^1 km^2$ to $10^3 km^2$. Primarily due to the paucity of data with adequate resolution and enough length, classical land surface water balance has seldom been applied to the estimation of evaporation at a regional scale ($10^4 km^2 - 10^6 km^2$).

As an alternative, numerous studies have attempted to estimate large-scale evaporation from the relatively abundant aerological data, utilizing either the atmospheric water balance concept or the similarity theory of planetary boundary layer properties. *Benton et al.* [1950] and *Benton and Estoque* [1954] pioneered studies of large-scale atmospheric water balance. *Benton et al.* [1950] focused on the water balance of the Mississippi Basin, considering both the atmospheric and the land surface branches of the hydrological cycle. *Benton and Estoque* [1954] studied the transfer of water vapor over the North American continent and estimated a water balance for this region. This approach was followed by *Rasmusson* [1967,1968,1971], who estimated the continental scale water balance for the region of North America using both the atmospheric and the terrestrial control volumes. Monthly values of evapotranspiration and change in storage of soil moisture were estimated based on observed values of atmospheric water vapor divergence, precipitation, and streamflow. *Rasmusson* [1977] reviewed the studies on the atmospheric water vapor transport, recommending the general application of vapor flux data in the routine computation of regional water balances, and the subsequent development of monthly, seasonal and long-term regional water balance climatologies. In addition, the atmospheric water balance approach has been applied at continental or global scale by *Starr and Peixoto* [1958], *Rosen and*

Omolayo [1981], *Peixoto et al.* [1982], *Peixoto and Oort* [1983], *Salstein et al.* [1983], *Bryan and Oort* [1984], *Savijarvi* [1988], *Brubaker et al.* [1994], *Roads et al.* [1994], *Oki et al.* [1995], *Higgins et al.* [1996], *Mo and Higgins* [1996], *Gutowski et al.* [1997] and *Ropelewski and Yarosh* [1998], among others. A complete introduction on the theoretical basis of the atmospheric water balance computations was given by *Peixoto and Oort* [1992, Chapter 12]. On the other hand, in recent years there has been interest in estimation of evaporation from large areas using the planetary boundary layer measurements [e.g. *Mawdsley and Brustaret,* 1979; *Abdulmumin et al.,* 1987; *Munley and Hipps,* 1991; *Sugita and Brutsaert*, 1991]. For a detailed discussion on the estimation of evaporation using these techniques, see the review by *Parlange et al.* [1995].

Apparently, there is an inconsistency in the scale to which the surface/subsurface water balance (SWB) approach and the atmospheric water balance (AWB) approach have been applied. Although the AWB approach has been employed since *Benton et al.* [1950], it has never been validated through a comparison of regional evaporation estimates from direct measurements or other independent studies, for example, regional scale water balance computed from the terrestrial branch of hydrology. To our knowledge, the only efforts made in this direction are those of *Abdulla et al.* [1996], *Berbery et al.* [1996], and more recently in PILPS 2c experiment (see *Liang et al.*, 1998). *Abdulla et al.* [1996] found a favorable agreement between the evaporation estimates based on a land-surface parameterization scheme VIC-2L [*Liang et al.,* 1994] and the estimates based on the AWB. *Berbery et al.* [1996] applied the National Center for Environmental Prediction's Eta model to study the seasonal variability of atmospheric branch of hydrological cycle in continental North America. Evaporation estimates obtained from the AWB approach were compared to the estimates produced from the Eta model. Still, the scarcity of data from ground truth measurements (especially soil moisture measurements) has limited the validation of the AWB approach using direct observations. Moreover, *Liang et al.* [1998] derived monthly evaporation estimates from 1980-1986 in the Red-Arkansas River basin using the radiosonde-based atmospheric water balance method in order to evaluate the evaporation simulations from 16 land surface models participating the PILPS 2c experiment. The error in their basin-average annual evaporation is found to be within 5%.

The soil moisture data collected in Illinois since 1981 [*Hollinger and Israd*, 1994], when used in conjunction with other available datasets (i.e., precipitation, snowfall, groundwater level, and streamflow), provide a unique opportunity to estimate regional evaporation in Illinois using the SWB approach. More importantly, these estimates can be compared to those obtained from the AWB approach. Annual evapotranspiration has been estimated by Illinois State Water Survey: *Jones* [1966, p.12] estimated the annual average evapotranspiration varying from 25 inches in northern Illinois to 30 inches in southern Illinois, based on the average precipitation and the average runoff from 43 stream gauging stations in Illinois. However, this paper focuses on estimation of monthly evaporation in Illinois from 1983 to 1994 over a regional scale ($\approx 2\times10^5$ km^2). The objective here is to investigate the validity of the AWB approach by comparing its evaporation estimates to those obtained by the SWB approach at a regional scale. Since the scale of interest in this study is comparable to the typical size of a GCM grid cell ($\approx 100\times100$ km^2 to $\approx 500\times500$ km^2), it is believed that if the two independent approaches yield similar estimates of regional evaporation, then future applications of the AWB approach to compute regional evaporation can aid in the validation of current land-surface schemes used in climate models.

The total area examined in this study is shown in Figure 2.3. The entire study area encompasses four grid cells with a size of $2.5^\circ\times2.5^\circ$ ($87.5^\circ W - 92.5^\circ W$, $37.5^\circ N - 42.5^\circ N$) which covers an area of approximately 240,000 Km^2. As shown in Figure 2.3, almost all of Illinois, except for the southern tip of the state, is covered by the study region along with some portions of surrounding states. The study region was chosen in an effort to strike a balance between using a larger area, which would provide more accurate atmospheric water vapor flux convergence estimates, and limiting the region to Illinois and its immediate area, so that the evaporation estimates from the AWB approach could be compared to those calculated from the SWB approach. *Rasmusson* [1968, 1971] demonstrated how using smaller areas decreases the accuracy of the estimates of water vapor flux convergence. He also argued that the small-scale spatial variations of atmospheric water vapor convergence are significant and can contribute additional inaccuracy when performing a water balance over smaller regions using spatially limited data. Specifically, *Rasmusson* [1968] indicated that the AWB approach is applicable for regions with area larger than 2×10^6 Km^2. The application over smaller areas is less reliable

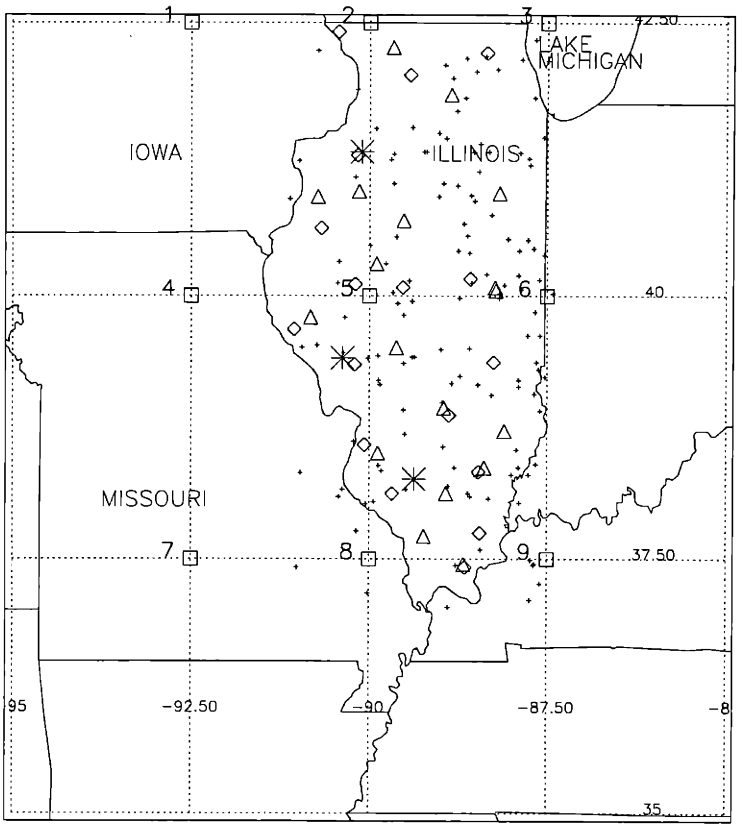

Figure 2.3 The total area examined in the Illinois water balance study: four grid cells with a size of $2.5^{\circ} \times 2.5^{\circ}$ ($87.5^{\circ}W - 92.5^{\circ}W$, $37.5^{\circ}N - 42.5^{\circ}N$).

especially when the size of the area is reduced to less than 10^5 Km^2 [*Rasmusson*, 1971]. This lower limit of scale, for the AWB approach to be possibly valid, corresponds to the scale of interest in this study. If the AWB approach can be shown at this scale (i.e., $10^5 - 10^6$ Km^2) to estimate the regional scale evaporation accurately, then those estimates have the potential for providing "observations" for the validation of GCM simulations.

The theories of two water balance computations, SWB and AWB, have been introduced in Section 2.1. Results and comparisons of the evaporation estimates made using these two approaches are presented in Sections 2.3.2 and 2.3.3, respectively. In Section 2.3.4, the sensitivity of the regional evaporation estimates from the AWB computations to the domain size is investigated. The sensitivity of specified parameters to the evaporation estimates from the SWB is also presented in this section. A short summary is given in Section 2.3.5.

2.3.2 Estimation of Evaporation Using Surface/subsurface water balance (SWB) and Atmospheric Water Balance (AWB)

Equations (2.3) and (2.10) constitute the basis of the mass balance methods for the estimation of regional evaporation [*Brutsaert*, 1982]. These two equations are valid for all scales. However, the accuracy by which each of the terms on the right hand sides of (2.3) and (2.10) can be evaluated varies depending on the spatial and temporal resolutions of the data used. Particularly, it should be noted that precipitation measurements from rain gauges tend to have a systematic negative bias, in that they underestimate the actual precipitation occurring over an area due to the local wind effects around the gauge. This can be especially pronounced during the winter months when snow occurs because the snowflakes are much more prone to wind deflection than raindrops. According to *Larson and Peck* [1974], rain gauges can underestimate rainfall up to 20% for a wind of 20 mph. For snowfall this value is likely go up by at least another 10%. *Groisman and Legates* [1994] estimated the average gauge undercatch bias of precipitation measurements is 9% of the annual precipitation for the continental United States, with a seasonal maximum of 15% in winter and a minimum of 5% in summer. The negative bias of precipitation measurement may result in the underestimation of evaporation, especially during the winter. However, inspection of (2.3) and (2.10) reveals that the bias affects both evaporation estimates from the SWB and AWB to an equal extent.

Figure 2.4 illustrates the 12-year (1983-1994) average seasonal variability of snow accumulation depth ($\overline{W_S}$), soil saturation ($\bar{s}$), and groundwater level ($\overline{H}$) in Illinois. These hydrological quantities correspond to the water storage in three distinct reservoirs: unsaturated soil reservoir, aquifer reservoir, and surface reservoir. For the two subsurface reservoirs, a similarity in the seasonal cycle is clearly demonstrated in Figure 2.4 with a peak of surface water storage occurring in March and a trough in August or September. The snow depth shown in Figure 2.4 is the 129-station average snow accumulation depth on the last day of each month. Figure 2.5 shows the average days within a month when there are snow accumulations, and the seasonal cycle of snowfall in Illinois. The snow data shown in Figures 2.4 and 2.5 have been converted into the water equivalent by multiplying by 0.1. The long-term (1983-1994) average

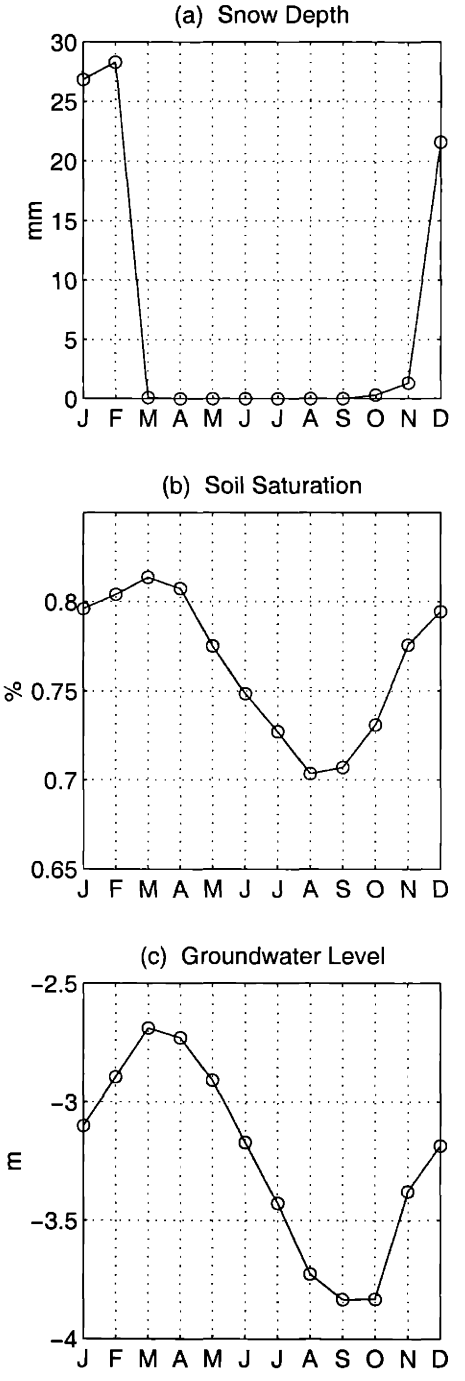

Figure 2.4 12-year (1983-1994) mean seasonal cycles of the state-average (a) snow depth, (b) soil saturation, and (c) water table in Illinois.

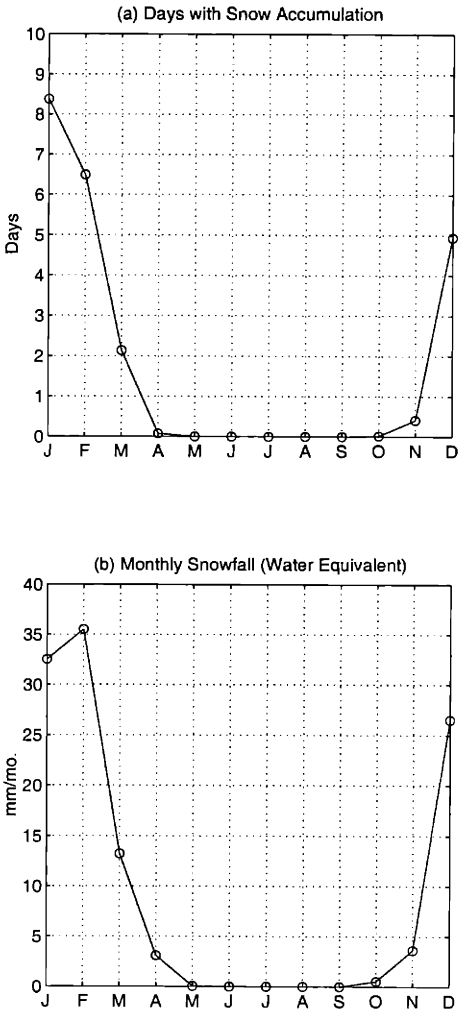

Figure 2.5 12-year (1983-1994) average (a) days within a month with snow accumulations in Illinois; (b) seasonal cycle of snowfall in Illinois.

annual snowfall is about 115 cm/yr., which is less than the average annual snowfall for North America $35^{\circ} \times 45^{\circ} N$ (i.e., 140 cm/yr., see Table 3 of *Groissman and Legates*, 1994). Actually, Illinois is not a snowy state even by Mid-western standards [*J. Angel*, climatologist, ISWS, personal communication]. The major reason is that Illinois locates at the upwind direction of Lake Michigan such that the lake-effect snow is irrelevant. Although the snow amount comprises a significant fraction of winter precipitation in Illinois, close examinations of the snow data reveal that, after a day with snow occurrence, the snow accumulation lasted only through the subsequent 1-5 days for most of the cases. Therefore we inferred the snow storage effect in Illinois is insignificant in comparison with other hydrological quantities involved in monthly

water balance computations. Given the limited role of snow in Illinois, we will employ (2.3) in conjunction with observations of $\overline{P}, \overline{R}, \overline{n}, \overline{s}$ and $\overline{H}$ to estimate the regional evaporation $\overline{E}$ in Illinois during the period 1983 to 1994.

Before the implementation of evaporation estimation procedure, two soil parameters in (2.3), the root-zone depth $\overline{D}$ and specific yield $\overline{S_y}$ should be determined. Constant values representing the regional scale average soil properties are estimated and used in this study since the paucity of data excludes the possibility to characterize the spatial patterns of these parameters.

Root-zone depth, from which the soil water is available for evapotranspiration, can be extremely variable within the range of a few centimeters to a few meters according to the different soil textures and vegetation characteristics. The determination of mean root-zone depth was initially performed by calculating the change in soil water storage for all of the available surface layers. It was found that the water stored below 1 m soil layer has much less variations than those stored within top 0.5 m soil layers. However, since the soil moisture data is available down to about 2m the mean root-zone depth was taken as 2 m in this study in order to avoid underestimation of the available storage volume of soil.

The mean specific yield $\overline{S_y}$ in (2.3) is also considered as a constant. Several sources of information can be utilized to infer the representative value of $\overline{S_y}$. The first source is the study of hydrological budgets from three small watersheds in Illinois by *Schicht and Walton* [1961]. Their analysis of groundwater recessions of different duration yielded a steady value of $\overline{S_y}$ equals to 0.08. Next, judging from the soil logs taken from 19 access holes of neutron probe in Illinois [*Hollinger and Isard*, 1994; Table 2], the soil textures at the soil moisture measurement sites are silt loam with only two exceptions. One of nineteen stations is silt clay loam and the other one is loamy sand. Further, according to the soil map provided by *FAO-UNESCO* [1975], the USDA (U.S. Department of Agriculture) soil texture class in Illinois is "fine silt" with the drainage characteristic as "imperfect, moderate to moderate slow permeability". According to the compilation of typical values of specific yield by *Johnson* [1967; also see *Domenico* and *Schwartz*, 1990, p.69] for various soils, the representative specific yield in the unconfined silt

loam aquifers in Illinois is specified as 0.08 in this study, which is exactly the value found by *Schicht and Walton* [1961]. Therefore $\overline{S_y} = 0.08$ was used in this study. Scientists from ISWS [*A. Visocky*, ISWS, personal communication] have suggested that $\overline{S_y} \cong 0.08 - 0.1$ is an appropriate estimate for the unconfined aquifers in Illinois. Sensitivity analysis was also conducted that indicates the variation within a possible range of $\overline{S_y}$ (0.05-0.10) has negligible effect on the changes in monthly evaporation estimates, as discussed later in Section 2.3.4.

In the following we present the estimates of monthly evaporation derived from the SWB and AWB computations. Table 2.2 summarizes the 12-year average annual soil and atmospheric water balances. Annual evaporation is about 660 mm, which falls within the range of the annual evaporation estimate (i.e., 25-30 inches per year) by *Jones* [1966]. Annual total runoff is about 314 mm, which comprises about 32% of the annual precipitation (975 mm.). The annual convergence of atmospheric moisture into this region is about 294 mm. (Table 2.2). The difference between runoff and convergence is about 6.3% of runoff, which is comparable to the accuracy of the estimates themselves. This suggests that any additional lateral and downward fluxes (leakage) across the boundary of the study region are indeed negligible (see equation 2.11).

Figure 2.6a illustrates the mean seasonal cycle of each surface/subsurface water balance component (precipitation, evaporation, runoff, and storage changes in the unsaturated and saturated zones). The 12-year average annual evaporation and runoff are approximately 70% and 30% of the annual precipitation (Table 2.2). For the evaporation estimates, a seasonal cycle is clearly demonstrated with a peak close to 120 mm/mo. during the summer (June-August) and a trough of almost zero during the winter (December-February). From May to August, the average monthly evaporation exceeds that of precipitation, while during the winter months evaporation falls well below the average precipitation. Upon examination of each individual year some evaporation estimates during the late fall and winter months appear to be below zero because of their limited accuracy.

	P (mm)	E_{soil} (mm)	R (mm)	s (%)	H (m)	$nD\frac{\partial s}{\partial t}$ (mm)	$S_y\frac{\partial H}{\partial t}$ (mm)	$E_{atmo.}$ (mm)	C (mm)
Jan	39.2	1.50	27.7	35.9	-3.10	7.2	2.9	0.4	41.4
Feb	50.2	-2.5	28.7	36.3	-2.89	7.5	16.5	-0.4	50.2
Mar	77.1	12.3	39.5	36.7	-2.69	8.9	16.4	12.6	66.6
Apr	90.0	59.0	41.2	36.4	-2.73	-6.9	-3.3	51.7	45.8
May	94.8	108.7	32.3	34.8	-2.91	-31.9	-14.3	96.9	2.8
Jun	89.3	112.0	24.6	33.5	-3.17	-26.2	-21.0	122.5	-22.4
Jul	97.3	117.5	20.9	32.5	-3.43	-20.6	-20.5	126.9	-32.0
Aug	83.5	114.6	14.8	31.4	-3.73	-21.9	-23.9	120.4	-42.4
Sep	89.0	80.5	15.2	31.5	-3.83	1.8	-8.6	74.1	7.9
Oct	83.0	42.5	16.6	32.6	-3.83	23.8	0.1	50.6	31.1
Nov	112.5	9.9	22.7	34.8	-3.38	43.5	36.4	21.0	82.9
Dec	69.0	3.8	30.0	35.8	-3.19	19.8	15.3	5.5	62.1
Ave.	81.2	55.0	26.2	34.4	-3.24	0.42	-0.33	56.9	24.5
Total	974.8	659.8	314.1	-	-	4.98	-4.01	682.2	293.7

P: precipitation; E_{soil} : evaporation estimated from soil water balance; R: river flow; s: soil moisture content; H: groundwater level; $E_{atmo.}$: evaporation estimated from atmospheric water balance; C: convergence of atmospheric moisture.

$nD\frac{\partial s}{\partial t}$: change in unsaturated (soil) storage. $S_y\frac{\partial H}{\partial t}$: change in saturated (aquifer) storage.

Table 2.2 12-year (1983-1984) Average Monthly Surface/subsurface Water Balance and Atmospheric Water Balance Components in Illinois

The contributions of changes in both unsaturated and saturated storage to the annual water balance are small (i.e., $0.4\% - 0.5\%$, see Table 2.2). However, from month to month these storage changes can be significant because of their apparent seasonal cycles (Figure 2.5a). For some months, the sum of the changes in soil moisture storage and in groundwater storage amount to almost 70% of the corresponding monthly precipitation. Considering the unsaturated and saturated zone as a whole, the seasonal cycle of the change in monthly subsurface storage has a maximum of 80 mm/mo. in November and a minimum of -47 mm/mo. in June, which constitutes a large contribution to the monthly water budget. On the other hand, rainfall is uniform throughout the year, although conditions during the spring, summer and fall are relatively wet in

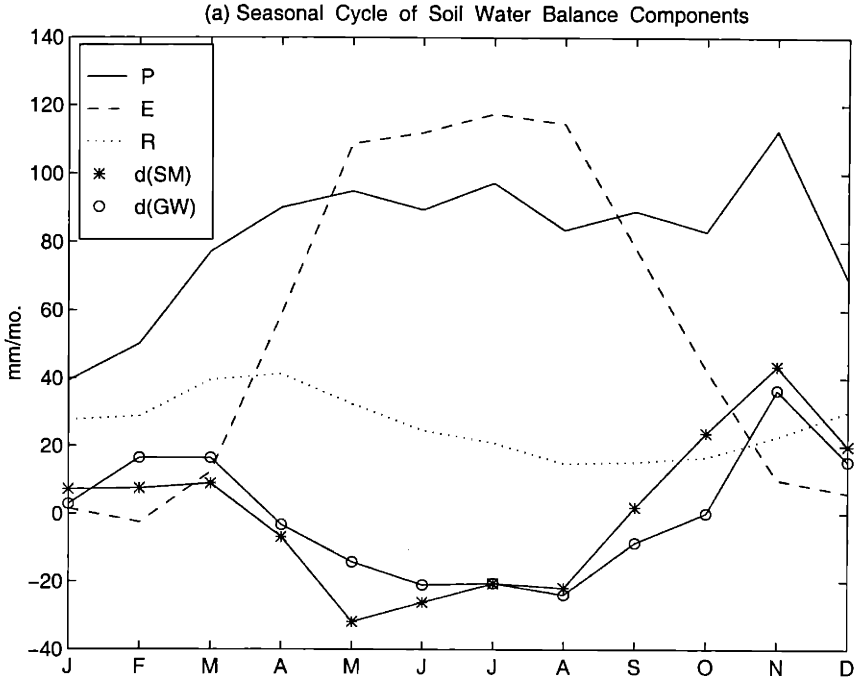

Figure 2.6(a) Seasonal cycle of the surface/subsurface water balance components in Illinois. *P*: precipitation; *E*: evaporation estimate from the surface/subsurface water balance; *R*: streamflow; d(SM): change in the soil moisture storage ($=nD\,ds/dt$), d(GW): change in the groundwater storage ($= S_y\,dH/dt$).

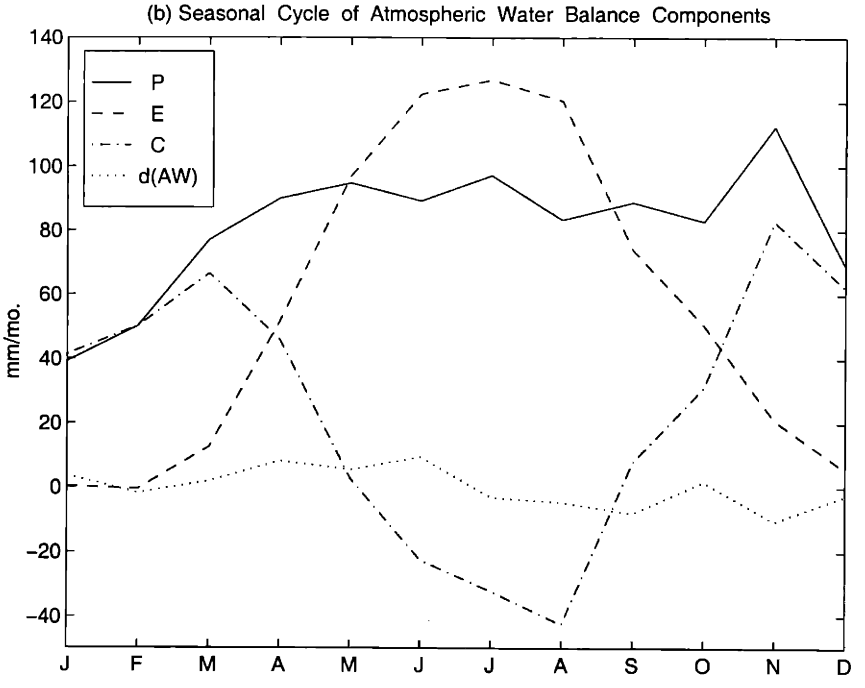

Figure 2.6(b) Seasonal cycle of the atmospheric water balance components in Illinois. *P*: precipitation; *C*: atmospheric water vapor convergence; *E*: evaporation estimate from the atmospheric water balance; d(AW): change in the atmospheric water storage ($=dW_a/dt$).

comparison with the relatively dry winter conditions (see Figure 2.6a and Table 2.2). The strong seasonal cycle of incoming solar radiation forces a similar cycle in evaporation, which then propagates through the soil down to the groundwater aquifer to dictate similar patterns of seasonal variability in soil moisture and groundwater levels. The seasonal cycle of evaporation is reflected in the changes of monthly unsaturated and saturated storage. Due to the same order of magnitude of both subsurface storage changes, the incorporation of the change in groundwater storage is indispensable for monthly surface/subsurface water balance computation in humid areas such as Illinois, since fluctuations in the shallow groundwater table level cause a significant variation in saturated storage at the monthly time scale.

The evaporation estimates from the AWB approach are presented as follows. On average, the total evaporation $E_{atmo.}$ over a year is 682 mm, and the net convergence of water vapor is 294 mm (Table 2.2). Again, the annual evaporation estimate is close to that estimated by *Jones* [1966]. As expected, the change in atmospheric storage $\partial\overline{W_a}/\partial t$ is small (usually less than 10 mm/mo.), and integrates to zero over the annual time scale (Table 2.2). The mean monthly values over the 12-year record of evaporation $E_{atmo.}$, along with precipitation P, convergence C, and change in storage $\partial\overline{W_a}/\partial t$, are shown in Figure 2.6b. A seasonal cycle for the evaporation estimates with a peak more than 120 mm/mo. during the summer (June-August) is clearly seen in this figure. Evaporation is lowest in the winter months with a trough almost equal to zero (December-February). Similar to the SWB computation, during the months of May, June, July and August the evaporation rate exceeds the precipitation rate. Atmospheric moisture diverges away from this region, and the subsurface storage of water acts as a significant source of water to the atmosphere. However, these patterns are reversed during the remaining months of the year: precipitation exceeds evaporation, significant amounts of atmospheric moisture converges towards the region, and this helps to replenish the subsurface storage of water before the onset of dry conditions in the following summer.

In February, the AWB approach gives an average evaporation equal to –0.45 mm/mo. Although small, this is the only negative value among the twelve monthly evaporation estimates. Interestingly, February is also the only month when the SWB approach yields a negative average

evaporation estimate (Table 2.2). Upon examination of the individual years some values of $E_{atmo.}$ during the late fall and winter are negative. In most cases the negative values are within 0 to -10 mm/mo.. However, in an extreme case such as November 1991 the evaporation estimate $E_{atmo.}$ is on the order of –49 mm/mo. In his study *Rasmusson* [1971] also found negative evaporation estimates during the fall and winter months. He argued that the error is most likely introduced in the measurement of precipitation and computation of convergence. As discussed earlier, the negative bias of precipitation may be the primary source of error for the underestimation of winter evaporation, with the remaining error most likely resulting from the estimation of convergence. The latter has been discussed in detail by *Rasmusson* [1977].

The impact of the undersampling of winter precipitation on the evaporation estimates can be roughly evaluated by increasing winter precipitation by 15%, according to the study by *Groisman and Legates* [1994]. The resulting average evaporation estimates in winter months increase from 3.8 mm (December), 1.5 mm (January), and –2.5 mm (February) to 16.4 mm, 7.4 mm, and 5.0 mm, respectively.

It is important to look at the AWB equation and note how each component affects the estimate of evaporation. From (2.11) it can be seen that precipitation $\overline{P}$ and changes in atmospheric storage $\partial\overline{W_a}/\partial t$ affect evaporation $\overline{E}$ positively, that is, an increase in $\overline{P}$ or $\partial\overline{W_a}/\partial t$ will increase $\overline{E}$. Conversely, $\overline{E}$ is negatively related to convergence $\overline{C}$. Therefore, when $\overline{C}$ becomes more positive (negative), $\overline{E}$ decreases (increases). As mentioned earlier changes in atmospheric storage are small and therefore have little impact on evaporation. While precipitation is slightly lower in the winter, evaporation is expected to be at its lowest because of limited solar radiation, which is consistent with the positive convergence throughout the fall and winter months. During the summer months, precipitation is abundant, and evaporation is expected to be highest due to the seasonal pattern of incoming solar energy. This is consistent with the strong negative peak in convergence for almost every summer. It is interesting to note that, while the seasonal variability of the evaporation estimates based on the SWB approach is largely balanced by the seasonal pattern of subsurface storage rather than by the lateral water fluxes (runoff), the reverse is true for the evaporation estimates based on the AWB approach.

The seasonal pattern of evaporation estimates from the AWB approach is almost entirely balanced by the seasonal pattern of lateral fluxes of water vapors, and not by the changes in storage. This contrast reflects a fundamental difference in the hydrology of the land and atmospheric branches of the regional water cycle. The differences in the memories of the two systems underscore the importance of the land in creating climate persistence in atmospheric states.

2.3.3 Comparison of Evaporation Estimates

Annually, the difference between the evaporation estimates from the SWB and the AWB is 22 mm/yr. Since changes in both the atmospheric and subsurface water storage are negligible over the annual time scale, the difference between two evaporation estimates is thus equal to the difference between the annual totals of atmospheric convergence and runoff. The comparison between the time series of two evaporation estimates, E_{soil} from (2.3) and $E_{atmo.}$ from (2.10), is shown in Figure 2.7 for each of 12 years. The average of the difference between the two evaporation estimates is 1.8 mm/mo., and the standard deviation is 37 mm/mo.. The two estimates agree reasonably well in the timing and magnitude of the seasonal pattern of evaporation; however, significant differences are evident in some estimates of evaporation. Twenty-three monthly evaporation estimates during the 12 years (15% of total estimates) have differences larger than 50 mm/mo.. The largest difference between E_{soil} and $E_{atmo.}$ is 108 mm/mo. in October 1986 when an unreasonable negative $E_{soil} = -72$ mm/mo. is obtained from the soil approach. Further, for June 1988, $E_{soil} = 102$ mm/mo. and $E_{atmo.} = 197$ mm/mo., which has a difference of 95 mm/mo. The evaporation estimates are also compared on a monthly basis by plotting the estimates from the SWB approach versus the estimates from the AWB approach (Figure 2.8). For perfect estimates, the data would lie along the 45° line. The coefficient of correlation between the time series of E_{soil} and $E_{atmo.}$ is 0.785. Also shown in this figure is the best-fit line derived by linear regression: $E_{soil} = 0.92E_{atmo.}$, which reflects the annual 22mm difference between two estimates of annual evaporation (see Table 2.2).

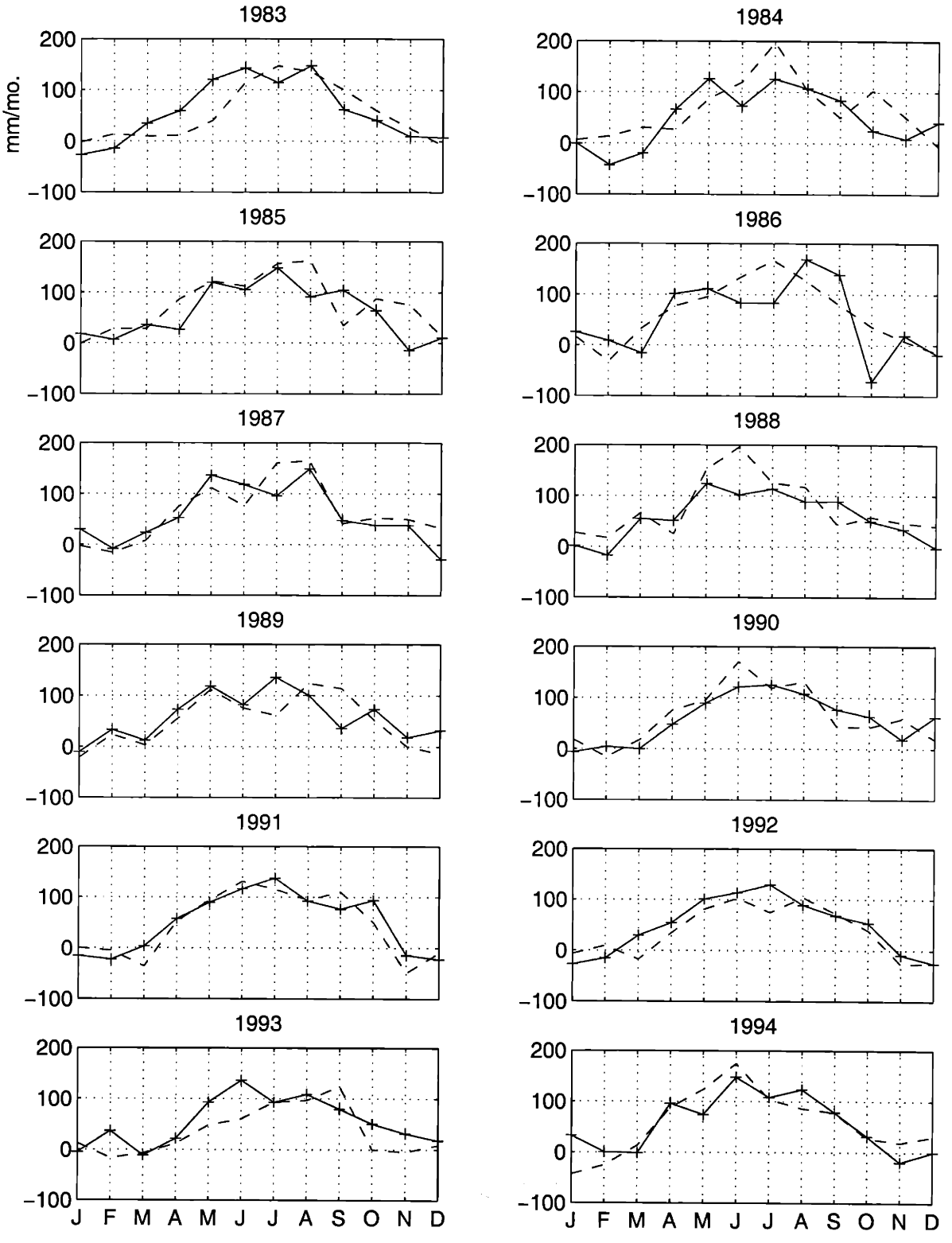

Figure 2.7 12-year time series of evaporations estimated from surface/subsurface water balance approach (solid line) and atmospheric water balance approach (dash line) from 1983 to 1994.

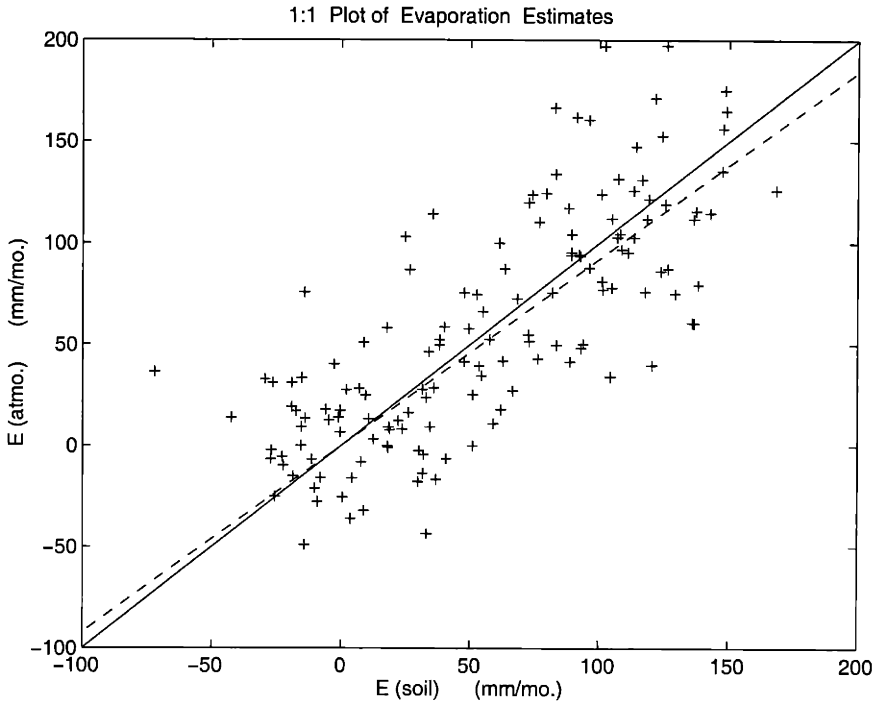

Figure 2.8 Plot of evaporation estimates from surface/subsurface water balance approach (SWB) versus evaporation estimates from atmospheric water balance (AWB) approach.

The seasonal cycles of two evaporation estimates are presented in Table 2.2 and plotted in Figure 2.9 for comparison. The standard errors of the mean evaporation are indicated by the error bars. For climatological estimates using the 12 years of data, the error is calculated as $STD_i/\sqrt{12}$, where STD_i is the standard deviation of evaporation estimates in month i. Also shown in this figure is the potential evaporation from the monthly Class A pan evaporation compiled by *Farnsworth and Thompson* [1982] for the United States. The evaporation measurements from Class A pans are available only from April to October. These pans are removed each fall around the middle of October and reinstalled around the middle of March. Farnsworth and Thompson suggested that potential evaporation from moist natural surfaces (i.e., shallow lake, wet soil) is roughly 70% of the Class A pan evaporation for the same meteorological conditions. Thus, potential evaporation is derived by multiplying a pan coefficient of 0.7 to their pan evaporation data. From Figure 2.9, the two estimates E_{soil} and $E_{atmo.}$ agree reasonably well for most of the months, however small differences on the order of 10 mm/mo. occur during late spring and summer. Both estimates predict peak evaporation in

July of approximately 120 mm/mo. and a minimum but slightly negative evaporation in February. For both estimates the evaporation is less than the precipitation during most of the year except for summer, when evaporation exceeds precipitation (see Table 2.2). Both estimates predict that evaporation can exceed precipitation by up to 40% in August. Over the entire year, however, evaporation is approximately 70% of precipitation. The seasonal evolution of both evaporation estimates follows closely to that of potential evaporation. The peak of the estimates occurred in the summer months with a magnitude of about 80%-90% of potential evaporation. This is indicative of the atmospheric control on evaporation in Illinois. According to the classification of climate by *Thronthwaite* [1948], Illinois belongs to the region where there is no water deficiency throughout the year. The non-water-stressed evaporation can be perceived in terms of the close agreement between the seasonal pattern of evaporation with that of net radiation (although not shown here). This implies that the variability of evaporation in Illinois is mainly controlled by the variability of energy supply.

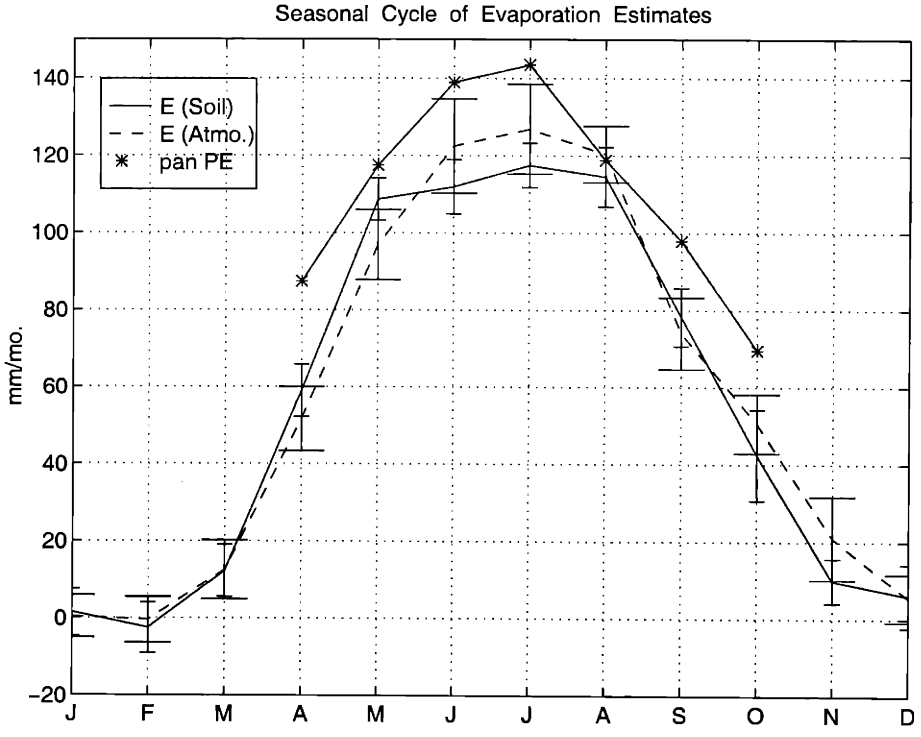

Figure 2.9 Seasonal cycles of evaporation estimated from SWB approach (solid line) and AWB approach (dash line), and potential evaporation (from April to October) calculated from Class A pan evaporation tabulated by *Farnsworth and Thompson* [1982]. The error bar indicates the standard error of the climatological estimates of evaporation. The wide error bars correspond to the evaporation estimates from the AWB, while the narrow ones correspond to those from AWB.

The difference between the climatologies of E_{soil} and $E_{atmo.}$ has the mean value of 1.8 mm and the standard deviation of 7.5 mm. The evaporation estimates during the summer are expected to be closer to the true evaporation than that during the winter because of the significant rain gauge bias, particularly during the winter snowfall periods. The two approaches produce almost identical climatologies of evaporation. In light of the fact that independent datasets were used in the two approaches, this result is encouraging: the AWB approach has the potential for the accurate estimation of the climatology of regional evaporation at least for humid regions at a scale similar to that of Illinois ($\sim 10^5$ Km^2).

2.3.4 Sensitivity Analysis

So far the above discussion has centered on estimates made corresponding to the whole study region ($\cong 250{,}000$ km^2, hereafter referred to as Area 1, see Figure 2.10). In order to test whether the AWB approach can be applied to even smaller regions, estimates were computed for several areas within the same study region: Area 2 ($\approx 500 \times 250$ km^2), Area 3 ($\approx 250 \times 250$ km^2), and Area 4 ($\approx 250 \times 250$ km^2), see Figure 2.10. To estimate evaporation for these areas, the same AWB approach described above was used. The only changes involved were the precipitation data and flux calculations. For precipitation, only those gauges within each area were used. The mean precipitation over the 12 years for each area is shown in Figure 2.11a. From this figure, precipitation does not change significantly; however, there is more precipitation in Area 4 and less precipitation in Area 3 except in summer, while Area 2 has approximately the same amount of precipitation as Area 1. The fluxes which are calculated to determine the convergence also change based on which node makes up the boundary of a specific area. For Areas 3 and 4 only four boundary nodes are available, so the estimates for these areas are most prone to error. The mean convergence over the twelve years for each of the four areas is shown in Figure 2.11b. All four of the convergence estimates exhibit a similar pattern in terms of two maximum peaks in spring and November and a large negative peak in August. For Areas 1 and 2 the results are very similar, however for Areas 3 and 4 the results differs significantly. The mean change in storage $\partial \overline{W_a}/\partial t$ over 12 years shows little sensitivity to changes in area (Figure 2.11c). The differences

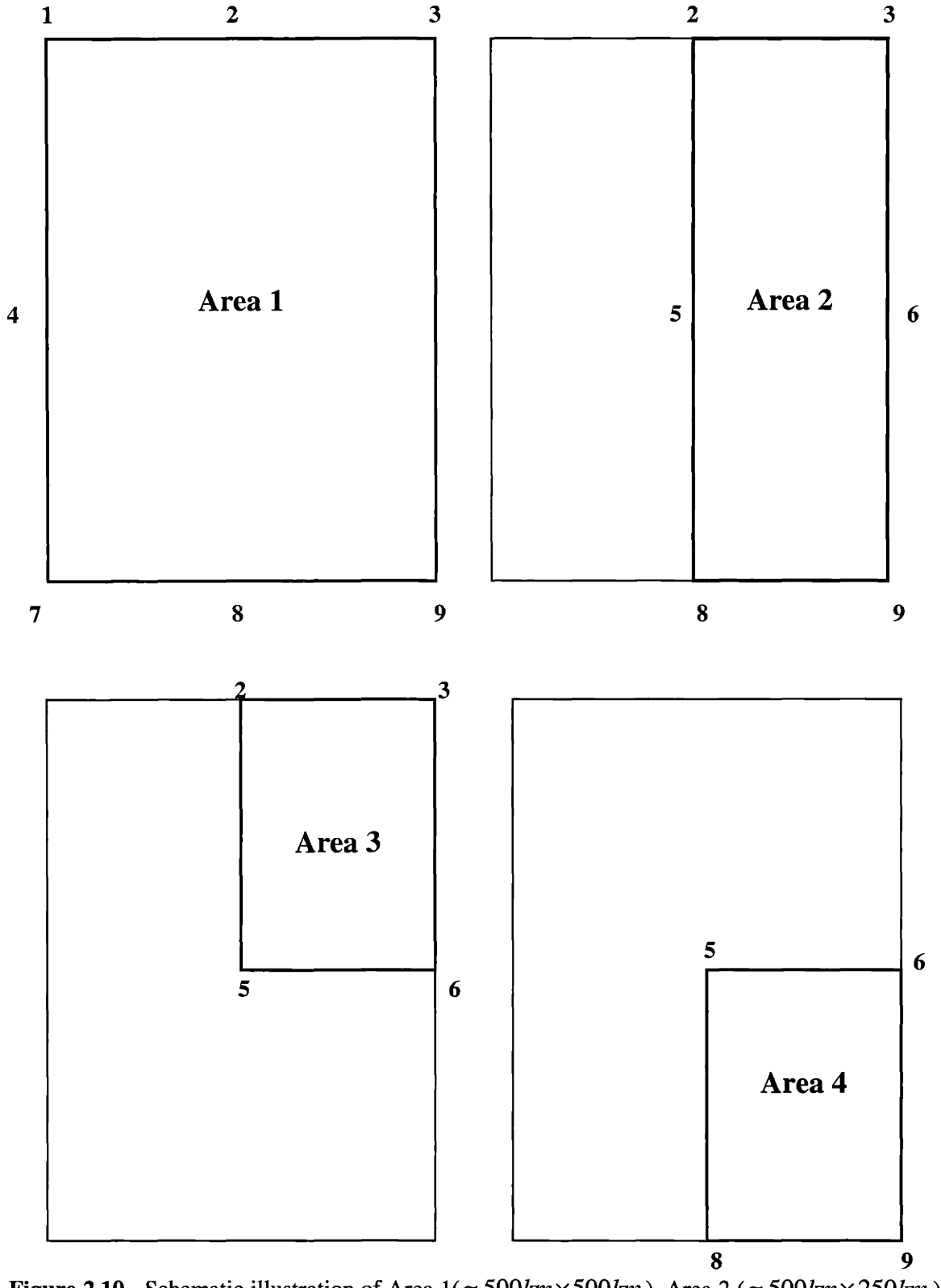

Figure 2.10 Schematic illustration of Area 1($\approx 500km \times 500km$), Area 2 ($\approx 500km \times 250km$), Area 3 ($\approx 250km \times 250km$) and Area 4 ($\approx 250km \times 250km$). The numbers marked on the boundaries of areas correspond to the nine grid points of NCEP/NCAR atmospheric data shown in Figure 2.3.

in convergence between the different areas stem from two factors: the limited accuracy of land extent of the available observations and the pattern of atmospheric circulation in this region. Specifically, the calculations of $\partial \overline{W_a}/\partial t$ and convergence use the same specific humidity data, therefore it can be inferred that the humidity is not the sensitive variable to the size of area. Instead, wind velocities, the only other atmospheric variable used to calculate the fluxes (see (2.9)), is the one which causes the difference in convergence as shown in Figure 2.11b. As mentioned earlier, *Rasmusson* [1968, 1971] stated that the AWB approach is more accurate for large areas, and this statement is indeed valid when such a small area is examined ($\cong 62{,}500\ km^2$).

The mean monthly evaporation for each area is shown in Figure 2.11d. The evaporation results are similar for Areas 1 and 2. The evaporation estimates for Area 3 are significantly lower due to the differences in the convergence as shown in Figure 2.11b. For eight out of twelve months the evaporation estimates for Area 3 are negative, which underscores the error involved in the estimates.

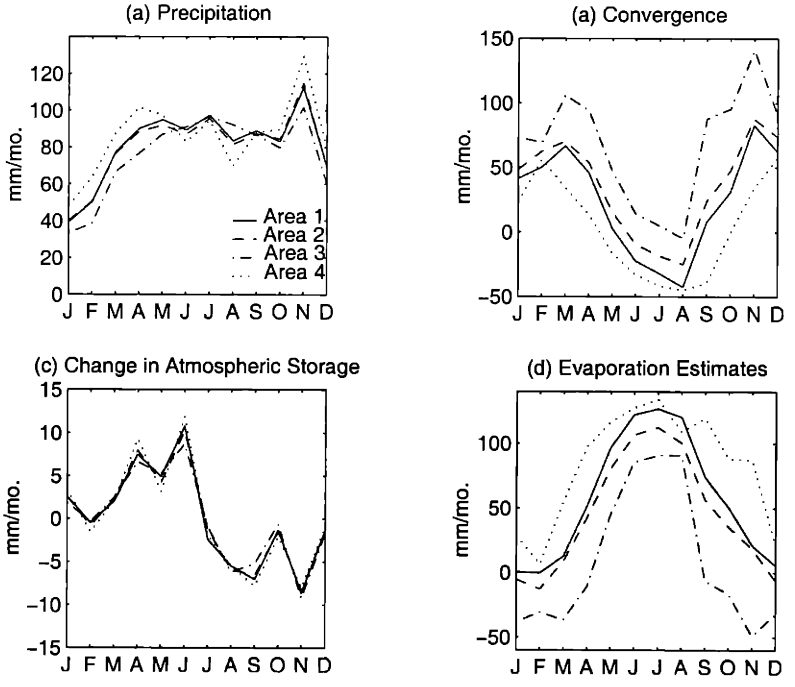

Figure 2.11 12-year monthly averages of (a) precipitation (b) atmospheric water vapor convergence (c) change in atmospheric storage (d) evaporation estimated from atmospheric water balance approach for four different areas shown in Figure 2.10.

Three principal factors controlling the accuracy of atmospheric flux computations were identified by *Rasmusson* [1968, p.721]. He stated that "in order to obtain satisfactory results, an adequate aerological network must exist, the region considered must not be too small, and the time period over which the observations are averaged must be of sufficient length to render the effect of random errors negligible." Since the atmospheric flux field exhibits significant diurnal variations [*Rasmusson*, 1967], using a finer temporal resolution of wind velocity measurements may alleviate the inaccuracy of atmospheric flux computations. From the study of the Upper Mississippi Basin where the water transport by the nocturnal low-level jet is a significant source of water vapor, *Gutowski et al.* [1997] suggested that six-hourly rawinsonde data appear to be the minimally acceptable frequency for the characterization of the temporal variability of water transport. This resolution is consistent with that used in this study, thus we believe the temporal resolution of rawinsonde data is not the main source of the estimate errors in Area 3. The twelve-year average period used in this study is expected to be long enough to give a reliable estimation of average atmospheric convergence. The most probable source of error thus lies in that the spatial resolution of aerological network ($2.5^\circ \times 2.5^\circ$) cannot resolve the significant feature of atmospheric circulation in Area 3. Therefore, we concluded that the evaporation estimates for Area 3 are not consistent with other areas. Also, whatever causes the error in Area 3 may in fact bias the estimates for other areas using node 3. This fact reiterates the need to use as large an area as possible in order to yield more accurate estimates of convergence. Since the estimates of evaporation for Area 3 were deemed inaccurate, our conclusion drawn from the sensitivity analysis is that the accuracy of the AWB approach is rather poor when the scale of the study area is smaller than about $10^5 km^2$.

Two lumped parameters required for the estimation of evaporation from SWB, the root-zone depth $\overline{D}$ and specific yield $\overline{S_y}$, were estimated as 2 meters and 0.08 as previously described. The sensitivity of evaporation estimates from the SWB computations to these parameters can be investigated by varying them within a reasonable range of values. The results are presented in Figures 2.12a and 2.12b. The climatology of the evaporation estimates is insensitive to a specified $\overline{D}$ larger than one meter (Figure 2.12a). The range of the monthly evaporation estimates is slightly larger when larger $\overline{D}$ is used. The annual evaporation estimates

corresponding to $\overline{D}$=50 cm, 110 cm, and 200 cm are 663.8 mm, 661.9 mm, and 659.8 mm, respectively. Such a result is anticipated since the soil water storage in the deep root-zone (1-2 meters) in Illinois maintains close to soil field capacity throughout the year [*Hollinger and Isard*, 1994]. However, the specified yield $\overline{S_y}$ affects the evaporation estimates to a slightly larger extent (Figure 2.12b). Large $\overline{S_y}$ amplifies the effect of groundwater storage, leading to larger summer evaporation estimates and lower winter estimates, due to the opposite sign of the amount $\overline{P}-(\overline{E}+\overline{R})$ in different seasons. Moreover, unrealistic large negative evaporation estimates during the winter months result from specifying $\overline{S_y}$ as large as 0.15, which suggest the representative $\overline{S_y}$ should range between 0.05-0.1 approximately.

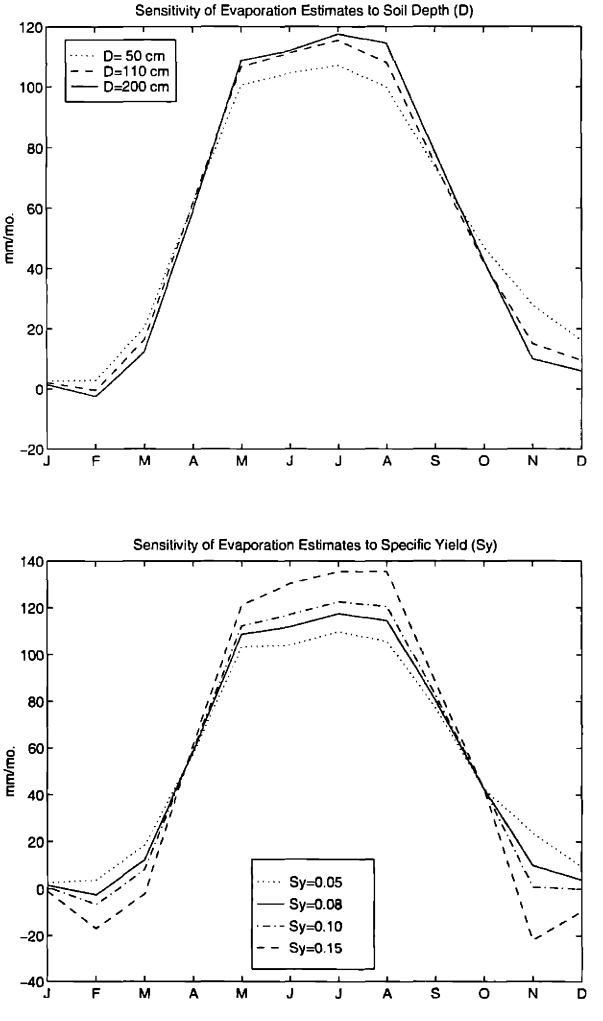

Figure 2.12 The sensitivity of the seasonal cycle of the evaporation estimates from surface/subsurface water balance to (a) root-zone depth and (b) specific yield.

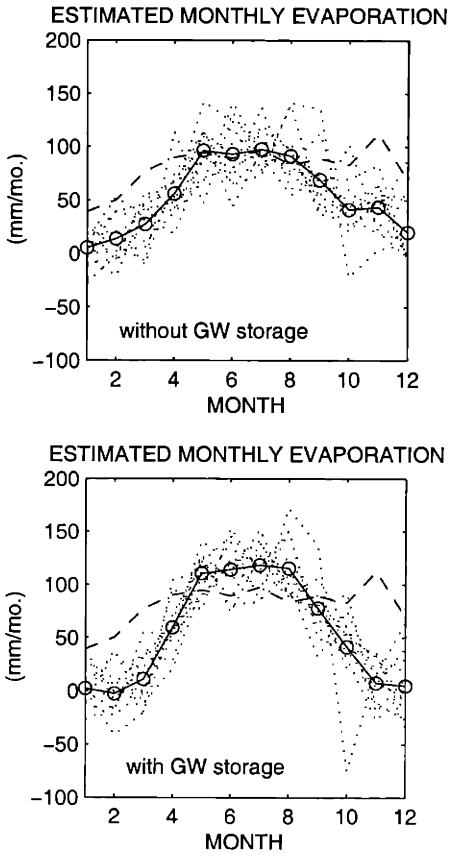

Figure 2.13 Seasonal cycles of the estimated evaporation (a) with (b) without the consideration of groundwater storage in the surface/subsurface water balance equation.

In the early stage of the evaporation estimation, groundwater storage was recognized as an important SWB component since its importance has been commonly ignored in the land surface modeling community. It has been commonly though that the residual of precipitation minus evaporation and streamflow would be balanced simply by the change of soil moisture storage. Figure 2.13 compares between the evaporation estimates from the SWB equation (2.3) (Figure 2.6a) and the estimates without considering the groundwater storage change in equation (2.3). From this figure, it can be seen that the estimated evaporation without considering groundwater storage underestimates the range of the seasonal cycle. It fails to exceed the corresponding precipitation from May to August as indicated by the estimation using the AWB approach, while overestimates the evaporation from November to February.

2.3.5 Summary

We have described in this section the regional scale hydrological cycle of Illinois, including the land and atmospheric branches, based on an extensive dataset on most of the hydrological variables. Since direct observations on evaporation are not available, two different approaches, based on surface/subsurface water balance (SWB) and atmospheric water balance (AWB), were applied to estimate the monthly regional evaporation over Illinois from 1983 to 1994. The following conclusions can be drawn:

(1) Estimates of evaporation based on the AWB approach have been compared to consistent estimates of evaporation based on the SWB approach. To our knowledge, this is the first time such a comparison has been made. The annual totals of evaporation estimates from both approaches are consistent with the previous study by Illinois state water Survey [*Jones*, 1966]. The climatologies of the monthly evaporation estimates from the two approaches agree reasonably well, and within a 10% error. However, substantial differences exist between the two estimates of evaporation for individual months. In light of the fact that two different datasets were used in the two approaches, this result is encouraging: the AWB approach is accurate enough for the estimation of the climatology of regional evaporation, at least for humid regions at a scale similar to that of Illinois ($\sim 10^5\ Km^2$).

(2) Since the magnitude of the change in subsurface storage can be nearly twice as large as runoff at the monthly time scale, the seasonal variability of evaporation estimates based on surface/subsurface water balance is mainly balanced by the seasonal variability of subsurface storage rather than the lateral water fluxes (runoff). Conversely, the seasonal variability of the evaporation estimates based on atmospheric water balance is almost entirely balanced by the seasonal variability of lateral fluxes of water vapor. On an annual basis, the net storage changes in the land surface and atmosphere are both zero. Annual runoff is in close agreement with the convergence of atmospheric water vapor.

(3) Although the AWB approach has been shown to be promising for the accurate estimation of regional evaporation at a scale of about $\sim 10^5\ Km^2$, this approach is more prone to error as the

size of the study area decreases. This conclusion is obtained from the observed divergence among the evaporation estimates from the AWB for small areas, especially for Area 3 ($\approx 250 \times 250\ km^2$) where estimates based on AWB approach are not accurate. Therefore, the accuracy cannot be warranted if the scale of the study area is smaller than $10^5 km^2$.

(4) For the calculation of SWB for humid regions such as Illinois where the groundwater table is rather shallow, the incorporation of the change in groundwater storage is indispensable since it contributes a significant portion of water storage at the monthly time scale.

2.4 Summary of the Regional Hydrological Cycle in Illinois

In this chapter, two water balance computations, one from the land surface branch and the other from the atmospheric branch of hydrology, were employed to estimate the 12-year (1983-1994) monthly evaporation in Illinois. This estimation completes the quantitative description of the regional-scale hydrological cycle in Illinois since evaporation is the only unknown variables in both the surface/subsurface water balance equation (2.3) and the atmospheric water balance equation (2.11).

Table 2.3 summarizes the average annual water balance in Illinois from 1983-1994. Rainfall over Illinois is 975 mm/year; 70% of that water is returned to the atmosphere through evaporation, with runoff contributing the remaining 30%, which is 314 mm/year. The convergence of atmospheric moisture towards this region is 294 mm/year. The difference between these two fluxes is about 20 mm/year, which is comparable to the accuracy of the estimates themselves. Since for a consist water balance of the atmosphere and of the soil, these two fluxes has to be equivalent; the above comparison suggests that any additional lateral land surface fluxes (leakages) are of negligible magnitude.

	P (mm/yr.)	*E (mm/yr.)*	*R (mm/yr.)*	*C (mm/yr.)*	*s (%)*	*H (m)*
Average	975	671	314	294	34.4	-3.24

P: precipitation.
E: evaporation
R: streamflow
C: atmospheric water vapor convergence
s: soil moisture content
H: groundwater level

Table 2.3 12-year (1983-1984) Average Annual Water Balance in Illinois

Although the changes in soil moisture storage and groundwater storage are both significant at the monthly time scale (with a magnitude equivalent to the monthly runoff), their contributions to the annual water budget are small (i.e., < 0.5%). It follows from Eqs. (2.1) and (2.2) that the annual precipitation is partitioned into evaporation, surface runoff, and groundwater runoff. The amount of (12-year) average annual groundwater runoff is approximately equal to that of groundwater recharge, since the average groundwater storage integrates to zero at the annual time scale.

The regional hydrological fluxes (precipitation, evaporation, streamflow, atmospheric moisture convergence), as well as the changes in the subsurface water storage, exhibit significant seasonal variability (Figures 2.6). Rainfall is uniform throughout the year, although conditions during the spring (March, April, and May), summer (June, July, and August) and fall (September, October, and November) seasons are relatively wet in comparison with the relatively dry conditions during the winter season (December, January, February). Evaporation has a strong seasonal cycle with high evaporation rates (>120 mm/mo.) during the summer season (June-August) and practically no evaporation during the winter season. During the summer, the evaporation rates in this region are similar in magnitude to the high evaporation rates that have been observed by *Shuttleworth* [1988] for the Amazon rainforest. During the summer months, the evaporation rate exceeds the precipitation rate, atmospheric moisture diverges away from this region, and the subsurface storage of water acts as a significant source of water to the atmosphere. However, these patterns are reversed during the remaining months of the year: precipitation exceeds evaporation, a significant amount of atmospheric moisture converges towards the region, and that helps to replenish the subsurface storage of water before the onset of dry conditions in the following summer.

The strong seasonal cycle of incoming solar radiation, evaporation, soil moisture, water table depth (from the local ground surface), and streamflow are related to each other through the water cycle (Figure 2.14). The strong seasonal cycle of incoming solar radiation leaves its signature on the soil moisture content through evaporation. The difference between effective precipitation and evaporation from the soil represents the natural replenishment rate of the soil water reservoir. Since precipitation shows no clear seasonal pattern, the seasonal cycle of evaporation leaves a

clear signature on the seasonal cycle of soil moisture content as seen in Figure 2.14. The recharge from the soil water reservoir to the groundwater reservoir is a slow process regulated by the variability in the soil moisture content. Hence, as seen in Figure 2.14, the seasonal cycle for the water table depth lags that of soil moisture content by about one month, which is consistent with the conclusion of *Changnon et al.* [1988]. The seasonal cycle of streamflow follows closely that of water table depth as seen in Figure 2.14. Examination of the seasonal cycle of snow depth (Figure 2.4) suggests that snow melting in spring has a relatively small magnitude, and is likely to have a minor impact on streamflow. As a result, the peak of streamflow during the spring season is attributable to high water table depths during that season.

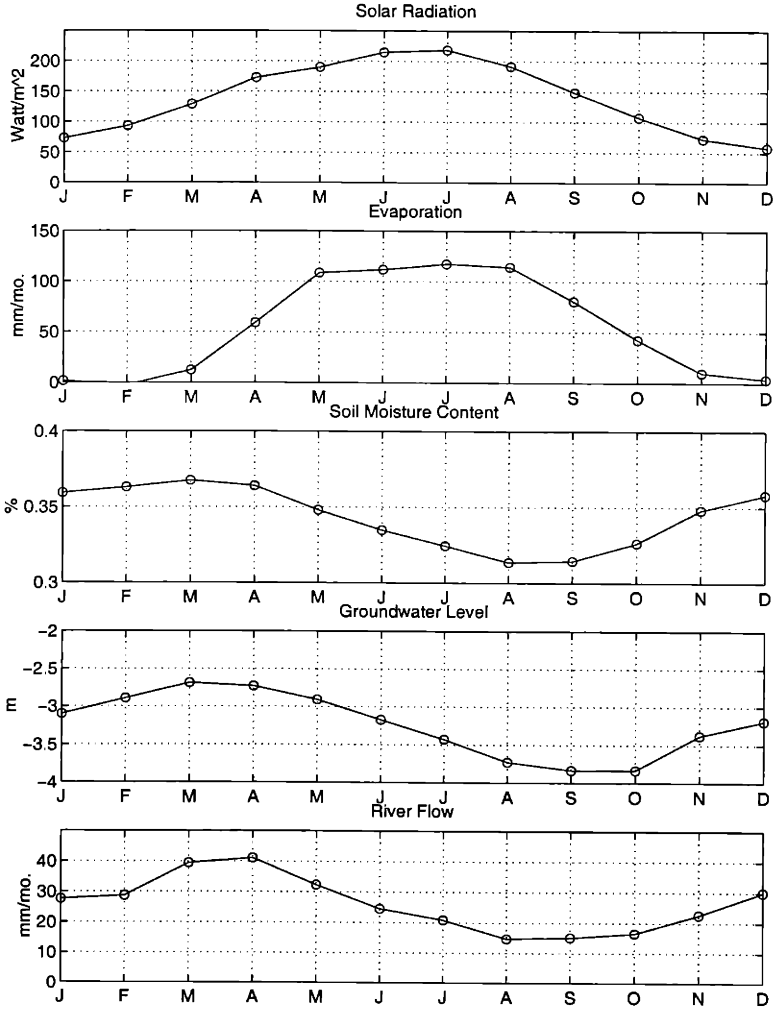

Figure 2.14 Seasonal cycle of incoming solar radiation, evaporation estimate, soil moisture content, water table depth and streamflow.

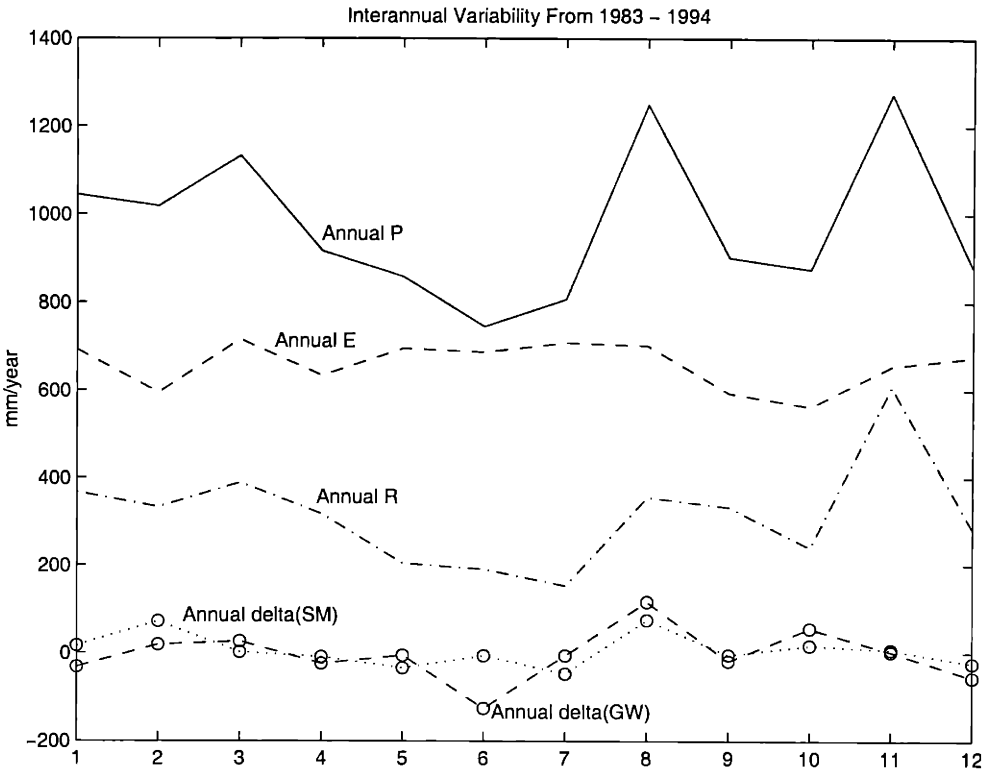

Figure 2.15 Plots of annual amounts of precipitation, evaporation, streamflow, as well as the storage changes in both the soil moisture and shallow unconfined aquifer from 1983-1994

In order to evaluate the interannual variability of the individual water balance components, the annual amounts of precipitation, evaporation, streamflow, as well as the storage changes in both the soil moisture and shallow unconfined aquifer from 1983-1994 are shown in Figure 2.15. The evaporation plotted in this figure is the average of the estimates from the surface/subsurface water balance computation and atmospheric water balance computation. It can be noted from this figure that (1) the annual streamflow exhibits significant interannual variability which primarily follows the pattern of the interannual variability of precipitation, while the interannual variability of evaporation is relatively small; (2) The annual water storage changes in two subsurface reservoirs (soil moisture and groundwater) are about zero and of similar pattern in most of the 12-years except 1988 and 1990. In the extremely try year 1988, the storage in groundwater aquifer declines significantly to replenish soil moisture such that the annual change in aquifer storage is as large as 150 mm/year, while the change in soil moisture remains about zero. In 1990, both reservoirs receive the replenishment due to the large precipitation (~1200 mm/year)

in that year. Moreover, notice the interesting fact that the storage changes in two reservoirs followed the nearly identical pattern in all 12 years but 1988, which suggests the different response of the shallow aquifer to the drought in contrast to the soil moisture. This point will be explored in detail using the statistic anomaly analysis in the next chapter.

In summary, the strong seasonal cycle of solar radiation forces a similar cycle in evaporation, which then propagates through the soil hydrology to dictate the observed patterns in the seasonal variability of soil moisture content and water table depth. The seasonal cycle of streamflow follows closely that of water table depth that suggests a significant contribution by the groundwater runoff to observed streamflow in Illinois.

In the next chapter, we will investigate the roles that shallow groundwater aquifer plays in the regional-scale hydroclimatology of Illinois (which is the main theme of this thesis) based on the results of the 12-year (1983-1994) water balance study performed in this chapter.

Chapter 3 Statistical Analysis of the Relations Between Water Balance Components in Illinois

Based on the results obtained from the 12-year water balance study presented in Chapter 2, the interrelationships between various water balance components will be investigated in Section 3.1 by using basic statistical techniques (correlation, spectrum, and regression analysis). In Section 3.2, we will discuss the patterns of the hydrological anomalies (i.e., flood and drought conditions) in the different hydrological variables and describe how these anomalies propagate through the different reservoirs of the water cycle. In Section 3.3, the regional-scale groundwater recharge, which couples the soil moisture water balance equation (Eq. 2.1) to the unconfined aquifer water balance equation (Eq. 2.2), will be estimated. The objective in the groundwater recharge estimation is to investigate the impact of shallow water table on the root-zone soil moisture profile and subsequently on the evaporation. This is followed by Section 3.4 in which the roles of shallow aquifers in the regional hydroclimatology in Illinois are summarized.

3.1 Interrelationships between the Components of the Hydrological Cycle

The interrelationships between the observed components of the hydrological cycle (i.e., precipitation, soil moisture, water table depth, and streamflow) in Illinois are investigated by the statistical analysis of the 12-year (1983-1994) monthly time series of these components. First, Table 3.1 summarizes the cross-correlation coefficients at lag zero (i.e., at the same month) between various components. Inspections of this table reveal that (1) streamflow, soil moisture, and water table depth are all poorly correlated with the corresponding precipitation, (2) the hydrologic variable accounting for most of the streamflow variability is the water table depth, and (3) water table depth is highly correlated with soil moisture, suggesting close interaction between the dynamics of unsaturated and saturated zones.

Correlation	*P*	*SM*	*H*	*R*
P	1	0.11	0.19	0.33
SM	0.11	1	0.69	0.62
H	0.19	0.69	1	0.80
R	0.33	0.62	0.80	1

P: precipitation; *R*: streamflow; *SM*: soil moisture content; *H*: groundwater level.

Table 3.1 The Correlation Coefficients Between the 12-year (1983-1984) Monthly Precipitation, Soil Moisture Content, Groundwater Level, and Streamflow

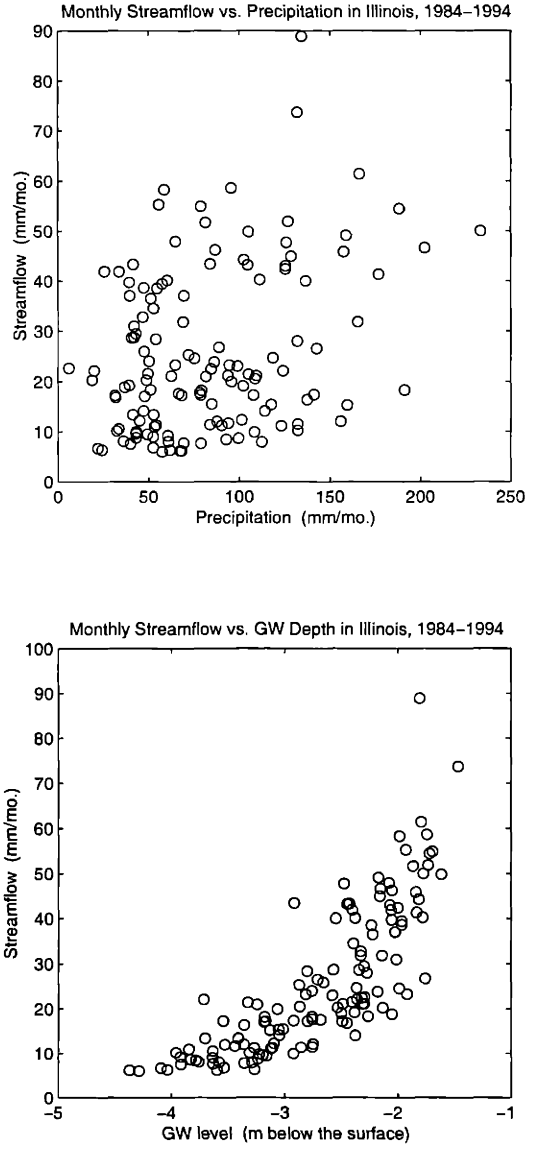

Figure 3.1 Plots of monthly (a) precipitation, (b) water table depth versus monthly streamflow during 1983-1994 in Illinois.

The 12-year monthly streamflow is plotted against the corresponding monthly precipitation and water table depth in Figures 3.1 (a) and (b), respectively. In consistency with Table 3.1, no distinct relationship can be observed between precipitation and streamflow. However, there is a strong nonlinear relationship between water table depth and streamflow. The correlation coefficients in Table 3.1 indicate that while water table depth alone explains about 65% of the variance of streamflow, precipitation alone explains only about 10% of the same variance. Similar observations on the nonlinear groundwater-rating curve (i.e., relationship between groundwater discharge to the stream and groundwater level) have been reported by *Rasmussen and Andreasen* [1959] for Maryland, by *Schicht and Walton* [1961] for Illinois, by *Lizarraga* [1978] and *Senn* [1980] for New Mexico, and by *Stagnitti et al.* [1989, 1992] for Connecticut. However, it should be indicated that most of these previous studies were based on the observations at a small scale ($\leq 10^3 km^2$), whereas the data used in this study are the spatially averaged hydrological variables over the Illinois ($\sim 10^5$ Km^2). To our knowledge, the nonlinear nature of the groundwater-rating curve at such a large scale has not been reported previously in hydrological literature.

A scatter plot between water table depth and soil moisture is shown in Figure 3.2. The same plot is also stratified into four seasons to emphasize the seasonal difference in the dependence between water table depth and soil moisture. As noted, a nearly linear relationship exists between water table depth and soil saturation with a cross-correlation coefficient of 0.77. The cross-correlation is more significant in summer (R=0.78) and autumn (R=0.86) than in the rest of a year. Given that the data of soil saturation and water table depth are the spatial averages over the Illinois rather than the point measurements, the linear relationship suggests strong interaction between the unsaturated and saturated zones at the regional scale in Illinois.

The autocorrelation functions and spectral density functions of 12-year monthly atmospheric moisture convergence, precipitation, soil moisture, streamflow, and water table depth from 1983-

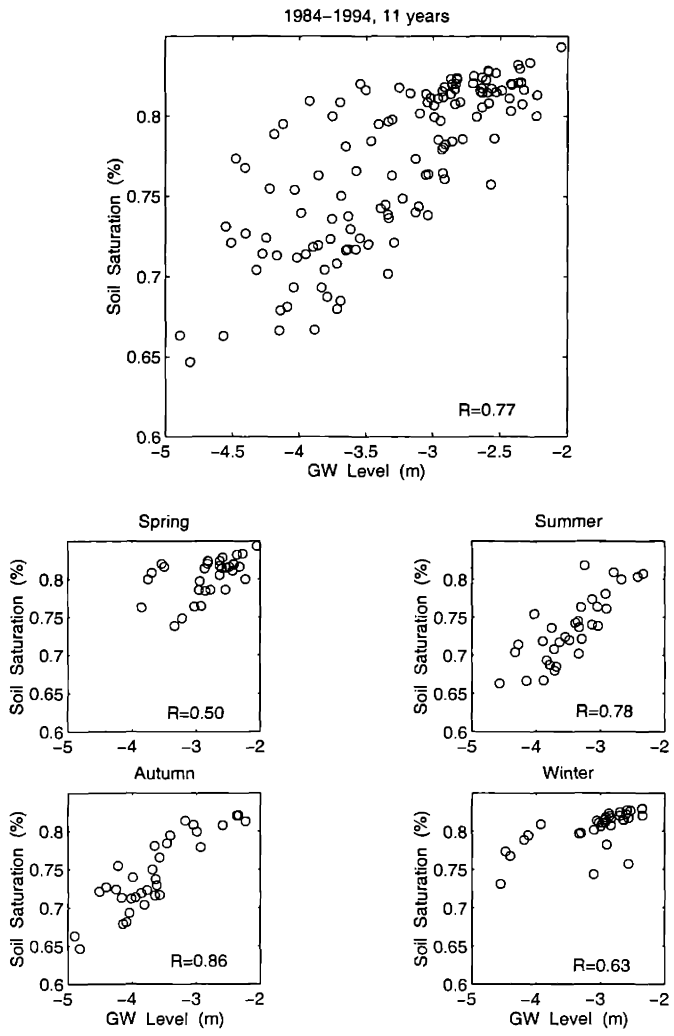

Figure 3.2 (a) Plot of monthly soil saturation degree versus monthly water table depth during 1983-1994 in Illinois. (b) Same as (a), but on a seasonal basis.

1994 are plotted in Figure 3.3. The seasonal cycles of these water balance components except precipitation are clearly shown in this plot. There is no clear seasonal cycle in precipitation.

In summary, for Illinois significant correlation exists between soil moisture, water table depth, and streamflow, but not precipitation. Streamflow is highly correlated with water table depth rather than precipitation at the regional scale in Illinois. Moreover, a significant linear relationship exists between root-zone soil saturation and water table depth during the summer and autumn, which indicates strong interactions between the unsaturated and saturated zones.

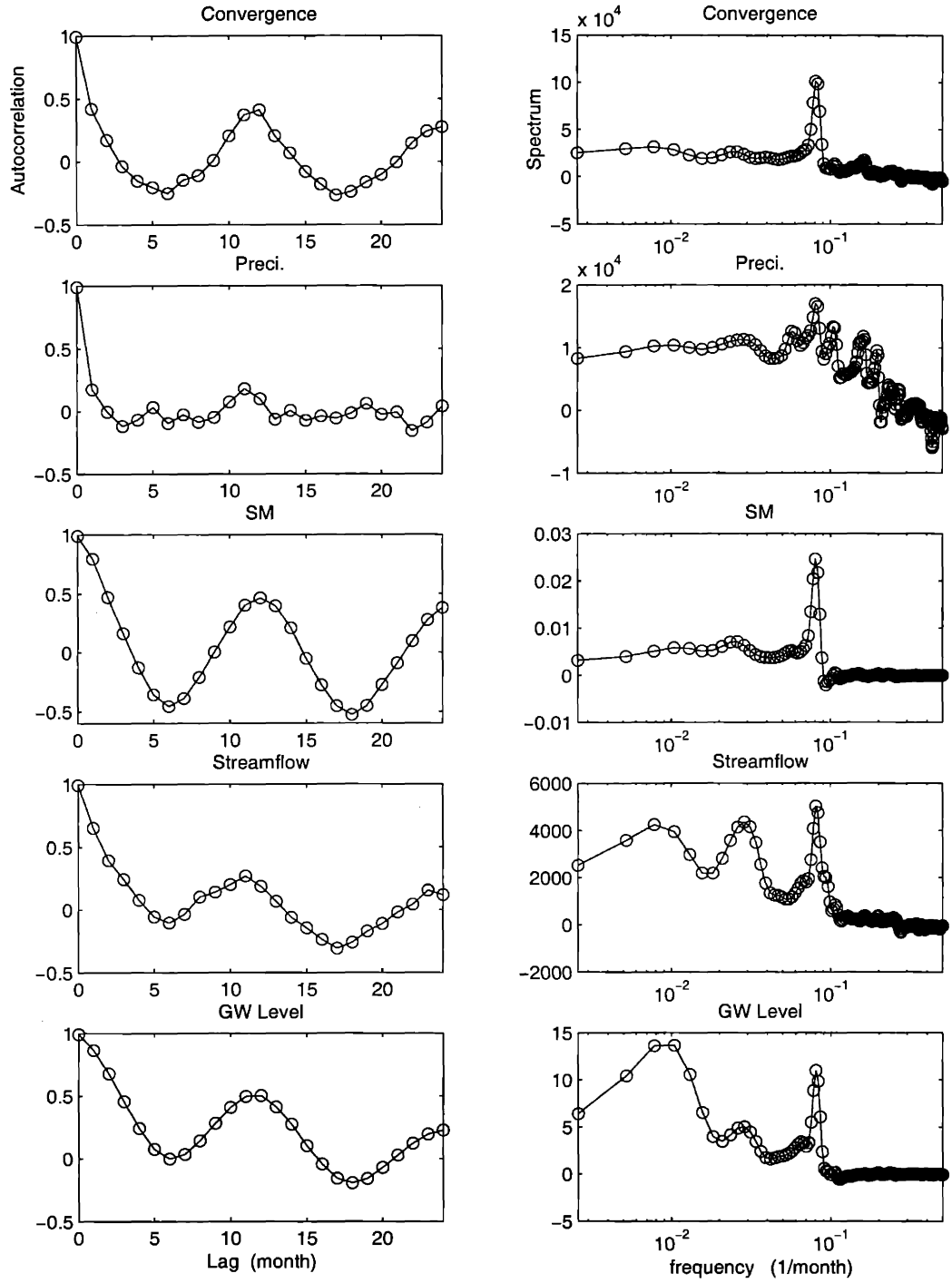

Figure 3.3 The autocorrelation functions and the spectra for the atmospheric moisture convergence, precipitation, soil moisture content, groundwater level, and streamflow.

3.2 Statistical Analysis of Hydrological Anomalies

In section 3.1 we discussed the interrelationships among various hydrological variables. In this section, we consider standardized anomalies of the observed variables from their corresponding monthly averages. Specifically, we investigate how hydrological anomalies, which define droughts and floods, propagate within the water cycle at the regional scale of Illinois. In particular, we investigate the response of the regional groundwater level to droughts and floods. Understanding the mechanisms of natural variability in the regional water cycle is a necessary step before we can make any credible predictions about the impact of future climate change on the hydrology and water resources in this important agricultural region.

Figure 3.4, which is taken from *Changnon* [1987], illustrates schematically how precipitation deficiencies during a hypothetical 4-year period are translated in delayed fashion through other components of the hydrologic cycle. The statistical relationship between precipitation and

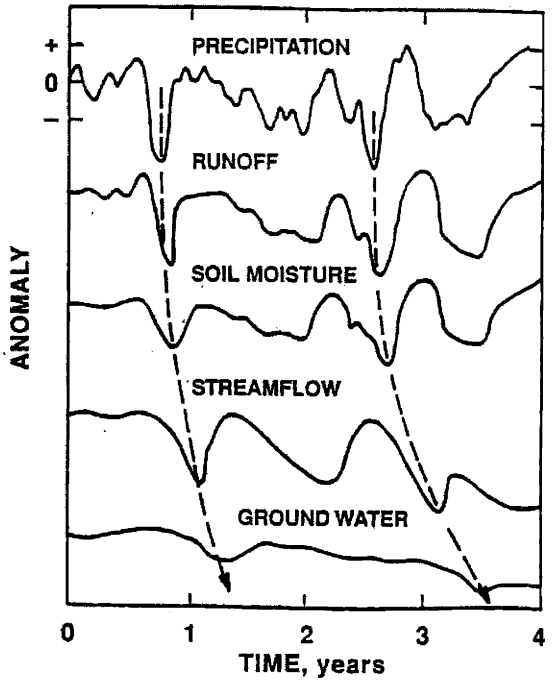

Figure 3.4 The propagation of the precipitation anomaly through the soil branch of the hydrological cycle down to the groundwater aquifer. (From *Changnon,* 1987)

groundwater levels, which is implied by Figure 3.4, has been studied by *Changnon et al.* [1988]. A significant correlation has been found between precipitation in any month and groundwater level in the following month. Thus, the temporal pattern of water level in groundwater aquifers should lag precipitation patterns by about one month. An example for this association is presented by *Olson* [1982] who studied the response of the groundwater system in Illinois to the drought event of 1980-1981. *Changnon et al.* [1988] calibrated a time series model using the data for the period 1960-1979 to predict the groundwater levels during the 1980-81 drought. The possible effects on flooding due to the gradually wetter climate in Illinois since 1940 have been addressed by *Changnon* [1983]. *Kohlhase* [1987] reported a significant rise in groundwater level in the East St. Louis area of Illinois between 1981-1985. *Smith and Richman* [1993] investigated the hydrologic and water resource effects induced by a change from a dryer to a wetter climatic regime over Illinois. They have shown evidence of a consistent increase by about one meter in the seasonal cycle of groundwater level for the period of 1970-90 compared to that of 1950-70. *Smith and Richman* [1993] indicated "this rise in well level may have been climatically driven but comparatively little is known about the response of shallow water able to long-term climate shifts".

In this section, we investigate the patters of hydrological droughts and floods in Illinois as they propagate from the atmosphere into the soil and down to the groundwater aquifer. The average climatology as well as the corresponding anomalies, namely droughts and floods, in several hydrological variables will be investigated. These variables include the flux of atmospheric water vapor, precipitation, soil moisture content, groundwater level, and streamflow. The response of the groundwater level to droughts and floods is investigated using direct observations. The mechanisms responsible for these observed patterns of hydrological anomalies are identified in observations and investigated theoretically using analytical techniques.

3.2.1 Anomalies in the Regional Hydrological Cycle: Droughts and Floods

First, we consider standardized anomalies of these observed variables from their corresponding monthly averages. For each variable, we estimate the average and standard deviation corresponding to each of the twelve months of the year. The differences between any observed variable and the corresponding monthly average for that variable and for that month of the year were first computed. Then, to compute standardized anomalies, these differences were normalized by the corresponding standard deviations. Figure 3.5 presents times series of the resulting anomalies in the following variables: convergence of atmospheric moisture, precipitation, soil moisture content, groundwater level, and streamflow. This figure describes how the anomalies in the large-scale atmospheric circulation propagate through the hydrological cycle to determine the magnitude of precipitation, which then regulate the variability in soil moisture conditions and recharge to aquifers, resulting in a clear signature of the circulation anomalies on the levels of groundwater and streamflow. While precipitation plays a minor role in shaping the natural variability in the regional hydrological cycle at the seasonal timescale, variability in precipitation is the major factor in shaping the natural variability in the regional hydrological cycle at the inter-annual timescale.

The persistence characteristics of the observed hydrological anomalies have been analyzed by using their auto-correlation and spectral density functions (Figure 3.6). As observed from Figure 3.6, the correlation timescales of atmospheric moisture convergence and precipitation are shorter than 1 month (i.e., within one lag), whereas the correlation timescales of soil moisture, groundwater level, and streamflow are about 3, 12, and 3 months, respectively. As the circulation anomalies propagate through the system, the high frequency contributions to the hydrological signal are smoothed out and their contributions to the overall variance are reduced. This is indeed true for the propagation of the signal from the atmospheric circulation to precipitation, to the soil moisture, and then to the groundwater levels (see Figure 3.5). The soil water reservoir and groundwater reservoirs act as two adjacent low-pass filters of the atmospheric forcing as it propagates through the hydrological cycle. However, the fluctuations in streamflow reflect the variability in precipitation (through the surface runoff production mechanisms) as well as the

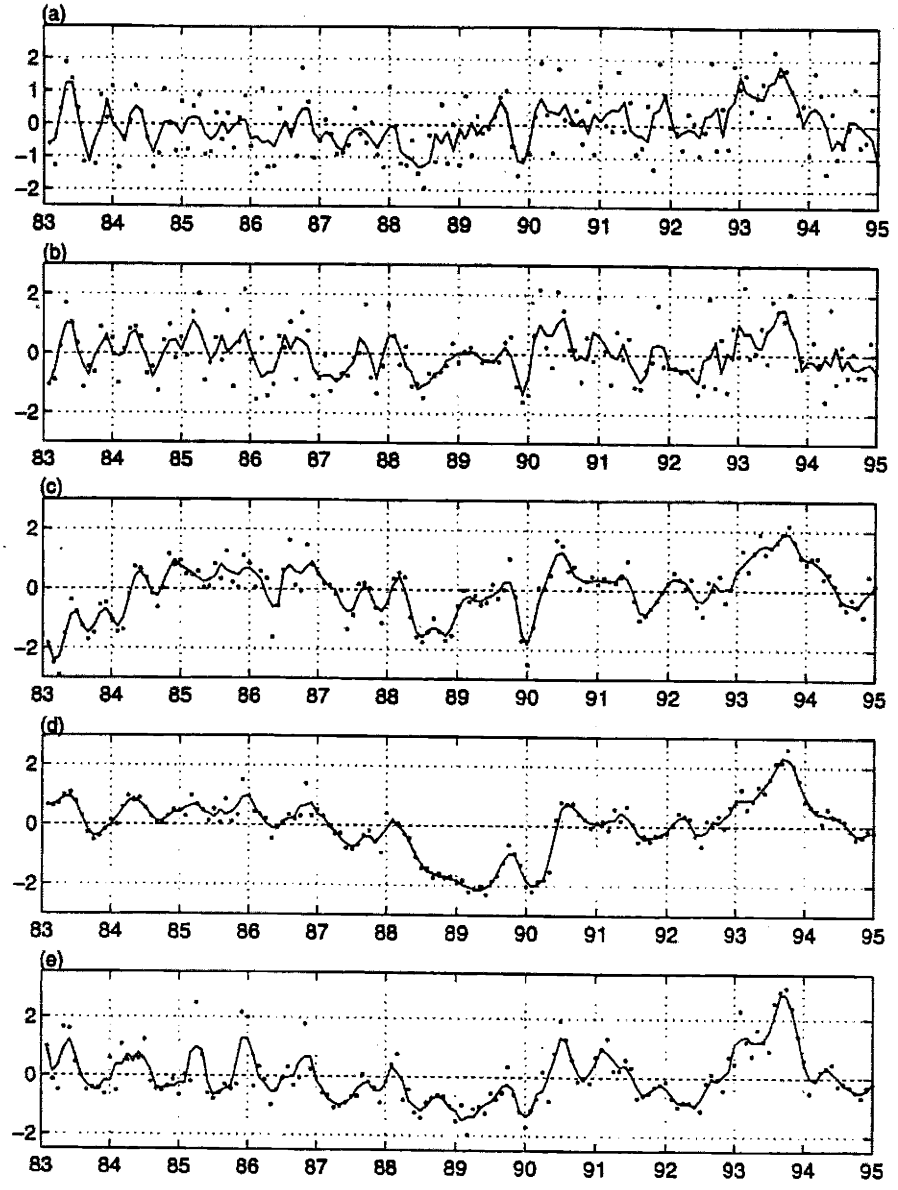

Figure 3.5 12-year (1983-1994) monthly time series of the normalized anomalies of (a) atmospheric moisture convergence, (b) precipitation, (c) soil moisture content, (d) groundwater level, (e) streamflow from 1983 to 1994 in Illinois. The continuous line is a 12-month moving average.

groundwater level (through groundwater runoff). As a result fluctuations in streamflow are richer in the high frequency components compared to groundwater level fluctuations.

Several small-scale droughts and floods with anomaly magnitudes of about 1 standard deviation and duration of about few months characterize the first 5 years of this analysis (1983 to

1987). Although the magnitude of any of these events is rather small, each hydrological anomaly leaves a clear signature on all the hydrologic variables considered (as seen in Figure 3.5). Moreover, the degree of persistence in these anomalies increases as they propagate through the soil hydrology, from the initial forcing by the atmospheric circulation to the eventual response by the groundwater aquifer.

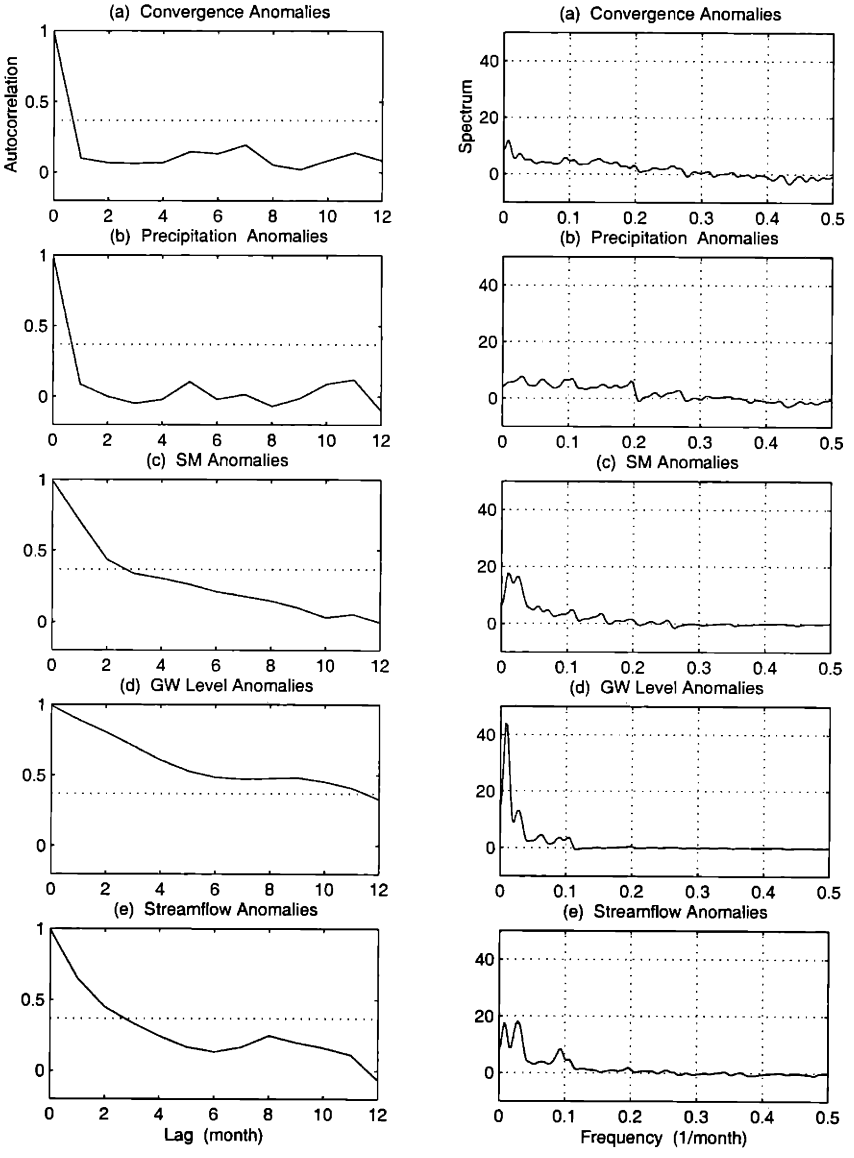

Figure 3.6 The auto-correlation function and the corresponding spectrum of the normalized anomalies of 12-year (1983-1994) monthly (a) atmospheric moisture convergence, (b) precipitation, (c) soil moisture content, (d) groundwater level, (e) streamflow in Illinois. The dashed line (i.e., correlation coefficient =1/e=0.367) line in the auto-correlation plot is the e-folding correlation timescale.

The following seven years (1988 to 1994) were marked by the occurrence of two extreme summer anomalies: the drought of 1988 and the flood of 1993. Both events were associated with hydrological anomalies that had magnitudes of about two standard deviations and extended for about a year. The response of the hydrological cycle to these two events will be examined in some detail as examples for significant summer floods and droughts. The drought of 1988 was triggered by anomalous divergence in the atmospheric circulation that started in February of 1988 and continued for most of the spring and summer seasons of 1988. A similar anomaly in precipitation was observed starting early spring and extending through the spring and summer seasons. However, the corresponding soil moisture anomaly persisted longer and dry conditions were observed throughout the spring, summer, and fall seasons of 1988. The response of the groundwater level was even more dramatic, with relatively low levels persisting until the end of the fall season of the following year. Another drought episode that occurred in the fall of 1989, triggered a further decrease in the aquifer level, before full recovery during 1990. The observed anomalies on precipitation and groundwater level left clear signatures on observed streamflow.

The 1993 flood was triggered by anomalous atmospheric convergence that started during the fall of 1992 and persisted for about a year, resulting in a precipitation anomaly with a similar persistence pattern. However, the corresponding soil moisture anomaly persisted throughout the spring, summer, fall and winter seasons, and well into the following year and up to the early summer of 1994. The level of water in the groundwater aquifer experienced a persistent rising trend starting in the fall of 1992, and continuing for about a year until the fall of 1993, when it leveled off, followed by a sharp decline, and eventually returned to normal levels during the spring of 1994. The corresponding pattern of streamflow anomaly was very similar to that of the groundwater level anomaly suggesting a strong association between the two variables during this wet episode.

The patterns of hydrological anomalies in soil moisture content for the 1988 drought and 1993 flood will be compared. The 1993 flood left a significantly more persistent signature on the soil moisture content when compared to the signature of the 1988 drought. While the soil moisture content returned to its normal levels by the end of 1988, a similar recovery did not occur until the early summer of 1994. Although, some difference in the recovery patterns would

be expected as a result of different characteristics of the two precipitation anomalies, the large differences between the observed patterns invite additional explanations. The climatology of the regional hydrological cycle (see Figure 2.6) indicates that the fall and winter seasons are the wet seasons for soil hydrology, when precipitation exceeds evaporation by a large magnitude. This surplus helps in first replenishing the soil water reservoir, from the normally dry summer conditions to the normally wet winter conditions, and then in recharging the excess water to the groundwater reservoir. Following the summer drought of 1988, the soil moisture recovered to normal levels quickly, however the groundwater level continued to decline throughout the following fall and winter seasons. This contrast suggests that the normal rainfall levels observed during the fall and winter seasons of 1988, were consumed in replenishing the anomalous dry summer conditions back to the normal winter soil moisture conditions, at the expense of the normal rate of recharge to the groundwater levels. As a result the groundwater levels continued to decline as observed. In comparison, under the usual conditions of low evaporation during the fall and winter of 1993, the recharge from the soil water reservoir to the aquifers was not efficient enough to dissipate the wet soil moisture anomaly. As a result, the wet soil moisture anomaly persisted until the onset of the following summer season.

The response of the groundwater level to the 1988 drought and 1993 flood was exactly opposite to that of soil water reservoir. A more persistent dry anomaly was observed in 1988 compared to a less persistent wet anomaly in 1993. The observations on streamflow show a wet anomaly of extreme magnitude and short duration that took place in the late summer and early fall of 1993. This event was followed by a sharp decline in groundwater level suggesting that groundwater runoff acts as an efficient dissipation mechanism of wet anomalies in groundwater levels. The association between anomalies in streamflow and groundwater level is less evident during the long recession of aquifer level in 1988 and 1989. There is no apparent negative feedback that could act as a dissipation mechanism for the drought conditions.

3.2.2 Application of the Crossing Theory to the Study of Floods and Droughts in Illinois

The crossing theory was first developed by *Rice* [1945] for analysis of the statistical properties of random noise, and was extended by *Cramer and Leadbetter* [1967]. The previous application of the crossing theory in hydrology has been summarized by *Bras and Rodriquez-Iturbe* [1985, pp. 240-261]. The theory deals with the properties of excursions of random processes, say, a hydrologic time series of runoff, above (i.e., floods) or below (i.e, droughts) a certain threshold value of the processes [*Bras and Rodriguez-Iturbe*, 198, pp. 240-261; *Nordin and Rosbjerg*, 1970]. It provides a definitive measure of persistence in hydrological time series. Figure 3.7, taken from *Bras and Rodriguez-Iturbe* [1985], shows a discrete time series, *Y(t)*, normalized to have zero mean and unit variance. The quantities of interest in the figure are: (1) the time between upcrossing or downcrossing (B_u^+ or B_u^-), which measures the frequency of occurrence of the floods (droughts); (2) the expected interval between zero crossings (l_0), which measures the persistence of floods (droughts); (3) the duration of excursions above or below a certain threshold value (l_u^+ or l_u^-), which measures the duration of a hydrological anomaly (floods or droughts) with certain magnitude; and (4) the area of an excursion above or below the

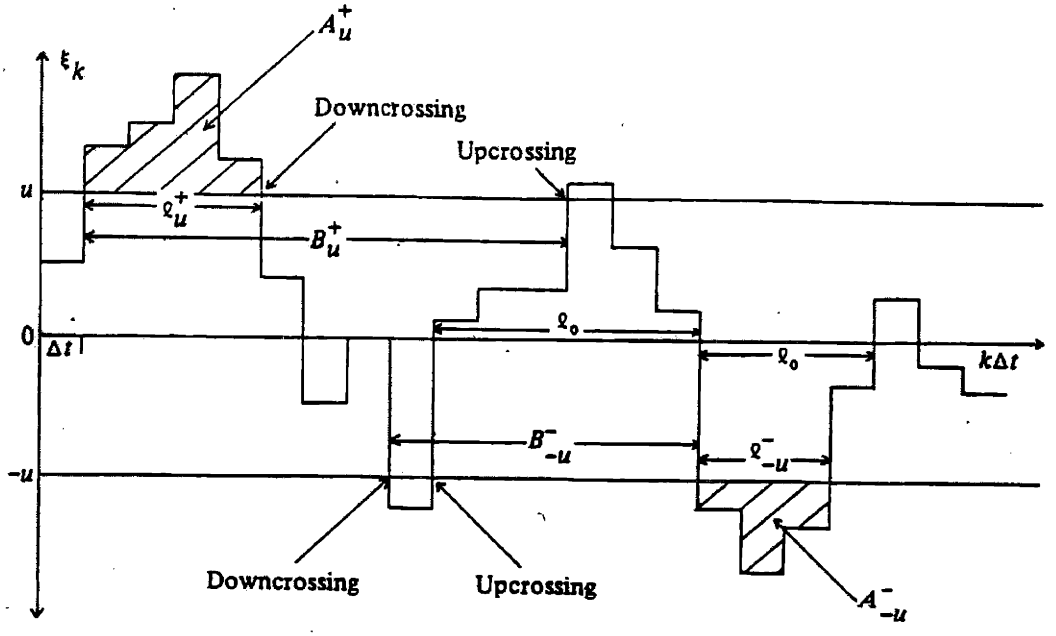

Figure 3.7 Discrete time series, normalized to have zero mean and unit variance. The figure shows all the relevant variables that are needed to describe a time series using crossing theory (see text for the definitions of all the variables). (From *Bras and Rodriguez-Iturbe* [1985])

threshold level (A_u^+ or A_u^-), which measures the cumulative magnitude of a hydrological anomaly above a threshold value, u. Given a hydrologic time series with sufficient length, all these crossing statistics, B_u^+, B_u^-, l_0, l_u^+, l_u^-, A_u^+ and A_u^-, are easily estimated. The analytical formula of these crossing statistics available has been developed for Gaussian processes. For a non-Gaussian process (with skewness coefficient large than about 0.2, *Nordin and Rosbjerg*, 1970), significant difference from the theoretical derivation would be anticipated depending on the degree of the deviation from the normality assumption.

A useful absolute measure of persistence is the ratio $E[l_u^+]/E[l_0]$, which measures the average duration of floods or droughts in terms of the length between zero crossings. For a discrete process with lag-one autocorrelation, this ratio can be derived theoretically as following [*Nordin and Rosbjerg*, 1970, Eq. 26]:

$$\frac{E[l_u^+]}{E[l_0]} = \frac{[\frac{1}{2} - (\frac{1}{\pi})\arcsin\phi(1)]pr\{Y > u\}}{pr\{Y > u\} - pr\{Y_1 > u, Y_2 > u\}} \tag{3.1}$$

Where the $\phi(1)$ is the value of autocorrelation of Y for the first lag interval. The probability distribution function (PDF) of Y, and the joint PDF between two arbitrary Y values, Y_1 and Y_2, are written as

$$pr\{Y > u\} = \frac{1}{\sqrt{2\pi}} \int_u^\infty e^{-\frac{1}{2}x^2} dx \tag{3.2}$$

$$pr\{Y_1 > u, Y_2 > u\} = \frac{1}{2\pi[1-\phi(1)^2]^{\frac{1}{2}}} \int_u^\infty \int_u^\infty \exp\left\{-\frac{u_1^2 - 2u_1u_2 + u_2^2}{2[1-\phi(1)^2]}\right\} du_1 du_2 \tag{3.3}$$

Another useful absolute measure, the expected value of A_u^+, can be estimated by dividing the area above (or below) an excursion level u by the number of excursions above (or below) u. For

a continuous Gaussian process, this quantity can be derived as [*Bras and Rodriguez-Iturbe*, 1985, p. 245]

$$E[A_u^+] = 2E[Z_1(T)]E[l_0]e^{u^2/2\sigma^2} \tag{3.4}$$

where

$$E[l_0] = \pi[\frac{\rho(0)}{2\rho(1)-2}]^{\frac{1}{2}}$$
$$E[Z_1(T)] = \frac{1}{\sigma\sqrt{2\pi}}\int_u^\infty (x-u)e^{-x^2/2\sigma^2}dx \tag{3.5}$$

slight modification is needed to apply (3.4) and (3.5) to a discrete time series such as annual streamflow records.

The $E[l_u^+]/E[l_0]$ in (3.1) provides an absolute measure of the average persistence in a hydrologic anomaly, whereas $E[A_u^+]$ provides an absolute measure of the mean magnitude of a hydrologic persistence above (or below) an anomaly level.

The relevant crossing statistics (i.e., $E[l_u^+]/E[l_0]$ and $E[A_u^+]$ here), can also be derived by Monte Carlo method. This is done by repetitive simulation of the time series having the identical statistical properties of the underlying random process. Although the analytical expressions for the confidence interval of $E[l_u^+]/E[l_0]$ and $E[A_u^+]$ are not available in literature, they can be inferred from the standard deviation of the simulated results by Monte Carlo simulation. First, 100 realizations of auto-regression AR(1) process were generated with zero-mean and unit variance, as well as the identical length and same lag-one autocorrelation coefficient as the original process, i.e., 27-year time series of precipitation and groundwater level. The same procedures of computing $E[l_u^+]/E[l_0]$ and $E[A_u^+]$ were performed with respect to these 100 realizations. The ensemble average was found to be exactly same with the theoretical results

given by (3.1)-(3.5). The one standard deviation, equivalent to the confidence interval, quantifies the statistical significance of the deviation in one single realization from the ensemble average behavior. For a Gaussian process, the crossing statistics should fall within the computed confidence interval.

In this section we use expanded data sets on precipitation and groundwater level covering the common period of 1970-1996 (see Figure 3.8). The state average variables are transformed into standardized anomalies by subtracting the monthly mean and then dividing by the corresponding standard deviation for that month. Floods (droughts) are characterized by the excursions of the anomalies above (below) a certain threshold. For floods we use positive thresholds; for droughts we use negative thresholds.

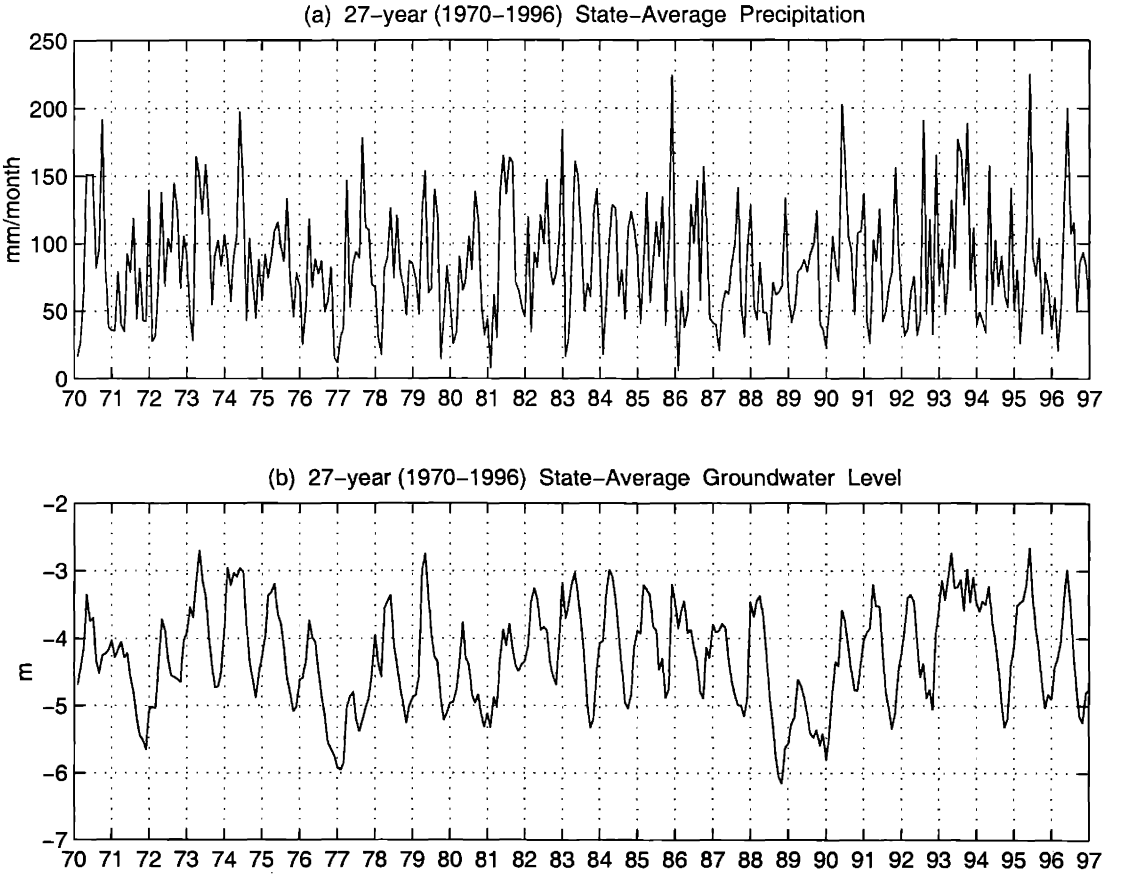

Figure 3.8 Time series of (a) precipitation and (b) groundwater level (1970-1996) from Illinois.

Figure 3.9 shows estimates of the average size of floods and droughts corresponding to different threshold levels. For precipitation, observed floods are consistently larger than the corresponding Gaussian floods, while observed droughts are smaller than the corresponding Gaussian droughts. This difference is interesting and is in general consistent with the positively skewed distribution of precipitation anomalies (not shown here). Identification of the physical mechanisms that are responsible for these statistical characteristics is an open subject for future research. For the groundwater level we observe a pattern of asymmetry that is the reverse of the pattern in precipitation anomalies: observed droughts are consistently larger than the corresponding Gaussian droughts, while observed floods are consistently smaller than the corresponding Gaussian floods.

A similar analysis was performed on another important characteristic of the observed floods and droughts: duration. We compared observed duration to the corresponding expected duration for Gaussian floods and droughts (see Figure 3.10). Again we see a reversal in the pattern of the observed asymmetry when comparing precipitation and groundwater level. Droughts (floods) are more (less) persistent in observed groundwater level than in the corresponding Gaussian process. This observed tendency for an increase (decrease) in the persistence and magnitude of droughts (floods) as they propagate from the atmosphere to the aquifer is an important characteristic of the regional hydrological cycle.

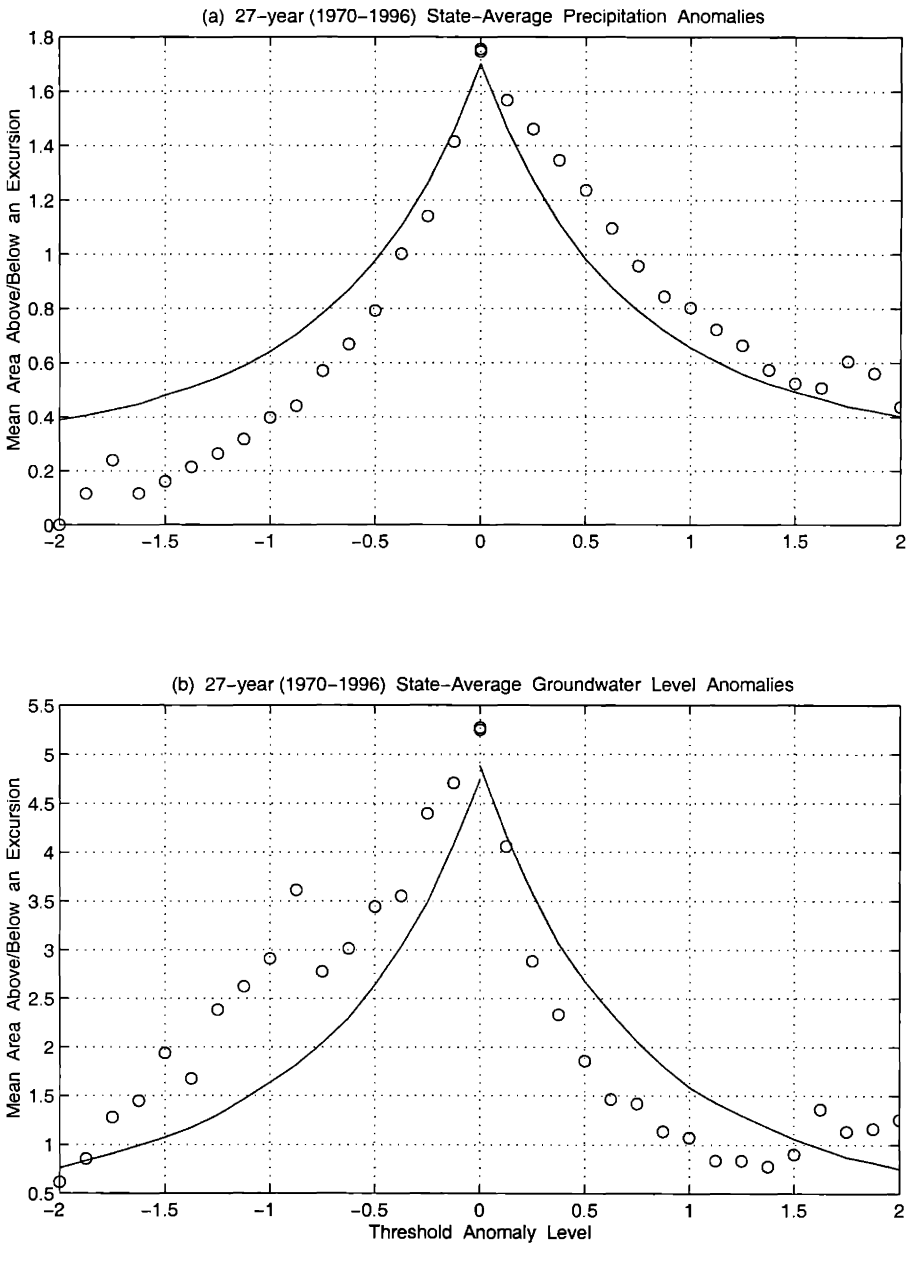

Figure 3.9 Mean area above (below) an excursion corresponding to positive (negative) threshold levels for (a) precipitation and (b) groundwater level. Circles are estimates from the observations of Figure 2.20. Continuous lines describe the theoretical relations for a symmetrical Gaussian stochastic process that has the same mean, standard deviation, and autocorrelation coefficient at lag 1.

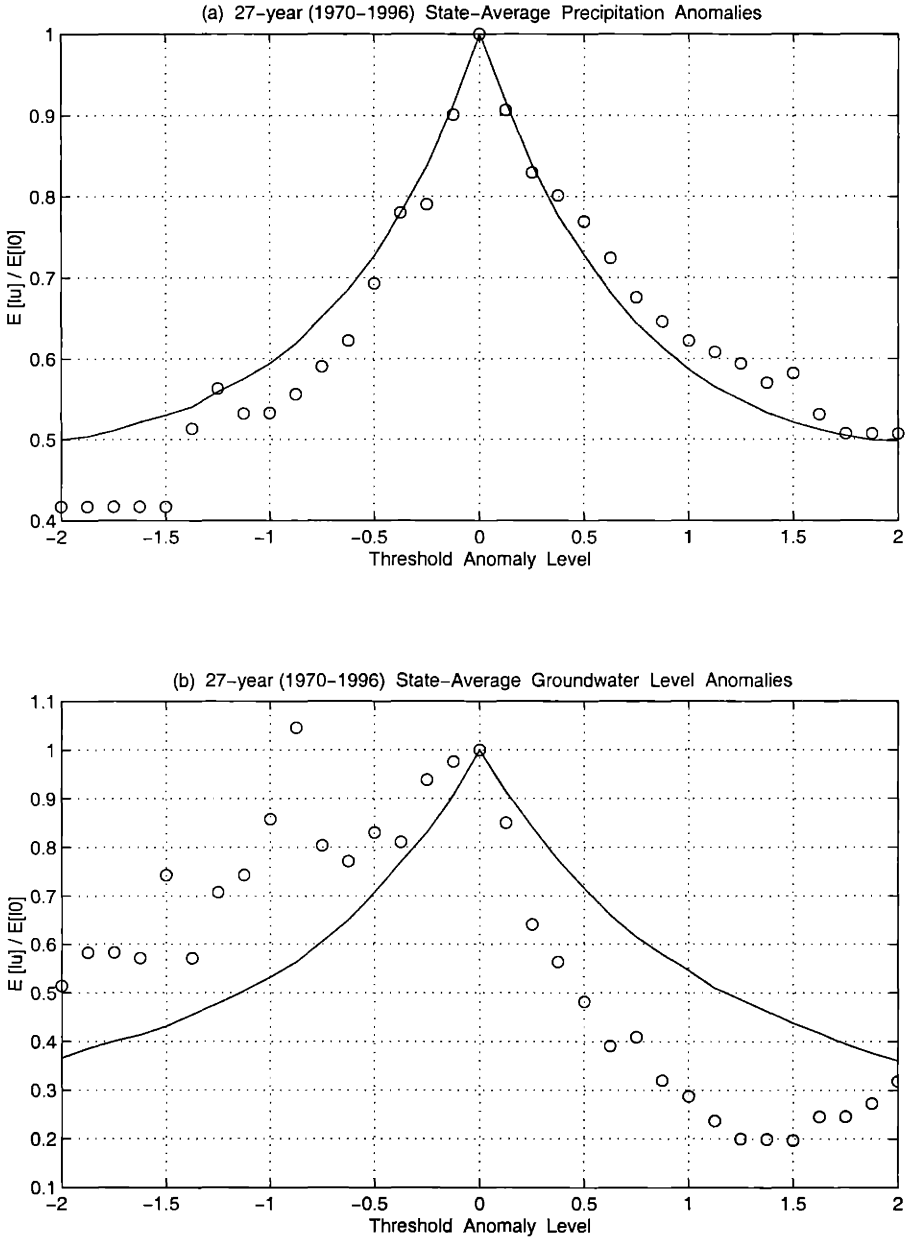

Figure 3.10 Normalized mean duration above (below) an excursion corresponding to positive (negative) threshold levels for (a) precipitation and (b) groundwater level. Circles are estimates from the observations of Figure 3.8. Continuous lines describe the theoretical relations for a symmetrical Gaussian stochastic process that has the same mean, standard deviation, and autocorrelation coefficient at lag 1.

3.2.3 Physical Basis of the Asymmetric Response of Aquifers to Floods and Droughts

In the previous sections we presented empirical evidence for the asymmetric response of aquifers to floods and droughts in Illinois. In this section we analyze the physical mechanisms that are responsible for these empirical observations. We propose that the nonlinear form of the groundwater-rating curve (i.e., functional relationship between groundwater discharge to the stream and groundwater level) is the key factor responsible for the different patterns of persistence that have been observed during floods and droughts. This nonlinearity is attributed mainly to the interactions between the groundwater level and the density of the stream channel network.

Here we perform a simple analysis of groundwater level fluctuations to support the hypothesis that the observed asymmetric response of aquifers is a natural result that follows from the nonlinear form of the groundwater-rating curve.

First, we need to characterize the groundwater-rating curve in Illinois. As shown in Figure 3.1b, the monthly streamflow is significantly more correlated to aquifer levels than to precipitation. Thus, an assumption can be made that Figure 3.1b describes reasonably well the general patterns of the relationship between groundwater flow and groundwater level. In Figure 3.1b, starting with the median of the observed groundwater levels (≈ -3.3 m, see Table 2.2), changes in H towards higher water levels are associated with a relatively large increase in observed streamflow per unit rise in groundwater level. However, changes in H toward lower water levels are associated with a significantly smaller sensitivity of observed streamflow. Precisely for this reason, we propose that groundwater aquifers act selectively to dissipate the wet anomalies in groundwater levels such as those experienced in 1993. Under the relatively dry conditions similar to those of 1988 and 1989 the groundwater runoff does not respond significantly to the drop in groundwater levels (see Figure 3.5). The only recovery mechanism for groundwater level is through occurrence of anomalous wet conditions, such as those experienced during the winter and spring seasons of 1990 leading to the eventual recovery from the drought conditions.

The hypothesis that the groundwater aquifers act selectively to dissipate wet anomalies, resulting in the observed asymmetric response of the groundwater level to droughts and floods, has been studied using a simple model of the groundwater aquifer. A lumped model of water level fluctuations in an unconfined aquifer is described by

$$S_y \frac{dH}{dt} = G - Q_g \tag{3.6}$$

where S_y is the specific yield, H is the groundwater level, G is the percolation (recharge) to the groundwater level and Q_g is the rate of groundwater runoff. In addition, we propose the following simple linear function to relate Q_g and H:

$$Q_g = Q_0 + K(H - H_0) \tag{3.7}$$

where H_0 is a constant reference level, Q_0 is the corresponding discharge level, and K is an outflow coefficient which is inversely proportional to the timescale of aquifer response. The observed relationship between Q_g and H is nonlinear (see Figure 3.1b). For this reason, (3.7) is not suitable to describe the observed aquifer system in Illinois. However, this linear function approximates the different segments in the observed relationship between Q_g and H such that K increases as we move from drought conditions into flood conditions. Studying the behavior of this simple system illustrates how the nonlinear form of the relationship between Q_g and H is responsible for the asymmetry in the response of the aquifer to floods and droughts. In order to estimate typical value of K, the data points in Figure 3.1b are divided into two groups: H > -4m and H < -4m. Then, two values of K were derived by linear regression analysis: K=0.006 for the dry condition (droughts) and K=0.025 for the wet condition (floods), a factor of 4 differences between wet and dry conditions (see Figure 3.11).

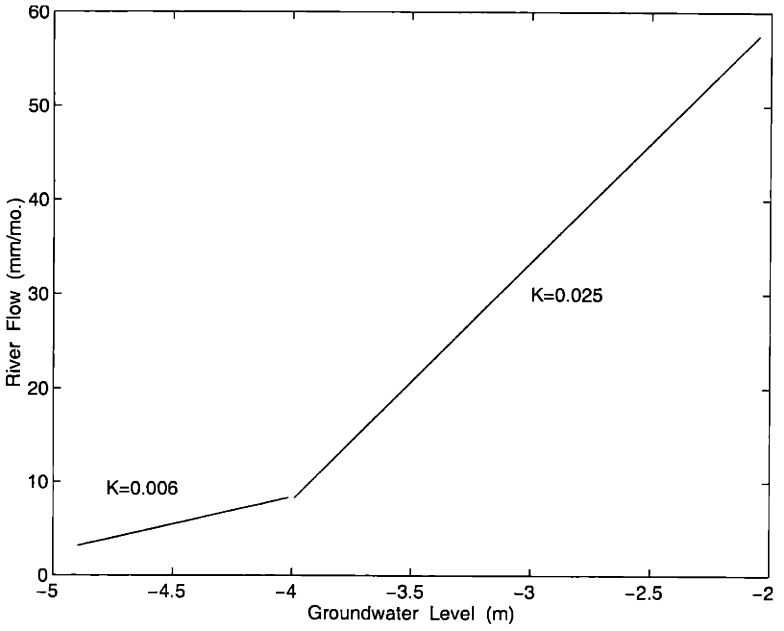

Figure 3.11 Linear representation of the relationship between streamflow and groundwater level obtained by performing a linear regression analysis of the data in Figure 3.1b.

The combination of (3.6) and (3.7) results in a simple linear model for groundwater level fluctuations as follows

$$S_y \frac{dH}{dt} = G - [Q_0 + K(H - H_o)] \tag{3.8}$$

This equation will be analyzed using stochastic analysis techniques after assuming that natural variability in recharge can be described by a stochastic process. The same equation can be analyzed deterministically. We choose to apply statistical analysis tools in order to achieve a realistic description of the natural variability of the groundwater system. The model of (3.8) is analogous to a first-order Markov process, except that the forcing G is not limited to be a pure random process. A similar model has been used to describe the response of phreatic aquifers to natural recharge by *Gelhar* [1993, p.64-70], assuming the outflow coefficient K to be a constant. Here we will consider the following two cases: K is large, corresponding to flood conditions, for which (3.8) describes a strongly dissipative system, and K is small, corresponding to drought conditions, for which (3.8) describes a weakly dissipative system.

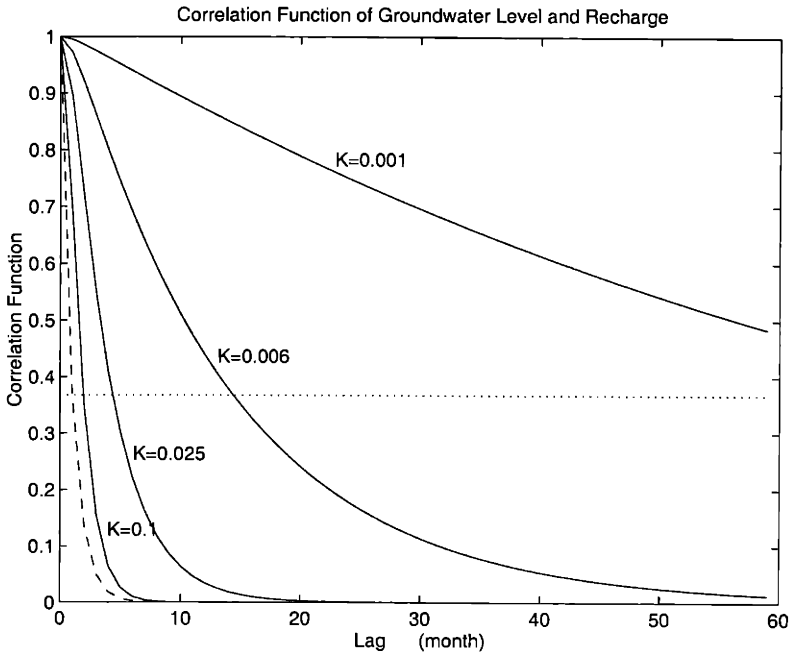

Figure 3.12 The autocorrelation function of groundwater level for several value of outflow constant K. The dotted line denotes the e-folding correlation timescale. (The correlation timescale of recharge is assumed to be 1 month).

The stochastic analysis of (3.8) is described in Appendix B. We assume that the forcing G is a stochastic process described by an exponential covariance function. Figure 3.12 shows the resulting covariance function of groundwater level $R_{hh}(\tau)$ for several values of outflow coefficient K. As K increases from 0.006 to 0.025 (see Figure 3.11) the correlation time scale of groundwater level decreases from about 14 months to 5 months. This is consistent with the observed difference in the persistence pattern of floods and droughts in Illinois. The dependence of the correlation time scale of groundwater level on K is shown in Figure 3.13 for a range of K values covering different conditions from droughts to floods. Decreasing K from K=0.1 to K=0.01 increases gradually the correlation timescale of groundwater level from about 1 to 9 months. A further decrease in K results in sharp increases in correlation timescale to a few years.

Functional expressions (other than (3.7)) describing the nonlinear relationship between groundwater runoff and groundwater level have been incorporated into the stochastic analysis using linearization technique. Although quantitative differences exist, the response of the

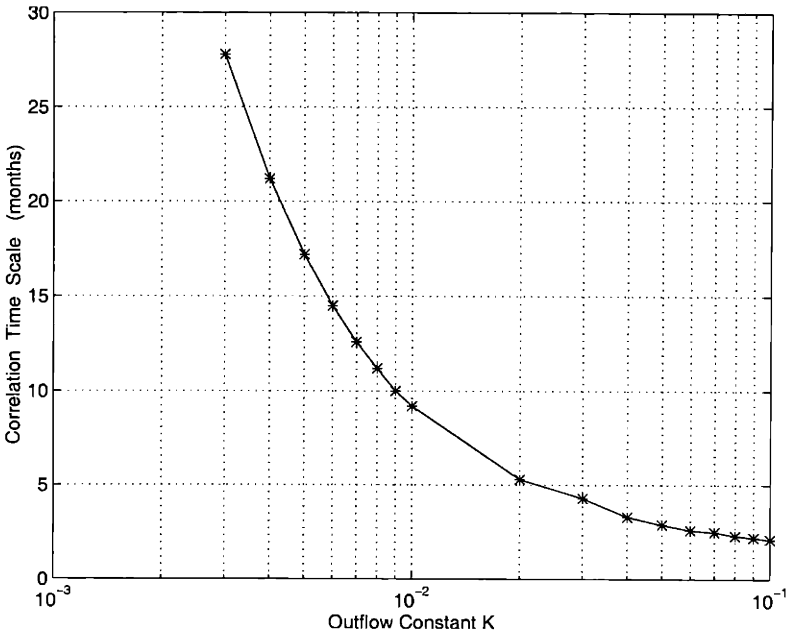

Figure 3.13 Plot of correlation timescale of groundwater level as a function of outflow constant K. (The correlation timescale of recharge is assumed to be 1 month).

groundwater aquifer to different anomalies is qualitatively similar regardless of the function used to describe the relationship between groundwater runoff and groundwater level. Similar results have also been obtained by assuming other types of covariance function (e.g., hole-type function) for the recharge instead of the exponential function in (A4). In summary, the asymmetric response of groundwater aquifers to hydrological anomalies can be explained as being due to the nonlinear form of groundwater rating curve.

Similar mechanisms for dissipation of anomalies have been identified for other meteorological and hydrological systems. For example, the large-scale long-term sea surface temperature anomalies can be explained as the response of the ocean to random short time-scale atmospheric forcing [*Hasselmann*, 1976]. Here, the dissipation mechanism is provided by the dependence of latent heat and sensible heat fluxes on sea surface temperature. Soil moisture anomalies can be conceived as the response of the soil reservoir to short time-scale precipitation forcing [*Delworth and Manabe*, 1988]. Here, the dissipation mechanism is provided by linear dependence of evaporation on soil moisture state. Similarly, groundwater aquifer anomalies result from short time-scale random forcing of recharge. However, the nonlinear nature of the

dependence of groundwater runoff on groundwater level results in the observed asymmetric response of groundwater level to droughts and floods.

3.2.4 Physical Basis of the Nonlinear Groundwater Rating Curve

Here we would like to discuss the physical basis of the nonlinearity in the groundwater rating curve. We consider a simple unconfined rectangular aquifer placed in a horizontal impermeable layer draining into a fully penetrating stream, (see Figure 3.14). Although this model is rather simple in comparison to the complexity of the natural system, studying the basic behavior of this model may offer some insight regarding the main physical factors in shaping the form of the groundwater rating curve. *Troch et al.* [1993] developed the following asymptotic relationship for describing the discharge into a channel of length L:

$$q_g \sim k h_r^2 D_d L \tag{3.9}$$

Where k is the hydraulic conductivity, h_r is the average groundwater level in this rectangular aquifer, D_d is the drainage density (total length of channels per unit area), and L is the total length of the channels, The same relationship can be expressed differently to describe the discharge per unit area,

$$Q_g \sim k h_r^2 D_d^2 \tag{3.10}$$

The dynamics of baseflow in this model reflect the dynamics in groundwater level fluctuations and the density of the drainage network, which is assumed to be constant in this simple model. These two factors appear explicitly in the above equation. The direct dependence of baseflow on the average groundwater level is regulated by the relative size of the fluctuations in groundwater level to the average depth of the aquifer, In locations where this ratio is relatively large, fluctuations in groundwater level are reflected significantly in h_r and baseflow. Otherwise, these

fluctuations would have a small impact on these variables and the direct dependence of baseflow on groundwater level can be approximated by a linear relationship.

However, in natural systems drainage density is a dynamic variable varying significantly as the channel network expands and contracts in response to fluctuations in groundwater level. Thus the following connection, rise in groundwater level $\rightarrow$ enhancement of drainage density $\rightarrow$ increase in baseflow, may provide an indirect pathway for relating groundwater level and baseflow. This pathway would tend to enhance, and under most conditions would even dominate, the relationship between groundwater level and baseflow. This is particularly true when the ratio of the fluctuations in groundwater level to the average saturated depth of the aquifer is of relatively small magnitude. Under those conditions variability in h_r would be insignificant. Figure 3.15 illustrates the relationship between drainage density and groundwater level. As the level of water rises, the groundwater table intersects with more and more sections of the river network. These sections then provide additional outlets for the aquifer to discharge water into streams. At the same time, a relatively dense drainage network favors a larger sensitivity of the hydraulic gradients to fluctuations in groundwater level. The geomorphology of the hillslopes and river networks play a significant role in dictating the nature of the dynamic relationship between groundwater level and drainage density.

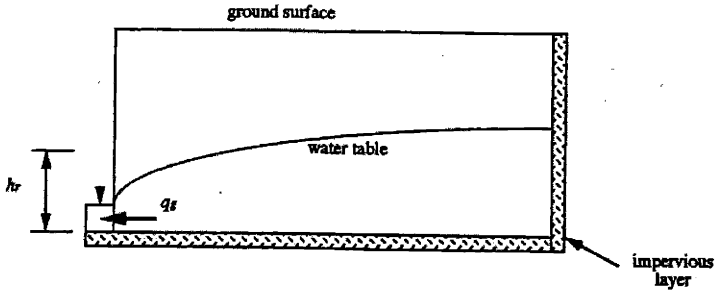

Figure 3.14 A schematic figure describing the simple groundwater flow configuration that has been measured in developing equation 3.9.

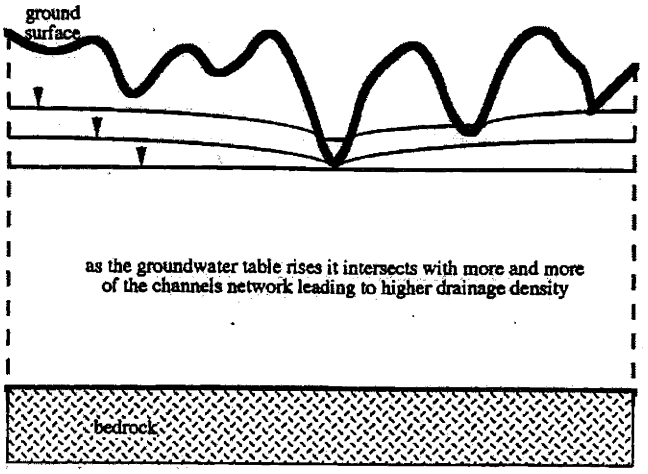

Figure 3.15 A schematic figure that illustrates the relationship between groundwater level and drainage density.

In Illinois the amplitude of the fluctuations in groundwater level varies between the different regions with a typical magnitude of a few meters. The saturated aquifer thickness varies significantly in the different geological zones. However, a typical scale would be in the order of a few tens of meters (see Appendix A). As a result, the ratio of the fluctuations in groundwater level to the average saturated depth of the aquifer would be of relatively small magnitude. Hence most likely the dependence of drainage density on groundwater level is the dominant pathway in shaping the nonlinear relationship between groundwater level and baseflow.

3.3 Estimation of the Regional-scale Groundwater Recharge

Recall that in Section 2.1 the surface/subsurface water balance equation (2.3) is the sum of the unsaturated zone water balance equation (2.1) and the unconfined aquifer water balance equation (2.2). The only connection between these two subsurface reservoirs is through the groundwater recharge flux (P_g) whose measurement is usually unavailable. In this section, we estimate the regional-scale groundwater recharge flux in Illinois in order to characterize the interactions between the soil moisture reservoir and groundwater reservoir. Groundwater evaporation is defined here as the water flux supplied from groundwater aquifer to the root-zone soil moisture for the subsequent evaporation use. Thus, negative groundwater recharge indicates the occurrence of groundwater evaporation. It is meaningful to explore if the groundwater evaporation contributes to the high rate of evaporation during the summer months in Illinois ($\cong$ 120 mm/month) as estimated in Section 2.3.

3.3.1 Literature Review

Recharge rates for aquifers must be estimated before groundwater resources can be evaluated and the impacts of aquifer development can be forecasted. In humid climates, water table often lies within several meters beneath ground surface and recharge from direct infiltration of precipitation can vary between 20%-50% or more of the mean annual precipitation [*Stephens*, 1996]. Groundwater recharge generally occurs in the period from the late fall through next spring [*Sophocleous and Perry*, 1985; *Mau and Winter*, 1997], whereas little recharge takes place during summer months due to high evapotranspiration rates. Abundant studies on groundwater recharge can be found in the hydrological literature; see the reviews by *Allison* [1988], *Gee and Hillel* [1988] and *Stephens* [1996, Chapter 2]. In the shallow water table areas, the large deficit in the root-zone soil moisture in summer exerts capillary force resulting in upward water flux from the aquifer to the root zone. From the analysis of observed recharge events in Kansas, *Sophocleous and Perry* [1985] found that under a shallow water table condition about 70% of the springtime recharge is lost by evapotranspiration during the subsequent summer and fall. Moreover, in many places groundwater is an important source of water for plant growth [e.g.,

Schmidhalter et al., 1994]. Plants can extract the moisture from the shallow water table for transpiration consumption during the growing season. *Maraux and Lafolie* [1998] found in a maize-sorghum cropland of Nicaragua that during the drought periods, the upward water flux reached 2 mm/day while the actual evapotranspiration of the crop is 2~4 mm/day. They concluded by stressing the importance of capillary rise in providing a significant part of water for crop transpiration use.

In contrast to groundwater recharge, groundwater evaporation has not been a widely explored subject. From a laboratory soil column measurement of evaporation, *Shaw and Smith* [1927] found that evaporation in Yolo loam soil is significant when groundwater table is less than 3 meters deep. *Remson and Fox* [1955] demonstrated that the discharge of groundwater by evapotranspiration from the shallow water table could be estimated by suitable application of the Richards equation. They identified the depth to water table as the most dominating factor that affects the ability of a particular soil to raise water to ground surface. *Gardner* [1958] showed analytically that the steady-state evaporation rate from a soil in the presence of a water table depends on the depth to water table, the soil capillary conductivity, and the capillary potential at ground surface. *Gardner and Fireman* [1958] found a good agreement between the laboratory measurements of evaporation and the theoretical solution of *Gardner* [1958]. They showed that for Chino clay and Pachappa sandy loam the evaporation rate decreases significantly as water table depth decreases from 1 to 3 meters below the surface. Moreover, they found upward movement and evaporation of water is possible with the water table as deep as more than 10 meters. *Willis* [1960] extended *Gardner* [1958]'s analytical analysis to a two-layered soil system in a shallow water table condition.

At the local scale, *Tschinkel* [1963] and *Daniel* [1976] estimated the magnitude of groundwater evaporation as only 0.04 mm/day and 0.17 mm/day, respectively. *Zecharias and Brutsaert* [1988] also reported small rates of groundwater evaporation (0.05-0.3 mm/day) from the investigation of 19 drainage basins in the Appalachian Plateaus. They concluded that groundwater evaporation constitutes only a minor portion of total basin evaporation. In contrast, significant groundwater evaporation has also been reported from field studies in playa environments where the water table approaches the ground surface. From an investigation of

groundwater inflow to a dry salt lake located in South Australia, *Allison and Barnes* [1985] estimated the range of groundwater evaporation varies between 90 and 230 mm/year with a mean of 170 mm/year. From a similar playa area in Australia, *Ullman* [1985] inferred from the analyses of the chloride and bromide profiles that the net groundwater evaporation rates lies between 9-28 mm/year. *Malek et al.* [1990], using Bowen-ratio method, estimated groundwater evaporation of 229 mm/year from a moist playa in a closed desert basin in eastern Utah. More recently, *Taylor et al.* [1997] compared three techniques in the estimation of groundwater evaporation at Owen Lake in the eastern California with annual precipitation of merely 100-140 mm. They concluded that mean groundwater evaporation from the playa surface ranges as large as 88~104 mm/year.

The observational evidences (*Sophocleous and Perry*, 1985; *Schuh et al.*, 1993; etc.) on the occurrence of upward water flux from the aquifer to the soil moisture are mostly for the small-scale watershed. Due to the complex spatial and temporal variability of the saturated-unsaturated zone interactions and the nonlinear physical processes involved, the significance of the groundwater evaporation at the regional-scale ($\sim 10^4 km^2 - 10^6 km^2$) hydrological cycle remains an open question. In section 3.3.2, we will estimate the regional-scale groundwater recharge flux using the water balance computation in conjunction with the multiple regression analysis. The major objective is to quantify the contribution of shallow groundwater to the regional-scale evaporation in Illinois. In section 3.3.3, we will present observational evidence on the occurrence of the regional-scale groundwater evaporation in Illinois based on the analysis of the observed soil moisture profiles.

3.3.2 Estimation of Regional Groundwater Recharge

In this section, the regional-scale monthly groundwater recharge flux in Illinois from 1983-1994 will be estimated by using water balance computations in conjunction with the regression analysis. It is expected that, if the mechanism of groundwater supply to evaporation is significant at the scale of Illinois, the estimated groundwater recharge flux would be negative during the summer months in Illinois.

For the readers' convenience, the regional-scale water balance equations for the soil moisture and for the unconfined aquifer (Section 2.3, Eqs. (2.1) and (2.2)) are repeated here respectively:

$$\overline{nD}\frac{\partial \bar{s}}{\partial t} = \bar{P} - \bar{E} - \overline{R_S} - \overline{P_G}$$

$$\overline{S_y}\frac{\partial \overline{H}}{\partial t} = \overline{P_G} - \overline{R_G}$$

There are 4 unknowns (evaporation E, groundwater recharge P_G, groundwater runoff R_G, and surface runoff R_S) in two equations. However, since the total runoff ($\bar{R} = \overline{R_S} + \overline{R_G}$) is known from streamflow records, E can be estimated by adding these 2 equations together as shown in Section 2.3:

$$\bar{E} = \bar{P} - (\bar{R} + \overline{nD}\frac{\partial \bar{s}}{\partial t} + \overline{S_y}\frac{\partial \overline{H}}{\partial t})$$

thus it reduces to 3 unknowns (P_G, R_G, and R_S) for the 2 water balance equations. Groundwater recharge P_G can be estimated if the measured streamflow can be separated into surface runoff and groundwater runoff components (i.e., hydrograph separation); but in general it is rather difficult to achieve. An alternative is to apply regression analysis. Since precipitation is the main forcing of surface runoff and aquifer level (H) is the main forcing of groundwater runoff, the hydrograph separation can be approximated with the aid of the regressions between streamflow, precipitation and groundwater level.

In the following, the relations between streamflow and other relevant hydrologic variables (precipitation, soil saturation degree, and groundwater level) are pursued using the multiple linear regression analysis. For simplicity, the seasonal dependence in the regression coefficients is not considered. The derived regression equations and the corresponding coefficients of determination, R^2, are summarized in Table 3.2. As shown in this table, groundwater level alone accounts for 64% of the variance in streamflow, while soil saturation and precipitation only

explain 38% and 11%, respectively. After combining soil saturation with groundwater level in the linear regression analysis, R^2 improves by only 1% due to the high correlation (R=0.69, Table 3.1) between soil saturation and groundwater level. Since the correlation between precipitation and groundwater level is weak (R=0.19, Table 3.1), it should be adequate to use the precipitation (as the surrogate of surface runoff) and the groundwater level (as the surrogate of surface runoff) as two independent variables in the regression equations. Considering the short timescale of the response of surface runoff, a linear relationship between surface runoff and precipitation is assumed: $R_S = \alpha P$, where α is the surface runoff coefficient. On the other hand, the dependence between groundwater runoff and groundwater level is nonlinear as shown in Figure 3.1b. Similar to the groundwater runoff formulation in the TOPMODEL [*Beven and Kirby*, 1979], groundwater runoff is parameterized here as:

$$R_G = R_0 \exp(-h) \tag{3.11}$$

where h is the distance from ground surface to water table, R_0 is the maximum groundwater runoff.

Therefore, streamflow can be expressed as:

$$R = R_S + R_G = \alpha P + R_0 \exp(-h) \tag{3.12}$$

Regression Equation	R^2
R= 0.13P +15.52	0.11
R= 189.11s -118.55	0.38
R= 20.16H +91.50	0.64
R= 0.11P +180.16s -120.27	0.44
R= 0.07P +19.29H +78.40	0.67
R= 39.38s +17.97H +54.25	0.65
R= 0.07P +41.32s +16.98H +43.48	0.68

P, R, s, and h is the precipitation, streamflow, soil saturation and groundwater level, respectively.

Table 3.2 The regression equations and the corresponding coefficient of determination (R^2) between streamflow and other water balance components

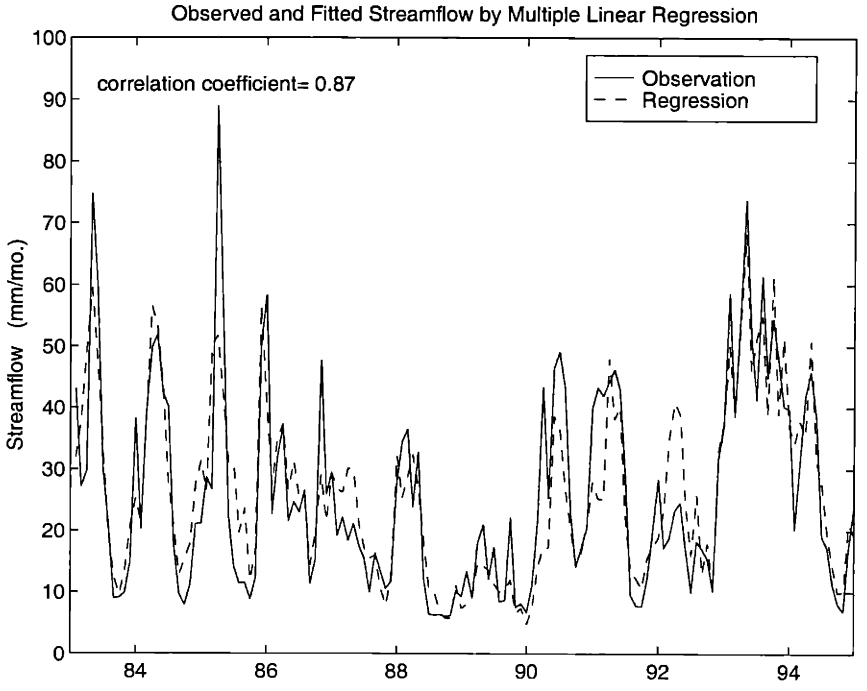

Figure 3.16 12-year (1983-1994) time series of observed streamflow versus fitted streamflow by using multiple linear regressions in Illinois.

Application of the multiple linear regression analysis to the 12-year (1983-1994) monthly data in Illinois yields the fitted streamflow: (R and P are in mm/month; h is in meter)

$$R_{fit} = 0.06P + 489.3\exp(-h) - 1.6 \tag{3.13}$$

with a high correlation coefficient of 0.87 between the observations and the fitted streamflow, R_{fit}, suggesting the variability in precipitation and groundwater level jointly explain about 75% of the variability in streamflow. The comparison between the fitted and the observed streamflow is given in Figure 3.16. As seen in this figure, the agreement between the fitted streamflow and the observations is remarkably well except the failure of the fitted streamflow to capture some flow peaks.

By comparing (3.12) to (3.13), the surface runoff coefficient α is estimated to be 0.06. Therefore, groundwater recharge flux can be calculated from (2.1):

$$\overline{P_G} = (1-\alpha)\overline{P} - \overline{E} - \overline{nD}\frac{ds}{dt} \tag{3.14}$$

or equivalently, from (2.2):

$$\overline{P_G} = \overline{R} - \alpha\overline{P} + \overline{S_y}\frac{d\overline{H}}{dt} \tag{3.15}$$

The seasonal cycle of the estimated groundwater recharge is plotted in Figure 3.17. The climatology of groundwater recharge exhibits two peaks and one trough. The first peak in March and the trough in August resemble the seasonal cycle of soil moisture (and also groundwater level) with a maximum in March and a minimum in August (Figure 2.4). Another peak of groundwater recharge in November is consistent with the maximum precipitation of a year. The 12-year monthly time series of groundwater recharge estimates range from –50 mm to 100 mm. The average annual groundwater recharge is 252 mm. (26% of precipitation), which is almost equal to the magnitude of groundwater runoff since the average 12-year average annual change

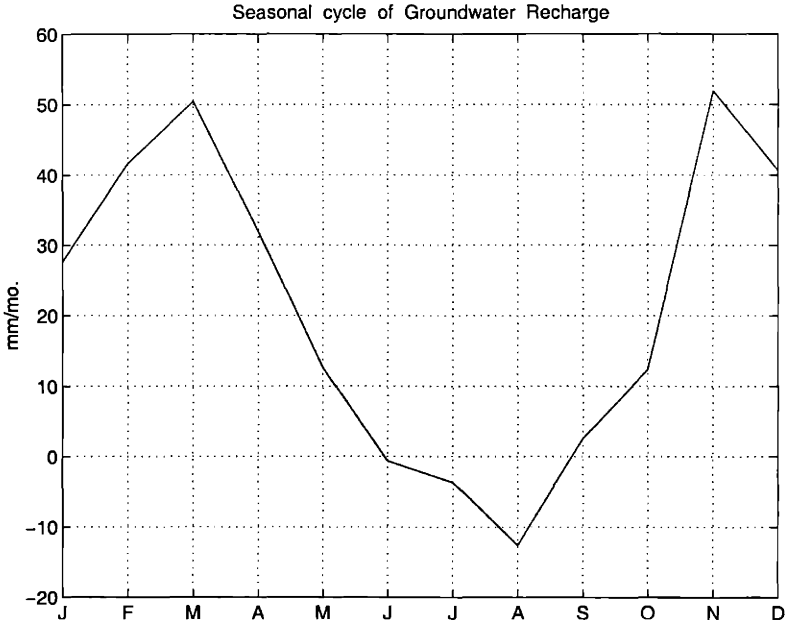

Figure 3.17 12-year (1983-1994) seasonal cycle of the estimated groundwater recharge fluxes.

in groundwater storage is nearly zero (Table 2.2). A significant amount of groundwater recharge occurs in (1) March when soil moisture is close to saturation such that most of the infiltrated water directly recharges the aquifer, and (2) November when precipitation is 140% of the average monthly value (Table 2.2). On the other hand, negative recharge (upward water flux: groundwater evaporation) occurs during summer months with a maximum of 14.2 mm/month in August. During summer months when the deficit in root-zone soil moisture is largest, upward water flux from the shallow aquifer replenishes the root-zone soil moisture resulting in the steep decline of water table (Figure 2.4). The magnitude of upward water fluxes (21.5 mm over three summer months) is consistent with the magnitudes of groundwater evaporation reported in previous studies (*Tschinkel*, 1963; *Daniel,* 1976; *Zecharias and Brutsaert*, 1988).

Due to the uncertainty in the estimation of α, the sensitivity is tested by varying α as 0.05, 0.10, to 0.15 (corresponding to 15%, 30%, and 45% of the total streamflow, respectively). As expected, a larger α (more surface runoff) results in a smaller groundwater recharge. The decrease in the recharge is less than 10 mm in each month as α varying from 0.05 to 0.15. Therefore it can be concluded that the groundwater recharge estimate has little sensitivity to the specified surface runoff coefficient, primarily because of the small magnitude of surface runoff comparing to other components in the water balance equations.

As seen in Table 2.2, the total amount of groundwater storage change and streamflow for the whole summer (June, July, August) are -65.4mm and 60.3mm, respectively. By assuming $R_G \cong 0.8R$, about 17mm of upward water flux is estimated to occur during the summer months in Illinois. Specifically, groundwater storage declines at a rate faster than the corresponding groundwater runoff during the summer months, suggesting a 17mm of upward water fluxes from the aquifer to the soil moisture for the whole summer.

It is interesting to note in July, streamflow, soil moisture change, and groundwater storage change all have a similar magnitude of about 20 mm/month, which is also equal to the magnitude of evaporation minus precipitation (Table 2.2). This implies in July, the low streamflow is sustained by groundwater discharge, whereas the soil moisture depletion is responsible for the

high evaporation demand exceeding the concurrent precipitation. In August, evaporation and the decrease in soil moisture storage remain nearly unchanged as in July. However, the precipitation decreases 14 mm from the last month. The deficit in evaporation over precipitation is supplied by the upward water fluxes from the unconfined aquifer which explains the negative peak of groundwater recharge in August as seen in Figure 3.17.

The 12-year monthly recharge estimates are plotted against precipitation in Figure 3.18. The same data is also plotted on a seasonal basis in this figure. Groundwater recharge is in general proportional to precipitation though the correlation between them is relatively low (R=0.44). The correlation between precipitation and groundwater recharge is strongest (R=0.82) in summer than in the rest of a year. Substantial amounts of groundwater recharge occur during spring, autumn, or winter. Significant recharge (i.e., >50 mm/month) can still take place during the spring and winter even when the corresponding precipitation is low, which is due to the nearly saturated soil moisture condition. In contrast, groundwater recharge is consistently negative in summer when precipitation is less than or equal to the long-term average (see Table 2.2), but the probability for the occurrence of upward water fluxes is virtually zero when precipitation is large than 100 mm/month irrespective of the season. This seasonal difference underscores the joint control of precipitation and soil moisture on the groundwater recharge.

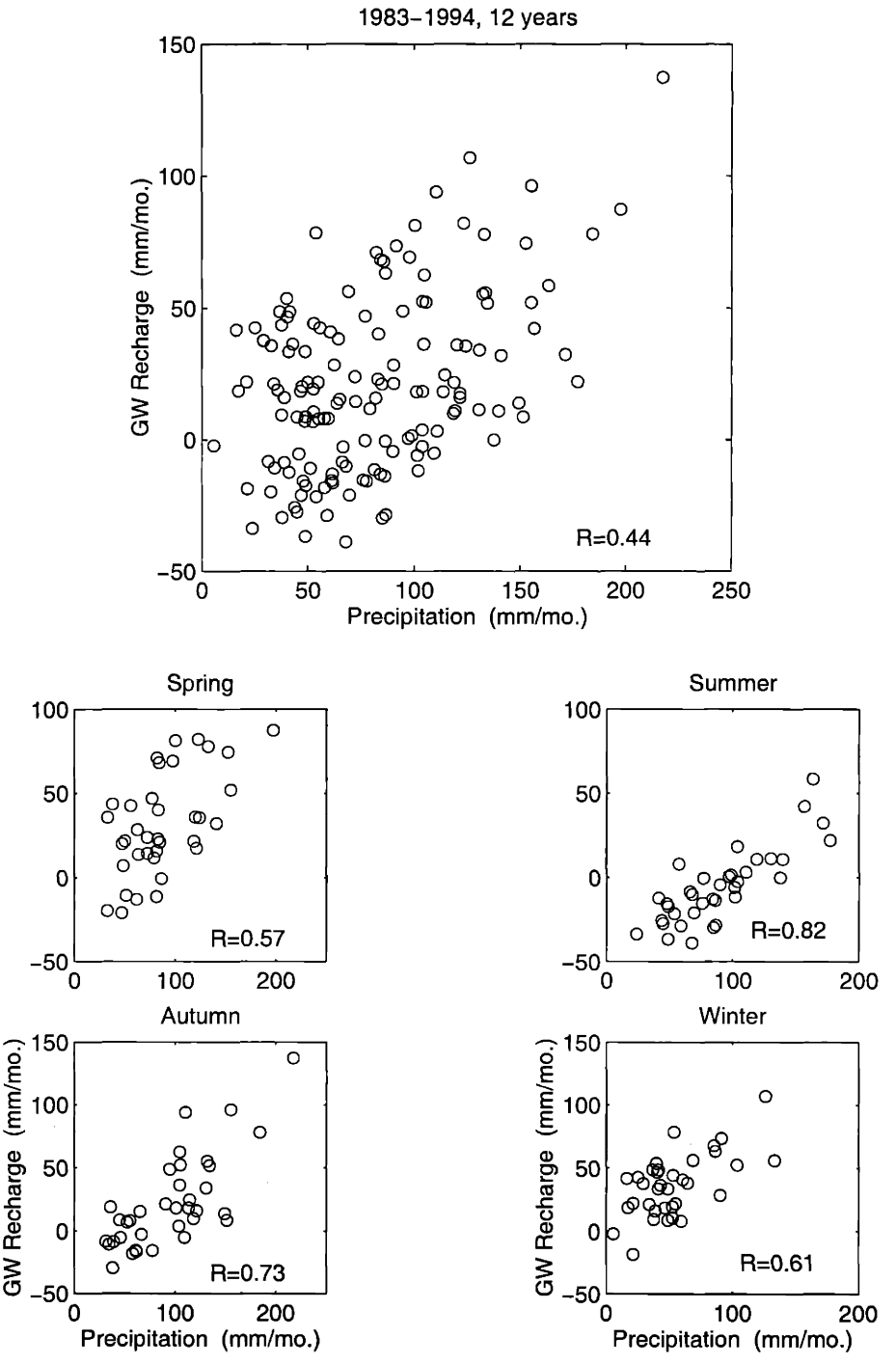

Figure 3.18 Scatter plots of 12-year (1983-1994) monthly groundwater recharge estimates versus the corresponding precipitation.

3.3.3 Observational Evidence of Regional-scale Groundwater Evaporation

From the 12-year (1983-1994) climatology of the hydrological cycle in Illinois in Table 2.2, it can be seen that in summer months (June, July and August) evaporation consistently exceeds precipitation about 20-30 mm/mo. Since the magnitude of streamflow in summer months is almost equal to the corresponding storage change in soil moisture, the summer evaporation would not exceed the corresponding precipitation without the supply of groundwater. Notice that (Table 2.2) the magnitude of the storage change in groundwater in summer months is close to that of the corresponding evaporation less precipitation. Moreover, the total changes in groundwater storage over the whole summer (June-August) are close to but slightly larger than the corresponding summer streamflow (i.e., 65.4mm versus 60.3mm). Reasonably assuming that groundwater runoff (basefow) is a certain large percentage of streamflow in summer months, the slightly larger magnitude of groundwater storage change over summer streamflow suggests the existence of another process depleting groundwater reservoir in summer months. Since the hydrological cycle in Illinois is a closed system, the potential groundwater discharge mechanism other than baseflow would be the upward water flux from water table to the overlying soils. Several additional observations support this argument. First, as observed from Figure 2.6a, the rate of decline in groundwater storage increases from April through the summer and reach the peak in August, while that in soil moisture storage lessens after the peak in May. Streamflow would increase if the accelerated depletion in groundwater storage from May to August is to contribute to the baseflow. However, Figure 2.6a shows the reverse trend: streamflow decreases from the spring until the late summer. Second, notice that evaporation increases from the late spring through the summer while precipitation is relatively uniform during this period, therefore the rate of depletion in soil water storage should increase if no additional sources of water could replenish the root-zone soil moisture during the summer. However, the soil moisture storage change and groundwater storage change exhibit an opposite trend from May to August (Figure 2.6a) suggesting a continuous water supply from the aquifer to the soil moisture in summer months.

The 12-year (1983-1994) monthly soil moisture data, collected by ISWS at 11 depths within the first 2 meters of soils below the surface, are used to characterize the vertical soil water flux

across the interface between any two adjacent soil layers. Since the driving force governing soil water movement is the hydraulic gradient, the measured soil moisture content is transformed into the capillary potential using the empirical soil water retention relationship proposed *by Clapp and Hornberger* [1978]: $\psi = \psi_S / s^B$, where s is the soil saturation; ψ_S is the soil matric potential (ψ) at saturation; B is an empirical parameter depending on the soil type. According to the soil map provided by FAO-UNESCO [1975], the dominant soil texture class in Illinois is silt loam. Following *Clapp and Hornberger* [1978, Table 2], B and ψ_S are taken as 5.3 and 786 mm, respectively. From the calculated soil matric potential, the direction as well as the magnitude of the vertical water fluxes in the interface of any two adjacent soil layers can be computed.

To quantify the average frequency on the occurrence of upward water fluxes in Illinois, direct spatial average over 16 measurement sites is avoided due to the nonlinear nature of the unsaturated flow process. Instead, the monthly probability for the occurrence of upward water fluxes at each soil layer interface is computed from the 12-year monthly time series of soil moisture. For each month, at each soil interface there are 16 * 12 = 192 samples, which should be sufficient to obtain a representative estimate for the occurrence frequency of upward water fluxes. The result is presented in the contour plot of Figure 3.19. As shown in the figure, the high probability (i.e., >90%) of the occurrence of upward fluxes locates at the soil layers about 50cm below the surface from May to August. On the other hand, the downward fluxes dominate at the deep soil layers (below 150 cm) throughout the year. The large probability of downward fluxes occurs during the spring when groundwater recharge rate is high. Moreover, the evolution of the probability curves in the middle soil layers (70-150 cm) shows a clear seasonal pattern associated with the seasonal cycle of groundwater recharge. This implies a gradual downward propagation of the soil layers within which the upward fluxes occur from spring through autumn in response to the high evapotranspiration demand in the upper soil layers. For example, the depth with 30% probability of upward fluxes moves downward from about 100cm in May to about 140cm in September. Given the generally shallow water table conditions in Illinois and the nearly constant soil moisture in deep soil layers (150cm-200cm) throughout a year, Figure 3.19 provides an observational evidence of the water supply from the shallow aquifers to the root-zone soil moisture in summer at the regional scale of Illinois.

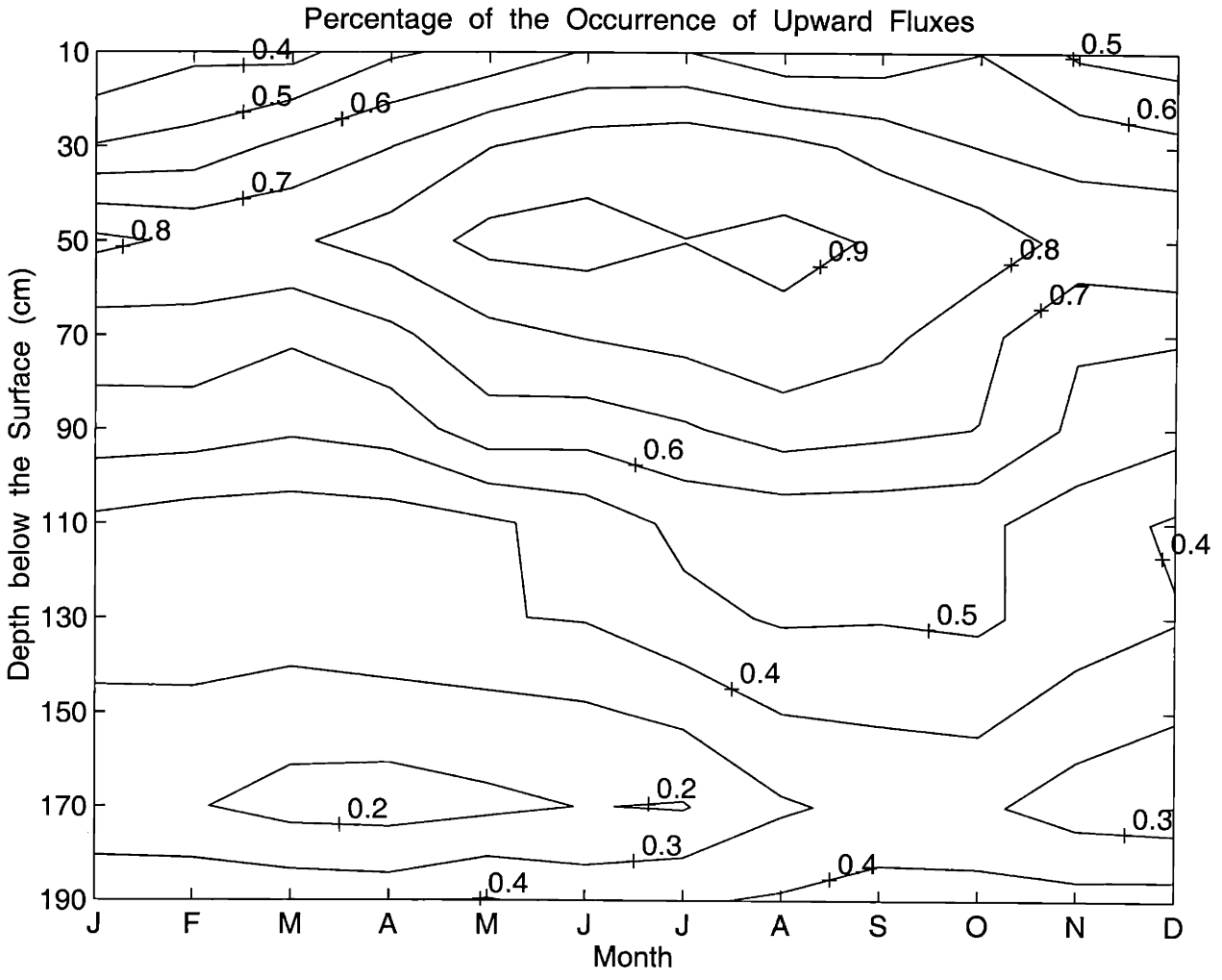

Figure 3.19 The contour plot of the probability of the occurrence of upward water fluxes in each soil layer interface at different depths for each month of a year.

3.4 Conclusions and Implications

We have investigated in this chapter various aspects of the regional-scale hydroclimatology in Illinois based on a 12-year (1983-1994) comprehensive dataset including most of the hydrometeorological variables. Among the major findings, of particular significance to the main theme of this thesis are the roles that shallow aquifers play in the regional-scale hydroclimatology of Illinois summarized in the following:

(1) The monthly change in groundwater storage is an important water balance component with a magnitude equals to the monthly change in soil moisture storage due to the generally shallow water table condition in Illinois (in average 3.2 m below the surface) so that unconfined aquifers respond sensitively to the fluctuations of regional climate.

(2) Examination of the observations on precipitation, water table depth, and streamflow reveals that streamflow is highly correlated with water table depth rather than precipitation at the regional scale. The state-average monthly water table depth explains 2/3 of the variance of average monthly streamflow in Illinois, while average monthly precipitation only explains less than 10% of the streamflow variance.

(3) The role of shallow aquifers in amplifying or dissipating the hydrologic anomalies (flood and drought) through the groundwater discharge to stream is analyzed by statistical techniques. It is found that the groundwater aquifers selectively amplifies the drought conditions while dissipates the floods conditions, which results in the observed asymmetric response of the groundwater level to the droughts and floods.

(4) It is found from the estimation of regional groundwater recharge that the shallow aquifers supply water to replenish the root-zone soil moisture during the summer, which helps to maintain a high summer evaporation rate in Illinois (~120 mm/mo.).

These findings obtained from the regional water balance study have implications for the land-surface parameterization schemes (LSPs) used in GCMs. One important conclusion, obtained from the recent evaluation of 23 LSPs using the observed data from the Cabauw site [i.e. pertaining to phase 2a of the Project for Intercomparison of Land-surface Parameterization Schemes, PILPS], is the existence of considerable inconsistency in the partitioning of annual runoff into its physical components among the various schemes [*Chen et al.,* 1997; *Beljaars and Bosveld*, 1997]. Observational evidence (shallow groundwater table 0-75 cm below surface, deep soil saturated throughout the year, and no overland flow observed) and site topography have indicated that downward drainage from the root-zone to a groundwater table and subsequent groundwater discharge is the main mode of runoff at this site. However, more than half of the LSPs generated significant amounts of overland flow and interflow. This is due to the inadequate assumption of free drainage from the root-zone commonly used in current LSPs. The identical problem was also encountered in using HAPEX-MOBILHY data in PILPS [*Shao and Henderson-Sellers*, 1996]. As summarized in the above, the changes in unsaturated and saturated storage in Illinois are equally important with a magnitude comparable to runoff. For the Cabauw site where similar hydroclimatic characteristics to Illinois exist, measurements of soil moisture, groundwater level, and runoff are not available for model evaluation. The question about the role that groundwater aquifers play in the regional water balance cannot be answered. Based on direct observations in Illinois, we have shown from this study that groundwater aquifer acts as a long-memory reservoir which stores excessive soil water. For the purpose of improving current LSPs, this study can provide observational support to help in the parameterization of groundwater storage.

The observed response of the groundwater aquifer to major droughts and floods in the atmosphere and soil water reservoir (Figure 3.5) also have important implications regarding the impact on regional groundwater level (hence regional water resources) due to any climate change scenario. Several climate change studies have concluded that the evident increase in the concentration of greenhouse gases in the Earth atmosphere is likely to enhance the frequency and severity of drought conditions during summer in mid-latitudes (e.g. *Manabe et al.* 1981, *Rind et al.* 1990, *Wethrald and Manabe* 1995, and *Kattenberg et al.* 1996). This prediction is consistent with an increase in evaporation that exceeds the corresponding increase in precipitation due to

the intensification of the hydrological cycle. The credibility of this prediction is rather limited because of the limitations on the climate model simulations by the inaccuracy in the land surface parameterization schemes, as well as the parameterizations of moist convection, clouds, among others. It should be emphasized that any significant regional change scenario for the mid-western United States has important implications on the regional agriculture and the national economy in general, and for this reason its consequences has to be investigated carefully. However, most of the current LSPs in climate models used in global change studies do not include adequate representations of groundwater aquifers. For this reason such models could not simulate the response of groundwater aquifer to climate change. The results of the present study suggest that a change to relatively dry climate may be reflected in groundwater levels in an amplified way; that is, the frequency of the occurrence of prolonged droughts would be enhanced. Consequently, a tendency towards dryer conditions in terms of precipitation and soil moisture over Illinois is likely to result from the feedback of the severe drought conditions in groundwater levels.

Chapter 4 The Representation of Water Table Dynamics

4.1 Introduction of the LSX Land Surface Scheme

The land surface scheme "LSX" (i.e., Land-Surface-Transfer Scheme) developed by NCAR (National Center for Atmospheric Research) scientists (*Pollard and Thompson*, 1995; *Thompson and Pollard*, 1995; *Bonan*, 1993) is used as the modeling tool in this study. It is also the land surface scheme used in the dynamic biosphere model "IBIS" (Integrated BIosphere Simulator, *Foley et al.*, 1996). The LSX computes exchanges of momentum, energy, and water mass in the soil-vegetation-atmosphere system with explicit accounts for vegetation effects. The design of LSX borrows heavily from BATS and SiB, and is intermediate in complexity between these two models. There are two vegetation layers in the LSX, an upper layer ("trees") and a lower layer ("grass"). Three main equation sets are employed in the LSX to simulate the water, energy, and momentum fluxes near the land surface. The first set of equations simulates vegetation temperature, canopy-air temperature and specific humidity. Another set of equations predicts the amount of intercepted water and the precipitation through the canopy. The last set of equations governs the dynamics of soil water. A multi-layer soil model is used in the LSX to simulate the fluxes of energy and water in the upper few meters of soil. For each layer, there are three prognostic variables: temperature, liquid water content, and ice content. The physics governing the movement of liquid water are described by the Richards equation:

$$n\frac{\partial s}{\partial t} = \frac{\partial}{\partial z}(-K_{unsat.}(s) + D(s)\frac{\partial s}{\partial z})$$
$$K_{unsat.}(s) = K_S s^{2B+3}; \qquad D(s) = K_S \psi_S B s^{B+2}; \tag{4.1}$$

where n is the soil porosity, s is the soil saturation degree; K_S and $K_{unsat.}$ are respectively the saturated and unsaturated hydraulic conductivity, ψ_S is the soil matric potential (ψ) at saturation, B is an empirical constant depending on the soil type, and D is the soil diffusion coefficient. The two terms inside the parenthesis of Eq. (4.1) are the gravity drainage flux and

the capillary diffusion flux, respectively, both of which has highly nonlinear dependence on the soil saturation *s*. The boundary conditions at the bottom of the lowest soil layer could be gravity drainage, no flux, or a flux in between determined by the specification of an empirical drainage coefficient between 0 to 1. The upper boundary is specified by the effective surface infiltration rate equal to rainfall minus evaporation. When the surface layer is saturated, any excess rainfall minus evaporation becomes surface runoff. As in most of the land surface schemes, the total runoff generated is the sum of the soil drainage and the surface runoff in the LSX model. For other details about the LSX model, the readers are referred to the appendex of *Pollard and Thompson* [1995] and *Thompson and Pollard* [1995].

The original LSX model does not account for the spatial variability of climate forcings (primarily precipitation) and land surface characteristics. Due to the significant impacts of the subgrid variability of precipitation on the surface water balance as shown by several past sudies (*Entekhabi and Eagleson*, 1989; *Pitman et al.*, 1990), the canopy model in the LSX has been modified to incorporate the statistical interception scheme developed by *Eltahir and Bras* [1993] who used the statistical-dynamical approach to take into account the sub-grid spatial variabilities of both precipiation and canopy storage size. The significant outcome of applying this statistical intercept scheme is reduction of interception loss, as will be shown later.

In the next section we run the LSX in Illinois by using the observed atmospheric forcing to test its ability to reproduce the regional hydroclimatolgy of Illinois as summarized in Chapter 2. The observational data on streamflow, soil moisture, water table depth, as well as the estimates of evaporation from water balance computations, will be used to validate the simulations of the LSX.

4.2 LSX Simulations in Illinois (In the Absence of Water Table Representation)

In this section the ability of LSX to reproduce the observed hydroclimatology in Illinois during an 11-year period (1984–1994) is tested. All the simulations conducted here are in an off-line mode; that is, using the prescribed atmospheric forcings to drive the model rather than coupling land surface schems to climate models. The test domain is the whole state of Illinois with the scale ~ 400km x 300km, which is comparable to the typical size of a GCM grid cell.

To drive the LSX in an off-line fashion, seven input atmospheric forcing (i.e., precipitation, near-surface air temperature, air humidity, air pressure, shortwave and longwave radiations, and near-surface wind speed) are prepared from either direct observations or the product of the NCEP/NCAR reanalysis. The sampling inteval of the atmospheric forcing is 1 hour. Precipitation is retrieved from the Earthinfo Inc. hourly dataset from which 52 rain gauges in Illinois with the data covergae above 90% during 1984-1994 are selected to derive the mean precipitation in Illinois. Because of the high density of rain gauges, the arithmetic average of the 52-station precipitation records is considered as the mean precipitation in Illinois. To correct the missing data in the EarthInfo hourly dataset, the total precipitation for each day of the 11-year period is adjusted to be consistent with the arithmetic average of the 129-station daily precipitation data provided by the Midwest Climate Center (MCC). Moreover, the near-surface air temperature, air humidity, and air pressure are taken from the NCDC (National climate Data Center) Surface Airway hourly dataset. There are 11 NCDC stations located in or near the Illinois which are used to derive the state-average values by simple averaging. In addition, the shortwave and longwave radiations are interpolated from the 6-hourly NCEP/NCAR reanalysis data to the hourly resolution, and then adjusted their monthly mean to be consistent with the NASA SRB (Surface Radiation Budget) monthly dataset, which contains global information on both net longwave radiation and net solar radiation. Finally, the near-surface wind speed is taken from the the 6-hourly NCEP/NCAR reanalysis data and interpolated to the hourly resolution. The 11-year (1984-1994) average climatologies of the 7 atmospheric forcings in Illinois are shown in Figure 4.1.

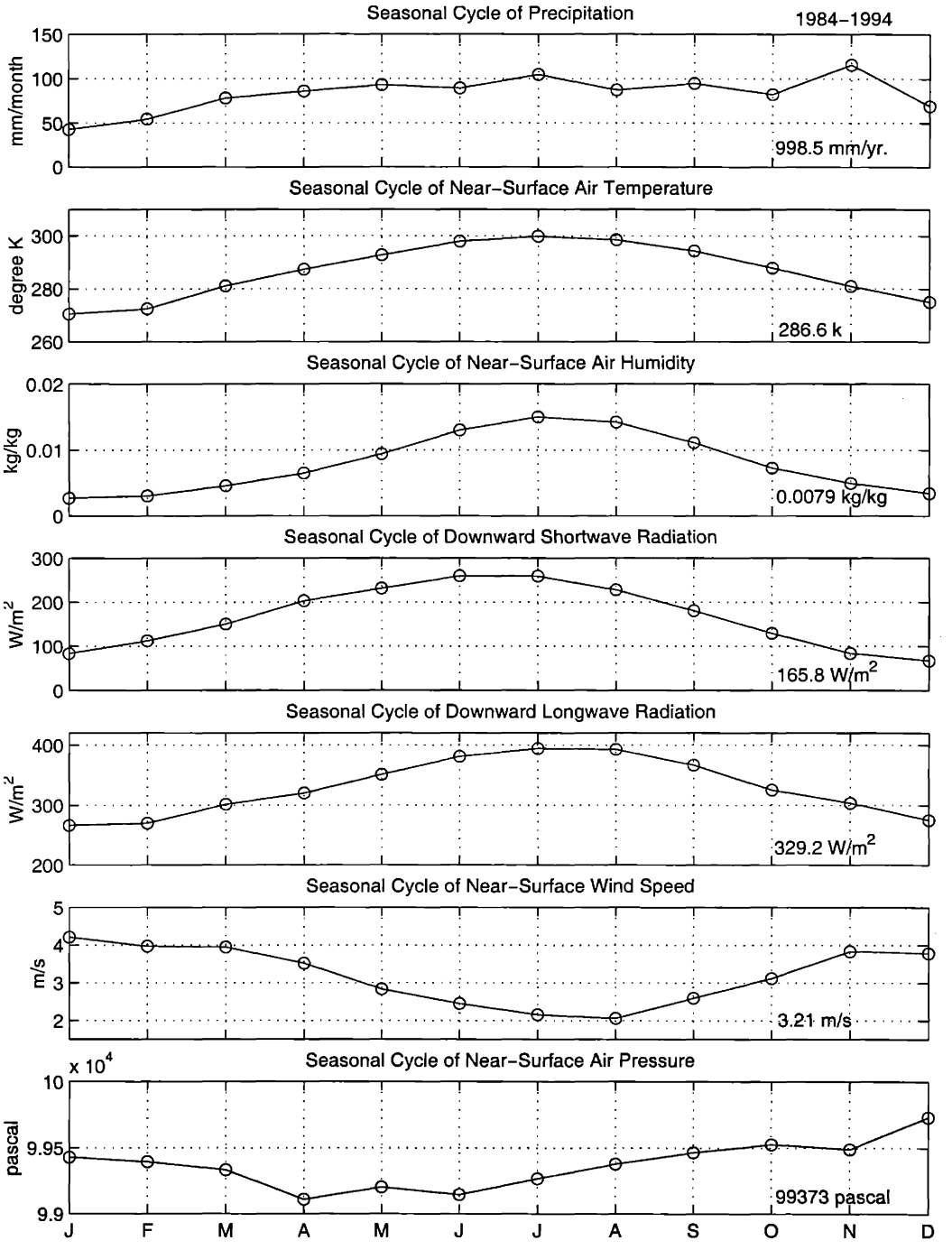

Figure 4.1 The 11-year (1984-1994) average climatologies of the seven atmospheric forcing used in the LSX simulations in Illinois.

In order to ensure the simulation results independent of the uncertain initial condition of hydrologic states (e.g., soil moisture, soil temperature, capopy storage, etc.), three identical spin-up years all with the forcings of 1984 are added ahead of the 1984-1994 simulation to bring the system to the hydrological equilibrium after the 3-year spin-up simulations. Hydrological equilibrium is reached when the deviations in the annual water and heat balance are negligible from year to year. As to how many years of spin-up are required to reach equilibrium depends on the memory of the models, but in general it takes longer to reach equlibrium for a dry year than for a wet year. For the LSX simulation in Illinois, 3 spin-up years are found to be sufficient to reach equilibium. This procedure of adding spin-up years has been widely used for the off-line testing of land surface schemes during the different phases of the PILPS.

Model validation is based on the comprehensive hydrological dataset of Illinos as summarized in section 2.2. The data used for model validation include the observed monthly time series of soil moisture, water table depth, streamflow, as well as the evaporation and groundwater recharge estimated from water balance computations as presented in Chapter 2.

The dominant soil type in Illinois is silt loam or silty clay loam inferred from the soil texture descriptions in 19 soil moisture measurement sites provided by *Hollinger and Isard* [1994]. The Illinois soil moisture dataset also includes the measurements of soil porosity, field capacity, and wilting point. The specification of the saturated hydraulic conductivity (K_S), soil exponent (B), and soil matric potential at saturation (ψ_S) for the silt loam soils was based on the tabulation of *Rawls et. al.* [1982]. Moreover, the dominant landcover in Illinois is 60% cropland and 20% short grass. Since crop is absent in the vegetation look-up table in the LSX, the vegetation cover is specified as the shortglass with a C3 photosynthetic pathway. This is consisitent with *Delire and Foley* [1999] who used C3 grass to simulate a crop site in the HAPEX-Mobilhy site in France. In addition, a seasonal cycle of Leaf Area Index (LAI) with a maximum in summer and zero in winter is imposed based on the avaialble information of the crop growing characteristics in Illinois [e.g. *Vinnikov et al.,* 1999] .

As discussed in section 1.1, a common weakness in the current generation of land surface schemes is the specification of the lower boundary condition in the soil model. Most schemes

specify a gravity drainage boundary condition or a linear function of gravity drainage condition. For the LSX, the bottom boundary condition of the soil moisture was specified as the unsaturated conductivity of the lowest layer multiplied by an empirical drainage coefficient ranging from 0 (i.e., no flux, bedrock condition) to 1 (i.e., gravity drainage condition). Since this coefficient dictates the rate of drainage out of the soil column, it has profound impacts on the entire set of hydrologic states and fluxes and hence on the partitioning of precipitation into runoff and evaporation. Unfortunately, it is in practice impossible to measure this coefficient in the field, therefore it is often treated as a tunning parameter with rather ambiguous physical meaning.

In order to investigate the sensitivity of the lower boundary condition types to the LSX simulation, the 11-year (1984-1994) simulations of two contrasting extreme cases, one with the gravity drainage condition at the bottom of the soil column (hereafter referred to as case A), and the other with the no-flux (bedrock) condition (as case B), were conducted. Both off-line simulations were driven by the identical hourly atmospheric forcings and parameters as summarized in the above. It should be pointed out that these two extreme cases are selected here to illustrate the sensitivity of the land surface model simulation to the specification of the drainage coefficient. Of course, it is possible to tune the drainage coefficient to be a value between 0 and 1 so that the simulated fluxes and states can better match the correspoing observations as the common practice of most current LSPs. As stated earlier, however, this coefficient in essence lacks of realistic physical meaning, and its constant value may not be able to simulate the dynamic drainage conditions such as the capillary rise from the aquifer to the unsaturatd zone.

Results from the simulation of case A are presented in Figure 4.2. Figure 4.2(a) shows the comparison between the 11-year average seasonal cycle of the simulated total runoff in case A and the observations. Figure 4.2 (b)-(c) plots the seasonal cycles of two runoff components in the LSX, soil drainage and surface runoff. Notice that the observed soil drainage is actually the groundwater rechrage estimated from water balance computations in section 3.3. Figure 4.2 (d)-(e) shows the 11-year monthly time series of soil drainage and total runoff in comparison with the corresponsing monthly observations. As seen in the panel (a) of this figure, runoff is underestimated from June through October by 5-10 mm/month. Since surface runoff only

contributes a small percentage of the monthly streamflow in this simulation, the underestimation is primarily caused by the inadquate modeling of soil drainage in the LSX. A notable example seen in the panel (e) is the extended dry summer span from 1987 to 1989 when streamflow was largely sustained by baseflow. Without a groundwater component in the LSX, the simulated streamflow in summer is significantly underestimated due to the small magnitude of the soil drainage. Moreover, soil drainage is poorly simulated with the range of its seasonal cycle

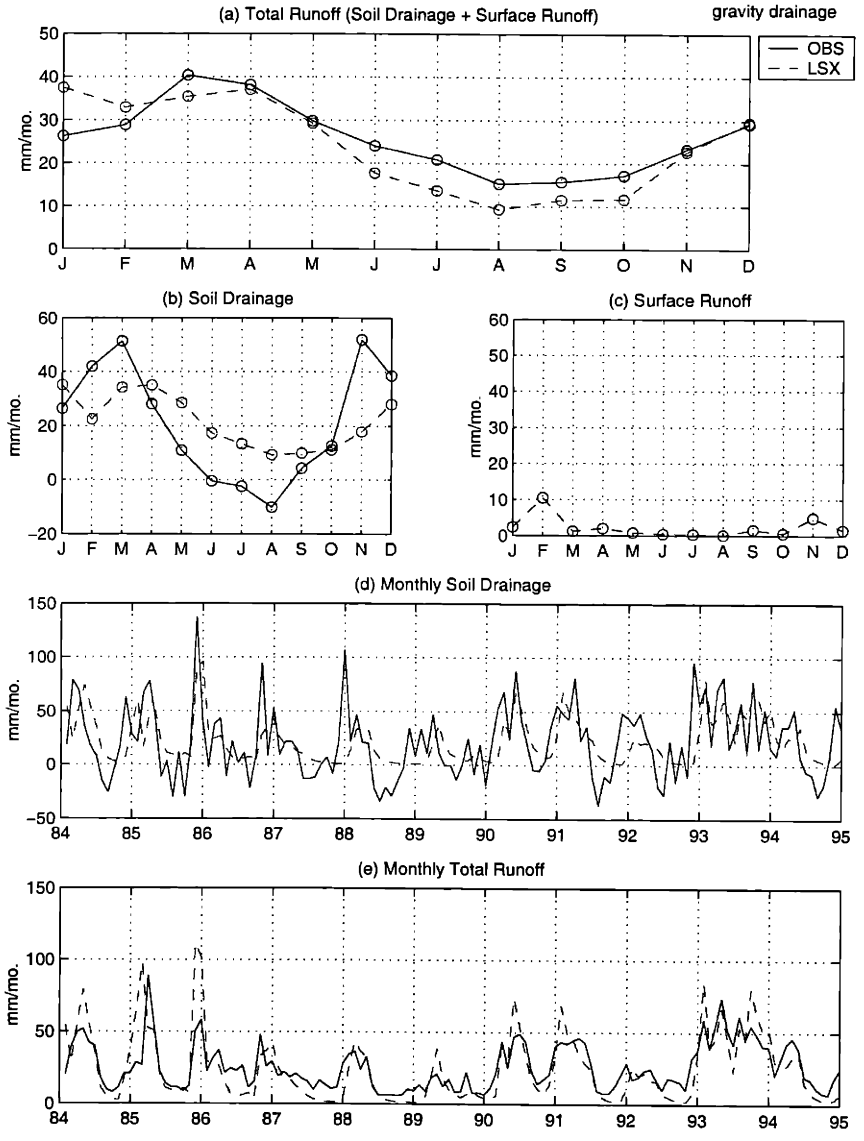

Figure 4.2 Case A (i.e., gravity drainage boundary condition): 11-year (1984-1994) average seasonal cycles of (a) the simulated total runoff in comparison with the observations, (b) the simulated soil drainage in comparison with the estimates of groundwater recharge from water balance computations, and (c) the simulated surface runoff. Panels (d) and (e) are 11-year monthly time series of soil drainage and total runoff, respectively, in comparison with the monthly time series of observations.

considerably smaller than the observations. Although the estimated groundwater recharge from water balance computations exhibits a negative peak (i.e., upward water flux) during summer months, the LSX fails to reproduce any upward flux during the 11-year simulation period owing to incorrect specification of the gravity drainage boundary condition. In addition, the simulated soil drainage flux during the winter and spring months is significantly underestimated and unable to capture the double peaks of soil drainage in November and March.

Figure 4.3 provides the comparisons with the observations similar to Figure 4.2, but for the case B (no-flux condition). In this case, runoff is solely contributed from surface runoff due to

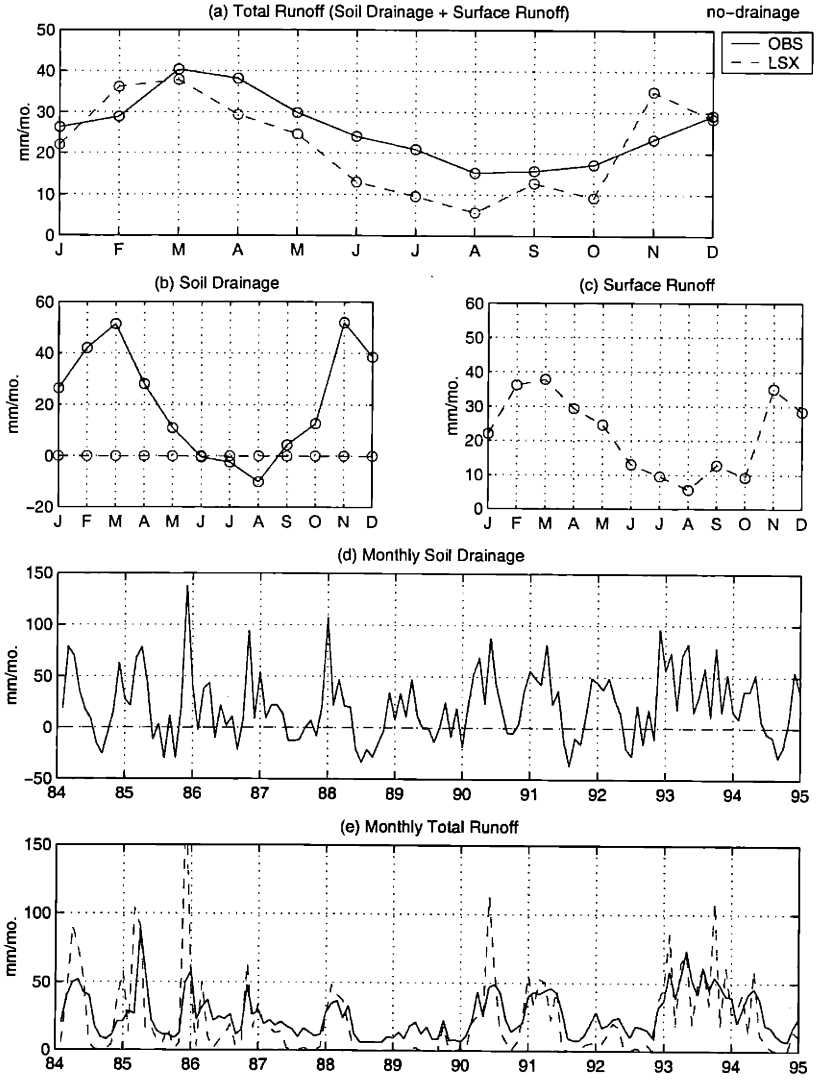

Figure 4.3 Same as Figure 4.2, but for the case B (i.e., no-flux boundary condition).

the shutdown of soil drainage. The overall pattern of the biases in the simulated total runoff is similar to that in the case A, but with a greater degree of deviations from the observations. For example, the peaks of streamflow were significantly overestimated (in 1984, 1986, and 1990), while nearly zero streamflow was generated during the dry summer periods from 1987 to 89.

The seasonal cycles of soil saturation degree for both cases A and B in the 11 soil layers (consistent with the vertical sampling resolution of the soil moisture data in Illinois) are compared to the observations in Figures 4.4 and 4.5, repectively. As clearly seen, neither case is close to the observed soil moisture. For the case A (Figure 4.4), a dry bias is observed from the simulated soil saturation in all the soil layers below 70cm from the surface. Due to the absence of water table, the lower soil layers persistently drain water out which is responsible for the underestimated soil moisture in these layers. In contrast, a consistent wet bias is noted in each of the 11 soil layers for the case B (Figure 4.5). Due to the shutdown of soil drainage in case B, the simulated soil moisture below 1m from the surface is close to saturation in the entire year. The wet bias in the lower soil layers propogates to the upper layers which leads to unrealistically large amounts of surface runoff (Figure 4.3).

Figure 4.6 presents the seasonal cycles of the simulated total evaporation for both cases in comparison with the observations. The "observations" in this figure is the evaporation estimates from water balance computations presented in Section 2.3. Also plotted in this figure is the three components of evaporation: transpiration, soil evaporation, and interception loss. As seen from this figure, both cases simulate the seasonal cycle of evaporation similar to each other except that the case B produces a slightly higher transpiration in summer due to the higher soil moisture than case A. Given that the soil moisture condition is drastically different between two cases, the similarity in the simulated evaporation between these two cases suggests that the water in Illinois is not a limiting factor for evaporation rather than implying that groundwater treatment has little impact on the simulated evaporation. Again, it is possible to tune the drainage coefficient in LSX to improve the soil moisture simulations. Moreover, the comparison with the observations indicates that both cases slightly underestimate evaporation in summer but significantly overestimate evaporation in winter.

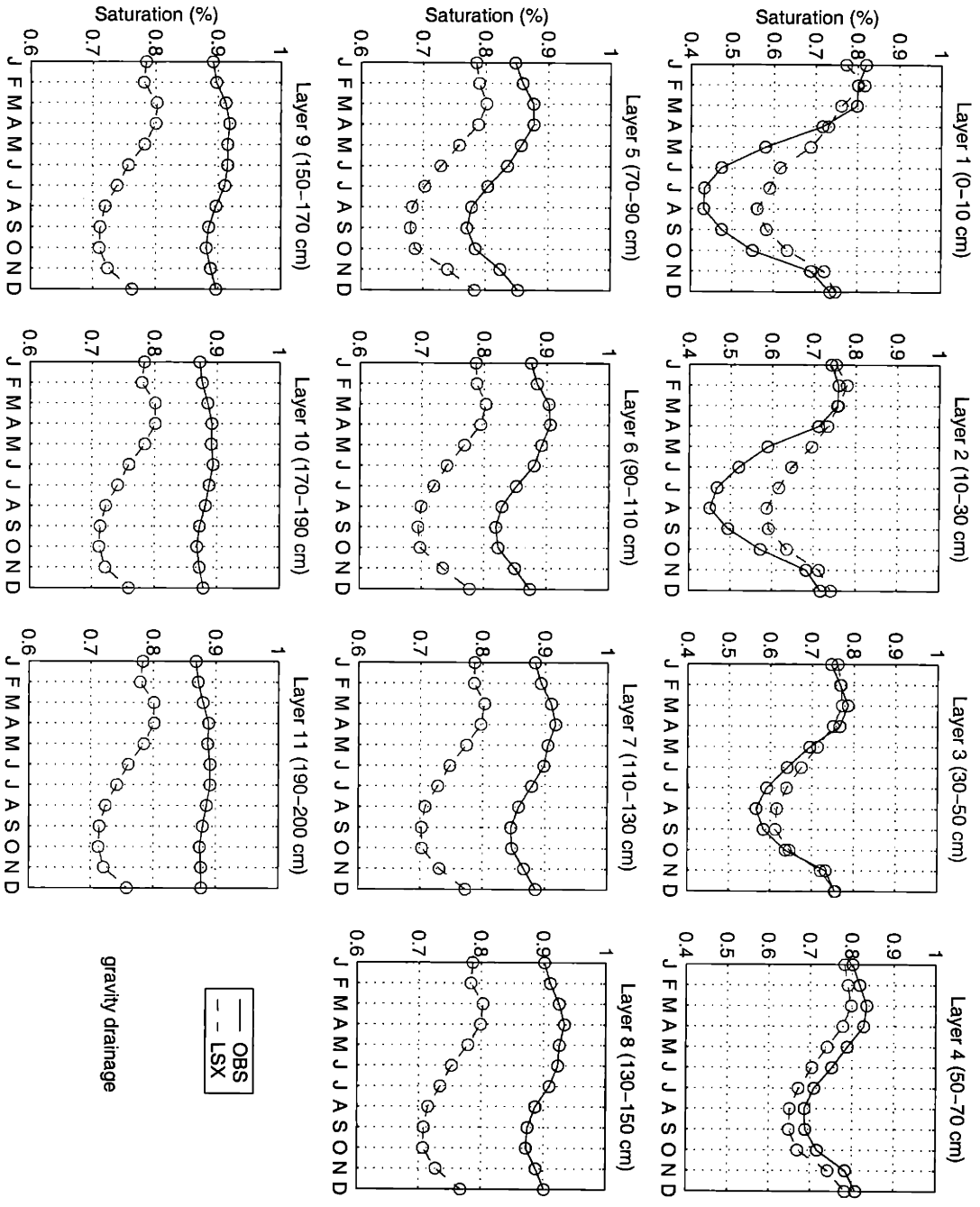

Figure 4.4 The 11-year (1984-1994) seasonal cycles of the simulated soil saturation degree for the case A (i.e., gravity drainage boundary condition) in 11 soil layers from 0-2m below the surface in comparison with the observations.

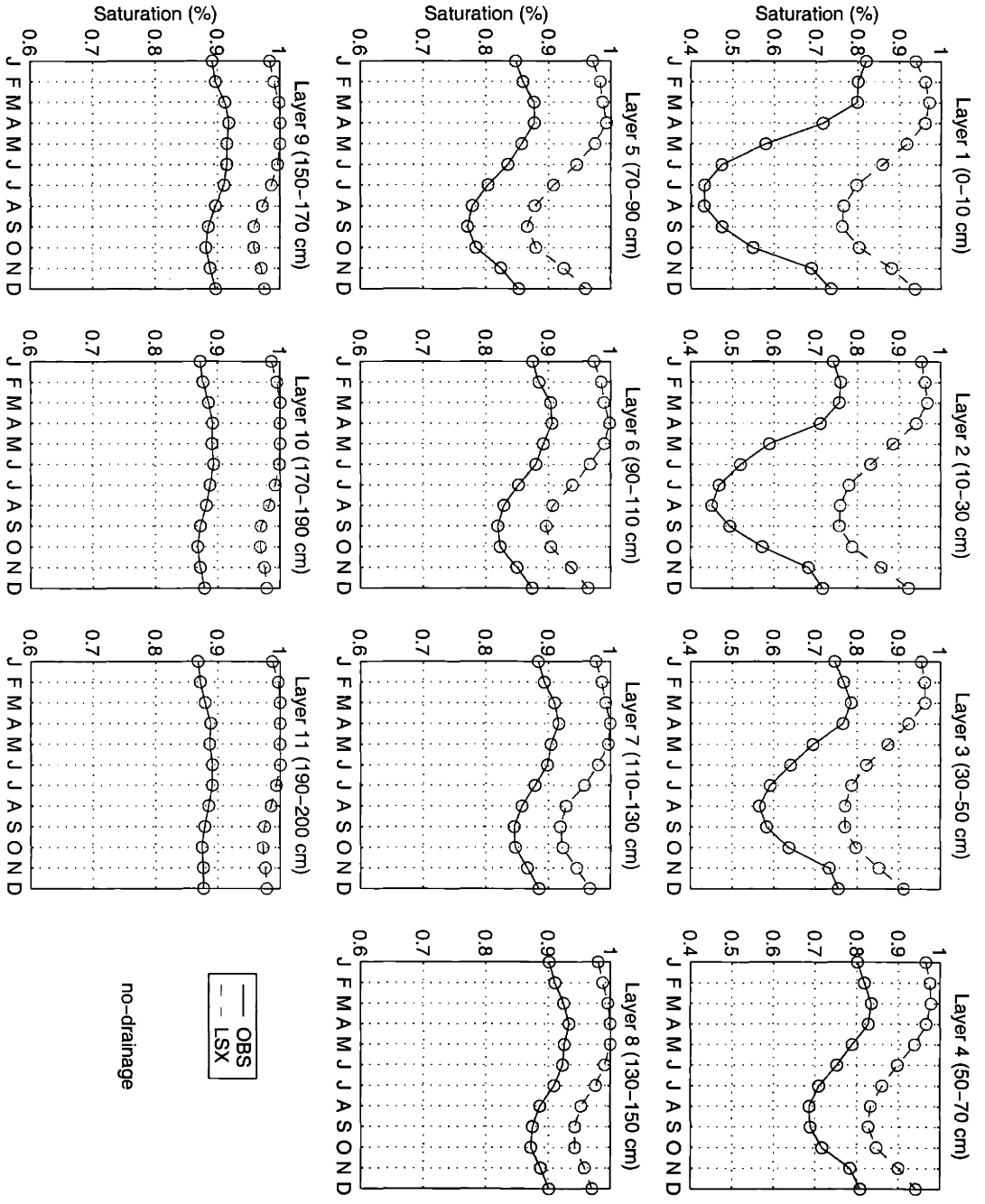

Figure 4.5 Same as Figure 4.4, but for the case B (i.e., no-flux boundary condition).

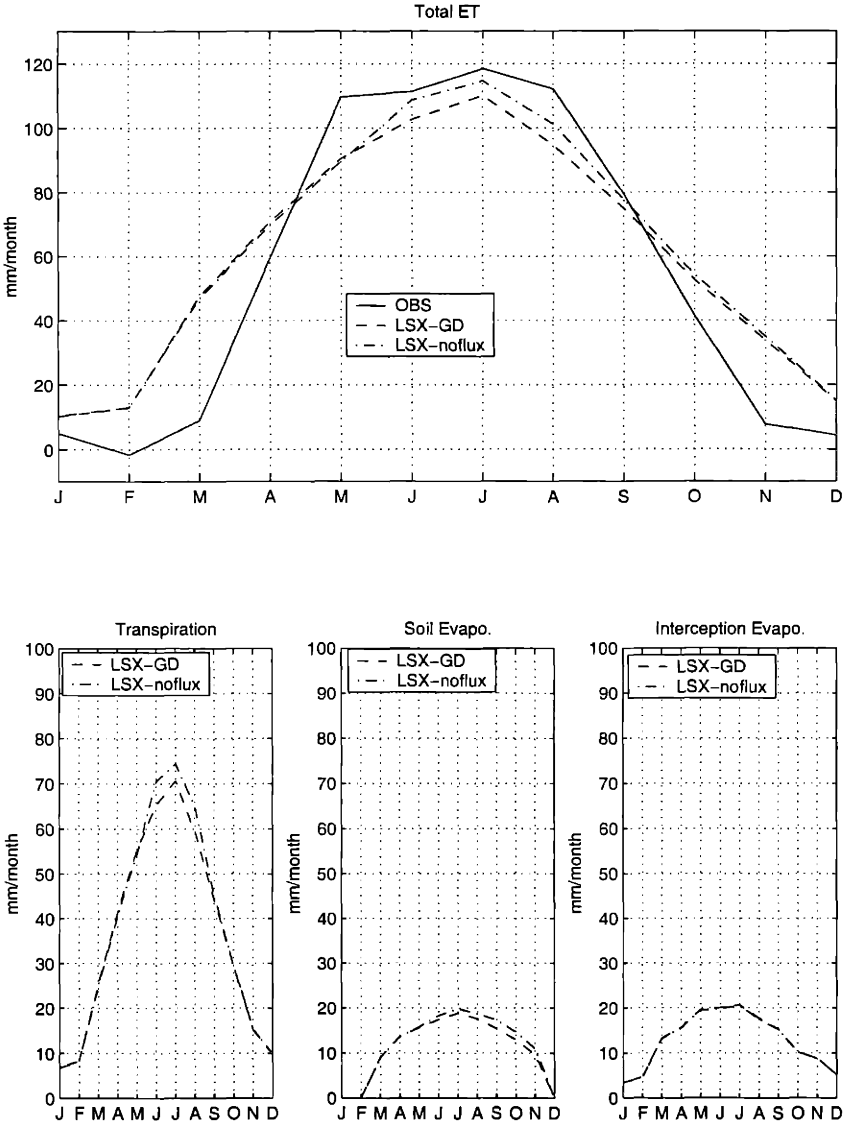

Figure 4.6 The 11-year (1984-1994) seasonal cycles of the simulated and observed total evaporation for both the cases A ("LSX-GD" in the figure) and B ("LSX-noflux"). Also shown in the figure are the seasonal cycles of the three components of the simulated evaporation: transpiration, soil evaporation, and interception loss.

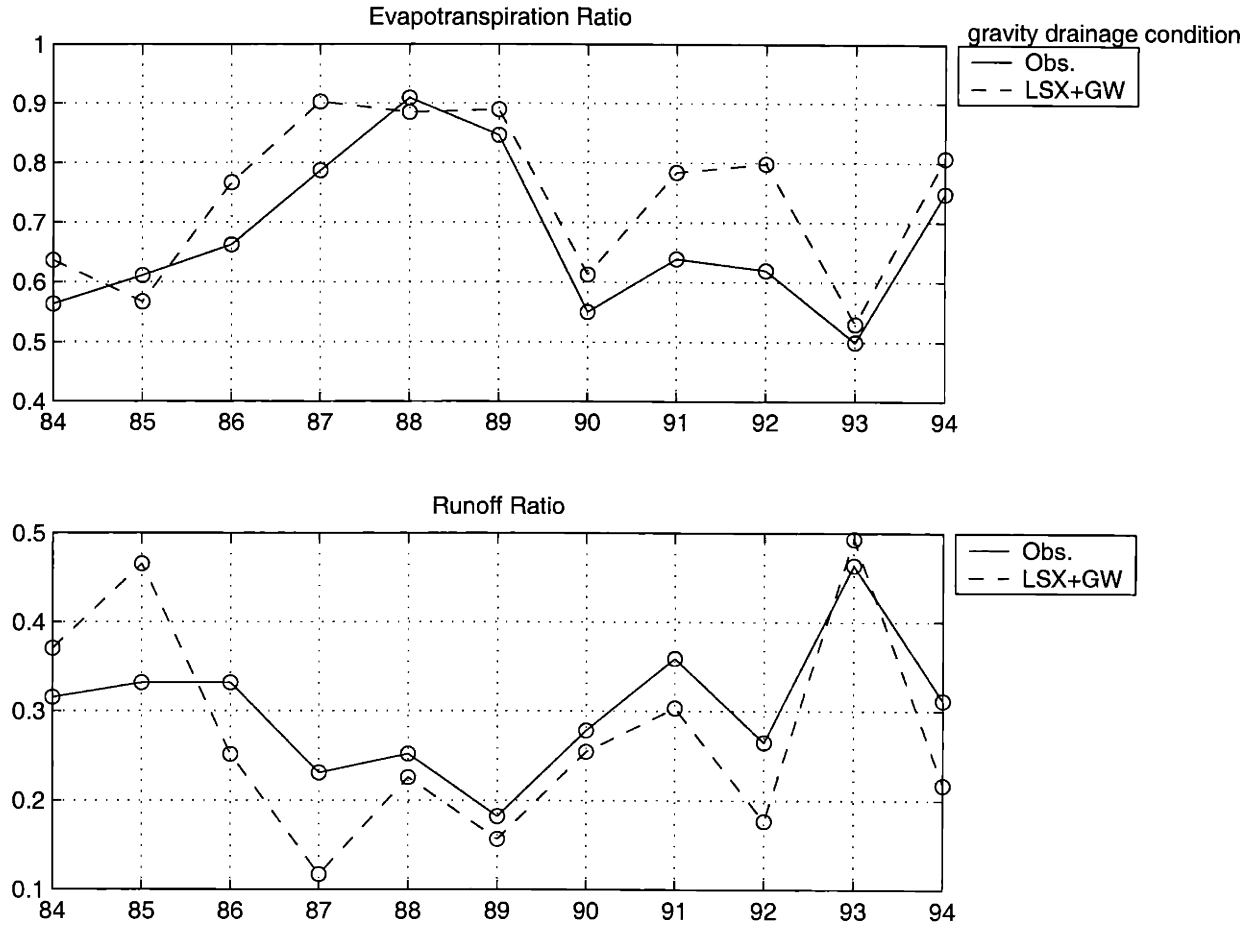

Figure 4.7 The evaporation ratio (i.e., annual total evaporation / precipitation) and runoff ratio (i.e., annual total runoff / precipitation) from 1984 to 1994 for the case A (i.e., gravity drainage boundary condition) in comparison with the observed ratios.

Finally, we evaluate the model performance at the annual time scale. Figure 4.7 shows the evaporation ratio (i.e., annual total evaporation / precipitation) and runoff ratio (i.e., annual total runoff / precipitation) from 1984 to 1994 for the case A in comparison with the observed evaporation and runoff ratios. From this figure, it can be seen that the LSX with a gravity drainage boundary condition simulates the correct evaporation and runoff ratios only in several years (1988, 89, 90, and 93), while large discrepancies can be noted for the rest of 11 years. Since soil mostiure is poorly simulated (Figure 4.3), it is possible that the occasional agreements with the observed ratios are the results of the cancellation of errors in the simulations rather than the proof of model skills.

As indicated in Figure 3.17 (p. 88), the water flux between the unsaturated and saturated zones (groundwater recharge) in Illinois is not always downward. Rather, it has a strong seasonal cycle with the upward water flux occurring in summer when diffusion flux outweighs gravity drainage flux due to the strong deficit in soil moisture. Most of the current land surface schemes do not allow for the occurrence of upward fluxes at the bottom of the soil model since they specify a gravity drainage-like condition as the lower boundary condition of soil moisture. The most critical outcome caused by the inappropriate lower boundary specification is the erroneous soil moisture profile that would affect the prediction of all the land surface water and heat fluxes. Comparing to the deep water table conditions, the presence of a shallow water table in general results in a decrease of the infiltration and an increase of the evapotranspiration due to the downward increase of moisture content. As found from the water balance computations in section 2.3, the high evaporation rate during the summer (~120 mm/month) in Illinois is partly sustained by shallow aquifers. It has shown in Figure 2.13 that the summer evaporation would be significantly underestimated without considering groundwater storage in the water balance equation. Therefore, we conclude that only by explicitly incorporating the water table dynamics in land surface schemes can we expect to have a realistic representation of land surface and subsurface hydrology, and hence a reliable partitioning of the land surface water and heat budgets. For this purpose, a simple lumped groundwater model designed for use in climate models will be proposed in the next section. The procedures of its coupling with the LSX will be presented. The coupled model will be tested in Illinois using the same forcing and validation data as in this section to investigate the improvement in model performance resulting from the incorporation of groundwater dynamics.

4.3 The Coupled Groundwater – Land Surface Model: LSXGW

The representation of water table dynamics in a land surface parameterization scheme (LSP) is the major issue in this thesis. This issue can be investigated through the following two steps: (1) Development of an unconfined aquifer model. This model should be able to simulate water table dynamics while computationally efficient enough to be used in climate models. The required parameters of the model should be parsimonious and can be estimated from the routinely measured hydrometeorological data or the commonly available data of aquifer attributes (section 4.3.1) (2) Coupling of the developed aquifer model with the LSX. The structure of the developed aquifer model should be flexible to be coupled to any land surface models (section 4.3.2).

4.3.1 Development of A Groundwater (GW) Model

A physically based groundwater flow model (e.g., MODFLOW, *McDonald and Harbaugh*, 1988) usually requires the discretization of the problem domain into a certain number of cells and numerically solves the multi-dimensional partial differential equations governing groundwater movement. Due to the large scale of a typical grid cell in climate models, such complicated numerical computations may be too expensive to be applied in climate models, and also too detailed given the objective of the model development. An alternative with less computational cost and parameter requirement is the lumped-parameter water balance model. For an unconfined aquifer, the water balance equation can be written as:

$$S_y \frac{dH}{dt} = I_{gw} - Q_{gw} \tag{4.2}$$

where S_y is the specific yield of the unconfined aquifer, H is the groundwater level above the datum, I_{gw} is the groundwater recharge flux, and Q_{gw} is the groundwater discharge to streams (i.e., groundwater runoff). For the silt loam soil typical in Illinois, S_y has been estimated as 0.08 in section 2.3. I_{gw} is also the soil drainage flux at the interface between the unsaturated and

saturated zone, which is the sum of the (downward) gravity drainage flux from the soil to the aquifer and the (upward) diffusion flux from the water table to the soil (i.e., the terms inside the parenthesis of Eq. (4.1)). I_{gw} is the key process controlling the unsaturated-saturated zone interactions since it is the only linkage connecting these two zones.

Eq. (4.2) represents a non-linear reservoir since I_{gw} and Q_{gw} both have nonlinear dependence on H. I_{gw} is calculated from the soil saturation in the bottommost soil layer determined by numerically solving the Richards equation (4.1). I_{gw} has an implicit dependence on H since the vertical soil moisture profile closely depends on the location of water table. Furthermore, recall that there is a strong nonlinear relationship between the large-scale observed streamflow and the corresponding water table depth in Illinois (Figure 3.1). Examination of the observations on precipitation, water table depth, and streamflow suggests groundwater runoff Q_{gw} is much larger than the surface runoff Q_S in the regional scale in Illinois. We have estimated in section 3.3 that Q_{gw} contributes about 80% of streamflow in Illinois, and for this reason the observed streamflow is a good surrogate for groundwater runoff. Therefore it is believed that Figure 3.1 describes reasonably well the general features of the nonlinear relationship between Q_{gw} and H.

A regression analysis was performed with respect to the 11-year (1984-1994) monthly average streamflow and water table depth. By assuming groundwater is 80% of streamflow as discussed in section 3.3. The following regression equation was derived:

$$Q_{gw} = \frac{164.7}{D_{gw}^{\,2}} - 1.42 \qquad (unit: mm/month) \tag{4.3}$$

with the correlation coefficient of 0.842. We have changed the exponent on the Q_{gw}-D_{gw} relationship from –1, -2, -3, to -4, and found that the inverse square dependence gives the highest correlation coefficient. In the next section, the simple unconfined aquifer model (Eqs. (4.2) and (4.3)) will be interactively coupled with the soil model in the LSX.

4.3.2 Coupling Groundwater Model to the LSX Model (LSXGW)

The soil model in the LSX is properly modified to accommodate the developed unconfined aquifer model. In the original LSX, the boundary condition at the bottom of the soil column is the drainage flux. In order to locate the lower boundary of the soil column at the water table, the flux boundary condition in LSX is modified to the concentration boundary condition by specifying the soil saturation in the lowest soil layer equals to one. Notice that such a boundary is actually where the top of the capillary fringe rather than the water table is located. However, it is possible to convert the top of the capillary fringe to the actual water table depth by approximating the thickness of the capillary fringe. For the silt loam soils typical in Illinois, the thickness of capillary fringe is about 50 cm [*Philip*, 1969].

By coupling Eq. (4.2) to the single soil column model in the LSX, the total length of the unsaturated soil column varies in response to the fluctuations in water table depth. Therefore, the number of the unsaturated soil layers varies with time since the vertical resolution of the soil model is fixed. In order to locate the water table position more accurately and capture the sharp moisture gradient near the water table, a fine resolution soil model is adopted. The specification of the soil layer geometry is flexible and the number of total layers is determined by the water table condition and the bedrock position. Here total 50 soil layers are used: 10cm each for the first 1 meter of soils and 20cm each from below 1 to 9 meters. If the water table locates within the layer n for a specific time step, the soil layers from 1 to (n-1) are unsaturated, and the soil moisture in these (n-1) layers would be solved by the Richards equation at that time step. If the water table falls below 9 meters, the soil model and aquifer model are basically decoupled and the gravity drainage boundary condition applies. This treatment is advantageous because it does not specify unjustified common boundary conditions such as gravity drainage or no flux conditions. Another reason in favor of the fine resolution model is because the magnitude of diffusion flux depends on the distance between the centers of two adjacent bottom layers (see Eq. 4.1), thus the thickness of soil layers should be as thin as possible in order to remove this sensitivity.

For each time step, the groundwater model simultaneously receives the drainage flux from the overlying soil column (i.e., groundwater recharge) and discharges runoff into streams. The water table position is updated accordingly at the end of each time step. The direction of the soil drainage flux can be downward or upward depends on the relative magnitude of the gravity drainage and diffusion fluxes. For the next time step, the soil moisture is updated according to the new position of water table by solving the Richards equation. By doing so, the interactions between the unsaturated and saturated zones are explicitly represented.

From Eq. (4.2), if I_{gw} is negative (upward flux from the water table), water table would go down since Q_{gw} is always positive. However, if both I_{gw} and Q_{gw} are positive, water table may go up or go down depending on the relative magnitude of these two fluxes. In either case, it forms a negative feedback that brings water table back to its equilibrium position. When water table goes up, Q_{gw} begins to increase and I_{gw} begins to decrease due to the stronger upward diffusion flux caused by the steeper moisture gradient. Both mechanisms have the effect of bringing water table down. On the other hand, when the water table goes down, Q_{gw} decreases and I_{gw} increases due to the weaker diffusion flux as a result of the smoother soil moisture gradient. The effect of both mechanisms is to increase the amount of water in the aquifer and hence to raise the water table.

4.3.3 Model Testing in Illinois

The coupled model LSXGW has been tested in Illinois using the identical atmospheric forcing and model parameters as that used in the LSX simulation (section 4.2). The results for the 11-year (1984-1994) LSXGW simulation are summarized in the follwing. First, the evaporation ratio and runoff ratio from 1984 to 1994 are shown in Figure 4.8 against the observations. In general, the LSXGW reproduces the observed interannual variability reasonably well, although small deviations (~10%) from observations remain during 1991-1993. The comparison of this figure with the LSX simulation (without groundwater representation) in Figure 4.7 indicates that the partitioning of the annual precipitation into evaporation and runoff is

significantly improved after incorporating the water table dynamics. Figure 4.9 shows the (11-year) average seasonal cycles of the simulated water table depth, soil drainage (i.e., groundwater recharge), and the total runoff (as well as its two components, groundwater runoff and surface runoff) of the LSXGW simulation in comparison with the corresponding observations. Figure 4.10 shows the seasonal cycles of the total evaporation and its three components (transpiration, soil evaporation and interception loss) in comparisons with the observations. Moreover, the seasonal cycles of the observed and simulated soil saturation in 11 soil layers are compared in Figure 4.11.

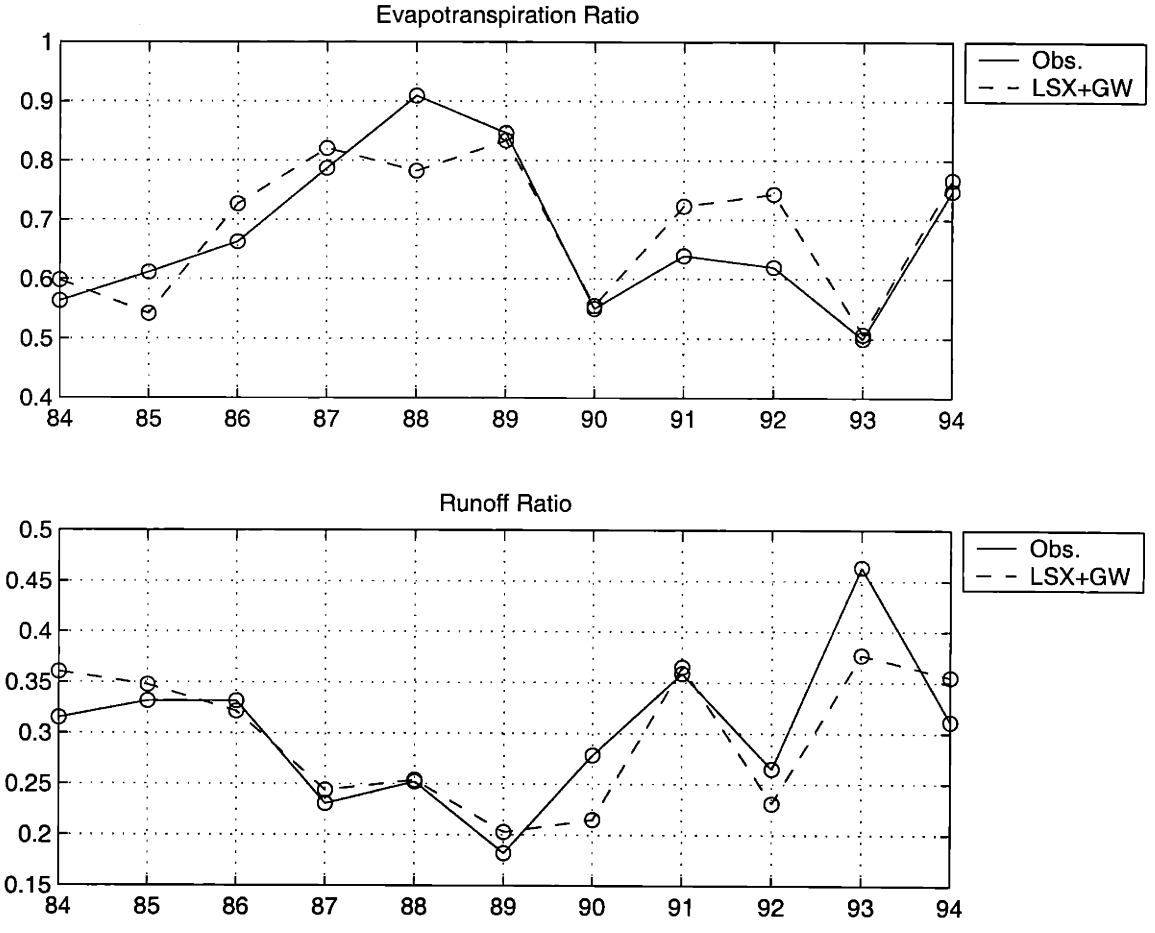

Figure 4.8 The simulated evaporation ratio and runoff ratio from 1984 to 1994 in comparison with the observations.

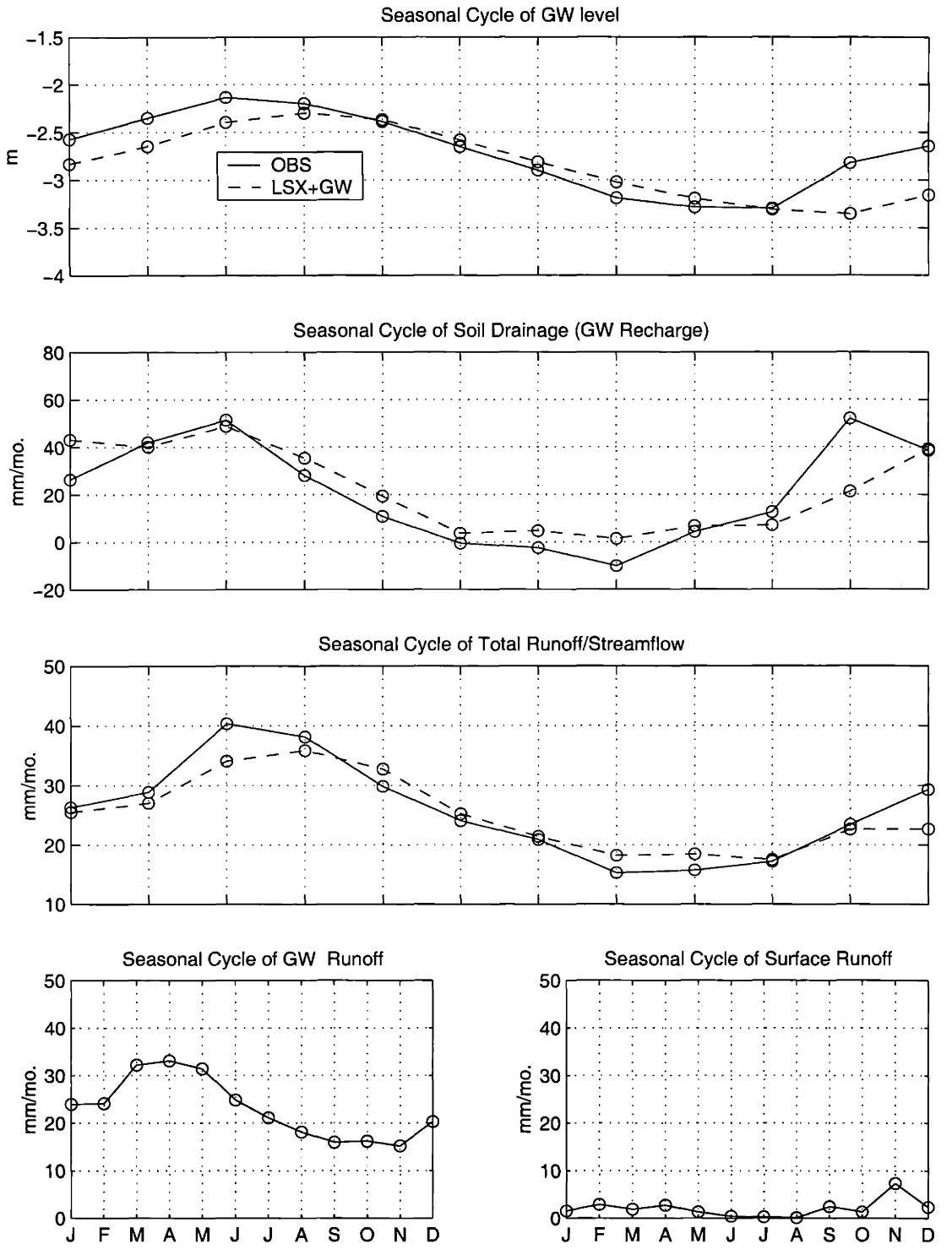

Figure 4.9 The 11-year (1984-1994) average seasonal cycles of the simulated water table depth, soil drainage (i.e., groundwater recharge), and total runoff from the LSXGW simulation in comparison with the corresponding observations. The seasonal cycles of two runoff components, groundwater runoff and surface runoff, are also shown in this figure.

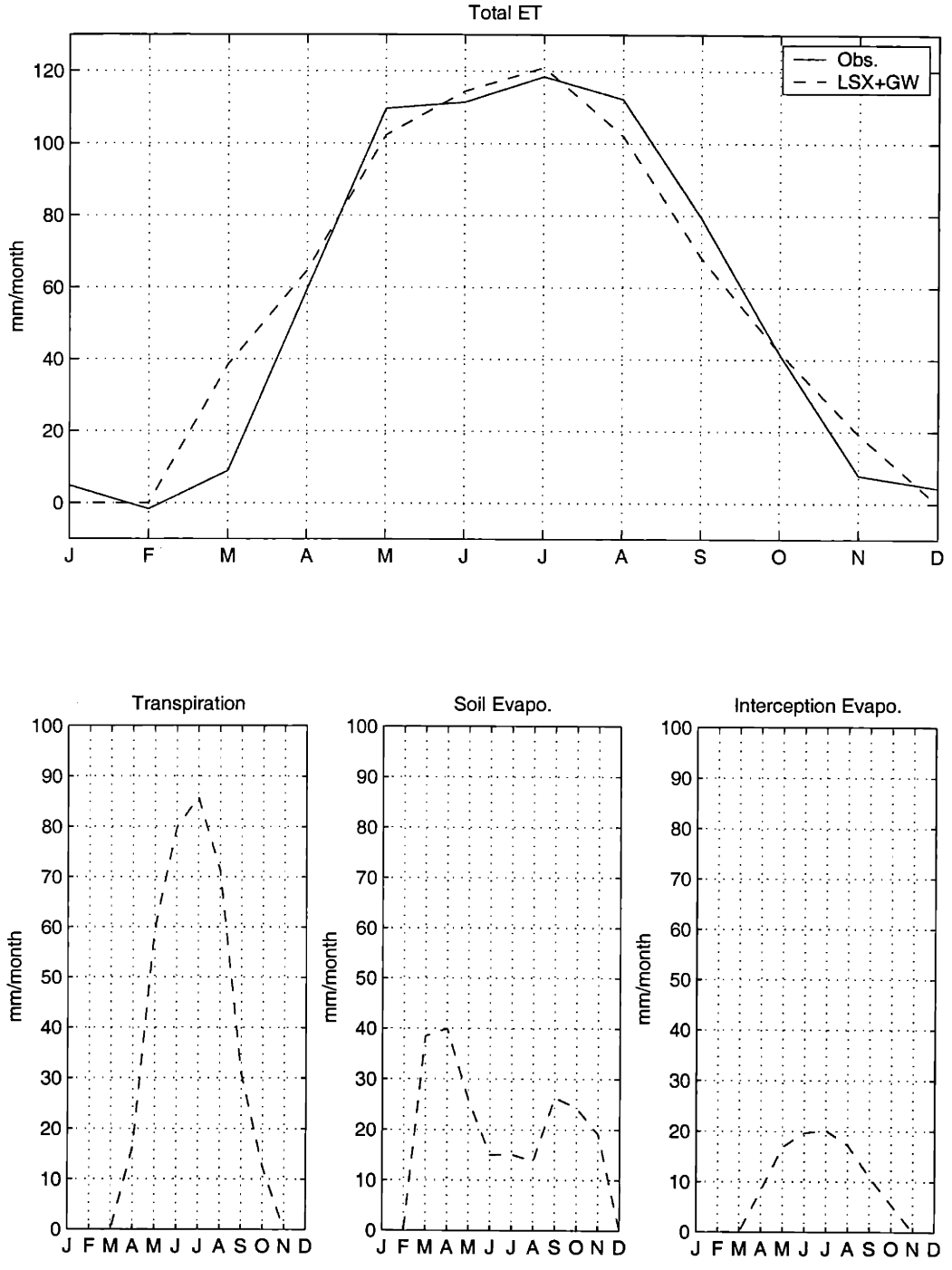

Figure 4.10 The 11-year (1984-1994) average seasonal cycles of total evaporation and its three components: transpiration, soil evaporation, and interception loss. The observation in this figure is the evaporation estimate from the water balance computations in section 2.3.

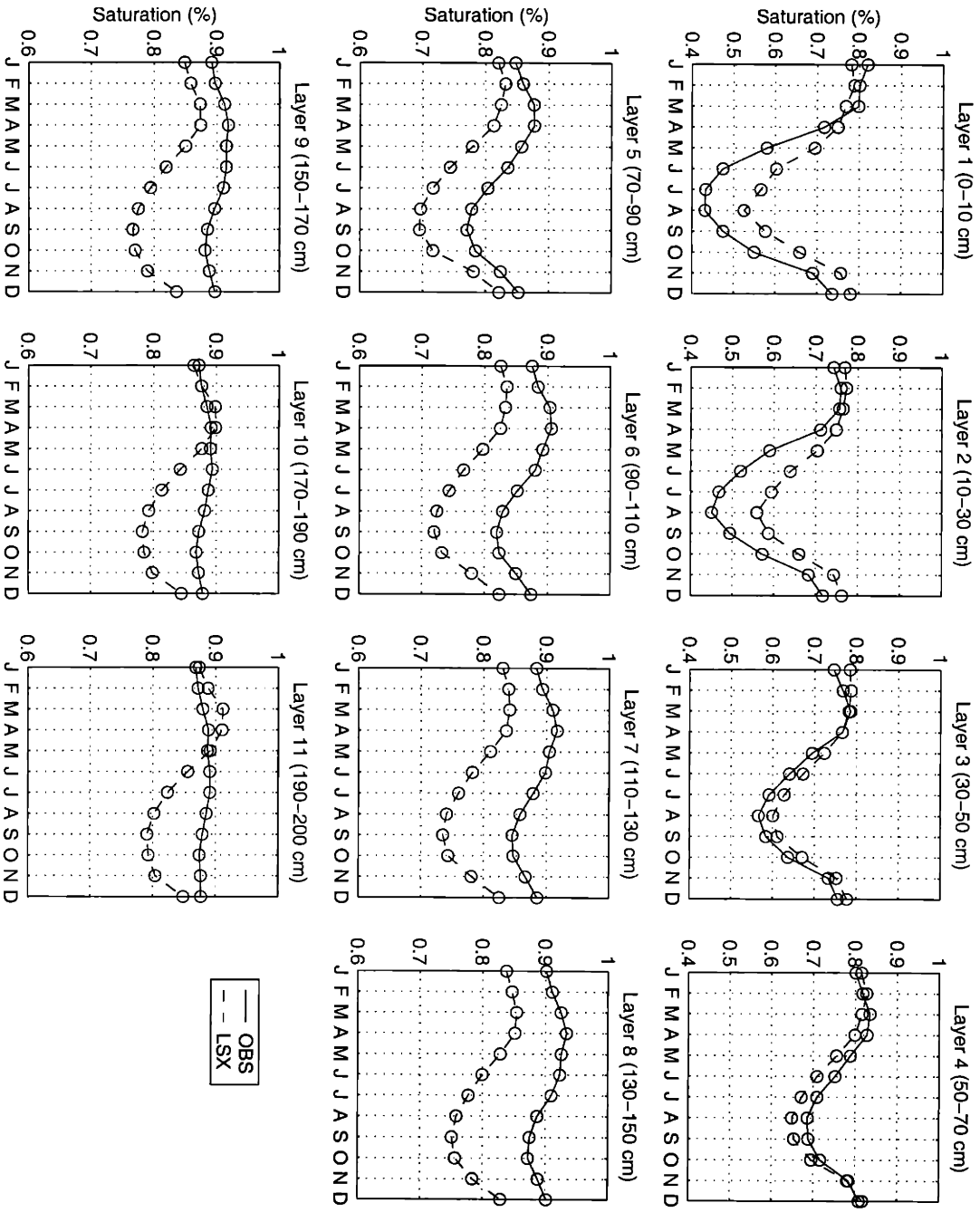

Figure 4.11 The 11-year (1984-1994) average seasonal cycles of the observed and the simulated soil saturation degrees in 11 soil layers from 0-2m below the surface.

The overall remarkable agreement between the LSXGW simulation and the observation as shown in Figures 4.8 - 4.11 indicates that the incorporation of groundwater model has resulted in significant improvement in the simulated land surface hydrology. The seasonal cycles of the simulated total runoff as well as soil drainage match the observations significantly better than the simulations by the LSX (Figures 4.2 and 4.3). Moreover, the simulated soil moisture profile by the LSXGW (Figure 4.11) has greatly improved the large biases found in the LSX simulations (Figures 4.5 and 4.6). However, the LSXGW simulations still have some shortcomings that need further improvements. The 11-year monthly time series of water table depth, soil drainage (groundwater recharge), and the total runoff are plotted in comparison with observations in Figure 4.12. As seen from this figure, there is a lag in the predicted water table depth by the LSXGW during the periods of 1988-1989 and 1992-1993. Furthermore, the observed negative groundwater recharge (upward water fluxes) in the summer months is not well reproduced by the LSXGW especially in 1985, 1988, and 1991. The LSXGW indeed simulates small upward fluxes in certain summer months, but its average seasonal cycle (Figure 4.9) fails to reproduce the observed negative groundwater recharge in summer months. The major reason responsible for this deficiency is that the impacts of spatial variability in water table depth have not been incorporated in the LSXGW. For example, the severe drought condition in 1988 resulted in a larger than average decrease in groundwater level for some regions in Illinois. Since the LSXGW only simulates the average water table depth over the Illinois, the effects of the anomalously low water table depth in some sub-areas in Illinois cannot be incorporated. Similarly, the upward water fluxes from the aquifer to the unsaturated zone take place only in the shallow water table regions. Without the consideration of the spatial variability of water table depth, the LSXGW cannot simulate the correct average magnitude of upward water fluxes. The important issue of the spatial variability of water table depth will be addressed in Chapter 5.

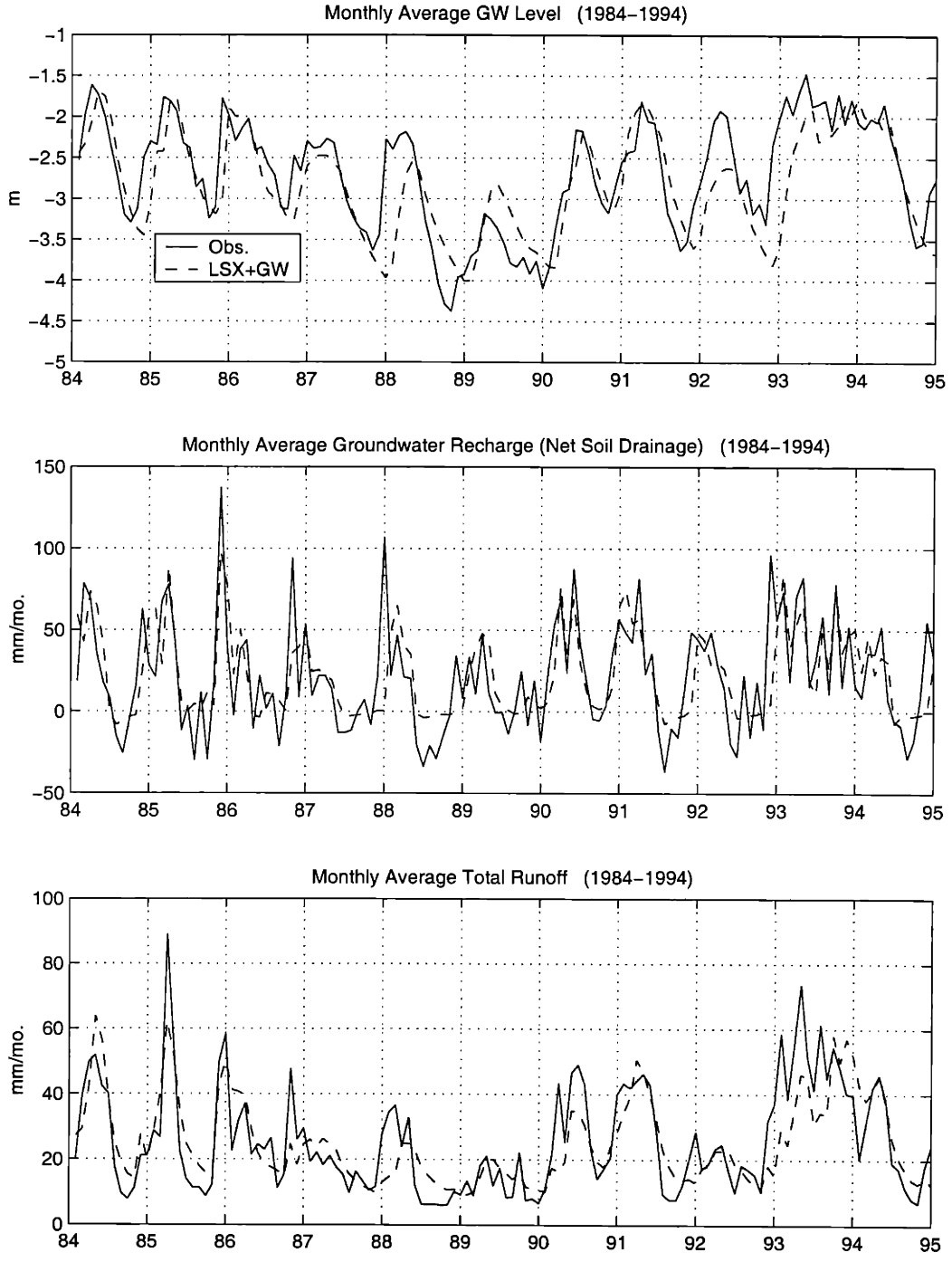

Figure 4.12 The 1984-1994 monthly time series of water table level, soil drainage, and total runoff in comparison with the corresponding monthly observations in Illinois.

Chapter 5 The Representation of Sub-grid Variability of Water Table Depth

5.1 Theoretical Development

In Section 4.3 a simple unconfined aquifer model is developed and interactively coupled to the LSX. The coupled model (LSXGW) has been tested in Illinois for an 11-year period from 1984 to 1994. It is found from the comparison with the observations that although the incorporation of groundwater dynamics has improved the model performance there are still certain biases possibly due to the neglect of the spatial variability of water table depth (WTD). In this chapter, the issue of sub-grid variability will be addressed. A new methodology combining the statistical-dynamical (SD) approach and the mosaic approach will be proposed to incorporate the sub-grid variability of WTD into the LSXGW.

Figure 5.1 shows the 11-year average seasonal cycles of the WTD at 15 monitoring wells in the Illinois. These 15 wells are selected from the total 18 monitoring wells in Illinois because of their availability of the complete records from 1984-1994. These wells are all in the unconfined condition and remote from pumping centers. As shown in Figure 5.1, WTD exhibits significant variability with the range of 0-15 meters below the surface. The research problem addressed here is, how these local-scale spatial heterogeneities of WTD be represented in the LSXGW, and how would they impact the regional-scale hydroclimatology in Illinois.

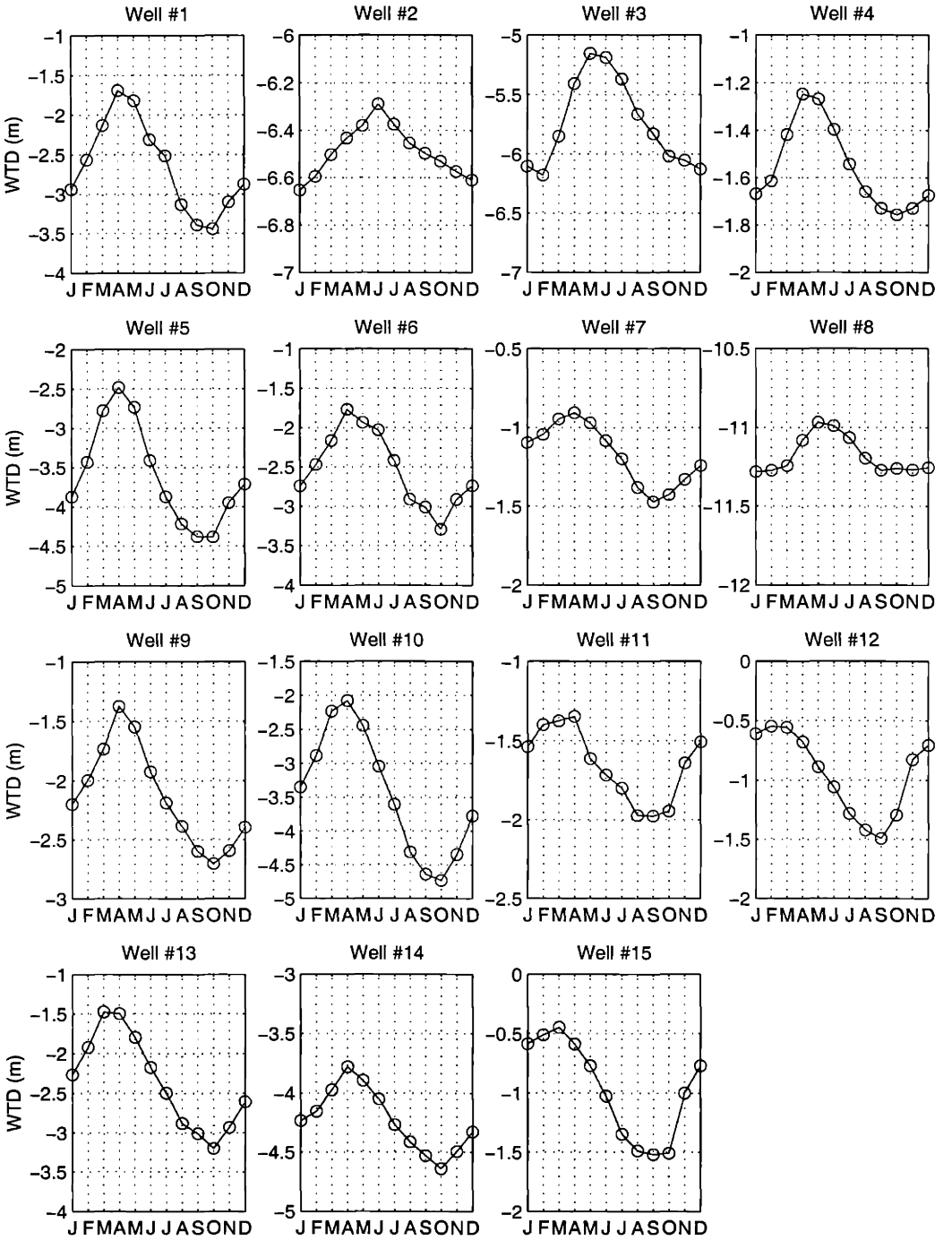

Figure 5.1 Long-term (1966-1996) average seasonal cycles of the water table depth (WTD) at 15 monitoring wells located in Illinois.

5.1.1 The Representation of Sub-grid Variability of WTD in Groundwater Runoff

In Section 4.3, the water balance equation for an unconfined aquifer is described as:

$$S_y \frac{dH}{dt} = I_{gw} - Q_{gw}$$

This equation is to be used at the grid scale of climate models although the water balance itself is valid at any scale. Due to the large scale of application (several tens kilometers to several hundreds kilometers) relative to the typical scale of most hydrological processes (i.e., several hundreds meters to several kilometers), the issue of the sub-grid variability cannot be ignored. Specifically, the effects of the spatial variability of the groundwater level (H) on the macro-scale groundwater recharge (I_{gw}) and groundwater discharge to streams (Q_{gw}) should be incorporated into the LSXGW.

Recall that there is a strong nonlinear relationship between the state-average streamflow and water table depth (WTD) in Illinois as shown in Figure 3.1 (p.56). It is meaningful to investigate if such a nonlinear dependence can also be observed at the small scale. Figure 5.2 shows the scatter plot of the 11-year (1984 -1994) observed monthly WTD versus the streamflow in the nearby stream gauges in eight locations of Illinois. The distances between these groundwater wells and stream gauges range between 5-30 kilometers. As observed from this figure, streamflow is generated when water table is above a threshold depth. The scatter plots of streamflow versus rainfall in these eight locations show little correlation between them, which together with the correlation shown in Figure 5.2 suggest that these streams are fed by the neighboring unconfined aquifers. In fact, some of these streams are ephemeral which desiccates in summer when the water table is low and connects with the unconfined aquifers during the high water table seasons.

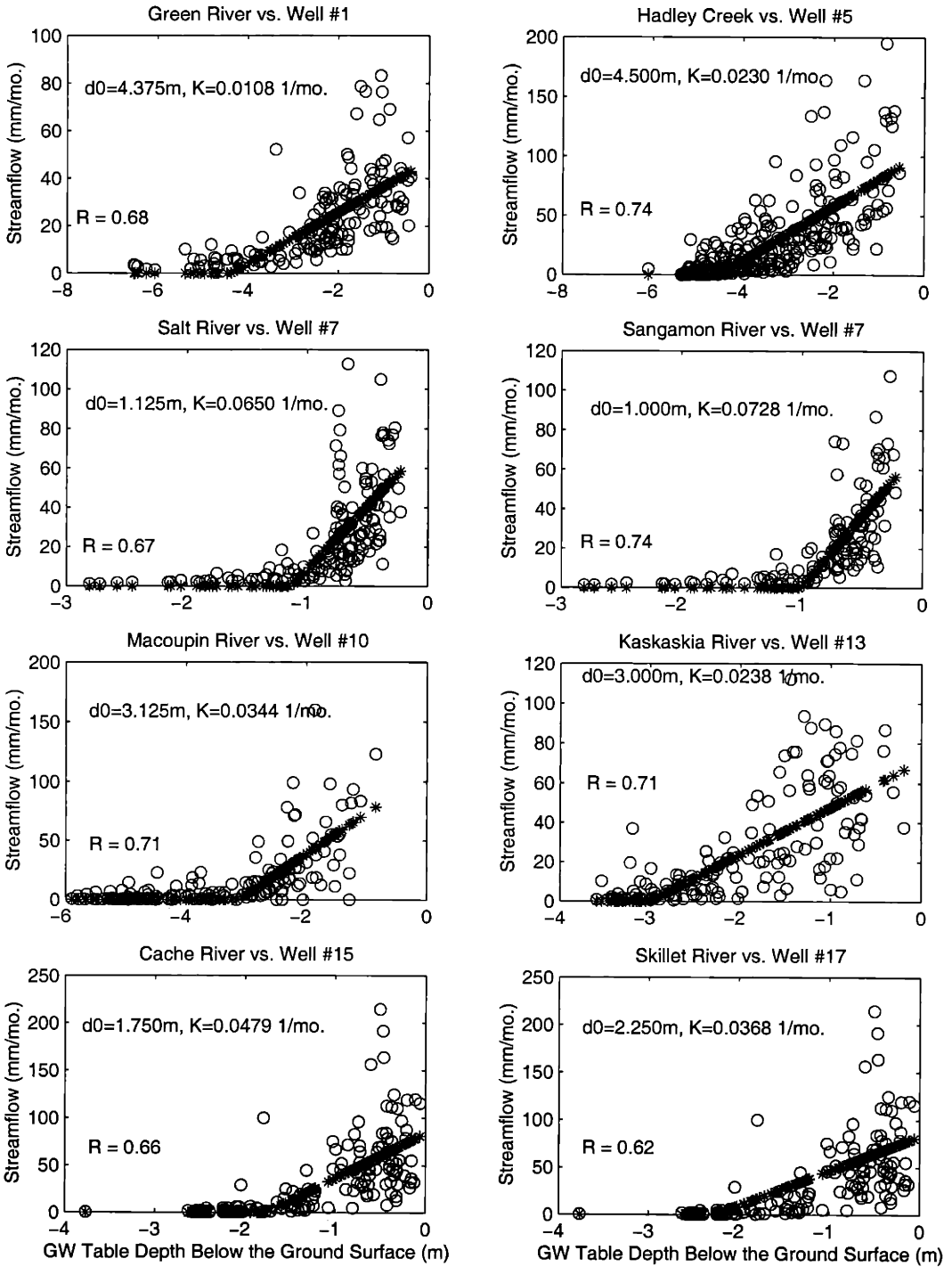

Figure 5.2 The scatter plots of the observed monthly WTD versus the corresponding nearby streamflow from 1984 to 1994 in eight locations in Illinois. Also shown in the Figure are the optimized parameters (d_0 and K) and the corresponding correlation coefficients derived from the least absolute error criterion.

Based on the observations in Figure 5.2, groundwater runoff at a catchment can be formulated as:

$$\begin{aligned} Q_{gw} &= K(d_0 - d_{gw}) \qquad if \quad 0 \le d_{gw} \le d_0 \\ Q_{gw} &= 0 \qquad\qquad\quad if \quad d_{gw} \ge d_0 \end{aligned} \tag{5.1}$$

where Q_{gw} [L/T] is the groundwater runoff, d_{gw} (≥ 0) [L] is the water table depth (WTD), and K [1/T] is the outflow constant inversely proportional to the aquifer residence time. Notice that d_{gw} is always positive. Eq. (5.1) is a threshold-type nonlinear function, which assumes a constant threshold storage, d_0 [L], independent of time, before groundwater runoff occurs. The threshold storage d_0 is a function of the catchment topography relative to the stream network, while the outflow constant K is mainly a function of soil properties. Both d_0 and K are catchment-scale parameters.

The groundwater runoff function in Eq. (5.1) is fitted to the observations in Figure 5.2 by using the least-absolute-error (LAE) criterion. The best-fit lines are obtained by varying d_0 and K simultaneously within the reasonabel ranges until the optimal values are found that minimizes the sum of the absolute errors. Because high streamflow contains more contributions from surface runoff, the LAE criterion is chose over the commonly used least-square-error criterion in order to reduce the bias caused by assuming that streamflow is the same as groundwater runoff. The derived optimal parameters (d_0 and K) and the fitted groundwater runoff in these eight locations are also shown in Figure 5.2. Although the magnitude of streamflow is assumed to be approximately equivalent to the groundwater runoff, it is believed that the minor part of streamflow coming from surface runoff would not significantly influence the estimations of d_0 and K.

While applying water balance equation (4.2) to the grid scale of climate models, the grid scale fluxes, I_{gw} and Q_{gw}, cannot be determined solely from the grid-average groundwater level H because of the nonlinear dependence between them. A statistical-dynamical (SD) approach is

proposed in the following to account for the effect of the sub-grid variability of WTD on the grid scale Q_{gw}. Concerning the effect of the sub-grid variability of I_{gw}, it will be dealt with in Section 5.1.2. The objective here is to derive the grid scale groundwater-rating curve (i.e., the functional relationship between groundwater level and groundwater runoff) by using statistical information on the sub-grid distribution of WTD.

To investigate the sub-grid distribution of WTD, the histogram of the 11-year (1984-94) average WTD (d_{gw}) at 14 wells in Illinois is plotted in Figure 5.3a. According to this figure, the following two-parameter Gamma distribution is assumed to be the PDF (probablity density function) of d_{gw}:

$$f(d_{gw}) = \frac{\lambda^{\alpha}}{\Gamma(\alpha)} d_{gw}^{\alpha-1} e^{-\lambda d_{gw}} \tag{5.2}$$

where $\Gamma(\alpha)$ is the Gamma function; α (shape parameter) and λ (scale parameter) are two parameters related each other through the grid-average WTD $E[d_{gw}]$:

$$\lambda = \frac{\alpha}{E[d_{gw}]} \tag{5.3}$$

The coefficient of variation of the WTD distribution is:

$$c.o.v. = \frac{1}{\alpha^2} \tag{5.4}$$

for a given α, the scale of the PDF $f(d_{gw})$ is dynamically shifted based on the time varying $E[d_{gw}]$. The PDFs for different values of α are plotted in Figure 5.3b. If $\alpha = 1$, the PDF collapse to the exponential distribution; while if α approaches infinite, the PDF approaches the Gaussian distribution.

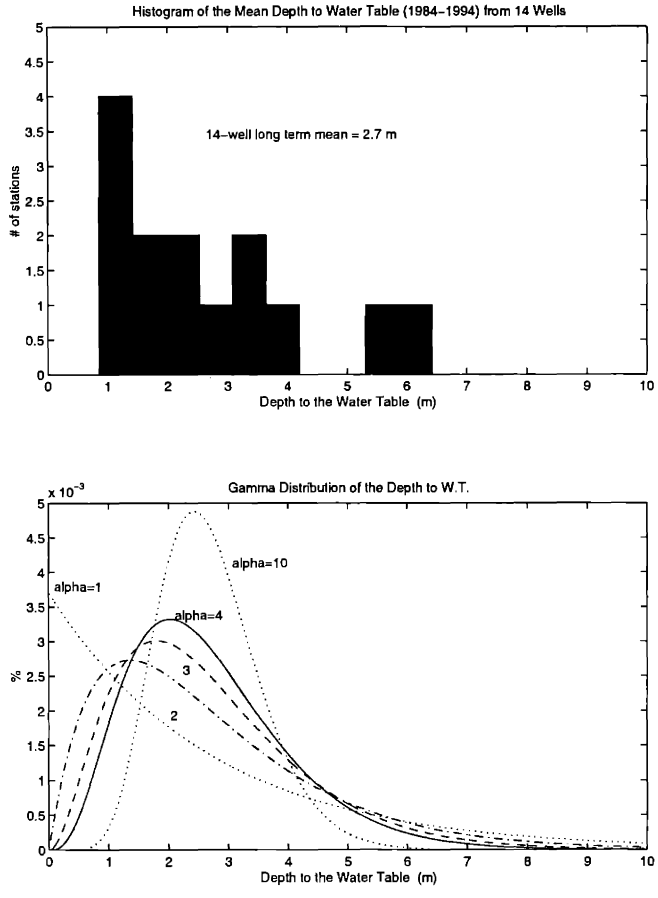

Figure 5.3 (a) The histogram of the 11-year (1984-1994) average WTD from 15 wells in Illinois; (b) The PDF of a Gamma distribution used to fit the histogram of WTD for different values of scale parameters α.

The grid scale groundwater runoff can be derived by integrating the point groundwater runoff function in Eq. (5.1) with respect to the PDF of d_{gw} in Eq. (5.2):

$$E[Q_{gw}] = \int_{d_{gw}=0}^{d_{gw}=d_0} K(d_0 - d_{gw}) f(d_{gw}) d(d_{gw})$$

$$= \frac{K\lambda^{\alpha}}{\Gamma(\alpha)} \left\{ d_0 \left[\frac{(\alpha-1)!}{\lambda^{\alpha}} - e^{-\lambda d_0} \sum_{k=0}^{\alpha-1} \frac{(\alpha-1)!}{k!} \frac{d_0^{\,k}}{\lambda^{\alpha-k}} \right] - \left[\frac{\alpha!}{\lambda^{\alpha+1}} - e^{-\lambda d_0} \sum_{k=0}^{\alpha} \frac{\alpha!}{k!} \frac{d_0^{\,k}}{\lambda^{\alpha-k+1}} \right] \right\} \tag{5.5}$$

Figure 5.4 plots $E[Q_{gw}]$ versus $E[d_{gw}]$ for α=1, 2, 3, and 4, respectively, in comparison with the observed state-average grounwater rating curve. The effective parameters (i.e., d_0=2.64 m and K=0.0393 1/month) introduced in Eq. (5.1) to plot Figure 5.4 are the arithmetic averages of the local-scale parameters in those 8 locations shown in Figure 5.2. Only the curves for α=1-4 are shown since the sensitivity of the rating curve to α decreases significantly as α increases. The close agreement between the theoretical $E[Q_{gw}]$ (for α=3 or 4) and the observation in this figure indicate the suitability of the proposed SD approach in the statistical integration of the sub-grid scale groundwater runoff function to the grid scale groundwater rating-curve.

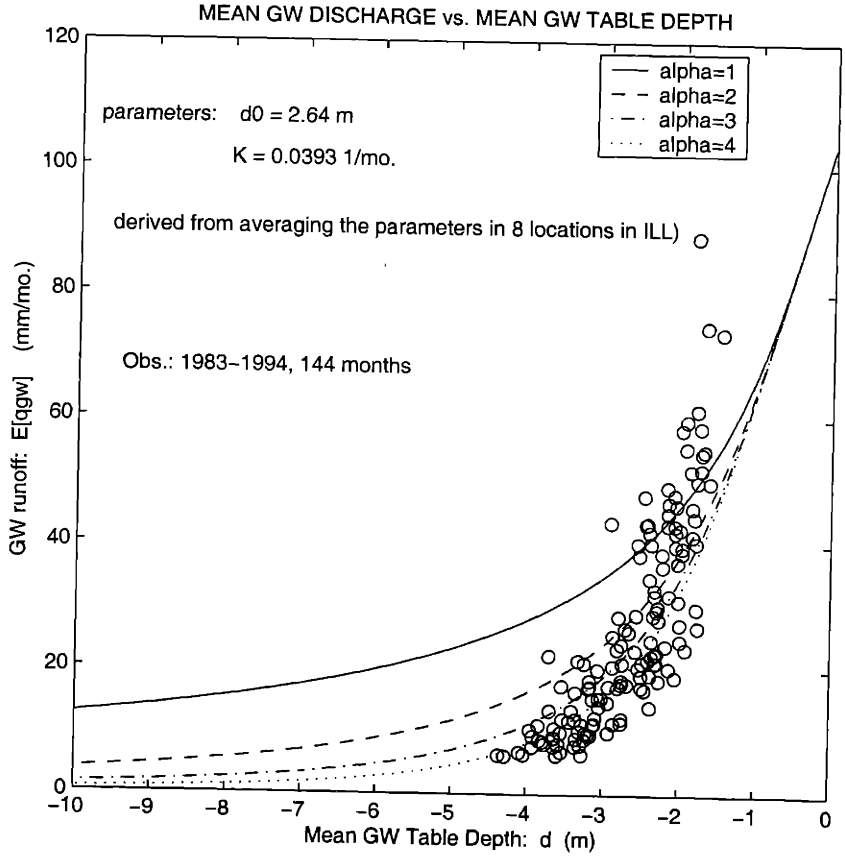

Figure 5.4 Grid-scale groundwater rating-curve: the average groundwater runoff ($E[Q_{gw}]$) versus the average WTD (E[d_{gw}]) for different values of α. The circles in the Figure are the observed state-average groundwater rating-curve in Illinois.

5.1.2 The Representation of Sub-grid variability of WTD in Groundwater Recharge

In section 5.1.1, a statistical-dynamical (SD) approach was proposed to account for the effects of the sub-grid variability of WTD in the grid scale groundwater runoff. However, the impacts of sub-grid variability in the unsaturated-saturated zone interactions have not been incorporated into the LSXGW. That is, the calculation of the grid scale groundwater recharge is based solely on the grid-average WTD without considering its sub-grid variability.

A new methodology based on the mosaic approach is proposed in the following to deal with this issue. First, a grid cell is divided into a class of sub-grids based on the WTD. The areas with similar WTD are grouped into the same class, say, 0-1m, 1-2m, ...etc. These sub-grids coexist within a grid with their individual area fraction variable over time according to the varying grid-average WTD. Unlike the traditional mosaic approach, these absolute geographic locations of these sub-grids are not fixed. The sub-grids with a shallow water table would locate near the runoff contributing areas and stream channels, whereas those with a deep water table would locate close to the groundwater divide (mountain ridge). The fraction of each sub-grid varies according to the dynamic PDF of WTD (see Eqs. 5.2 and 5.3) and can be determined analytically. For example, if a grid is divided into three sub-grids each with a different WTD ranges ($0-d_1, d_1-d_2$ and d_2-d_3, respectively), the fractions of each sub-grid can be derived as follows:

$$A = A_1 + A_2 + A_3 = \int_{d_{gw}=0}^{d_{gw}=d_3} f(d_{gw})d(d_{gw}) = \frac{\lambda^\alpha}{\Gamma(\alpha)}\left[\frac{(\alpha-1)!}{\lambda^\alpha} - e^{-\lambda d_3}\sum_{k=0}^{\alpha-1}\frac{(\alpha-1)!}{k!}\frac{{d_3}^k}{\lambda^{\alpha-k}}\right]$$

$$A_1 = \int_{d_{gw}=0}^{d_{gw}=d_1} f(d_{gw})d(d_{gw}) = \frac{\lambda^\alpha}{\Gamma(\alpha)}\left[\frac{(\alpha-1)!}{\lambda^\alpha} - e^{-\lambda d_1}\sum_{k=0}^{\alpha-1}\frac{(\alpha-1)!}{k!}\frac{{d_1}^k}{\lambda^{\alpha-k}}\right]$$

$$A_2 = \int_{d_{gw}=0}^{d_{gw}=d_2} f(d_{gw})d(d_{gw}) - \int_{d_{gw}=0}^{d_{gw}=d_1} f(d_{gw})d(d_{gw}); \qquad A_3 = \int_{d_{gw}=0}^{d_{gw}=d_3} f(d_{gw})d(d_{gw}) - \int_{d_{gw}=0}^{d_{gw}=d_2} f(d_{gw})d(d_{gw})$$

(5.6)

In each time step each sub-grid is simulated independently using the LSXGW. The differences among sub-grids are primarily caused by the different water table conditions. The

grid-scale hydrological fluxes are computed at the end of each time step by averaging all the sub-grid fluxes weighted by their individual fractions. Only one single lumped groundwater reservoir is represented for a grid which receives the groundwater recharge from all sub-grids. The groundwater discharge to stream depends on the WTD in the lumped groundwater reservoir. According to the grid-scale groundwater rechage and groudwater discharge fluxes, the grid-average WTD is updated using the water balance equation (4.2) for the next time step.

By using the mosaic approach, the dynamic expansion and contraction of the runoff contributing areas can be quantitatively simulated, and the runoff generation from different hydrological regimes within a grid can be computed separately in a consistent way. Better yet, due to the nature of the mosaic approach the spatial distributions of the entire set of hydrological variables can be obtained, which are valuable information for downscaling the results of climate model simulation from the regional scale to the local scale.

5.2 Results of the One-Column and Multi-Column LSXGW Simulations

Two 11-year (1984-1994) off-line simulations using the LSXGW in Illinois were conducted. The first incorporates the SD approach developed in Section 5.1.1 to account for the effects of the sub-grid variability of water table depth (WTD) in the grid-scale groundwater runoff. This is denoted as "one-column simulation" since there is no grid subdivision in this case. In the second simulation not only the SD approach but the mosaic approach (section 5.1.2) are included in the LSXGW to account for the effects of WTD sub-grid variability on both the groundwater runoff and the groundwater recharge. In this case, which is denoted as "10-column simulation", a grid is subdivided into 10 sub-grids with the WTD of 0-1m, 1-2m, ...,8-9m, and larger than 9m, respectively.

The results of these two 11-year simulations are presented in the following. First, Table 5.1 summarizes the 11-year average annual water balance in comparison with the corresponding observations. It can be seen from Table 5.1 that in general the partitioning of the annual precipitation into evaporation and runoff by the LSXGW is fairly well although the LSXGW slightly overestimates the evaporation by 20 mm/year and underestimates runoff by the same amount. Moreover, it is interesting to note that the partitioning of the annual precipitation into evaporation and runoff is rather similar between the 1-COL and the 10-COL. However, by comparing the 1-COL case with the 10-COL case, two marked differences in Table 5.1 can be

	P	*E*	*I*	*R*	*Rg*	*Rs*
Observations	**998.5**	**656.6**	**253.2**	**309.3**	**-**	**-**
1-column simulation	**998.5**	**674.3**	**264.2**	**296.9**	**269.8**	**27.1**
10-column simulation	**998.5**	**677.6**	**219.2**	**298.4**	**224.6**	**73.8**

P: precipitation; *E*: total evaporation, *I:* groundwater recharge; *R*: total runoff; *Rg*: groundwater runoff; *Rs*: surface runoff. Units are all in mm/year.

Table 5.1 11-year (1984-1994) average annual water balance for the LSX 1-column and 10-clumn simulations in comparison with the corresponding observations

noted: (1) In the 10-COL case 24.7% (73.8 mm/year) of the total runoff comes from surface runoff compared to only 9.1% (27.1 mm/year) in the 1-COL case. The 10-COL case is closer to the estimation in Section 3.3 where the surface runoff is estimated to be about 20% of the total runoff in Illinois; (2) The groundwater recharge simulated in the 10-COL case is 20% less than that in the 1-COL case. Both of these two differences can be attributed to the representation of the hydrology in the shallow water table areas in the 10-COL simulation. One favorable outcome resulted from the grid subdivision in the 10-COL case is the provision of realistic vertical soil moisture profiles under various water table conditions as opposed to only one single profile as in the 1-COL case. Since most of the surface runoff are generated from the shallow water table areas, the grid subdivision is important to realistically model the runoff generation dynamics in the near-stream runoff contributing areas.

Figure 5.5 plots the annual evaporation ratio (i.e., annual total evaporation / precipitation), annual runoff ratio (i.e., annual total runoff / precipitation) and the sum of these two ratios from 1984 to 1994 for both 1-column and 10-column cases against the corresponding observations. It can be seen from this figure that the LSXGW faithfullly reproduces the interannual variability of the annual evaporation and runoff ratios. The fact that the sum of these two ratios from year to year is not always equal to one highlights the importance of groundwater storage at the inter-annual timescale. Furthermore, notice that the differences in the annual evaporation and runoff ratios between the 1-COL and 10-COL cases are not discernible, which suggests the effect of sub-grid variability of WTD on the partitioning of precipitation into evaporation and runoff is negligible for this simulation period of 1984-1994 in Illinois.

Figure 5.6 compares the simulated 11-year average seasonal cycles of the water table depth (WTD), soil drainage (groundwater recharge), and total runoff for both the 1-COL and 10-COL cases to the corresponding observations. Two major runoff component (groundwater runoff and surface runoff) are also plotted in the figure. In general, the simulations of both cases agree reasonably well with the observations in the timing and magnitude of the seasonal pattern despite some differences exist between the two cases. However, both cases fail to capture the peak of grounwater recharge in November when the monthly precipitation is at maximum, and as a result the simulated groundwater level is unable to recover as much as the observation indicates during

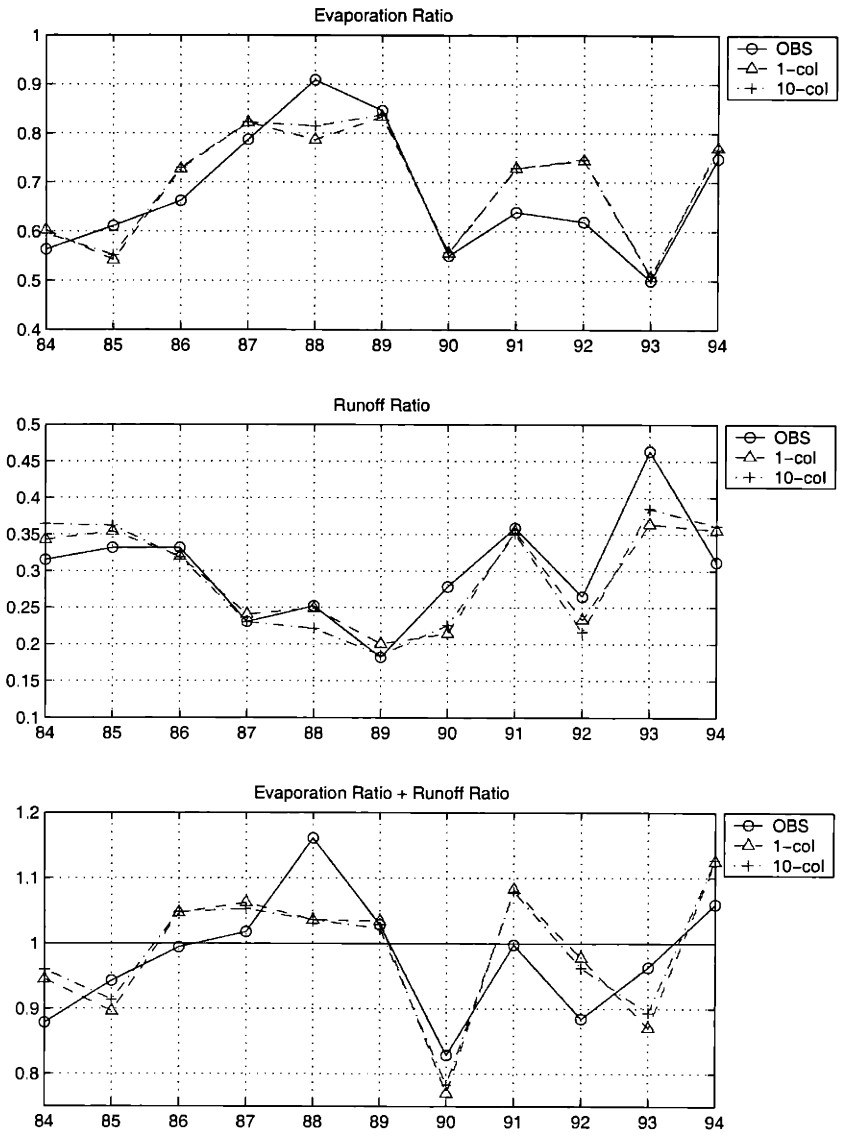

Figure 5.5 The observed and simulated (for both 1-col and 10-col cases) annual evaporation ratio (i.e., annual total evaporation / precipitation) and annual runoff ratio (i.e., annual total runoff / precipitation) from 1984 to 1994.

the winter months. This bias eventually results in the underestimation of the streamflow peak in early spring.

To demonstrate the ability of the LSXGW in simulating the interannual variability, 11-year monthly time series of the simulated WTD soil drainage, and total runoff are plotted in Figure 5.7 in comparison with the corresponding observations. It can be seen that overall the LSXGW faithfully reproduces the observed interannual variability of these variables. Despite some minor

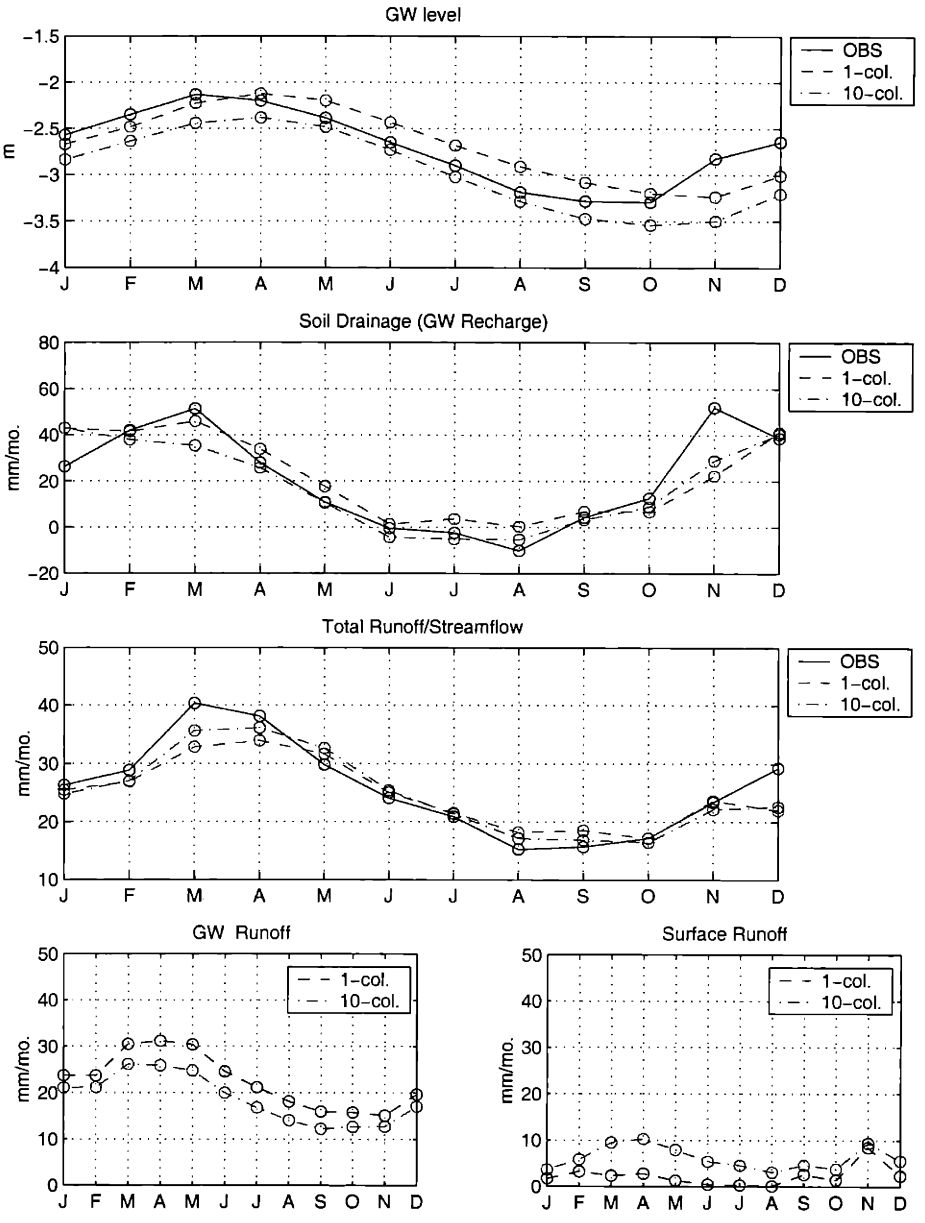

Figure 5.6 11-year (1984-1994) average seasonal cycles of water table depth, soil drainage (groundwater recharge), total runoff, and the two major components of runoff, groundwater runoff and surface runoff.

biases observed in the simulated water table depth especially during the extended drought period from the middle of 1988 to 1989, the simulations of soil drainage (groundwater drainage) and total runoff are remarkably close to the observation in the 11-year period. In particular, the LSXGW model reproduces the observed negative groundwater recharge (upward water flux) in most of the summer in from 1984-1995. Comparing this recharge simulation to that in Figure

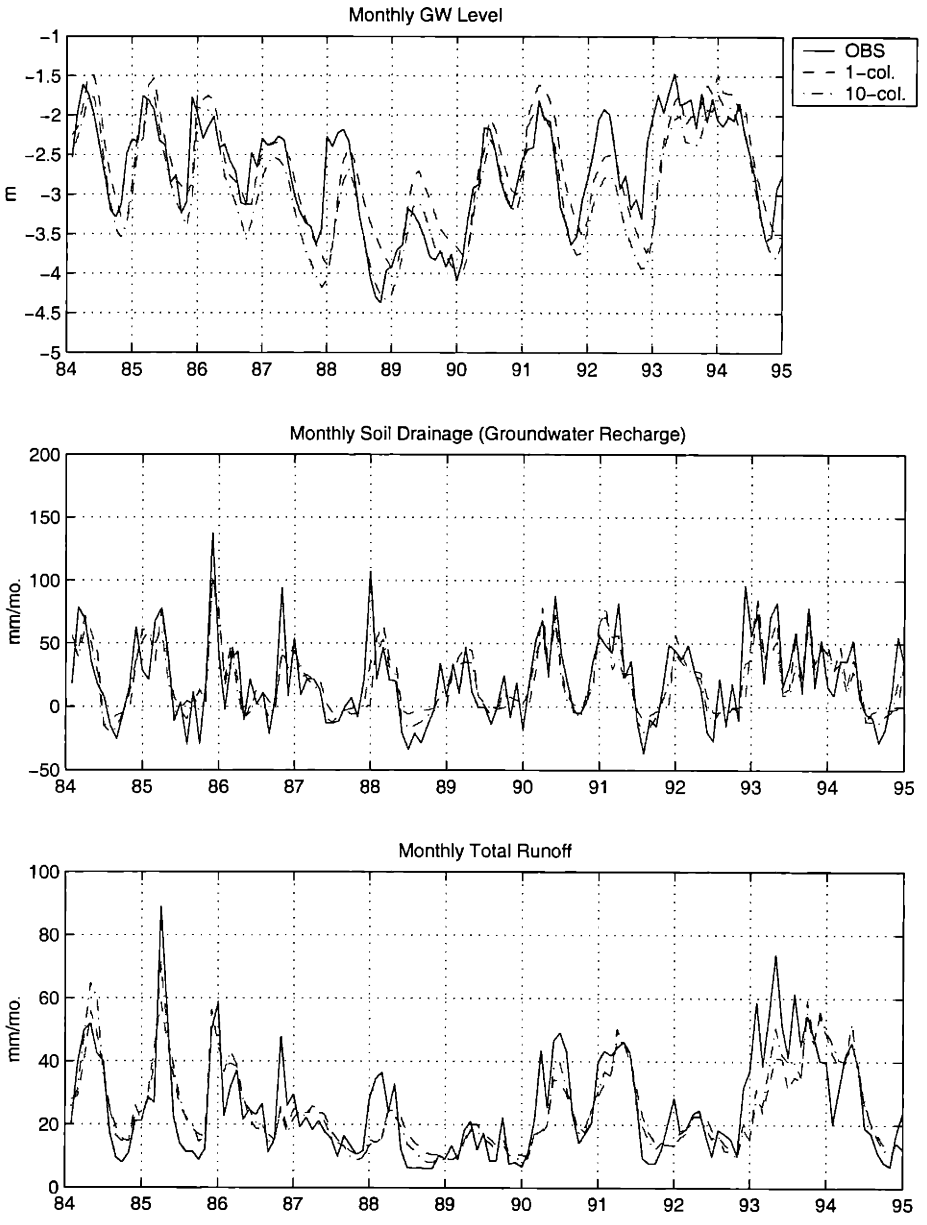

Figure 5.7 The simulated 11-year (1984-1994) monthly time series of (a) water table level, (b) groundwater recharge, and (c) total runoff for both 1-col and 10-col cases in comparison with the observations.

4.6, a significant improvement due to the incorporation of the sub-grid variability of WTD is clear. Moreover, it is rather encouraging that the model picks up the anomalously low (high) water table depth and streamflow during the drought (flood) year 1988 (1993) reasonably well.

The average seasonal cycle of the total evaporation and the corresponding 11-year monthly time series are plotted against the observations in Figure 5.8 The seasonal cycles of the

evaporation simulated in both the 1-COL and 10-COL cases agree well with the observed seasonal pattern of evaporation except in early spring when LSXGW overestimates the evaporation probably due to the inaccuracy in the seasonal cycle of the leaf area index (LAI). Notice that the differences in the simulated evaporation between the 1-COL and 10-COL cases from month to month are not discernible, which suggests the effect of sub-grid variability of WTD on the grid scale evaporation is negligible for this simulation period from 1984-1994 in Illinois.

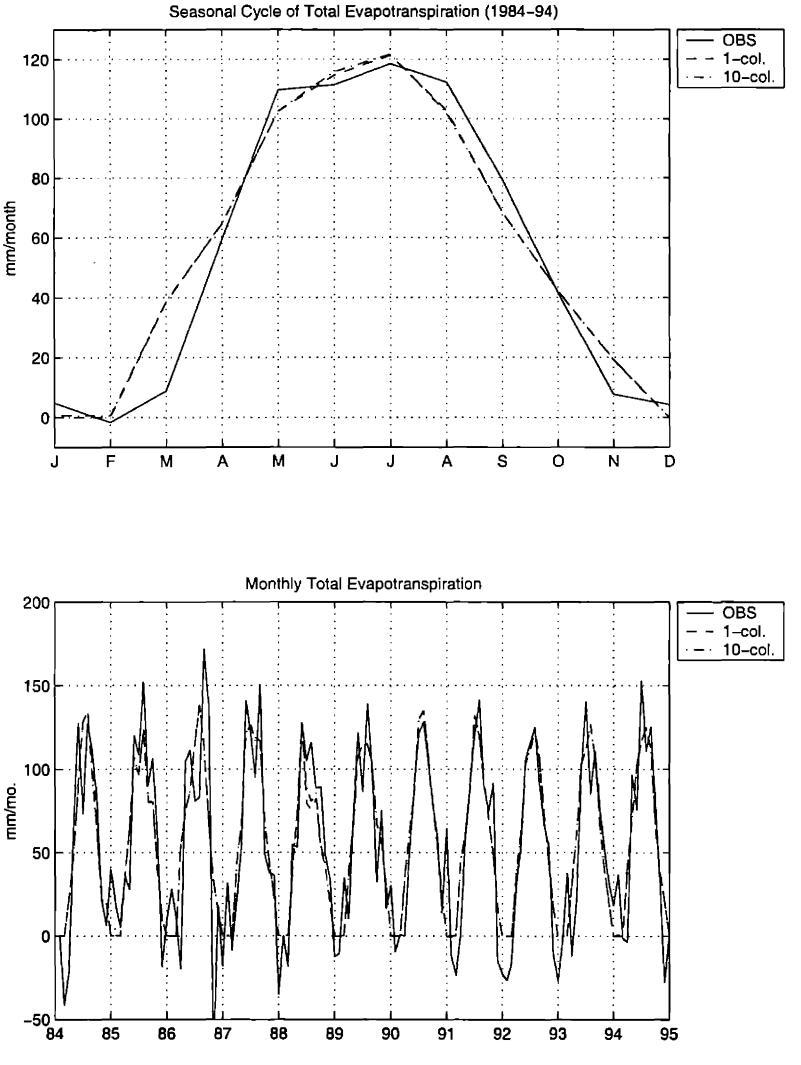

Figure 5.8 11-year (1984-1994) average seasonal cycle of the observed and simulated total evaporation and the corresponding 11-year monthly time series.

Figure 5.9 shows the 11-year climatology of the simulated and the measured soil saturation degree in the 11 soil layers from 0 to 2m below the surface. Again, both cases simulate soil saturation rather close to each other. The most notable bias seen from this figure is that the soil saturation in the surface layers (0-30cm) experiences insufficient drying during the growing season, which is probably related to the specification of the root distribution and/or the LAI inaccuracy as mentioned above. However, the simulation in the layers from 70-170cm is underestimated up to 10% of the saturation, and that in the deep soil layers (170-200 cm) overestimates the amplitude of the seasonal cycles.

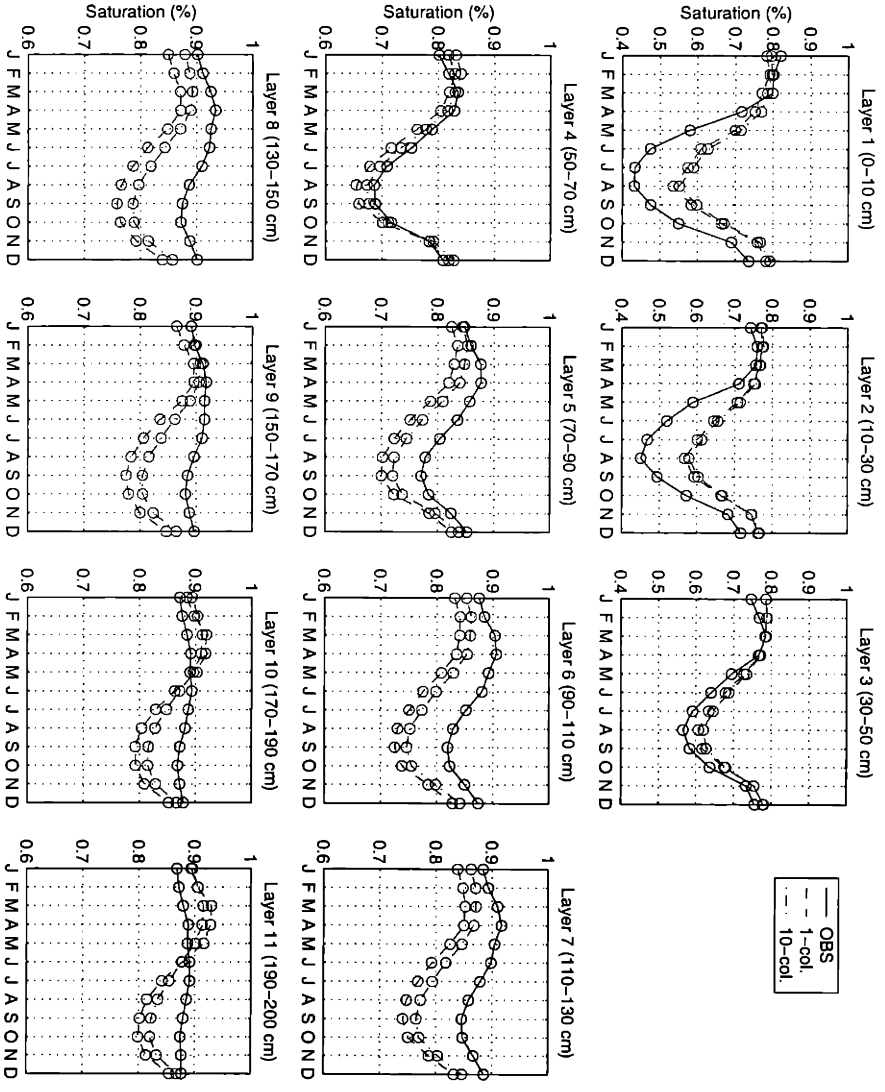

Figure 5.9 11-year (1984-1994) average seasonal cycles of the observed simulated soil saturation from 0 to 2 m below the groundwater surface.

The 11-year monthly time series of the simulated soil saturation are compared with the observations in Figure 5.10. It is encouraging to see that the LSXGW accurately simulates the dry soil moisture anamolies in the surface layers in 1984, 1988 and 1991, as well as the wet anamoly during the flood year 1993. This demonstrates the capability of the LSXGW in simulating the soil moisture dynamics under the drought and flood conditions. However, there are still some notable deficiencies including the consistent dry bias and the exaggerated amplitude of the soil moisture in the 50-150cm soil layers, and the insufficient drying of the soil moisture in the 0-30cm dring the summer of 1985, 86, 89 and 90. The simulated soil moisture in the surface layers (0-30cm) exhibits the observed summer drying only for the dry years when the water stress is strong, which is the main factor responsible for the insufficient drying in the seasonal cycle of the simulated surface soil moisture as shown in Figure 5.9.

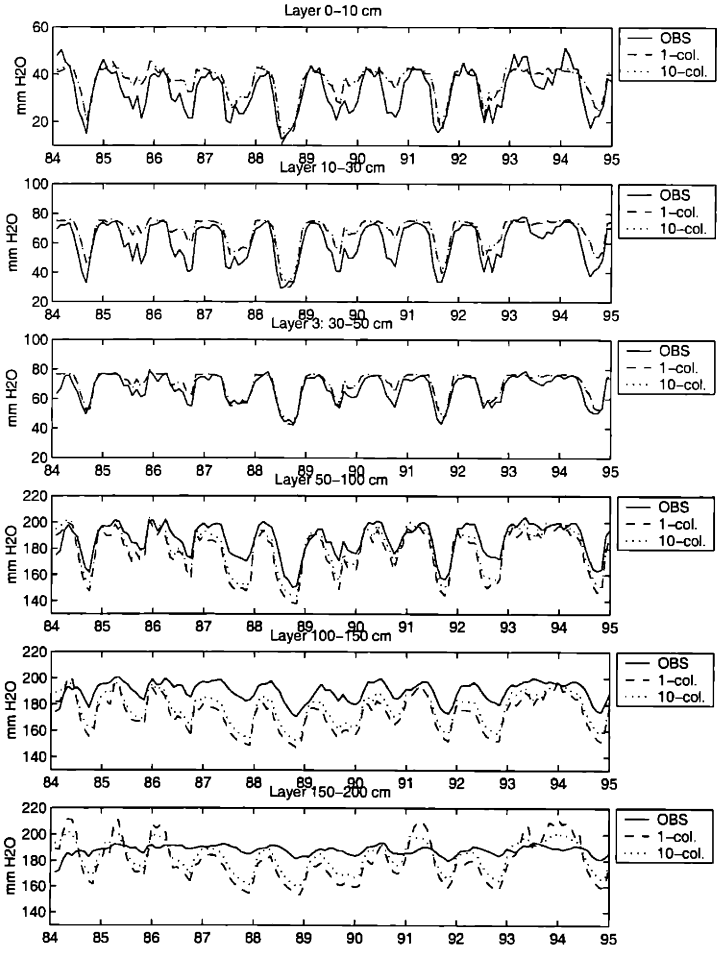

Figure 5.10 11-year monthly (1984-1994) time series of the simulated soil water depth from 0-2m below the ground surface.

In summary, by explicitly modeling the water table dynamics and incorporating the sub-grid variability of WTD in the LSXGW, most of the simulated hydrological states and fluxes agree reasonably well with the observations in Illinois. In addition to the long-term climatologies, the LSXGW also faithfully reproduces the interannual variability of these hydrological variables as shown in Figures 5.6, 5.8, and 5.10.

One interesting point which can be observed from the last several figures is that most of the hydrological variables simulated in the 1-COL case and the 10-COL case are rather similar. The major reason for this similarity is that the Illinois is humid and rarely under the water-stressed condition. The simulation errors in the 1-COL case induced by using only the average WTD in the calculation of aveage fluxes are possibly canceled each other. However, this might not be true for the arid or semi-arid climate frequently under the water-stressed condition. Under such circumstances, the nonlinearity in the associated physical processes as well as the nonuniform distribution of the hydrological states would significantly deviate the resulting average hydrological fluxes from the fluxes calculated from the average hydrological states or parameters. Moreover, the arid regions have their own modeling issues which is beyond the scope of the present research. Two striking examples are the difficulties in the streamflow simulation encountered in the application of the VIC-2L model (*Liang et al.*,1994) to the semiarid and arid regions in Arkansas-Red River basin as reported by *Abdulla and Lettenmaier* [1997], and to a dry subcatchment in the Columbia River basin as reported by *Nijssen et al.* [1997].

The insufficient summer drying of the surface soil moisture in several years between 1984-1994 as shown in Figure 5.10 is probably caused by the sub-grid variability of the surface soil moisture. *Entekhabi and Eagleson* [1989] have shown that by accounting for the sub-grid variability of the surface soil moisture, surface runoff increases due to its threshold triggering characteristic. Although the sub-grid scheme of water table depth developed herein actually also implicitly accounts for the heterogeneous soil moisture profile (especially near the water table) as a result of the various WTD at different locations, the variability of the soil moisture near the surface caused by the sub-grid variability of precipitation is not yet considered. It is the sub-grid variability of the surface soil moisture that would significantly impact the effective infiltration

and surface runoff, which would then feedback to impact the soil moituste profile. We plan to include a sub-grid surface soil moisture scheme into LSXGW in the near future.

Another possibility that might cause the overestimation of surface soil moisture (as well as the underestimated surface runoff in the 1-COL case) is the unrealistic temporal pattern precipitation forcing. The temporal statistics (e.g., the average length of wet and dry spells, the total rainy hours percentage, and the mean precipitation intensity conditioned upon rain) of the grid-average precipitation are significantly distorted in both the spatial and temporal averaging processes. The precipitation forcing used in the LSXGW simulations is the average from the observations in 100 plus stations in Illinois. Since the averaging process has effectively smoothed out the temperoal variability in precipitation in terms of magnitude and frequency, soil moisture is too wet in summer due to the reduced length of dry spells, and surface runoff is too low due to the reduced rainstorm magnitudes. Perhaps more likely, the simulation biases in the surface soil moisture and surface runoff might simply reflect certain degrees of model deficiencies.

A product of the 10-COL simulation is the spatial distributions of the entire set of hydrological variables at the sub-grid scale. For example, Figures 5.11 illustrates the 11-year average seasonal cycles of groundwater recharge and surface runoff in each of the ten sub-grids for the 10-COL simulation. Several important points can be noted from this figure: (1) The sub-grids with a shallower water table have more intensive interactions between the unsaturated and saturated zones as indicated by the lager amplitude in the seasonal cycles of groundwater recharge. (2) The groundwater recharge in column 1 (i.e., with the WTD of 0-1m) is always negative (upward fluxes) throughout a year. The magnitude of the upward groundwater fluxes reaches the peak in summer (~100 mm/mo.). Other than the column 1, upward water fluxes occur only during the summer for those sub-grids with the water depth shallower than 3m. (3) Surface runoff is generated almost completely from the column 1; other sub-grids only contribute a negligible amount of surface runoff in November when the precipitation is at maximum in a year.

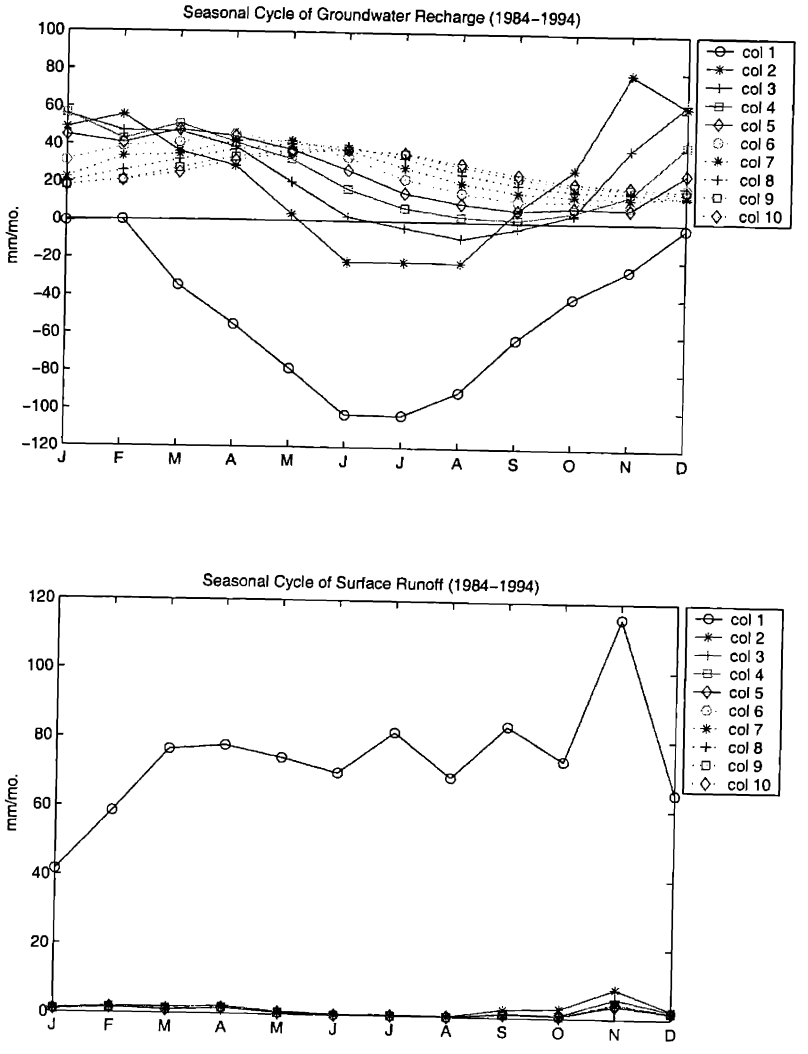

Figure 5.11 11-year (1984-1994) average seasonal cycles of the (a) groundwater recharge and (b) surface runoff. Column 1 denotes the subgrid with a water table shallower than 1m below the surface, while column 10 with a water table deeper than 9m.

To demonstrate the influences of water table position on evaporation, the 11-year (1984-1994) average seasonal cycles and monthly time series of the total evaporation in each sub-grid are plotted in Figure 5.12. From this figure, it can be seen that the sub-grids with a shallow water table (0-3m) have slightly higher evaporation during the growing season. Also the differences in evaporation between the shallow WTD sub-grids can be classified only under the water-stressed condition such like years 1988 and 1991. The fact that the shallow water table regions having a higher evaporation than other regions suggests the groundwater supply to the root zone soil

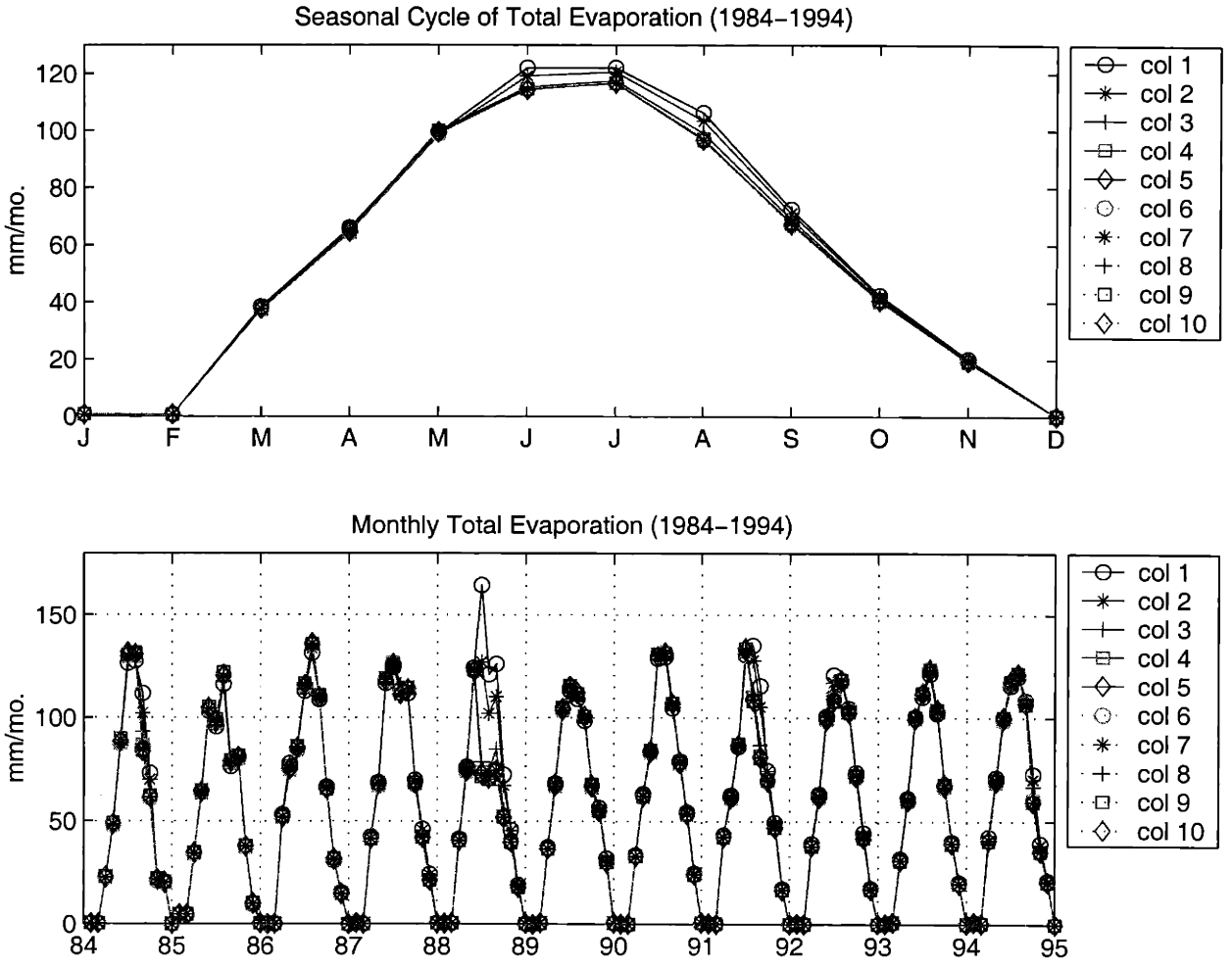

Figure 5.12 11-year (1984-1994) average seasonal cycle and the 11-year monthly time series of the total evaporation in each of the 10 columns.

moisture for maintaining the high evapotranspiration rate during the summer, which has been identified as one of the major roles that unconfined aquifers play in the regional hydroclimatology in Illinois.

Figure 5.13 plots the 11-year monthly time series of the area fraction for each of the 10 columns. As seen in this figure, the fraction of the shallow (deep) water table sub-grids decreases (increases) during the drought year 1988. The opposite trend can be observed during the flood year of 1993. By analytically integrating the dynamically shifted PDF of water table depth (WTD) over a certain WTD interval, the dynamic expansion and contraction of the

corresponding area fraction with the WTD in that interval can be quantitatively traced with consistency by the proposed methodology combining the SD and the mosaic approaches.

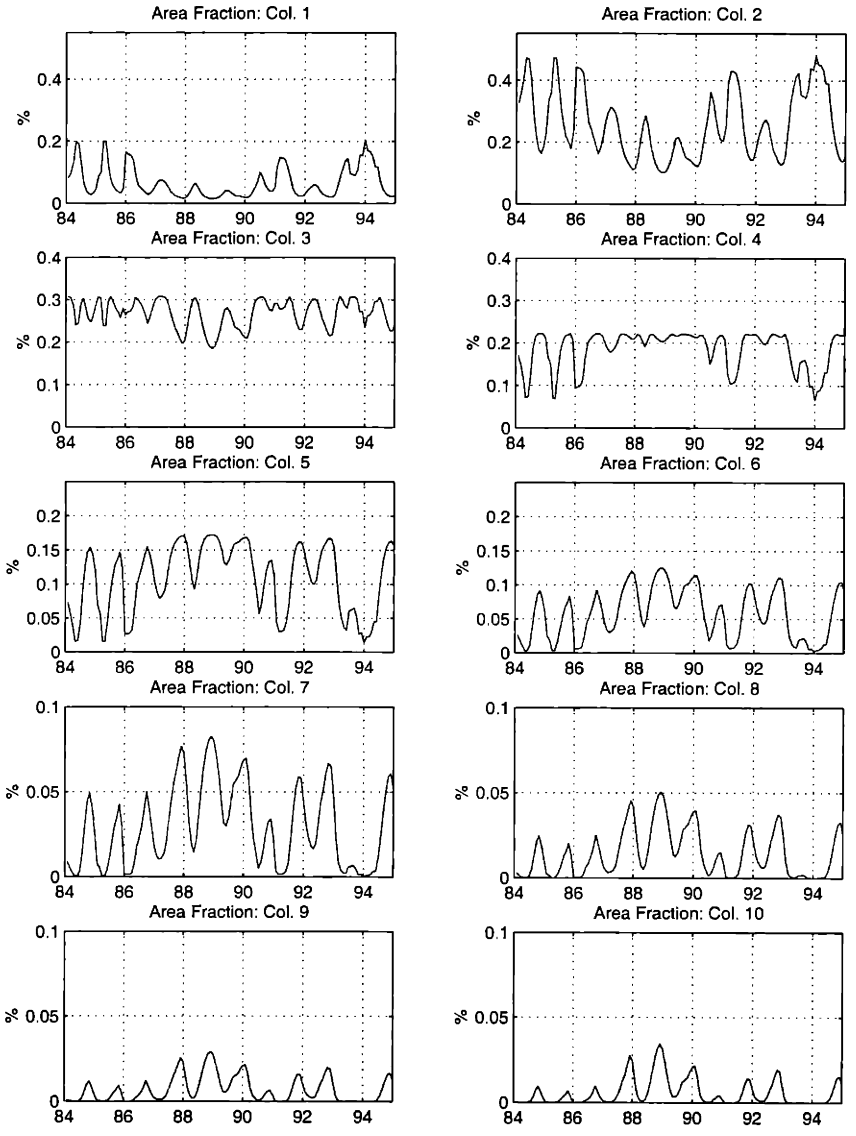

Figure 5.13 11-year (1984-1994) monthly time series of the area fraction in each of the 10 columns. The Col. 1 is the area with water table depth (WTD) between 0-1 m below the surface; The Col. 2 is the area with water table depth (WTD) between 1-2 m below the surface;...,; The Col. 10 is the area with water table depth (WTD) between 9-10m below the surface.

A sensitivity experiment is designed to investigate the model response to the water-stressed condition. An 11-year (1984-1994), 10-COL LSXGW similation is carried out in which the precipitation is cut down 50% in each time step while all the other aspects of the simulation remain unchanged. Prior to the 11-year simulation, twenty spin-up years with the identical forcing with the 1984 were added to ensure the system was in equilibrim in the beinning of 11-year simulation. In contrast to all the previous LSXGW simulations in Illinois (which take only 4 years to spin-up), the dry case (50% precipitation) needs much more spin-up years for the LSXGW to reach equilibrium. During the 20 spin-up years with 50% reduction in precipitation, groundwater level kept on decreasing until it reached an equlibrium at the depth of about 10m below the surface as a result of the small magnitude in groundwater recharge. The nonlinearity in the water balance is significant in that the groundwater runoff (about 25 mm/yr.) decreases by more than 90% from the original 100% precipitation simulation. Figure 5.14 shows the 11-year (1984-1994) average seasonal cycles and the monthly time series of the total evaporation in each sub-grid for the 50% precpitation case. Unlike the 100% precipitation case (Figure 5.12), the differences in the evaporation for the sub-grids with WTD from 0-5m are significant from May to October. It is interesting to note that even under the 50% precipitation condition the sub-grid with the shallowest water table (i.e., column 1) still has a high evaporation rate during the summer. This phenomena suggests that the evaporation in the shallow water area is still without water stress even with 50% reduction of precipitation. However, the 11-year average area fraction of column 1 in the 50% precipitation case is less than 1%, thus the average annual evaporation is much smaller than the 100% precipitation case. In contrast to Figure 5.12, the difference in the simulated evaporation for columns 1-3 is significant in every year except 1993. The differences reach the maximum in the drought year 1988. In 1988, all the 10 columns have significantly reductions in evaporation except colume 1. The comparison between Figure 5.14 and Figure 5.12 underscores the significance of the shallow aquifer in maintaining the nonwater-stressed condition by supplying water to the root zone for the evaporation use.

In summary, the proposed methodology in this chapter combines the strengths of the statistical-dynamical approach and the mosaic approach to account for the effects of the sub-grid variability of WTD in the groundwater runoff and groundwater recharge. It explicitly subdivides a model grid into several sub-grids based on the WTD in the calculation of the grid scale

groundwater recharge. By doing so, the prognostic states in each sub-grid can be traced with consistency from step to step without losing the memory. Moreover, the model uses a statistical-dynamical approach to integrate the point-scale groundwater runoff function to the grid scale. There are at most only 4 parameters (d_{gw}, K, α, and S_y) need to be specified in the developed aquifer model. The specific yield S_y can be determined from the soil type. As discussed in section 5.1.1, the shape parameter α of the assumed Gamma distribution is not sensitive to the grid scale groundwater runoff (Eq. 5.5) if $\alpha \geq 4$. Moreover, the computational cost is rather economical due to the nature of a lumped-parameter model. Therefore, it can be

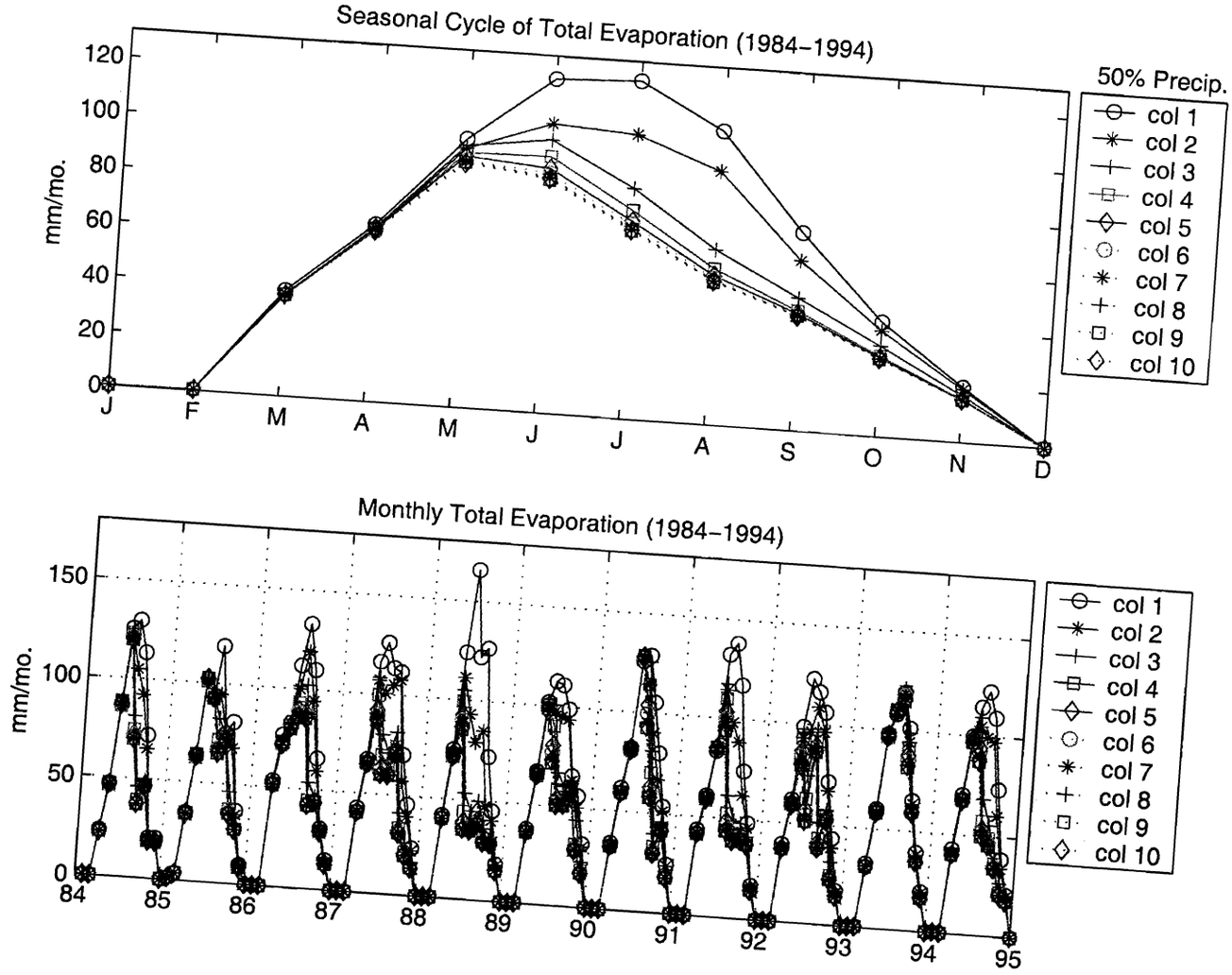

Figure 5.14 Same as Figure 5.12, but for the 50% precipitation case. 11-year (1984-1994) average seasonal cycle and the 11-year monthly time series of the total evaporation in each of the 10 columns

concluded that the LSXGW model is parametrically parsimonious and computationally efficient, thus it is suitable for use in climate models. Moreover, the valuable product is the statistical information on the spatial distributions of the associated hydrologic variables. This information usually not provided in current land surface schemes is valuable in many hydroclimatic applications such as the assessment of the impacts of climate changes on the regional water resources.

5.3 Spatial Heterogeneity of Groundwater Parameters

In section 5.1.1, we have derived the analytical expressions of the macro-scale groundwater runoff (Eq. (5.5)) from the statistical integration of the local-scale groundwater runoff function (Eq. (5.1)) over the assumed Gamma-type spatial distribution function of water table depth. The macro-scale groundwater runoff in Eq. (5.5) depends on the local-scale aquifer parameters (d_0 and K) in Eq. (5.1). For the typical scale of a grid square in climate models (~100-500 km), d_0 and K may exhibit significant sub-grid heterogeneity as a result of the spatially heterogeneous topography and soil properties. Moreover, usually more than one watershed locates within a grid square. It is not clear how to specify the effective values of d_0 and K in Eq. (5.5) that incorporate the variations in these two parameters from watershed to watershed.

In the following, an effort will be made to account for the spatial heterogeneity of d_0 and K in the macro-scale groundwater runoff expression (Eq. (5.5)). A simple analytical technique is used to incorporate the sub-grid variability of d_0 and K into Eq. (5.5) whereby the sensitivity of Eq. (5.5) to the variations in d_0 and K can be analyzed. In Eq. (5.5), α is the shape parameter of the specified Gamma distribution of water table depth. For $\alpha = 1$, Eq. (5.5) can be written as:

$$E[Q_{gw}] = K[d_0 - \frac{1}{\lambda} + \frac{1}{\lambda}e^{-\lambda d_0}] \tag{5.7}$$

for $\alpha = 2$,

$$E[Q_{gw}] = K[d_0 - \frac{2}{\lambda} + (\frac{2}{\lambda} + d_0)e^{-\lambda d_0}] \tag{5.8}$$

for $\alpha = 3$,

$$E[Q_{gw}] = K[d_0 - \frac{3}{\lambda} + (\frac{3}{\lambda} + 2d_0 + \frac{\lambda d_0^{\,2}}{2})e^{-\lambda d_0}] \tag{5.9}$$

for $\alpha = 4$,

$$E[Q_{gw}] = K[d_0 - \frac{4}{\lambda} + (\frac{4}{\lambda} + 3d_0 + \lambda d_0^{\,2} + \frac{\lambda^2 d_0^{\,3}}{6})e^{-\lambda d_0}] \tag{5.10}$$

5.3.1 Spatial Heterogeneity of d_0

Since the form of the PDF of d_0 is unknown, for the convenience of the analytical treatment the following simple uniform function is assumed to be the PDF of d_0,

$$\begin{aligned} f(d_0) &= \frac{1}{2w} \qquad \overline{d_0} - w \le d_0 \le \overline{d_0} + w \\ &= 0 \qquad\quad otherwise \end{aligned} \tag{5.11}$$

where $\overline{d_0}$ is the mean value of d_0 distribution; w is half of the range of d_0 distribution. The expressions of $E[Q_{gw}]$ that accounts for the spatial heterogeneity of d_0 can be derived by integrating Eqs (5.7)-(5.10) (for α =1-4) term by term with respect to d_0 distribution in (5.11) by using the following relationships:

$$\int_{\overline{d_0}-w}^{\overline{d_0}+w} d_0 f(d_0) d(d_0) = \overline{d_0} \tag{5.12}$$

$$\int_{\overline{d_0}-w}^{\overline{d_0}+w} e^{-\lambda d_0} f(d_0) d(d_0) = \frac{1}{2w\lambda}[e^{-\lambda(\overline{d_0}-w)} - e^{-\lambda(\overline{d_0}+w)}]$$

$$\int_{\overline{d_0}-w}^{\overline{d_0}+w} d_0 e^{-\lambda d_0} f(d_0) d(d_0) = \frac{1}{2w\lambda}[(\overline{d_0} - w + \frac{1}{\lambda})e^{-\lambda(\overline{d_0}-w)} - (\overline{d_0} + w + \frac{1}{\lambda})e^{-\lambda(\overline{d_0}+w)}]$$

$$\int_{\overline{d_0}-w}^{\overline{d_0}+w} {d_0}^2 e^{-\lambda d_0} f(d_0) d(d_0) = \frac{1}{2w\lambda}\left\{\begin{array}{l}[(\overline{d_0}^2 + (\frac{2}{\lambda} - 2w)\overline{d_0} + w^2 - \frac{2}{\lambda}w + \frac{2}{\lambda^2})e^{-\lambda(\overline{d_0}-w)} - \\ [\overline{d_0}^2 + (\frac{2}{\lambda} + 2w)\overline{d_0} + w^2 + \frac{2}{\lambda}w + \frac{2}{\lambda^2}]e^{-\lambda(\overline{d_0}+w)}\end{array}\right\}$$

$$\int_{\overline{d_0}-w}^{\overline{d_0}+w} {d_0}^3 e^{-\lambda d_0} f(d_0) d(d_0) = \frac{1}{2w\lambda}\left\{\begin{array}{l}[\overline{d_0}^3 + (\frac{3}{\lambda} - 3w)\overline{d_0}^2 + (3w^2 - \frac{6w}{\lambda} + \frac{6}{\lambda^2})\overline{d_0} + (-w^3 + \frac{3w^2}{\lambda} - \frac{6w}{\lambda^2} + \frac{6}{\lambda^3})]e^{-\lambda(\overline{d_0}-w)} - \\ [\overline{d_0}^3 + (\frac{3}{\lambda} + 3w)\overline{d_0}^2 + (3w^2 + \frac{6w}{\lambda} + \frac{6}{\lambda^2})\overline{d_0} + (w^3 + \frac{3w^2}{\lambda} + \frac{6w}{\lambda^2} + \frac{6}{\lambda^3})]e^{-\lambda(\overline{d_0}+w)}\end{array}\right\}$$

similar derivations can be repeated for any value of α. However, only the cases for $\alpha \le 4$ are discussed here.

The derived analytical expressions are plotted in Figure 5.15 by assuming d_0 has a uniform

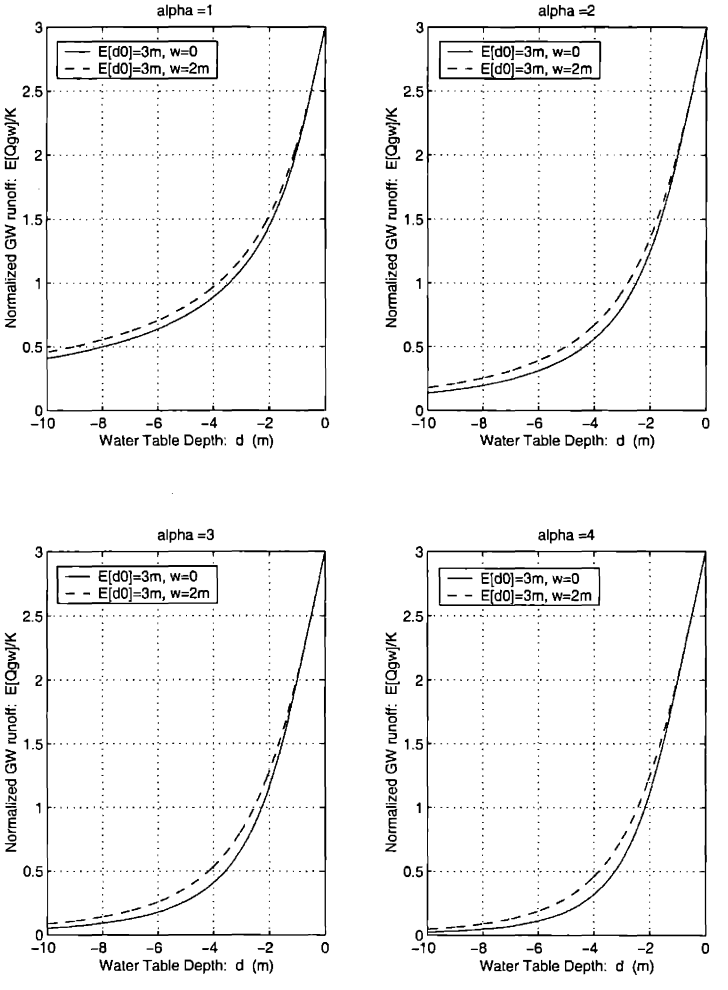

Figure 5.15 The effect of the spatial variability of d_0 (i.e., $\overline{d_0}$ =3m, w =2m in Eq. (5.12)) in the non-dimensional macro-scale groundwater runoff ($E[Q_{gw}]/K$) for different values of α.

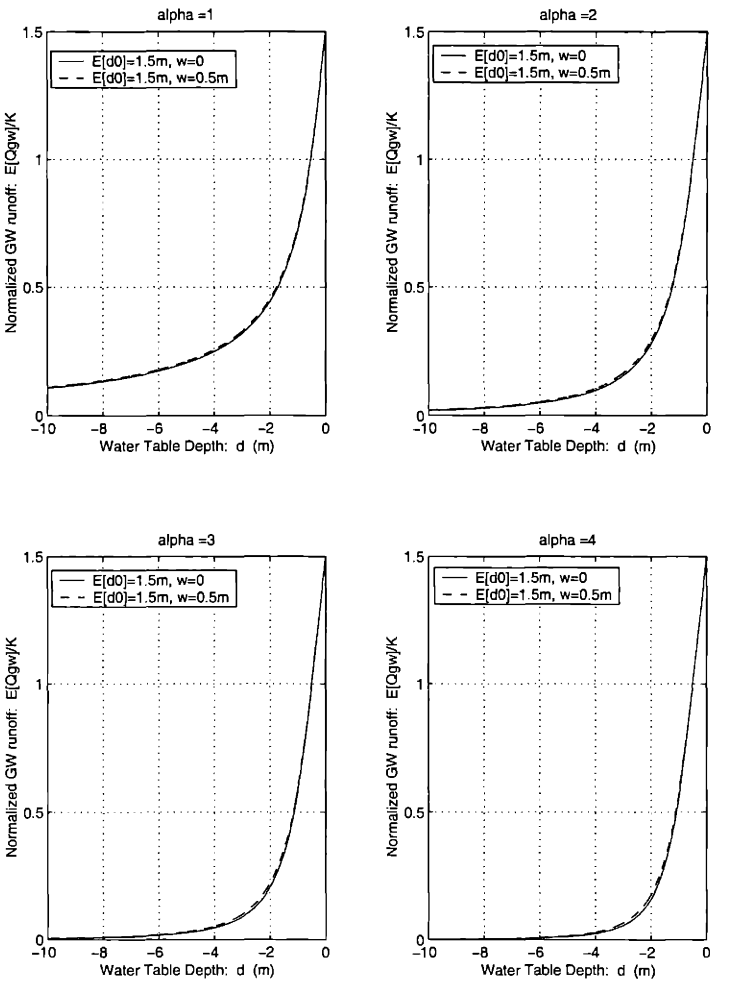

Figure 5.16 Same as Figure 5.15, but for a smaller spatial variability $\overline{d_0}$ =1.5m, w=0.5m in Eq. (5.12).

distribution between 1-5m; that is, $\overline{d_0}$ =3m, w=2m in Eq. (5.11). As seen from this figure, the macro-scale groundwater runoff in general shows little sensitivity to the heterogeneity in d_0. When the average water table is deep, the spatially heterogeneous d_0 results in slightly higher groundwater runoff than the constant d_0 due to the threshold nature of runoff triggering process. However, in this example the range of d_0 (1-5m) might be unrealistically wide. Figure 5.16 gives another example in which d_0 has a uniform distribution ranging from 1m to 2m (i.e., $\overline{d_0}$ =1.5m, w=0.5m in Eq. (5.11)). As seen in the figure, for this case the heterogeneity of d_0 does not have any impact on the macro-scale groundwater runoff.

5.3.2 Spatial Heterogeneity of K

It can be observed from Eq. (5.5) that K is just a multiplier ahead of the groundwater runoff equation. Therefore, it is trivial to derive the $E[Q_{gw}]$ expression that accounts for the spatial heterogeneity of K as following:

$$E[Q_{gw}] = \frac{\overline{K}\lambda^{\alpha}}{\Gamma(\alpha)}\left\{ d_0\left[\frac{(\alpha-1)!}{\lambda^{\alpha}} - e^{-\lambda d_0}\sum_{j=0}^{\alpha-1}\frac{(\alpha-1)!}{j!}\frac{{d_0}^{j}}{\lambda^{\alpha-j}} \right] - \left[\frac{\alpha!}{\lambda^{\alpha+1}} - e^{-\lambda d_0}\sum_{j=0}^{\alpha}\frac{\alpha!}{j!}\frac{{d_0}^{j}}{\lambda^{\alpha-j+1}} \right] \right\} \tag{5.13}$$

where $\overline{K}$ is the mean value of the K distribution. Notice that the macro-scale groundwater runoff depends only on the mean value of the K distribution, but not the form of its distribution.

5.4 Summary and Discussions

5.4.1 Summary of the LSXGW Modelling

Although traditionally water table position is conceived as one of the most basic variable in hydrology, the current generation of land surface schemes (LSPs) used in climate models typically negelects the representation of water table dynamics. For the shallow water table areas, such a simplification would result in significant errors in the predicted hydrological fluxes and states. It has been shown in Chapter 4 through two off-line simulations in Illinois that the LSX model, which is a representative of the current LSPs, fails to reproduce the observed hydroclimatology in Illinois probabaly due to the absence of water table dynamics.

As an effort to incorporate water table dynamics into LSPs, a lumped unconfined aquifer model is developed and interactively coupled to the soil model in the LSX. This aquifer model receives the recharge from the overlying soils and discharges groundwater runoff whereby the water table position is updated accordingly at the end of each time step. Groundwater runoff is parameterized as a nonlinear function of water table depth based on the observations in Illinois, while groundwater recharge is equal to the soil dainage flux computed from solving the Richards equation in the soil model. The aquifer model and the soil model in the LSX are interactively coupled through the soil drainage flux (groundwater recharge flux).

The issue of land surface variability of water table depth is also addressed. A new methodology, combining the strengths of the statistical-dynamical (SD) approach and the mosaic approach, is proposed to account for the effects of the sub-grid variability of water table depth (WTD) on the grid scale groundwater runoff and groundwater recharge. This combined approach statistically incorporates the unresolved sub-grid variability of WTD in the computation of the grid scale groundwater runoff, whereas consistently keeps tract of the prognostic variables within each sub-grid without losing memories between timesteps. It has the advantage that the dynamic expansion and contraction of the runoff contributing area can be explicity incorporated in the computations of runoff as well as other hydrological fluxes. Another useful product is the spatial

distributions of hydrological variables in all sub-grids, which are useful in downscaling the climate model simulation results to a smaller scale often needed in the studies of the impacts of climate changes on the regional water resources.

This coupled model (LSXGW) has been tested in Illinois for an 11-year perioid from 1984 to 1994. The simulation results indicate that most of the simulated hydrological states (e.g., water table depth and soil saturation) and fluxes (e.g., groundwater recharge, runoff, and evaporation) agree with the hydrological observations in Illinois reasonably well. The proposed aquifer model is suitable to be used in climate models in that it is parsimonious in terms of the required parameters and computationally efficient due to the lumped-parameter nature. Moreover, it was designed in a flexible way such that it can be easily coupled to any land surface scheme with very little modifications of the soil model codes.

5.4.2 Unsolved Issues Identified From the LSXGW Modelling

As concluded in 5.4.2, the developed non-linear unconfined aquifer model, when coupled to the LSX (collectively called LSXGW) and forced by the observed atmospheric forcing, is able to faithfully reproduce a 11-year (1984-1994) regional-scale hydroclimatology in Illinois. However, it should be recognized that the successful testing of the LSXGW in Illinois is largely attributed to the fact that the correct large-scale groundwater-rating curve is available from the observations. The agreement between the theoretical and the observed large-scale rating curves shown in Figure 5.4 results from the correct estimation of aquifer parameters. Two effective aquifer parameters, d_0 (characterizing the threshold depth above which the aquifer connects with the stream channel) and K (characterizing the discharge rate of aquifers), as well as the assumption on the spatial probability distribution function of WTD, are required as the input to the aquifer model. In section 5.2, d_0 and K were estimated at 8 locations in Illinois where the observations of WTD and a nearby streamflow gauges are available. However, it is impractical to expect these data, especially the water table depth, are usually available. Since the ultimate

goal of the development of LSXGW is its global implementation in climate models, the development of a universal parameter estimation procedure is most urgent challenge ahead.

In order to develop a global parameter estimation scheme, the following questions need to be explored:

(1) For most regions in the world the observation of WTD is not available, how to determine the groundwater-rating curve? Namely, how to estimate the effective parameters, primarily d_0 and K, in the LSXGW?

(2) In the Illinois study, d_0 and K within each catchment were estimated from the "point" WTD observations and the catchement-scale streamflow record. This is not necessary to be consistent with the mean aquifer storage-discharge relationship of the catchment.

(3) The effective parameters (d_0 and K) were derived from the arithmetic averages of the parameters estimated from 8 locations in Illinois. Since the underlying physical process of groundwater discharge to streams is non-linear, this simple aggregation procedure may not be sound.

A feasible solution to these questions is to use the streamflow records to calibrate d_0 and K. This has been attempted in several watersheds in Illinois; the results will be presented in the next chapter. Another alternative is to apply a physically-based, three-dimensional distributed watershed modeling system such like the MIKE-SHE (*Abbott et al.,* 1986) at the small grid scale to help estimate the required groundwater parameters in the LSXGW. The research tasks in using MIKE-SHE over several watersheds in Illinois will be discussed in another research report.

Chapter 6 Global Applicability – A Parameter Calibration Approach

6.1 Introduction

In the previous macro-scale LSXGW simulation, the groundwater parameters (d_0 and K) determining the average groundwater-rating curve (i.e., the relation between the aquifer storage and aquifer discharge) were estimated from several local-scale observations of water table depth and nearby streamflow records in Illinois. The simulated hydrological states and fluxes at the monthly and annual timescales are close to the corresponding observations or the estimates from the water balance analysis (i.e., evaporation and groundwater recharge). For that case, the specified groundwater-rating curve in the LSXGW simulation is reliable judging from the comparison with the observed macro-scale rating curve (see Figure 5.4). The LSXGW can therefore faithfully reproduce the 11-year (1984-1994) macro-scale hydroclimatology in Illinois.

However, when applying the LSXGW to other regions in the world, water table depth and streamflow observations required for the determination of groundwater-rating curve are rarely both available. Therefore, the development of a parameter estimation approach for determining the groundwater parameters is necessary for the practical global implementation of the developed LSXGW model.

Before the development of a parameter estimation approach, it is important to examine certain physical reasoning behind the non-linear groundwater-rating curve. The macro-scale rating curve in Figure 3.1b is the relationship between the Illinois state-average water table depth (WTD) and streamflow. The WTD is the average from 16 unconfined monitoring wells in Illinois. The streamflow is the average from 3 major river basins in Illinois which collectively consist of 2/3 of the total areas of Illinois. Several critical points regarding Figure 3.1b can be made here. First,

the streamflow is the sum of groundwater flow plus surface runoff, and perhaps other streamflow components, thus Figure 3.1b is in fact not the groundwater-rating curve. Previously in section 3.3 groundwater runoff was estimated to explain about 80% of the variance of monthly streamflow in Illinois based on the multiple regression analysis conducted with respect to the average precipitation, WTD, and streamflow. Accordingly, we assumed without further justification that Figure 3.1b is rather close to the groundwater-rating curve in Illinois given that groundwater is the dominant source for streamflow in Illinois rather than precipitation. However, for the pursuit of the relationship between WTD and groundwater runoff, the separation of the total streamflow into its components must be performed.

The physical meaning of the Figure 3.1b can be explained as, baseflow would increase as the water table rises according to the Darcy's law (larger hydraulic gradient and transmissivity). Concurrently, surface runoff would also increase due to the higher soil moisture (hence reduced available pore space for infiltration). That is, baseflow and surface flow will increase simultaneously as water table rises, and both mechanisms are highly non-linear. How to partition the total increase in streamflow into the increases in baseflow or surface runoff is the key challenge to deal with.

At the local scale, recall that the WTD at 8 groundwater monitoring wells in Illinois were plotted against the nearby streamflow observations in Figure 5.2. Based on this plot, the local LSXGW parameters (d_0 and K) were estimated via an optimized parameter search algorithm. The effective (macro-scale) parameters were then derived by arithmetically averaging the estimated local parameters. Despite the fact that the derived effective parameters reproduced reasonably well the observed macro-scale groundwater-rating curve (see Figure 5.4), the procedures raise three theoretical problems. First, similar to the above discussions at the macro-scale the streamflow rather than the baseflow was used in the parameter estimation which would result in a biased estimation of d_0 and K. Second, the adoption of the arithmetic averages as the aggregation criterion lacks any physical ground. A rigorous aggregation procedure based on the water balance should be developed for deriving the effective parameters. The third problem is that the local observations of WTD as shown in Figure 5.2 do not necessarily represent the

catchment-averaged WTD, thus the estimated effective parameters may not be accurate. If the sampling monitoring well locates at the mountain ridge (valley bottom) where the water table is deep (shallow), the estimated d_0 would be biased large (small) to reflect the local conditions.

Moreover, it also can be noted from Figure 5.2 that the nonlinear dependence between the WTD and the corresponding streamflow at the local scale is not as strong as that at the large scale (Figure 3.1b), suggesting either not all of these 8 watersheds have significant groundwater contribution to stream, or the locations of some of these wells do not represent the watershed-averaged WTD. Therefore, unlike at the macro-scale it is improper to assume that the plots in Figure 5.2 would be close to the local-scale groundwater-rating curve.

In the next section, we will attempt to apply the hydrograph separation technique to the streamflow in those 8 locations in Figure 5.2 in order to improve the estimation of the groundwater-rating curve.

6.2 Baseflow Estimation by Hydrograph Separation

Streamflow may be composed of surface flow, interflow, baseflow, or a combination of these (*Singh*, 1993). A major problem in hydrology is the prediction of groundwater contribution to the stream which bears extreme importance in water supply, irrigation, and flood control. According the definition of *Singh* [1968], baseflow is the net flow from groundwater storage to a stream. Moreover, according to *Hall* [1968], baseflow was defined as "the portion of flow that comes from groundwater storage or other delayed sources". Depending upon their interest, hydrologists have called it various names: groundwater flow, groundwater runoff, seepage flow, sustained flow, low flow, and perhaps others.

Perennial streams depend on groundwater flow for discharge between surface runoff events. The amount and duration of baseflow occurring in a stream depends on the amount of precipitation, the geologic conditions allowing infiltrated water to be stored underground, and the hydrogeologic and basin geomorphic controls governing groundwater flow to the stream. During wet periods, the water table continues to elevate and this increased elevation will increase both the hydraulic gradient and the (groundwater) drainage density, and hence increase the baseflow contribution to the stream. During dry periods, the opposite will occur and the baseflow will decrease.

[

The most direct way to estimate baseflow is through the hydrograph separation, a long-standing classic problem in hydrology. Numerous techniques of hydrograph separation have been proposed in the hydrological literature. Here we adopt the digital recursive filter technique, perhaps the most commonly used and the simplest, to attempt to separate baseflow from the daily streamflow records. The digital recursive filter technique was originally used in signal analysis and processing (*Lyne and Hollick*; 1979), and has recently been applied to separate baseflow from daily streamflow (*Nathen and McMahon*, 1990; *Chapman*, 1991; *Furey and Gupta*, 2001).

According to the theory of the digital recursive filter, the base flow in time t, $B(t)$, can be written as:

$$B(t) = cB(t-1) + 0.5(1-c)[F(t) + F(t-1)] \tag{6.1}$$

where the fast flow component, *F(t)*, can be estimated from the total streamflow *Y(t)*:

$$F(t) = \frac{(3c-1)}{(3-c)}F(t-1) + \frac{2}{(3-c)}[Y(t) - cY(t-1)] \tag{6.2}$$

c is the filter coefficient with the feasible range between 0.900-0.995. *Chapman* [1991] has suggested c=0.925 as a proper value. Eqs (6-1)-(6-2) is a low-pass filter in which the larger c is, the more high frequency components being filtered out. However, the differences in the estimated baseflow estimates from using different c values are significant only when c=0.975-0.995.

Although the digital filter technique bears no physical basis, it is an objective technique and easy to implement. It can effectively filter out high frequency components from the streamflow to a certain degree depending on the value of the filter coefficient used. Since the major objective here is to improve the estimation of groundwater-rating curve rather than the accurate quantification of baseflow, the adoption of the digital recursive filter is suitable.

The digital recursive filter is applied to the 11-year (1984-1995) daily streamflow records at those 8 catchments in Figure 5.2. The estimated daily baseflow is then aggregated to the monthly scale and plotted together with the streamflow in Figure 6.1. The long-term average baseflow ratio (i.e., baseflow/total streamflow) is also given in the figure. The optimal parameters (d_0 and K) fitting these groundwater-rating curves are derived by using the same automatic search algorithm as used in section 5.1. The groundwater-rating curve is plotted in the third panel of Figure 6.1, For comparison, the scatter plot of streamflow versus WTD and the fitted groundwater-rating curves (as those in Figure 5.2) are also plotted in Figure 6.1 (second panel). As seen from this figure, the major difference between using the total flow and baseflow is in the fitted outflow constant K, while all the d_0 are nearly identical in two cases.

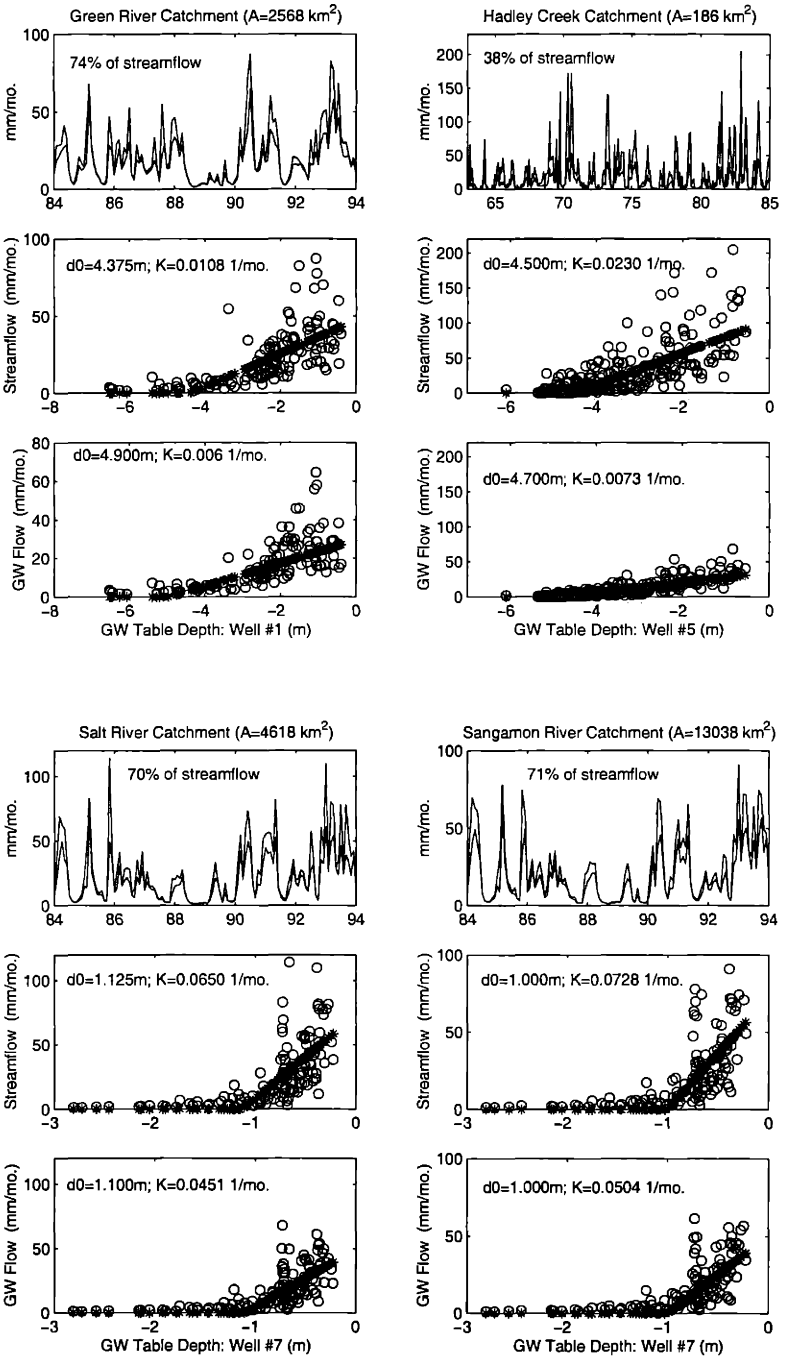

Figure 6.1 The first panel plots the 11-year (1984-94) monthly time series streamflow and baseflow estimated by using the recursive digital filter in eight locations in Illinois. The second (third) panel is the scatter plots of the observed monthly WTD versus the corresponding nearby streamflow (baseflow) from 1984 to 1994 in these eight locations. Also shown in this figure are the best-fit lines derived from the least absolute error criterion and the associated optimal parameters (d_0 and K).

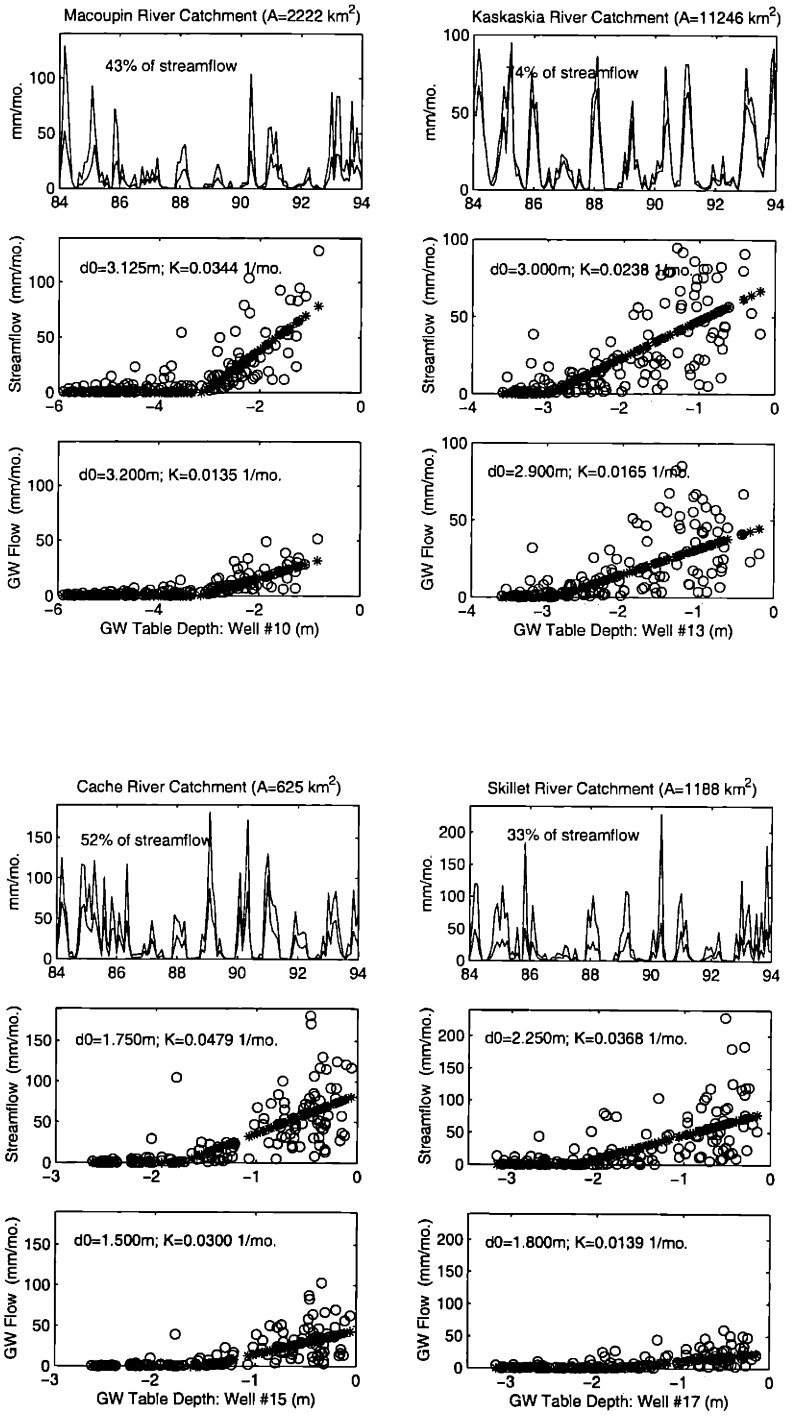

Figure 6.1 (Continued)

Previously in section 5.1, the effective parameters (d_0=2.641 m and K=0.0393 1/month) were estimated by the arithmetic averages of the local parameters in the 8 catchments. Here in this section the baseflow rather than the total flow is used, the derived arithmetic-averaged parameters are d_0=2.638 m and K=0.0228 1/month. Reasonably, the effective K decreases about 50% while d_0 remains nearly unchanged. These two sets of parameters are plugged into the macro-scale groundwater runoff expression in equation (5.5) and the resulting macro-scale groundwater-rating curves are plotted in Figure 6.2. It can be seen from Figure 6.2 that the revised groundwater-rating curve (using the baseflow instead of streamflow) form the lower envelop of the observations.

An 11-year LSXGW simulation identical to the one-column simulation presented in Chapter 5 except using a smaller K (=0.0228 1/month) is carried out. The results (not shown here) indicate a reduced baseflow and increased surface runoff by the similar amount. The runoff and evaporation ratios are rather close to the previous results.

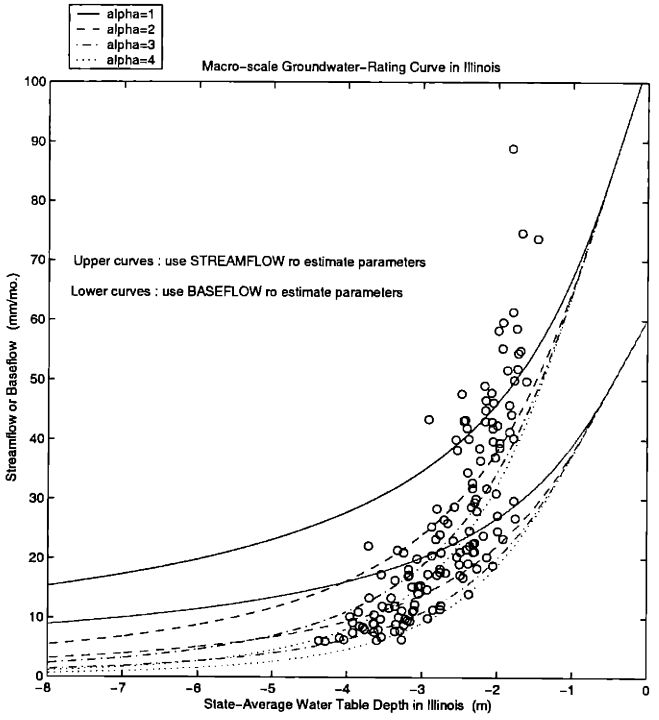

Figure 6.2 Macro-scale groundwater rating-curves in Illinois estimated from the WTD observations and the streamflow observations (the upper curves) or the estimated baseflow (the lower curves). The circles are the observed macro-scale groundwater rating-curve in Illinois

6.3 Parameter Calibration from the Streamflow Records

In this section, a parameter calibration approach based on the comparison of the streamflow from the off-line LSXGW simulation with the streamflow observation is proposed. The calibration parameters of the LSXGW include primarily d_0 and K, and secondarily other groundwater parameters (e.g. the shape parameter α and the specified yield S_y). In this section, we calibrate the LSXGW groundwater parameters in the following 4 basins in Illinois: Green River basin (2568 km^2), Cache River basin (625 km^2), salt River Basin (4618 km^2), and Kaskaskia River Basin (11246 km^2). These 4 basins have been plotted in Figure 5.2 to estimate the local groundwater parameters by statistical best-fit technique since each of them has a monitoring well observation. The atmospheric forcing (to drive the off-line LSXGW run) and the streamflow records are the required data for the proposed calibration approach. The WTD observations in the 4 basins will not be needed in the proposed calibration approach.

The values of the calibration parameters (d_0 and K) are adjusted progressively until the model-simulated streamflow matches the observations. The calibration focuses on the streamflow comparisons at the monthly and seasonal time scales. This is because from the viewpoint of climate modeling, it is more important to assure that the long-term (monthly and annually) streamflow simulation is realistic as opposed to its daily fluctuations. Moreover, since all the land surface schemes generate "runoff" rather than "streamflow", the comparison between the observation and the simulation at the daily time scale for a large-size river basin is problematic without employing a runoff routing scheme.

In the following, we present the application of the proposed parameter calibration approach to the Green River basin (2568 km^2). The LSXGW model is run by prescribing the atmospheric forcing at the Green River basin. The representative soil and vegetation parameters of this basin are also specified in the LSXGW. The calibration strategy is to adjust the value of d_0 first and then K. A smaller d_0 reduces the baseflow and the effect is more dramatic than reducing K during the low flow period, whereas the adjustment of K is more effective to capture the flow

peaks than d_0. Therefore, the value of d_0 is at first adjusted progressively until the simulated streamflow during the low flow period matches the filtered baseflow, then K is adjusted to capture the observed flow peaks.

Starting from an arbitrary initial guess of d_0 and K, Figure 6.3 shows the progressive improvement of the LSXGW simulated monthly streamflow in the Green River basin by adjusting d_0 from 4.0m to 1.0m. For the case of d_0=1.0 m and K=0.20 1/mo. (in the bottom of Figure 6.3), the simulated flow agrees well with the observation during the low flow periods, suggesting d_0=1.0m is closed to the optimal value. To match the flow peak, Figure 6.4 shows the gradual improvement by the adjustment of K from 0.20 to 0.40 1/mo. As seen in this figure, the flow peaks in 1985-87 and 1993 were significantly improved as K increases. Moreover, the 11-year (1984-1994) seasonal cycle of the simulated streamflow for the three cases in Figure 6.4 are given in Figure 6.5 in comparison with the observations. Again, this figure confirms d_0=1.0 m and K=0.40 1/mo. are close to the optimal values. Finally, due to the large increment of d_0 used in Figure 6.4, some fine-tuning of d_0(1.00m 1.25m, 1.50m, 1.75m) is given in Figure 6.6. Juding from this figure, d_0 should not exceed 1.25m in the Green River Basin.

The same calibration approach has also been applied to estimate the groundwater parameters in the Cache River Basin, Salt River Basin, and Kaskaskia River Basin. Figure 6.7 shows the progressive improvement of the simulated streamflow in the Cache River basin by different combination of d_0 and K. The left hand side of this figure shows the monthly comparison of the simulated flow against the observation, while the right hand side gives the corresponding comparision of the average seasonal cycles. By reducing d_0 to 0.60 m, the simulated flow starts to converge with the observed low flow condition. Then with d_0=0.60 m, a larger and a smaller K value was tested and finally concluded d_0=0.60 m and K=0.20 1/mo. are close to the optimal values for the Cache River Basin.

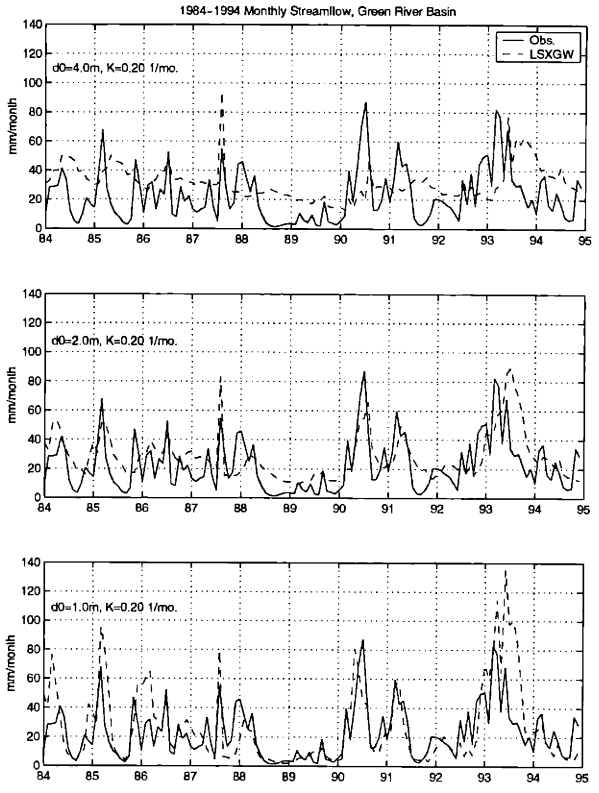

Figure 6.3 The progressive improvement of the LSXGW simulated monthly streamflow in the Green River basin by adjusting the value of d_0.

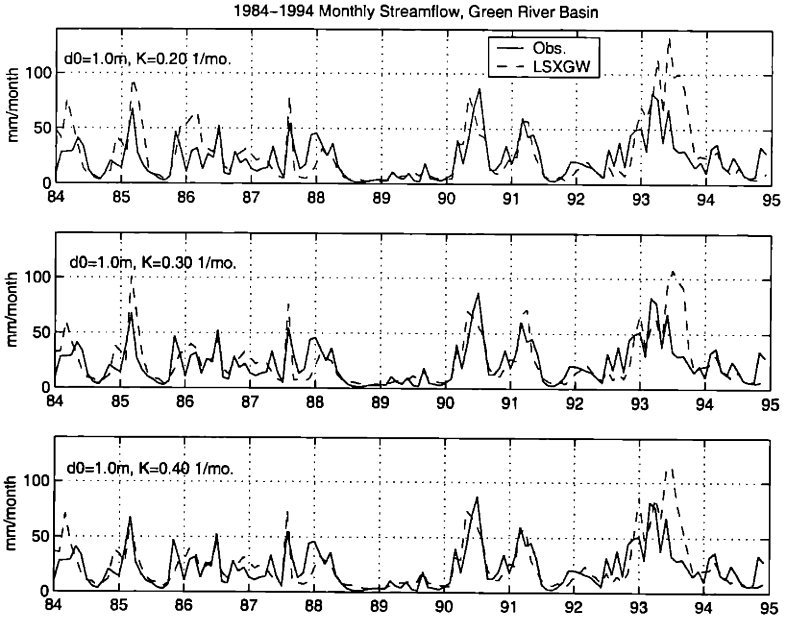

Figure 6.4 The progressive improvement of the LSXGW simulated monthly streamflow in the Green River basin by adjusting the value of K.

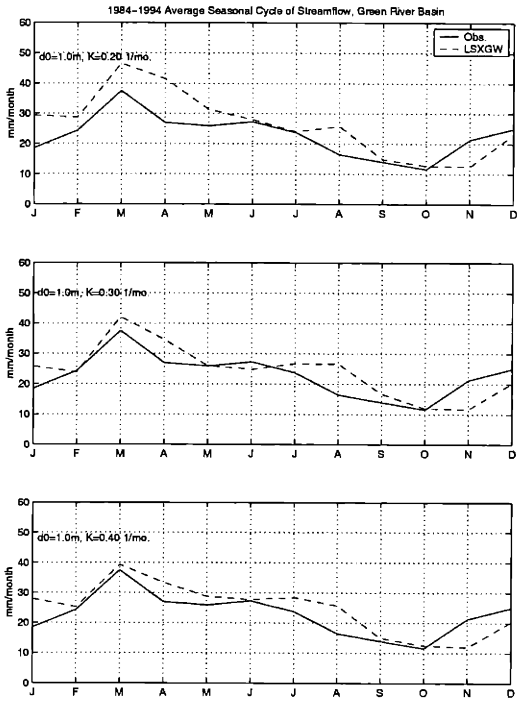

Figure 6.5 Average seasonal cycle of the simulated streamflow for the three cases in Figure 6.4.

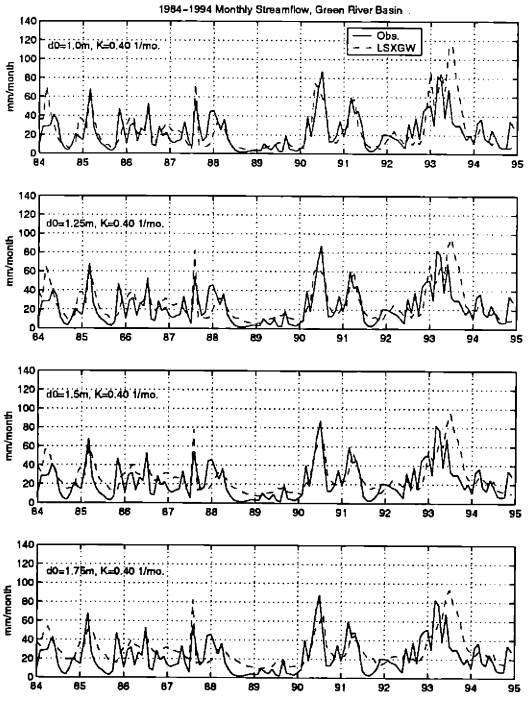

Figure 6.6 The effect of fine-tuning d_0 value in improving the LSXGW streamflow simulation in the Green River basin in Illinois.

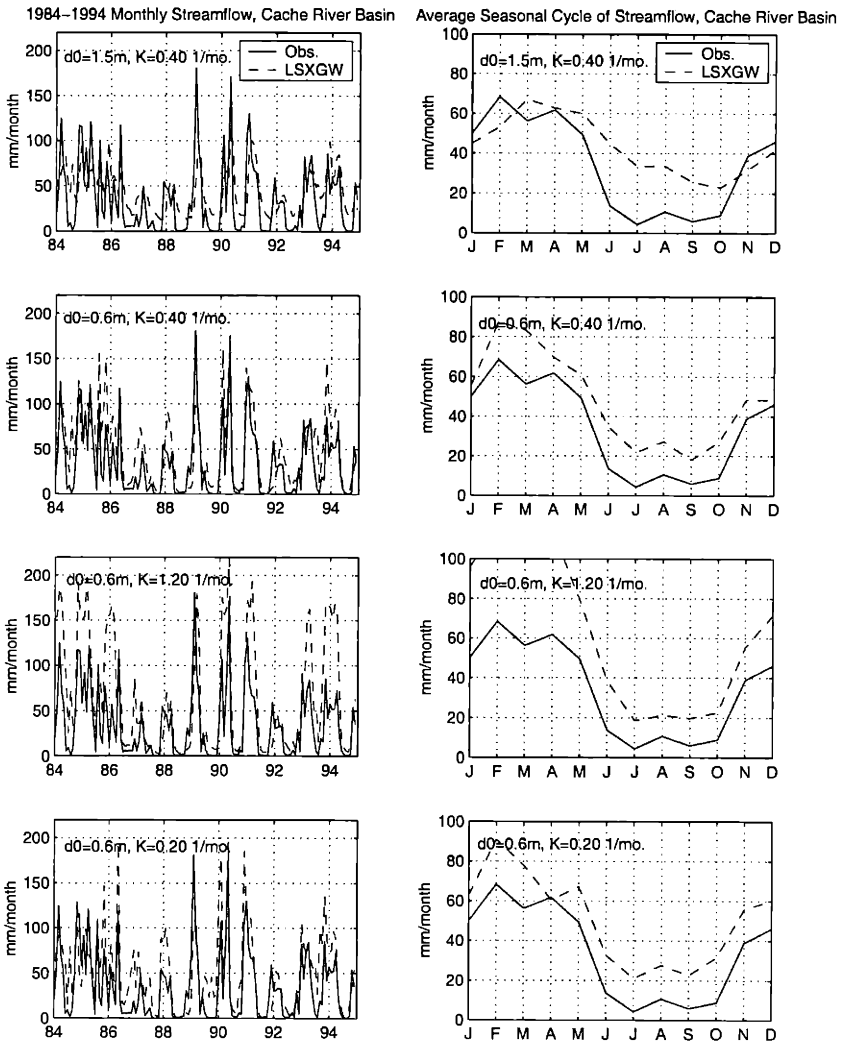

Figure 6.7 Progressive improvements in the LSXGW streamflow simulation in the Cache River basin in Illinois by calibrating d_0 and K values.

Figure 6.8 shows the similar plot to the Figure 6.7, but for the Salt River Basin. As shown, d_0=1.10 m and K=0.60 1/mo. are about the optimal values for this basin. Finally, the estimated optimal cases (d_0=1.00 m and K=0.40 1/mo.) for the Kaskaskia River Basin is compared wih the streamflow observation in Figure 6.9.

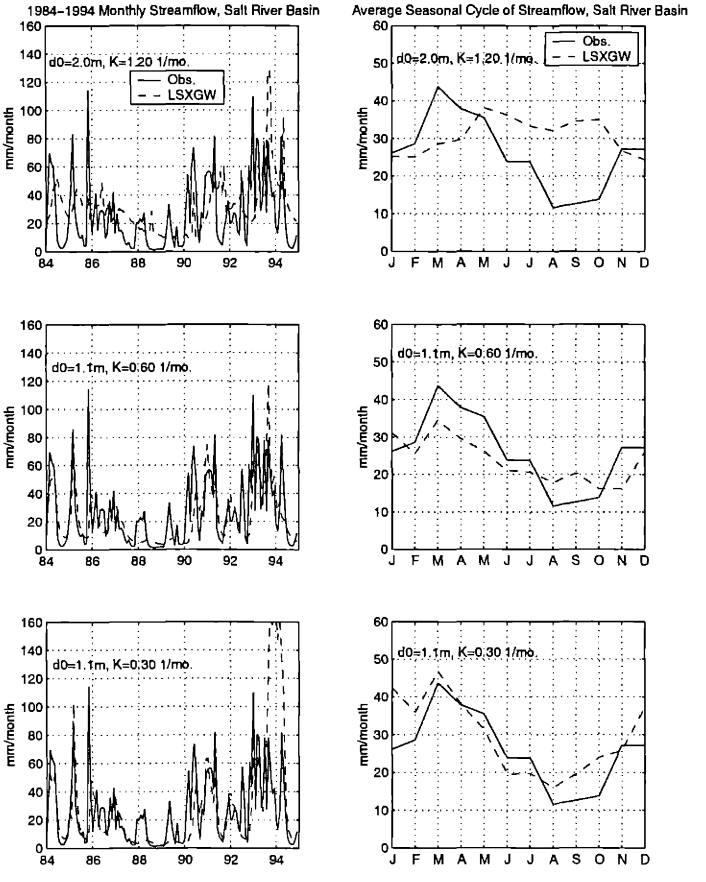

Figure 6.8 Progressive improvements in the LSXGW streamflow simulation in the Salt river basin in Illinois by calibrating d_0 and K values.

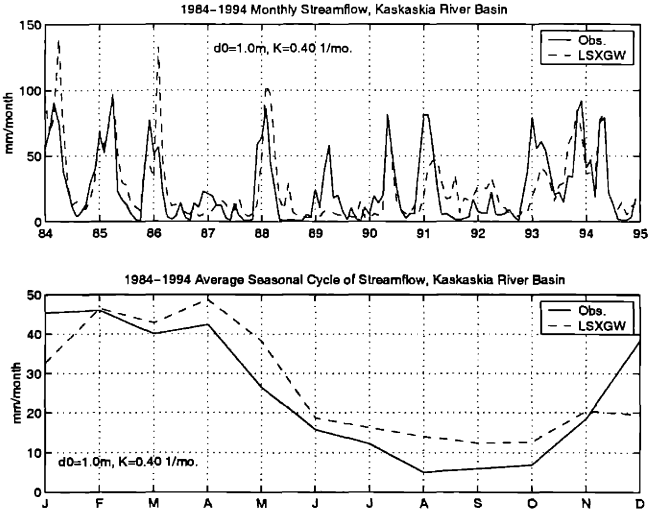

Figure 6.9 The comparsion of the monthly time series and the seasonal cycle between the simulated and the observed streamflow in the Kaskaskia River basin in Illinois. The LSXGW simulation uses the optimal groundwater parameters (d_0=1.00 m and K=0.40 1/mo.) estimated by calibration.

Parameter Calibration from the Baseflow Estimates

Another calibration approach slightly different from the first approach is proposed here. The second approach is based on the comparison of the LSXGW-simulated daily groundwater runoff against the daily baseflow estimated from the digital recursive filter. Similar to the first approach, the values of the calibration parameters d_0 and K are adjusted progressively until the simulated daily baseflow matches the filtered baseflow.

Here we only present the application of this approach to the Green River Basin, although it has also been applied to the Cache, Salt, and Kaskaskia River basins. First, the digital recursive filter is applied to estimate the baseflow from the 11-year daily streamflow record at the outlet of the Green River basin. Figure 6.10 shows the baseflow estimates from using various filter

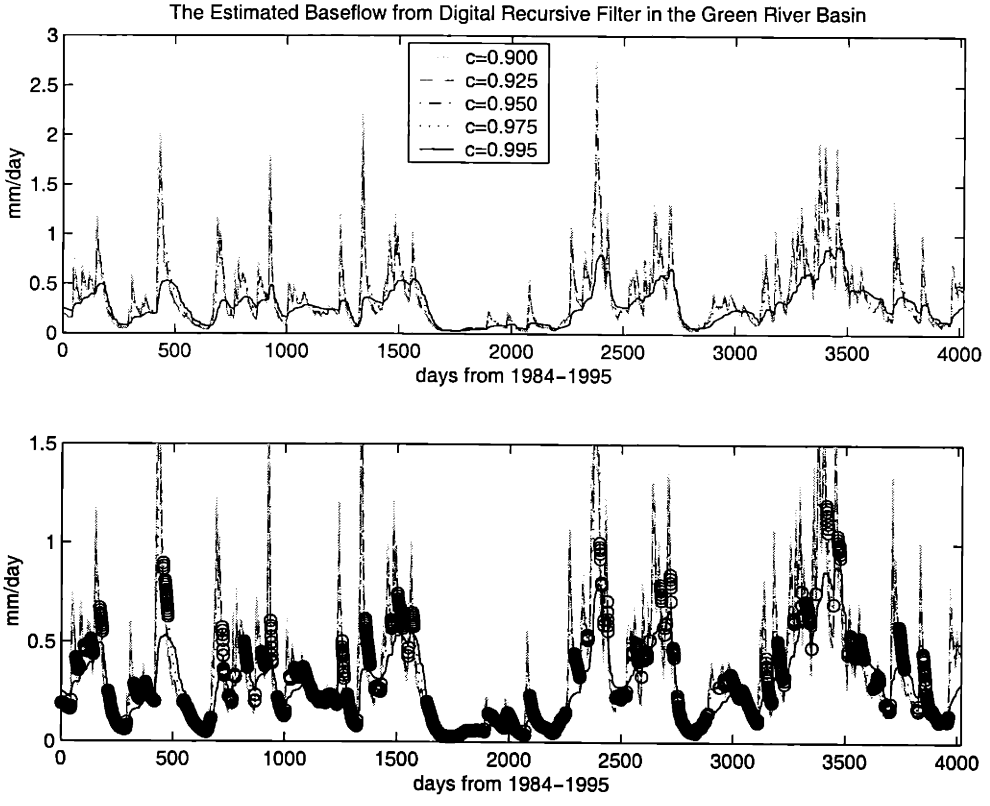

Figure 6.10 The baseflow estimates in the Green River basin using various filter ccoefficients. The lower panel shows the 2009 days (in black circles) in 1984-1995 when the baseflow estimates using various c values only differ within 0.1 mm/day.

coefficient, c=0.900, 0.925, 0.950, 0.975, and 0.995. A larger c filters out more high frequency components of the streamflow, thus the estimated baseflow is smaller in magnitude than specifying a smaller c. While the baseflow estimates from various c show noticeable differences at the high flow period, they actually converge to each other during the low flow period when baseflow dominates the streamflow. By specifying a criterion that the various baseflow estimates only differ within a threshold value, say, 0.1 mm/day, the baseflow on 2009 low flow days are screened from the 11-year period as the calibration objective (plotted as the black circles in Figure 6.10). This procedure avoids the uncertainty in determining the value of the unknown filter coefficient, but it does not assure the reproduction of the baseflow peak most of which occurring outside the selected calibration days.

After the initial try-and-error search of the reasonable ranges of d_0 and K, Figure 6.11 shows the progressive improvement of the simulated baseflow in the Green River basin on those 2009 selected days. The correlation coefficient between the filtered and simulated baseflow series is also given in this figure. It is found the optimal parameters are d_0=1.20 m and K=0.10-0.20 1/mo., which are colse to the values estimated from the other calibration approach based on the monthly streamflow comparioson. Figure 6.12 shows the similar daily comparison, but for the entire 11-year daily baseflow. As seen in these figures, by using the calibrated parameters the LSXGW can simulate the baseflow close to the filtered baseflow. However, not surprisingly, the simulated baseflow has difficulty in capturing some of the baseflow peaks.

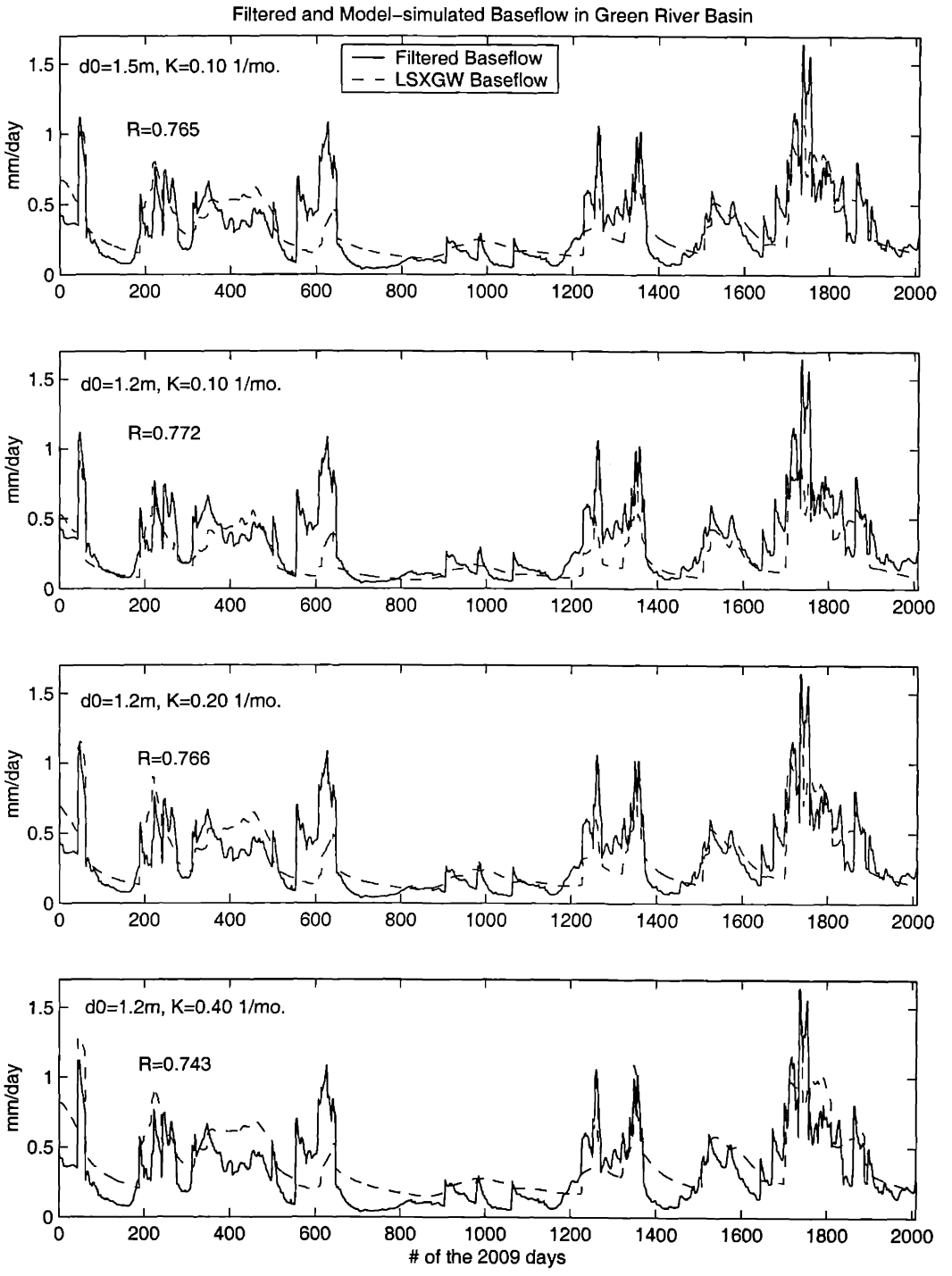

Figure 6.11 The progressive improvements of the LSXGW simulated baseflow by calibrating the groundwater parameters in the Green River basin on those 2009 selected days shown in Figure 6.10.

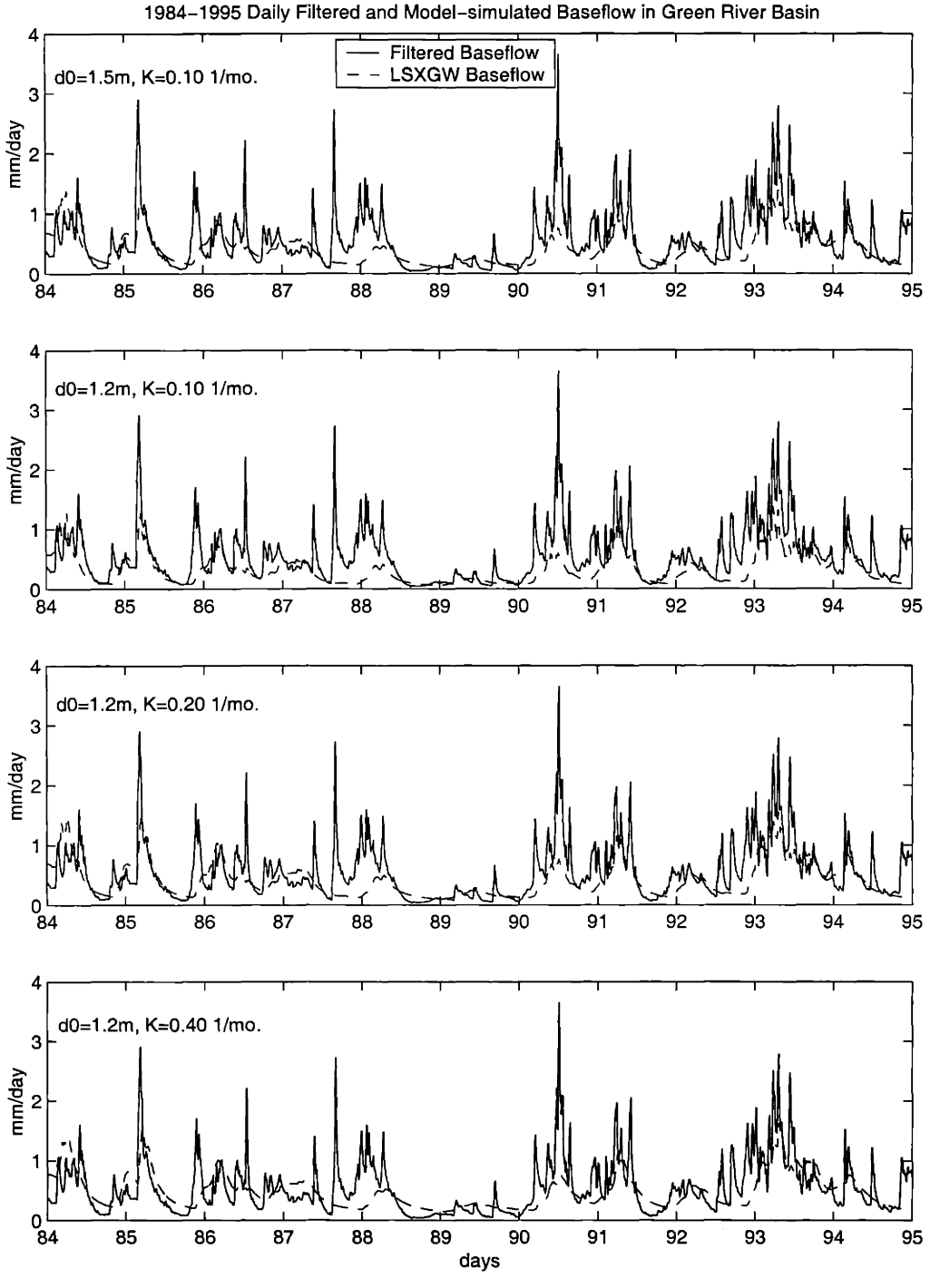

Figure 6.12 Similar to Figure 6.11, but for the entire 11-year period (4018 days).

Discussions

- In the first proposed calibration approach, the simulated monthly total runoff is calibrated against the observed streamflow. Since the simulated total runoff is the sum of surface runoff and groundwater runoff, the controlling parameters of the surface runoff parameterization in the LSXGW (the most important one is the capacity of surface retention, i.e., the puddle size) can also be considered as a calibrating parameter. However, the surface runoff parameterization in LSXGW, which is as the same as in the original parameterization of the LSX, is rather crude (see Appendix C). Only the type of infiltration-excess surface runoff is modeled in the surface runoff scheme of the LSX. In fact, most of the current land surface schemes do not simulate the saturated-excess surface runoff except the TOPMODEL-based land surface schemes such like *Famiglietti and Wood* [1994a], *Stieglitz et al.,* [1997], and *Koster et al.,* [2000].

  The surface runoff in the LSXGW is in general proportional to the storage in the puddle, which in turn is proportional to the effective rainfall reaching the surface (i.e., Hortonian runoff). This is not sound since the Dunne-type surface runoff (which is believed to be the main mode of surface runoff mechanism in Illinois) and the associated spatial variability of soil moisture are not represented in the LSXGW. It makes little sense to treat the size of the surface retention as a calibrating parameter since it does not directly relate to the major surface runoff generation mechanism in Illinois. The Dunne-type surface runoff closely depends on the saturation area dynamics, which is closely related to the water table dynamics developed in this thesis. The development of a revised surface runoff scheme based on the saturated area dynamics as shown in Figure 5.13 is a critical future research issue that will help improve the LSXGW simulation. Such kind of schemes with more mature treatment of saturation-excess surface runoff has been developed in VIC models (*Liang et al.*, 1994) as well as in the Mosaic model (*Koster et al.*, 2000).

- One shortcoming of the LSXGW simulation is the occasional inability to simulate the rising of baseflow when the water table is deep. An example is given in Figure 6.13 where the 1984-1994 precipitation forcing, the observed WTD (from a monitoring well maintained by ISWS) and the simulated WTD, and the filtered and the simulated

baseflow at the Kaskaskia River basin are shown. As seen, the simulated baseflow in general well matches the observation except in 1989 and 1990 when the simulated water table is at its deepest level during the 11-year (1984-1994). Since the simulated WTD and baseflow are intimately interrelated, the bias might reflect the difficulty in capturing the baseflow dynamics by only two calibration parameters. (Notice that in other well-known hydrological lumped model, say, the Sacramento model has 14 parameters to calibrate; the VIC model has also more than 5 parameters to calibrate!). However, when the number of calibration parameters increases, the task of the optimal parameter search would soon become unmanageable.

Moreover, the above problem might be due to the errors in the atmospheric forcings, primarily the precipitation. The monthly precipitation in the Kaskaskia River basin is shown in the first panel of Figure 6.13. It can be seen although the observed water table level and baseflow both increase in 1989, the concurrent precipitation cannot explain for this rising trend. This suggests that the single rain gage selected as the model forcing may not be accurate in this case. (Note that the observed water table depth is a point observation, while the model simulates the average water table fluctuations; they do not necessarily agree with each other. However, the observed water table depth indeed show the increase in 1989).

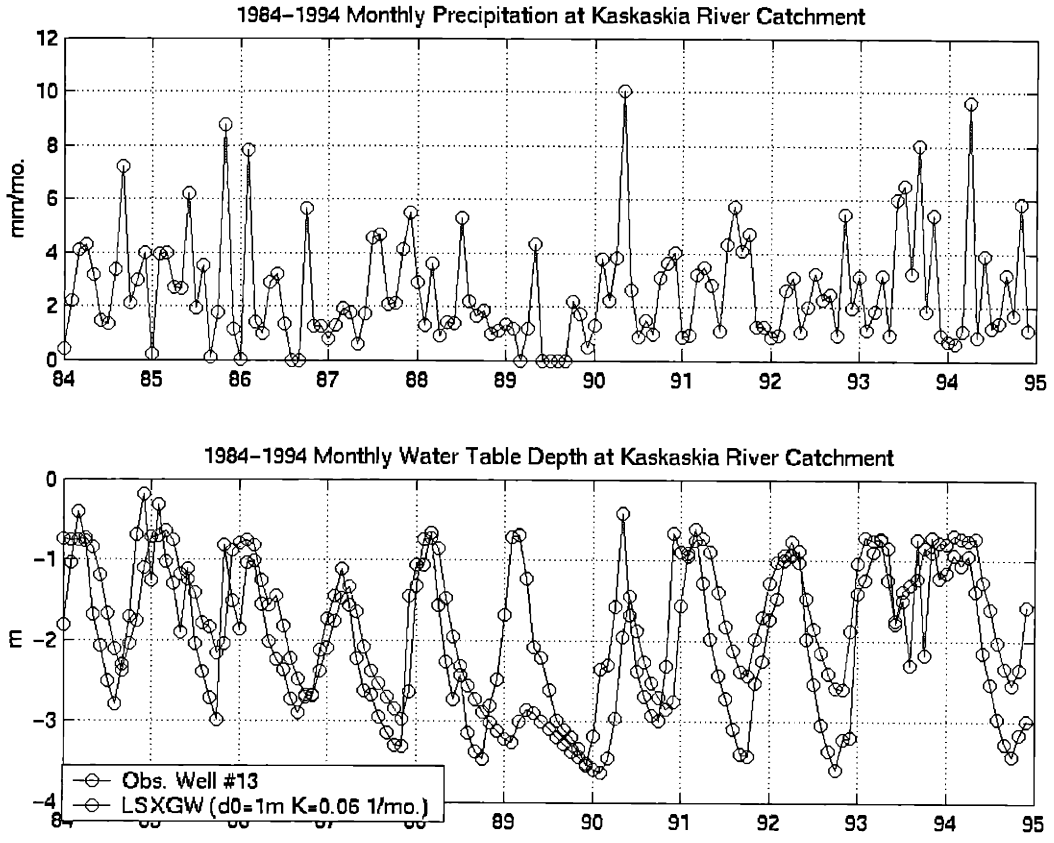

Figure 6.13 The 1984-1994 precipitation forcing, the observed water table depth (WTD, from the Illinois State Water Survey monitoring well #13) and the simulated WTD, and the filtered and the simulated baseflow at the Kaskaskia River basin.

- The sensitivities of (a) the shape parameter (α) of the assumed Gamma distribution of WTD and (b) the specific yield (S_y) on the simulated baseflow in the Green River basin are shown in Figure 6.14. In general, the difference caused by different α is significant during the period when baseflow is below its long-term average; a larger α (i.e., more towards the central distribution) leads to smaller baseflow due to the smaller fraction of shallow water table areas. However, it should be noted the impact of α is completely reflected on the groundwater-rating curve; therefore, the inaccuracy as a result of using erroneous α could be reconciled by calibrating the d_0 and K. Moreover, as expected the fluctuations of baseflow increase as S_y decreases. The general pattern of baseflow

evolution does not alter significantly for various S_y since the groundwater-rating curve is independent of the values of S_y. Therefore, it can be concluded the sensitivity of S_y on the simulated baseflow is low.

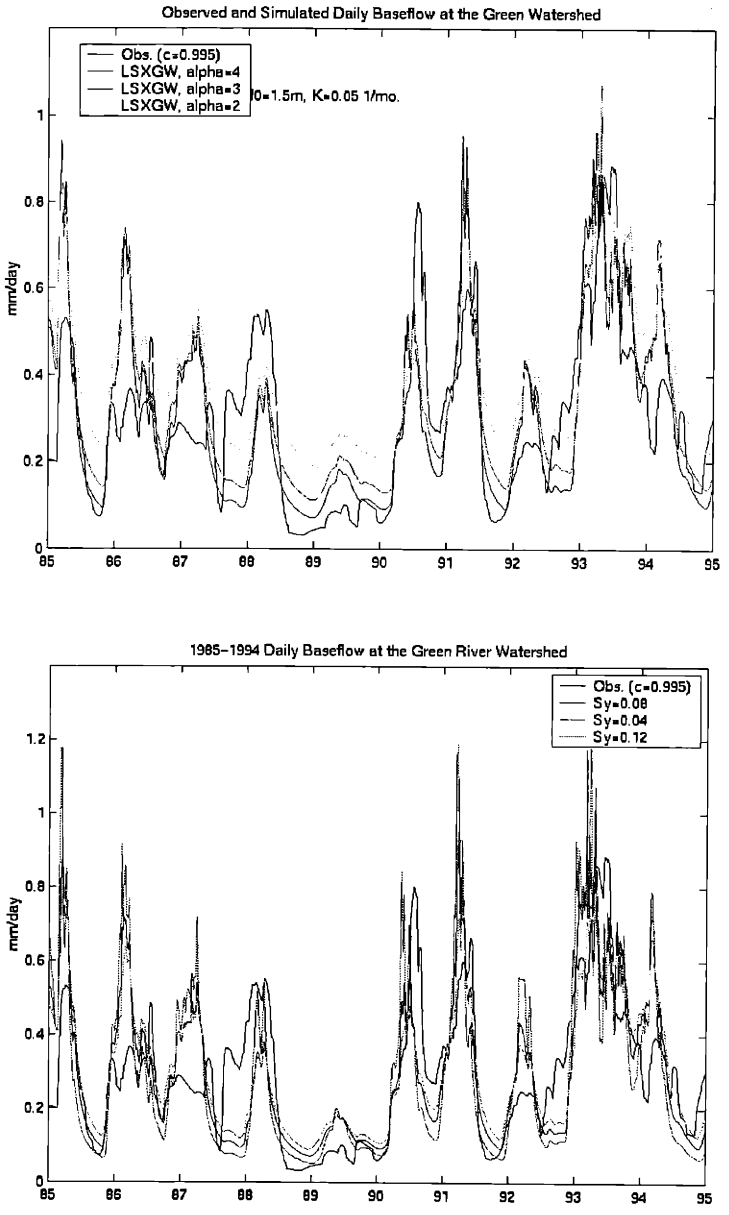

Figure 6.14 The sensitivities of (a) the shape parameter (α) of the assumed Gamma distribution of WTD and (b) the specific yield (S_y) on the simulated baseflow in the Green River basin.

6.4 Discussions and Future Directions

A parameter calibration approach has been proposed in this chapter as a necessary step for the global implementation of the LSXGW model. The practical application of this approach was demonstrated in several river basins in Illinois where the atmospheric forcing data and streamflow measurement are available. A critical issue to be addressed with this calibration approach is the issue of scaling. That is, at what scale is this methodology suitable?

The proposed calibration methodology is sound for any given river basin regardless of its scale since the streamflow used for the calibration has integrated the runoff generation process over the scale of that specific basin. However, cautions should be exercised when applying the calibration approach to the typical grid scale of climate models unless the catchment-based land surface scheme (e.g. *Koster et al.* 2000) in which watershed is the fundamental land surface unit is used. The reason is because the watershed scale does not coincide with the model grid scale. It is not clear how to average the calibrated parameters (and perhaps also the "process description", but let us accept the process description itself does not have scale transition problem or its scale issue can be reconciled by the suitable effective parameters) from the watershed scale to the grid scale. A grid may encompass several watersheds of different sizes; or conversely a large river basin may cover multiple grids; for example, in the PILPS phase 2c experiment the Red-Arkansas River Basin was divided into sixty-one $1^o \times 1^o$ rectangular grids.

In addition, the theory behind the groundwater model in the LSXGW was designed for a single watershed, not for a combination of several watersheds (which is more relevant to the grid size in climate models). This is because the current version of the LSXGW does not include a aggregation scheme to account for the actual variability of d_0 and K, which may vary from watershed to watershed. A parameter aggregation scheme to resolve the mismatch at the spatial scales has to be developed. This practical problem can be addressed through the following two directions:

(1) Modeling Study: run the LSXGW and use the proposed calibration approach in a nested river basin. Identify if any correlation can be found among the calibrated parameters in the sub-basins with various scales?

(2) Theory Development: extend the mathematical theory of LSXGW to statistically incorporate the spatial variability of d_0 and K. (The one presented in chapter 5.3 is a good analysis to start with, but the underlying assumptions there, like the uniform distribution of d_0, are too simplified for practical application). The development should base on the principle that streamflow in a large river basin is just a sum of many small ones!

As always, there is a mismatch between the scale of the observations and the scale at which land surface models are designed to be applied. One of the major goals of PILPS experiment phase 2c at the Red-Arkansas River basin is the calibration issue: test the ability of the schemes to transfer information about model parameters to other catchments and to the computational grid boxes. The decisions about whether to calibrate, which parameters to calibrate, and how to average to the computational grid scale were left to the participant modelers. The conclusion they derived was very limited: the calibrated model generally performs better those uncalibrated ones.

The scale issue we are dealing with now has not been rigorously answered in the literature of land surface modeling. The developed LSXGW model has accounted for the effects of the spatial variability of water table depth in the groundwater discharge, groundwater recharge, as well as implicitly in the soil moisture profile. However, the insufficient observations limit its global application at the climate model scale. Ideally, if we have enough observations of atmospheric forcing (primary raingages) and streamflow we can calibrate parameters from the LSXGW simulation at each catchment within a grid box, and then develop a parameter aggregation scheme base on the linearity of streamflow superposition to derive the grid-scale parameters. But this is not practical since first, we may not have so many atmospheric stations and streamflow records in most regions of the world, and the calibration approach itself is too tedious to implement globally. Another limitation imposed on the application of the parameter calibration

approach is the studies of the perturbed scenarios concerning future climate changes where the correct results are not known a priori. In those cases the only hope is to assume the parameters calibrated from the history streamflow records will remain unchanged under the future climate change conditions although the validity of this assumption is almost improvable.

Another totally different approach to determine the land surface model parameters is to develop the correlation between the model parameters and certain land surface attributes. Examples are *Koster et al.* [2000]; *Famiglietti and Wood* [1994]; and *Stieglitz et al.* [1997] who all developed their land surface models based on the relationships between topography and the sub-grid variability of hydrological processes. Since their models rely on the abundant topographic data rather than the atmospheric and hydrological observations to estimate parameters, they have no data constraint problem as in our proposed calibration approach. Moreover, due to the similarity in theoretical basis they are subject to the assumptions behind the TOPMODEL framework and share the common strengths and weakness of the TOPMODEL.

It is reasonable to expect that d_0 and K can be linked to certain basin geomorphologic attributes, aquifer soil and hydraulic properties, or basin climatology. If such correlations can be found, the groundwater parameters are possible to be estimated without both the streamflow records and groundwater level observations. A classification algorithm can be developed in which different regions can be categorized into different groups based on different combinations of groundwater parameters. Since the water table dynamics in a region can be uniquely characterized by it's groundwater-rating curve, regions in the same group form a hydrologically similar regime and share a similar groundwater-rating curve. Therefore, a global groundwater-rating "type-curves" can be developed which can be determined by the measured basin geomorphic and soil attributes, or climate variables.

Chapter 7 Conclusions and Future Directions

The availability of a multi-year comprehensive dataset on most of the hydrological variables in the large area of Illinois has facilitated the characterization of the regional-scale hydroclimatology in Illinois. Two independent water balance approaches, the surface/subsurface water balance approach and the atmospheric water balance approach, were used to quantify various water balance components in Illinois from 1983 to 1994. One of the major conclusions of this regional water balance study is that the incorporation of the change in groundwater storage into the water balance computations in the shallow water table regions is indispensable since groundwater aquifers provide a significant portion of water storage at the monthly and annual time scale.

Based on the findings in Illinois presented in Chapters 2 and 3, the roles that the regional-scale unconfined shallow aquifers play in the Illinois regional hydroclimatology can be summarized as follows:

1. Groundwater storage is a major water balance component whose storage is as important as soil moisture at monthly or longer time scale.
2. The regional-scale water table depth is highly correlated with the regional streamflow in a strong nonlinear manner (explains 2/3 of the streamflow variance)
3. The regional unconfined aquifer amplifies the drought climatic anomalies and dissipates the flood anomalies.
4. The regional unconfined aquifer provides water to the root-zone soil moisture for maintaining the high rate of summer evapotranspiration (~120 mm/month) in Illinois.

Despite its significance, the current generation of land surface schemes (LSPs) used in GCMs or numerical weather prediction models largely neglect the representation of groundwater aquifers, and consider the soil moisture as the only subsurface reservoir to store water. The major reason of the extreme importance of the land surface scheme to the predicted climate from atmospheric models is the long memory of soil moisture that can significantly impact the

exchanges of water and heat fluxes between the land surface and the atmosphere. Since at least in the shallow water table regions such as Illinois the storage capacity of the unconfined aquifer is comparable to that of soil moisture, such a simplified representation of subsurface hydrology would result in significant errors in the predicted land surface fluxes and states. Globally, where should the groundwater storage be represented in LSPs depends on the degree that groundwater component participates in the regional-scale water balance. For the humid regions with relatively mild topography, it would be reasonable to expect the water table in a significant portion of the region is close to the ground surface, hence it is necessary to include water table dynamics. In contrast, for arid or semi-arid regions where the precipitation less evaporation is small, the water table for most of the regions is deep or even may not exist, thus the land surface water balance can be closed without considering groundwater storage. The groundwater recharge, which in general is proportional to the precipitation minus evaporation, is a suitable indicator of whether the groundwater storage should be represented in LSPs or not.

These findings obtained from the regional water balance study have implications for the land-surface parameterization schemes (LSPs). In order to incorporate the water table dynamics into climate models, a lumped unconfined aquifer model was developed and interactively coupled to the land surface scheme LSX. This model is parsimonious and computationally efficient, hence it is suitable for the use in GCMs and numerical weather prediction models. A methodology combining the strengths of the statistical-dynamical approach and the mosaic approach is developed to account for the subgrid variability of water table depth (WTD).

This coupled LSXGW model has been tested in Illinois for an 11-year perioid from 1984 to 1994. The simulation results indicate that the simulated hydrological states (e.g., water table depth and soil saturation degree) and fluxes (e.g., groundwater recharge, total runoff, and total evaporation) all have remarkable agreements with the hydrological observations in Illinois.

However, it has been recognized that the excellent performance of the LSXGW in the Illlinois simulation is partially attributed to the successful reproduction of the grid-scale groundwater rating-curve. Specifically, the success stems from the reliable estimation of the required parameters (i.e., d_0 and K) in the aquifer model, namely due to the availability of the data on the

water table level and streamflow in Illinois. In practice it is impractical to expect that these data, especially water table observations, are globally available. Since the LSXGW is aimed to be used in climate models, the development of a globally feasible procedure of parameter estimation is necessary.

A parameter estimation procedure using the observed daily streamflow records to calibrate the groundwater model parameters (d_0 and K) is proposed. Its applicability has been demonstrated in several watersheds in Illinois. The calibration approach is suitable to be applied to the situation when the observations of precipitation and streamflow are available. Another parameter estimation approach to deal with the regions with scarce data is to develop the correlation between the model parameters and certain land surface attributes. Examples are the work by *Koster et al.* [2000], *Famiglietti and Wood* [1994a], and *Stieglitz et al.* [1997] who developed their land surface schemes based on the relationships between topography and the sub-grid variability of hydrological variables. The development of such kind of schemes for the estimation of LSXGW groundwater parameters is a future research topic.

The proposed methodology to account for the sub-grid variability, namely, a combination of the statistical-dynamic approach and the mosaic approach, is not new. The TOPMODEL-based land surface schemes (LSPs) developed by *Famiglietti and Wood* [1994a], and *Stieglitz et al.* [1997], and *Koster et al.* [2000] are indeed similar in concept to the LSXGW in this regard. All of these LSPs applied TOPMODEL equations to their land surface schemes and sub-divided a grid into several sub-regions in order to classify different hydrological regimes. The grid subdivision is a great improvement over the traditional single-column LSPs since it resolves the hydrologically most active areas, i.e., the near-channel runoff generation areas. This advantage is conceptually exactly the same as the multi-column models proposed in the section 5.2 of this thesis. However, the LSXGW model differs significantly from these TOPMODEL-based LSPs in that the water table depth rather than the topography-soil index is used as the criterion for grid subdivision. Water table depth not only controls the generation of groundwater runoff, it also dictates the seasonal variability of the expansion and contraction of the saturated areas and hence the generation of saturated-excess surface runoff. Therefore, in our view it is the most suitable variable to identify various hydrological regimes.

Another significant value of the developed LSXGW model is its ability of predicting the evolution of water table depth. In addition to the role that the land surface process plays in affecting atmospheric process, the land surface process also has important role in water resource management. For any study on the impact of regional climate change on the future groundwater resource, the prediction of water table depth is desirable. The proposed LSXGW model is well suited to be used in this kind of studies, which is still very scant in both hydrological and atmospheric literature.

An important previous work worthy of further discussion is the MOSAIC land surface models developed by *Koster et al.*, [2000]. The MOSAIC model used catchment-based approach for modeling the land surface processes in GCMs by partitioning continental areas into a mosaic of hydrologic catchments through analysis of surface elevation data. The sub-grid variability of soil moisture in a catchment was related to the topographic characteristics of that catchemnt in this model. In our view, the catchment-based approach is a superior strategy for the LSP modelers to adopt. Recall that the aggregation problem (scale problem) as discussed in section 6.4 stemming from the mismatch between the scale of observations (i.e., a watershed) and the scale at which LSPs were designed to be applied (i.e., a grid cell), the catchment-based approach apparently can alleviate this problem. The common practice in the land surface model calibration as well as model validation by using the streamflow observations at the river basin outlet is only valid when the size of the basin drainage area is comparable to the grid size of LSPs.

The developed LSXGW model has only been tested in Illinois. As discussed in section 5.2, dry regions have unique modeling issues that need to be addressed. Therefore, we plan to test the LSXGW in several contrasting environments. It would be worthwhile to investigate first, if the LSXGW can satisfactorily simulate the hydroclimatology in a water-deficient arid region such as Sahel in West Africa and the semiarid and arid regions in Arkansas-Red River basin of the PILPS phase 2c experiment.

References

Abdulla, F. A., D. P. Lettenmaier, E. F. Wood and J. A. Smith, Application of a macroscale hydrologic model to estimate the water balance of the Arkansas-Red River basin. *J. Geophys. Res. 101*, 7 449-7 459, 1996.

Abdulla, F. A., and D. P. Lettenmaier, Application of regional parameter estimation schemes to simulate the water balance of a large continental river, *J. Hydrology*, 197 (1-4), 230-257, 1997.

Abdulmumin, S., L. O. Myrup, and J. L. Hatfield, An energy balance approach to determine regional evapotranspiration based on planetary layer similarity theory and regularly recorded data. *Water Resour. Res. 23*, 2050-2058, 1987.

Abramopoulos, F., Rosenzweig, C. and Choudhury, B., Improved Ground Hydrology Calculations for Global Climate Models (GCMs): Soil Water Movement and Evapotranspiration, *J. Climate, 1,* 921-941, 1988.

Alley, W. M., On the treatment of evapotranspiration, soil moisture accounting and aquifer recharge in monthly water balance models. *Water Resour. Res. 20*, 1137-1149, 1984.

Avissar, R. and R. A. Pielke, A parameterization of heterogeneous land surface for atmospheric numerical models and its impacts on regional meteorology. *Mon. Wea. Rev., 117*, 2113-2136, 1989.

Avissar, R., Conceptual aspects of a statistical-dynamical approach to represent landscape subgrid-scale hetergeneities in atmospheric models. *J. Geophys. Res., 97,* 2729-2742, 1992.

Baumgartner, F. and E. Reichel, *The World Water Balance: Mean Annual Global, Continental and Maritime Precipitation, Evaporation and runoff.* Ordenbourg, Munich, 179 pp., 1975.

Beljaars, A. C. M., and F. C. Bosveld, Cabauw data for the validation of land surface parameterization schemes. *J. Climate 10*, 1172-1193, 1997.

Benton, G. S., R. T. Blackburn, and V. W. Snead, The role of the atmosphere in the hydrologic cycle. *Trans. Amer. Geophys. Union 31*, 61-73, 1950.

Benton, G. S., and M. A. Estoque, Water vapor transfer over the North American continent. *J. Meteoro. 11*, 462-477, 1954.

Berbery, E. H., E. M. Rasmusson, and K. E. Mitchell, Studies of North American continental-scale hydrology using Eta model forecast products. *J. Geophys. Res. 101*, D3, 7305-7319, 1996.

Beven, K., and M. J. Kirby, A physically based, variable contributing area model of basin hydrology, *Hydrol. Sci. J., 24,* 43-69, 1979.

Bonan, G. B., Influence of subgrid-scale heterogeneity in leaf area index, stomatal resistance, and soil moisture on grid-scale land-atmosphere interactions. *J. Climate, 6,* 1882-1897, 1993.

Bonan, G. B., Comparison of two land surface process models using prescribed forcing. *J. Geophys. Res., 99(D12),* 25,803-25,818, 1994

Bras, R. L., and I. Rodriquez-Iturbe, *Random Functions and Hydrology*, Addison-Wesley, Reading, Mass., 1985.

Bras, R. L., K. Curry, and R. Buchanan, The multivariate broken-line model revisited: A discussion on capabilities and limitations, *J. Hydro.,* 53, 31-51, 1981.

Brubaker K. L. and D. Entehkabi, and P. S. Eagleson, Atmospheric water vapor transport and continental hydrology over the Americas. J. *Hydrol. 155*, 407-428, 1994.

Brutsaert, W., *Evaporation into the Atmosphere*. D. Reidel, Dordecht, Holland, 1982.

Bryan, F. and A. Oort, Seasonal variation of the global water balance based on aerological data. *J. Geophys. Res. 89*, 11 717-11 730, 1984.

Changnon, S. A., G. Achtemeier, S. Hilberg, V. Knapp, R. Olson, W. Roberts and P. Vinzani, The 1980-1981 drought in Illinois: Causes, dimensions and impacts. Rep. of Investigation 102, Illinois State Water Survey, 78 pp., 1982.

Changnon, S. A., F. A. Huff, and C. F. Hsu, Relations between precipitation and shallow groundwater in Illinois. *J. Climate 1*, 1239-1250, 1988.

Charney, J. G., W. K. Quirk, S. –H. Chow, and J. Kornfield, A comparative study of the effects of albedo changes on drought in semi-arid regions, *J. Atmos. Sci., 34*, 1366-1385, 1977.

Chen, et al., Cabauw experimental results from the Project for Intercomparison of Land-Surface Parameterization Schemes. *J. Climate 10*, 1194-1215, 1997.

Chen, T. -H., Henderson-Sellers, A., and Qu, W., Behind the scenes of the Phase 2(a) experiment of the Project for Intercomparison of Land-surface Parameterization Schemes (PILPS): the Cabauw Story, Tech. Rep. 22, GEWEX Technical Note, IGPO Publication Series, 23 pp., 1996.

Delire C. and J. A. Foley, Evaluating the performance of a land surface/ecosystem model with biophysical measurements from contrasting environments. *J. Geophys. Res., 104(D14),* 16,895-16,909, 1999.

Delworth, T. L. and A. S. Manabe, The influence of potential evaporation on the variability of simulated soil wetness and climate. *J. of Climate 1*, 523-547, 1988.

Dirmeyer, P. A., A. J. Dolman, and N. Sato, The Global Soil Wetness Project: A pilot project for global land surface modeling and validation. *Bull. Amer. Meteor. Soc.*, **80**, 851-878, 1999.

Dickinson, R. E., Henderson-Sellers, A., and Kennedy, P.J., Biosphere-Atmosphere Transfer Scheme (BATS) Version 1e as Coupled to the NCAR Community Climate Model., NCAR Technical Note TN- 387 + STR, 72p., 1993.

Domenico, P. A. and F. A. Schwartz, *Physical and Chemical Hydrogeology*. John Wiley & Sons Inc., second edition, New York, 1990.

Eagleson, P. S., Climate, soil, and vegetation: 3. A simplified model of soil moisture movement in the liquid phase. *Water Resour. Res., 14(5),* 722-730, 1978.

Eltahir, E. A. B., and R. L. Bras, A description of rainfall interception over large areas. *J. Climate, 6,* 1002-1008, 1993.

Eltahir, E. A. B., and P. J. –F. Yeh, On the asymmetric response of groundwater level to floods and droughts in Illinois, *Water Resour. Res.* 35(4), 1199-1217, 1999.

Entekhabi, D. and P. Eagleson, Land surface hydrology parameterization for atmospheric general circulation models including subgrid scale spatial variability. *J. Climate, 2,* 816-831, 1989.

Ernstberger, H., and V. Sokolleck, Effects of land use on the hydrology of small basins in Hessen (Federal Republic of Germany), in the *New Approach in Water Balance Computations, Proceedings of the Hamburg Workshop*, IAHS Publ. No. 148, International Association of Hydrological Sciences, Wallingford, UK, p.147-157, 1985

Famiglietti, J., and E. Wood, Evapotranspiration and runoff from large area: Land surface hydrology for atmospheric general circulation models, in *Land Surface-Atmospheric Interactions for Climate Models*: Observations, Models, and Analyses, edited by E. Wood, Kluwer Academic Publishers, 1990.

Famiglietti, J., and E. Wood, Multiscale modeling of spatially variable water and energy balance processes, *Water Resour. Res.* 30, 3061-3078, 1994.

Famiglietti, J., and E. Wood, Application of multiscale water and energy balance models on a tallgrass prairie, *Water Resour. Res.* 30, 3?-3?, 1994.

Famiglietti, J., and E. Wood, Effects of spatial variability and scale on areally average evapotranspiration, *Water Resour. Res.* 30, 3?-3?, 1994.

FAO-UNESCO, *Soil Map of the World 1:5,000,000,* UNESCO, Paris, 1975.

Farnsworth, R. K., and E. S. Thompson, Mean monthly, seasonal, and annual pan evaporation for the United States, NOAA Tech. Rept. NWS 34, Silver Spring, MD, 1982

Findell, K. L., and E. A. B. Eltahir, An analysis of the soil moisture-rainfall feedback, based on direct observations from Illinois, *Water Resour. Res.* 33, 725-735, 1997.

Foley, J. A., C. I. Prentice, N. Ramankutty, S. Levis, D. Pollard, S. Sitch, and A. Haxeltine, An integrated biosphere model of land surface process, terrestrial carbon balance, and vegetation dynamics, *Global Biogeochem. Cycles, 10*, 603-628, 1996.

Gangopadhyaya, M., G. E. Ir. Harbeck, T. J. Nordenson, M. H. Omar, and V. A. Uryvaev, Measurement and estimation of evaporation and evapotranspiration, World Met. Organ., Tech. Note No. 83, WMO-No. 201.TP.105, 121 pp., 1966.

Giorgi, F., An approach for the representation of surface heterogeneity in land surface models, Part 1: Theoretical framework, *Mon. Wea. Rev., 125,* 1885-1899, 1997.

Giorgi, F., An approach for the representation of surface heterogeneity in land surface models, Part 2: Validation and sensitivity experiments, *Mon. Wea. Rev., 125,* 1900-1919, 1997.

Groisman, P. Ya., and D. R. Legates, The accuracy of United States precipitation data. *Bull. Amer. Meteo. Soc.,* 75, 215-227, 1994.

Gutowski, Jr. W. J., Y. Chen, and Z. Otles, Atmospheric water vapor transport in NCEP-NCAR reanalyses: comparison with river discharge in the Central United States. *Bull. Amer. Meteo. Soc.,* 78, 1957-1969, 1997.

Hendeson-Sellers, A., A. J. Pitman, P. K. Love, P. Irannejad, and T. H. Chen, The Project for Intercomparison of Land Surface Parameterization Schemes (PILPS): Phases 2 and 3. *Bull. Amer. Meteor. Soc.,* 76, 489-503, 1995.

Higgins, R. W., K. C. Mo, and S. D. Schubert, The moisture budget of the Central United states in spring as evaluated from the NCEP/NCAR and the NASA/DAO reanalyses. *Mon. Wea. Rev.* 124, 939-963, 1996.

Hollinger, S. E., and S. A. Isard, A soil moisture climatology of Illinois. *J.Climate 7*, 822-833, 1994.

Houghton, J. T., L. G. M. Filho, B. A. Callander, N. Harris, A. K. M. Kattenberg (eds), *Climate Change*, Cambridge University Press, Cambridge, 1995.

Johnson, A. I., Specific yield – compilation of specific yields for various materials. *U. S. Geol. Surv. Water-supply paper, 1662-D*, 1967.

Johnson, K. D., D. Entekhabi, and P. Eagleson, The implementation and validation of improved landsurface hydrology in an atmospheric general circulation model, Center for Global change Science, MIT, Report No. 11, 64 pp, 1992.

Jones, D. M., Variability of evapotranspiration in Illinois, Circular Report 89, Illinois State Water Survey, 13pp., 1966.

Kalnay, E., and co-authors, The NCEP/NCAR 40 years reanalysis project. *Bull. Amer. Meteo. Soc.,* 77, 437-471, 1996.

Kattelmann R. and K. Elder, Hydrologic characteristics and water balance of an alpine basin in the Sierra Nevada. *Water Resour. Res. 27*, 1553-1562, 1991.

King , J. E., Illinois climate in a geological scale: The last 10,000 years, in *Proceedings of the 12th Annual ENR Conference on Illions Climate*, pp. 9-14, Ill. Dep. Of Energy and Nat. Resour., Springfield, 1984.

Koster, R.D. and Suarez, M.J., Modelling the land surface boundary in climate models as a composite of independent vegetation stands, *J. Geophys. Res., 97*, 2697-2715, 1992.

Kunkel, K. E., S. A. Changnon, C. G. Lonnquist, and J. R. Angel, A real-time climate information system for the Midwestern United States. *Bull. Am. Meteorol. Soc. 71,* 1601-1609, 1990.

Larson, L. W., and E. L. Peck, Accuracy of precipitation measurements for hydrologic modeling. *Water Resour. Res. 10*, 857-863, 1974.

Leighton, M. M., G. E. Ekblaw, and L. Horberg, Physiographic Divisions of Illinois. *Rep. Of Investigation* 129, Illinois State Water Survey, 39 pp., 1948.

Lesack, L. F. W., Water balance and hydrologic characteristics of a rain forest catchment in the central Amazon basin. *Water Resour. Res. 29*, 759-773, 1993.

Leung, L. R. and S. J. Ghan, A subgrid parameterization of orographic precipitation. *Theor. Appl. Climatol.*, 52, 95-118, 1995.

Leung, L. R. and S. J. Ghan, Parameterizing subgrid orographic precipitation and surface cover in climate models, *Mon. Wea. Rev.*, 3271-3291, 1998

Liang, X., D. P. Lettenmaier, E. F. Wood, and S. J. Burges, A simple hydrologically model of land surface water and energy fluxes for GCMs. *J. Geophys. Res. 99,* 14,415-14,428, 1994.

Liang, X., E.F. Wood, D.P. Lettenmaier et al., The project for intercomparison of land-surface parameterization schemes (PILPS) phase-2c Red-Arkansas river basin experiment: 2. Spatial and temporal analysis of energy fluxes, Global and Planetary Change, *19*(1-4), 137-159, 1998.

Lohmann, D., D.P. Lettenmaier, X. Liang, E.F. Wood et al., The project for intercomparison of land-surface parameterization schemes (PILPS) phase-2c Red-Arkansas river basin experiment: 3. Spatial and temporal analysis of water fluxes, *Global and Planetary Change*, *19*(1-4), 161-179, 1998.

Malek, E., G. E. Bingham, D. Or, and G. McCurdy, Annual mesoscale study of water balance in a Great Basin heterogeneous desert valley. *J. Hydrol.* 191, 223-244, 1997.

Manabe, S., Climate and the ocean circulation: 1, The atmospheric circulation and the hydrology of the Earth's surface, *Mon. Weather Rev.*, 97, 739-805, 1969.

Manabe, S., R. T. Wetherald, and R. J. Stouffer, Summer dryness due to an increase of atmospheric CO2 concentration. *Climate Change*, 3, 347-386, 1981.

Mawdsley, J. A., and W. Brutsaert, Determination of regional evapotranspiration from upper air meteorological data. *Water Resour. Res., 13*, 539-548, 1979.

McGowan, M. and J. B. Williams, The water balance of an agricultural catchment, III The water balance. *J. Soil Sci. 31,* 245-262, 1980.

Miller, S. A., and P. S. Eagleson, Interaction of the saturated and unsaturated soil zones. Report number 284, Parsons Laboratory, MIT, 289 pp., 1982.

Mo, K. C., and R. W. Higgins, Large-scale atmospheric moisture transport as evaluated in the NCEP/NCAR and the NASA/DAO reanalyses. *J. Climate 9,* 1531-1545, 1996.

Munley, W. G., and L. E. Hipps, Estimation of regional evaporation for a tallgrass prairie from measurements of properties of the atmospheric boundary layer. *Water Resour. Res., 27*, 225-230, 1991.

Nichols, W. D., Estimating annual groundwater discharge by greasewood in areas of shallow groundwater groundwater in the northern Great Basin using an energy-combination model. *Water Resour. Res., 29(10)*, 2771-2778, 1993.

Nichols, W. D., Groundwater discharge by phreatophyte shrubs in the Great Basins as related to depth of groundwater. *Water Resour. Res., 30*(12), 3265-3274, 1994.

Nijssen B., D. P. Lettemnier, X. Liang, S. W. Wetzel and E. F. Wood, Streamflow simulation of continental-scale river basins, *Water Resour. Res., 33*(4), 711-724, 1997.

Oki, T., K. Musiake, H. Matsuyama, and K. Masuda, Global atmospheric water balance and runoff from large river basins. *Hydrol. Process. 9*, 411-434, 1995.

Parlange, M. B., W. E. Eichinger, and J. D. Albertson, Regional scale evaporation and the atmospheric boundary layer. *Rev. of Geophys. 33*(1), 99-124, 1995.

Peixoto, J. P., M. Almeida, R. D. Rosen and D. A. Salstein, Atmospheric moisture transport and the water balance of the Mediterranean Sea. *Water Resour. Res. 18*, 83-90, 1982.

Peixoto, J. P., and A. H. Oort, The atmospheric branch of the hydrological cycle and climate, *Variation in the Global Water Budget*, A. Street-Perrot and Co-editors, Ed., Reidel, 5-65, 1983.

Peixoto, J. P., and A. H. Oort, *Physics of Climate*, American Institute of Physics, New York, 1992.

Penman, H. L., The water balance of the Stour catchment area. *J. Inst. Water Eng. 4,* 457-469,1950.

Pitman, A. J., A. Henderson-Sellers, and Z. –L. Yang, Sensitivity of regional climates to localized precipitation in global models, *Nature, 346*, 734-737, 1990.

Pollard, D. and Thompson, S. L., Use of a land-surface-transfer scheme (LSX) in a global climate model: the response to doubling stomatal resistance, *Global and Planetary Change, 10*, 129-161, 1995.

Pruitt, W. O., and D. E. Angus, Large weighing lysimeter for measuring evapotranspiration. *Trans. Am. Soc. Agric. Eng. 3,* 13-15, 1960.

Rasmussen, W. C., and G. E. Anderasen, Hydrologic budget of the Beaverdam Creek Basin, MD., U.S. Geol. Survey, Water Supply Paper 1472, 106pp, 1959.

Rasmusson, E. M., Atmospheric water vapor transport and the water balance of North America: part 1. Characteristics of water vapor flux field. *Monthly Weather Review, 95*, 403-426, 1967.

Rasmusson, E. M., Atmospheric water vapor transport and the water balance of North America: part 2. Large-scale water balance investigations. *Monthly Weather Review, 96,* 720-734, 1968.

Rasmusson, E. M., A study of the hydrology of Eastern North America using atmospheric vapor flux data. *Monthly Weather Review, 97*, 119-135, 1971.

Rasmusson, E. M., Hydrological application of atmospheric vapor-flux analyses. *Hydrol. Rep. 11*, WMO, Geneva, 50 pp. 1977.

Rawls, W. J., D. L. Brakensiek, and K. E. Saxton, Estimation of Soil Water Properties, *Transac. of ASAE*, 1316-1320, 1982.

Rice, S. O., Mathematical analysis of random noise, *Bell Syst. Tech. J., 24*, 46-156, 1945.

Rind, D., R. Goldberg, J. Hansen, C. Rosenzweig, and R. Ruedy, Potential evapotranspiration and the likelihood of future draught. *J. Geophys. Res., 95*, 9983-10004, 1990.

Roads, J. O., S.-C., Chen, A. K. Guetter, and K. P. Georgakakos, Large-scale aspects of the United states hydrologic cycle. *Bull. Am. Meteorol. Soc. 75,* 1589-1610, 1994.

Roberts G. and R. J. Harding, The use of simple process-based models in the estimate of water balance for mixed land use catchments in East Africa. *J. Hydrol. 180*, 251-266, 1996.

Ropelewski, C. F. and E. S. Yarosh, The observed mean annual cycle of moisture budgets over the Central United States (1973-1992), accepted by *J. Climate*, 1998.

Rosen, R. D., and A. S. Omolayo, Exchange of water vapor between land and ocean in the Northern Hemisphere. *J. Geophys. Res. 86(C12),* 12,147-12,152, 1981.

Salstein, D. A., R. D. Rosen, and J. P. Peixoto, Modes of variability in annual hemispheric water vapor and transport fields. *J. Atmos. Sci. 40*, 788-803, 1983.

Savijarvi, H. I., Global energy and moisture budgets from rawinsonde data. *Mon. Wea. Rev., 116*, 417-430, 1988.

Schicht, R. G. and W. C. Walton, Hydrologic budgets fro three small watersheds in Illinois. *Rept. Of Investigation, 49*, Ill. State Water Survey, Champaign, 1961.

Sellers, P. J., Y. Mintz, Y. C. Sud, and A. Dalcher, A simple biosphere model (SiB) for use within general circulation models, *J. Atmos. Sci., 43*, 505-531, 1986.

Senn, R. B., A nonlinear reservoir lumped parameter model for the Herkenhoff farm located near San Acacia, New Mexico Institute of Technology, 1980.

Seth, A., F. Giorgi, and R. E. Dickinson, Simulating fluxes from heterogeneous land surfaces: Explicit subgrid method employing the biosphere-atmosphere transfer scheme (BATS), *J. Geophy. Res., 99*, 18,651-18,667, 1994.

Shao, Y. and A. Henderson-Sellers, Validation of soil moisture simulation in landsurface parameterization schemes with HAPEX data. *Global Planet. Change, 13,* 11-46, 1996.

Shukla, J., and Y. Mintz, Influence of land-surface evapotranspiration on the Earth's climate. *Science 215*, 1498-1500, 1982.

Shuttleworth, W. J., *Evaporation*, Institute of Hydrology, Report No. 56, Willingford, Oxon., UK., 1979.

Sivapalan, M., and R. A. Woods, Evaluation of the effects of general circulation model's subgrid variability and patchiness of rainfall and soil moisture on land surface water fluxes, in *Scale Issues in Hydrological Modeling*, J. D. Kalma and M. Sivapalan, Eds., John Wiley and sons, 453-473, 1995.

Stagnitti, F., J. -Y. Parlange, and C. W. Rose, Hydrology of a small wet catchment, *Hydrol. Processes*, 3, 137-150, 1989.

Stagnitti, F., J. -Y. Parlange, T. S. Steenhuis, M. B. Parlange, and C. W. Rose, A mathematical model of hillslope and watershed discharge, *Water Resour. Res. 28*, 2111-2122, 1992.

Starr, V. P. and J. Peixoto, On the global balance of water vapor and the hydrology of deserts. *Tellus 10,* 189-194, 1958.

Stieglitz, M., D. Rind, J. Famiglietti, and C. Rosenzweig, An efficient approach to modeling the topographic control of surface hydrology for the regional and global climate modeling, *J. Climate, 10*, 118-137, 1997.

Street-Perrott, A., M. Beran, and R. Ratcliffe, *Variations in the Global Water Budget*, D. Reidel, Dordrecht, Holland, 1983.

Sugita, M. and W. H. Brustaert, Daily evaporation over a region from lower boundary-layer profiles measured with radiosondes. *Water Resour. Res., 27*, 747-752, 1991.

Thompson, S. L. and D. Pollard, A global climate model (GENESIS) with a land-surface transfer scheme (LSX), Part 1: Present climate simulation, *J. Climate, 8,* 732-761, 1995.

Thronthwaite, C. W., An approach toward a rational classification of climate. *Geogr. Rev. 38,* 55-94, 1948.

Vandewiele, G. L., C. -Y. Xu, and N. L. Win, Methodology and comparative study of monthly water balance models in Belgium, China and Burma. *J. Hydrol. 134*, 315-347, 1992.

Van der Beken, A., and A. Herrmann (Ed.), *New Approaches in Water Balance Computations, IAHS Publ. 148*, International Association of Hydrological Sciences,
Wallingford, UK, 167pp. 1985.

Verseghy, D.L., 1991: CLASS: A Canadian land surface scheme for GCMs, I. Soil model, Int. J. Climatol., 11, 111-133.

Vinnikov, K. Y., A. Robock, S. Qiu, J. K. Entin, M. Owe, B. J. Choudhury, S. Hollinger, and E. G. Njoku, 1999: Satellite remote sensing of soil moisture in Illinois, United States. *J. Geophys. Res., 104(D4),* 4,145-4,168.

W. C. Walton, Ground-water recharge and runoff in Illinois. *Rept. Of Investigation, 48*, Ill. State Water Survey, Champaign, 1965.

Wetherald, R. T. and S. Manabe, The mechanism of summer dryness induced by greenhouse warming, *J. Climate, 8,* 3096-3108, 1995.

Wood, E. F., D. P. Lettenmaier, and V. G. Zartarian, A land-surface hydrology parameterization with subgrid variability for general circulation models, J. *Geophy. Res., 97*(D3), 2717-2728, 1992.

Xu C. –Y. and J. S. S. Halldin, Regional water balance modelling in the NOPEX area: development and application of monthly water balance. *J. Hydrol. 180*, 211-236, 1996.

Yeh, P. J. -F., M. Irizarry, and E. A. B. Eltahir, Hydroclimatology of Illinois: a comparison of monthly evaporation estimates based on atmospheric water balance and soil water balance. *J. Geophys. Res.,* 103 (D16), 19,823-19,837, 1998.

Yeh, P. J. –F., and E. A. B. Eltahir, The role of unconfined aquifers in supplying water for regional evapotranspiration during summer in Illinois, unpublished manuscript, 1998.

Zektser, I. S., and H. A. Loaiciga, Groundwater fluxes in the global hydrologic cycle: past, present and future, *J. Hydrol., 144*, 405-427, 1993.

Appendix A: Hydrogeology of Aquifers in Illinois

Here we provide a brief description of the hydrogeology in Illinois. For a detailed discussion of the topic, we recommended the earlier studies by the Illinois State Water Survey (ISWS) [*Leighton et al., 1948*; *Schicht and Walton*, 1961; *Prickett et al*, 1964; *Walton,* 1965, *Changnon* et al., 1988, etc.]. The following summary is based upon those studies.

Illinois has a wide diversity of soils including almost all the major types of soil found throughout the Midwest. The physiography of Illinois is composed largely of flat glacial prairies and rolling hills [*Changnon* et al., 1988]. Over 90% of Illinois lies mostly within the central lowland physiographic province and is essential a prairie plain. Illinois has the lowest mean elevation above sea level among mid-west states [*Leighton et al.,* 1948]. The relief over most of the state is moderate to slight; large-scale relief features are generally absent.

Large areas in Illinois are covered by unconsolidated deposits left by the glaciers. The glacial deposit commonly ranges from 50 to 200 feet (~15-60m) or more in thickness over Illinois. Glacial till is the principal constituent of the deposit. Till is typically a heterogeneous unsorted mixture of particles ranging in size from boulder to fine clay. In most places till contains a high percentage of silt and clay such that it has a low permeability and specific yield. Accumulations of wind-blown silt-size materials called loess are associated with glacial deposits. Deposits of loess cover most areas in Illinois to a depth varying from 4 to 25 feet (~1-8m). In addition, these glacial drifts contain extensive deposits of sand and gravel in two zones: near the surface (upper aquifer) and immediately above bedrock (lower aquifer). The upper and lower aquifers exceed 30 feet (~9m) in thickness at many places and are separated by clayey materials (confining bed) commonly exceeding 75 feet (~23m) in thickness.

Moreover, sand and gravel and bedrock aquifers are often deeply buried. The recharge to the aquifers is largely derived from direct precipitation through thick layers of till having low permeability. Groundwater recharge generally is at a maximum during the April and most

recharge occurs prior to July. In dry years there is very little recharge from July through November. Vertical leakage is often much less than the infiltration rates originated from precipitation to surface deposits, leading to a shallow water table condition in Illinois. In most of the state, the water table is very near the surface and shallow ponds, swamps, and poorly drained areas are widespread prior to settlement. Extensive surface and subsurface drainage are necessary to permit agricultural development.

The size and hydraulic properties of the groundwater reservoir in connection with streams determines the quantities of groundwater runoff, which comprises most of the runoff in the extended dry periods. According to an earlier study by ISWS [*Walton*, 1965, p. 17], groundwater runoff in Spring Creek of Illinois ranges from about 75 mm/year for dry years (i.e., the years of much below normal precipitation) to roughly 250 mm/year for wet years. The factor most difficult to evaluate in the determination of groundwater contribution to the streamflow is the hydraulic connection between aquifers and streamflow, and the associated thickness of the contributing aquifers. It is not clear whether the water level fluctuation in the observation wells used in this studies are indeed the indication of the hydraulic potential in those aquifers in proving the groundwater discharge to the streams in Illinois. However, as will be shown later, the close correspondence between the water table fluctuations and the magnitude of streamflow in Illinois indicates that at least, the water level in those shallow wells reflects to a large degree the conditions in the aquifers connected to the streams.

Appendix B: Stochastic Analysis of Equation (3.8)

Here we describe a stochastic analysis of (3.8). We will consider S_y, K, H_0 and Q_0 to be constants and H and G to be stationary random functions of time. Thus, H and G can be decomposed into a temporal average and a perturbation term ($H = \overline{H} + h$; $G = \overline{G} + g$); then by taking the expected value of (3.8) the following mean equation is derived

$$S_y \frac{d\overline{H}}{dt} = \overline{G} - Q_0 - K(\overline{H} - H_0) \tag{A1}$$

By subtracting equation (A1) from (3.8), we have

$$S_y \frac{dh}{dt} = g - Kh \tag{A2}$$

which is the perturbation equation governing the fluctuation of input forcing G and output H. The spectral density function of h, $S_{hh}(\omega)$, can be related to that of g, $S_{gg}(\omega)$, through the following relationship:

$$S_{hh}(\omega) = \frac{1}{S_y{}^2\omega^2 + K^2} S_{gg}(\omega) \tag{A3}$$

Considering the following exponential covariance function [*Gelhar,* 1993] for describing the groundwater recharge G:

$$R_{gg}(\tau) = \sigma_g^2 \exp(-\frac{|\tau|}{T_g}) \tag{A4}$$

where σ_g^2 and T_g are the variance and correlation time scale of recharge. Another related study on the hydroclimatology of Illinois [*Yeh and Eltahir*, unpublished manuscript] focusing on the estimation of groundwater recharge in Illinois has shown that the correlation time scale of recharge is about one month. This value will be used as T_g in the plots of Figures 3.12 and 3.13. The spectral density function corresponding to the exponential covariance function is

$$S_{gg}(\omega) = \frac{2\sigma_g^2 T_g}{\pi(1+\omega^2 T_g^2)} \tag{A5}$$

By substituting (A5) into (A3) and then taking the inverse Fourier transform, the covariance function of H can be derived as

$$R_{hh}(\tau) = \sigma_g^2 [\frac{S_y T_g}{K(S_y^2 - K^2 T_g^2)} \exp(-\frac{K|\tau|}{S_y}) + \frac{T_g^2}{(K^2 T_g^2 - S_y^2)} \exp(-\frac{|\tau|}{T_g})] \tag{A6}$$

The variance of H corresponds to $\tau = 0$

$$\sigma_h^2 = \frac{\sigma_g^2 T_g}{K(KT_g + S_y)} \tag{A7}$$

which implies the larger deviations from the long-term average of groundwater level for a smaller K (i.e., more toward drought conditions).

Appendix C: Surface Runoff Scheme in the LSX

The surface runoff generation in the original LSX model depends mainly on one parameter *wpudmax*: the maximum size of puddle. The puddle represents surface retention that receives and stores rainfall, and infiltrates water to soils. The default value of *wpudmax* in LSX is 5mm. There are the following two mechanisms for surface runoff generation in LSX:

(a) When puddle water storage exceeds *wpudmax;* the excess rainfall goes to surface runoff. (b) By assuming a uniform distribution of the sub-grid puddle size ranging between 0 and *wpudmax*, surface runoff occurs at a rate equal to rainfall rate multiplied by (*wpud / wpudmax*), where the prognostic variable *wpud* is the average water storage in puddles.

Therefore, surface runoff in LSX is in general proportional to rainfall intensity, but not directly related to the soil moisture in surface soils. Also, the amount of surface runoff generation depends strongly on the value of *wpudmax.* A large *wpudmax* inhibits the surface runoff generation and enhances infiltration. Therefore, the value of *wpudmax* determines the amount of infiltration and hence groundwater recharge. The shortcomings of the LSX surface runoff scheme have been reported by *Bonan* [1994].